



**HAL**  
open science

# Lipid Flippases from Plasmodium Parasites : from Heterologous Production towards Functional Characterization

Anaïs Lamy

► **To cite this version:**

Anaïs Lamy. Lipid Flippases from Plasmodium Parasites : from Heterologous Production towards Functional Characterization. Biochemistry, Molecular Biology. Université Paris-Saclay, 2018. English. NNT : 2018SACLS447 . tel-02426208

**HAL Id: tel-02426208**

**<https://theses.hal.science/tel-02426208>**

Submitted on 2 Jan 2020

**HAL** is a multi-disciplinary open access archive for the deposit and dissemination of scientific research documents, whether they are published or not. The documents may come from teaching and research institutions in France or abroad, or from public or private research centers.

L'archive ouverte pluridisciplinaire **HAL**, est destinée au dépôt et à la diffusion de documents scientifiques de niveau recherche, publiés ou non, émanant des établissements d'enseignement et de recherche français ou étrangers, des laboratoires publics ou privés.

# Lipid flippases of *Plasmodium* parasites: from heterologous production towards functional characterization

Thèse de doctorat de l'Université Paris-Saclay  
Préparée à l'Université Paris-Sud  
Et à l'I2BC, CEA-Saclay

École doctorale n°568  
Signalisations et réseaux intégratifs en biologie (Biosigne)  
Aspects Moléculaires et Cellulaires de la Biologie

Thèse présentée et soutenue à Gif-sur-Yvette, le 23/11/2018, par

**Anaïs Lamy**

Composition du Jury :

<b>Philippe Minard</b> Professeur, Université Paris-Sud (UMR 9198)	Président
<b>Bruno Miroux</b> Directeur de Recherche, INSERM (UMR 7099)	Rapporteur
<b>Renaud Wagner</b> Ingénieur de recherche (hors classe), CNRS (UMR 7242)	Rapporteur
<b>Isabelle Florent</b> Professeure, MNHN (UMR 7245)	Examinatrice
<b>Rosa Laura López-Marqués</b> Associate Professor, University of Copenhagen	Examinatrice
<b>José Luis Vázquez-Ibar</b> Chargé de Recherche, CNRS (UMR 9198)	Directeur de thèse



## Remerciements

Je voudrais tout d'abord remercier l'école doctorale Biosigne pour m'avoir accordé un financement de thèse.

Je veux remercier également les membres de mon jury pour avoir accepté d'être présent et pour leur bienveillance.

Je tiens à remercier Francis Haraux pour m'avoir accueillie au sein du laboratoire et pour sa super affiche pour ma soutenance de thèse !

Je voudrais remercier tout particulièrement mon directeur de thèse José Luis Vázquez-Ibar pour sa patience et son soutien durant ces 3 années. Pour avoir supporté mon caractère un peu « bitchy » à certains moments, mes longues phases de déprime et de m'avoir dopé à la charcuterie espagnole ! Et surtout pour son optimisme (qui n'a pas déteint sur moi malheureusement !).

Je remercie également Christine Jaxel, ma co-directrice de thèse, pour sa gentillesse, son écoute, nos discussions scientifiques ou personnelles, son aide précieuse lors de la rédaction et les chocolats anti-déprime.

Je voudrais remercier Cédric Montigny et Guillaume Lenoir pour leurs conseils et leur aide pour les manip, et les moments passés tous ensemble lors des déjeuners.

Je remercie Thibaud « Titi » Dieudonné pour son aide sur les manip surtout sur les derniers moments de cette thèse, pour les fous rires, les concours de qui fera le plus peur à l'autre en sortie de la pièce de culture et les partages de vidéos ridicules. Je te souhaite une bonne fin de thèse (courage, le pire reste à venir), et on se revoit pour ta soutenance.

Je remercie Maylis Lejeune qui comme moi est restée 3 années au labo pour son apprentissage et qui a brillamment réussi son master. Je la remercie pour sa bonne humeur et pour les pauses thé. Sa voix douce et le son feutré de ses pas dans le couloir vont me manquer ☺ !

Je remercie Valentine « Valentina » Guinot pour sa gentillesse et sa bonne humeur. Et je lui souhaite le meilleur pour la suite.

Je remercie Thomas Barbot et le félicite pour sa thèse obtenue quelques mois plus tôt. Merci pour les marrades au labo mais je n'ai pas oublié le vieux spoil tout pourri de Game of Thrones, mon cœur en est meurtri à jamais ...

Je tiens également à remercier Marc le Maire pour sa gentillesse, ses conseils et pour m'avoir accueillie lors du concours de l'ED et pour les partages de connaissances sur les loutres.

Je remercie Phillipe Champeil d'avoir partagé son bureau avec moi et d'avoir participé à la relecture de cette thèse sur son temps de retraité et de papi.

Les autres membres du LPSM, Manuel Garrigos, pour nos discussions et nos échanges de film et série ! Nadège Jamin, Véronica Beswick, Claire Lemaire, Stéphane Orłowski, Michel Roux, Anthony Rignani, et Ewerton Bruzaferro qui a fait son M2 avec nous et nous a aidé sur le projet.

Les deux personnes sans qui on est vite perdu au labo (en tout cas moi je l'étais) ; Pascale Filoche qui s'occupe de nous et de nos commandes et Josiane Piles qui faisait en sorte qu'on ait toujours notre matériel propre et à disposition. Surtout merci pour votre gentillesse et votre bienveillance envers moi.

Merci à tous pour votre gentillesse, pour l'ambiance au laboratoire sérieuse et moins sérieuse, Pour être venu lors de mes différentes répétitions, pour avoir joué le jeu lors des repas de Noël et pour les anniversaires.

Je remercie également toutes les personnes des autres labos du cea ou I2BC que j'ai pu rencontrer durant ma thèse.

Je remercie Sandrine Lecart de la plateforme Imagerie-gif de l'I2BC, qui m'a aidé et conseillé pour les images de microscopie confocale.

Je remercie toutes les personnes que j'ai pu rencontrer lors des deux années en tant qu'enseignante à l'Université Paris-Sud, particulièrement Aurélie Hua-Van, Marielle Valerio-Lepiniec, Sylvie Nessler et Agathe Urvoas.

Je remercie aussi les personnes que j'ai rencontré lors de mes différents stages en Licence et Master, l'équipe « Mollicutes » à l'INRA de Bordeaux et l'équipe « Métabolisme intermédiaire des Trypanosomes » au CNRS de Bordeaux, qui m'ont donné envie de continuer en thèse et faire de la recherche.

Hors du cadre du travail, je remercie énormément Sandra alias Rocky, la meilleure sparring partner que j'ai pu avoir. Mon mentor, merci pour son soutien, pour les fous rires et les soirées Hawaiï 5-0 ! Merci d'avoir été là pour moi pendant cette thèse et pour longtemps encore !

Je remercie le club de Krav Maga Combat Evolution qui m'a permis de me défouler et d'apprendre beaucoup aussi ! Je remercie les instructeurs Franck, Bauris, Ilker, Christophe, Fabrice, Benjamin et bien sûr toutes celles et ceux que j'ai rencontré, qui m'ont permis de leur taper dessus (et qui m'ont tapé dessus en retour !).

Je remercie bien évidemment les girls Elodie D et Charlotte (qui sont aussi folles que moi et à qui je souhaite bon courage pour leurs thèses respectives), Les bananes : Marie et Elodie B ; Jeanne, Clara, Cécile et Léonie, qui étant loin ou moins loin ont toujours été d'un soutien sans faille depuis de nombreuses années maintenant ! Merci d'être toujours là !

Je remercie également ma famille qui s'est agrandie cette année avec les naissances de mon petit cousin Léon et ma petite Cacahuète, ma nièce Olivia.



## Table of contents

Abbreviations .....	5
I. Introduction.....	8
I-1 Malaria.....	8
I-1-1 General information on the disease.....	8
I-1-2 Plasmodium parasites and their complex life cycle .....	9
I-1-3 Treatments and resistance .....	13
1. Symptoms and diagnosis.....	13
2. Protection: chemoprophylaxis, vaccines and vector control .....	15
3. Treatments .....	16
4. Mechanisms of action of antimalarial drugs and resistance to them .....	18
I-2 Membrane transport proteins from <i>Plasmodium falciparum</i> .....	20
I-2-1 Membrane transporters in the infected erythrocyte.....	21
I-2-2 Genetic studies on the membrane transporters.....	23
I-2-3 Heterologous expression of <i>Plasmodium</i> membrane transporters.....	24
I-3 P4-ATPases .....	26
I-3-1 P-type ATPases .....	26
1. General information and subfamilies.....	26
2. Structural characteristics:.....	27
3. Catalytic cycle of P-Type ATPases.....	28
I-3-2 P4-ATPases .....	30
1. Overview of the P4-ATPases .....	30
2. Regulation of the P4-ATPases .....	32
3. Transport mechanism of P4-ATPases: two different models.....	32
I-3-3 P4-ATPases and Cdc50 proteins in <i>Plasmodium</i> parasites.....	34
I-4 Project .....	36
II. Objectives.....	38
III. Results and discussion.....	39
III-1 Analysis of ATP2 and Cdc50 sequences present in the genome of <i>Plasmodium</i> species .....	39
III-2 Expression of ATP2 and potentially associated Cdc50 subunits in <i>S. cerevisiae</i> .....	45
III-2-1 Construction of expression plasmid vectors .....	47
III-2-2 Expression tests in small-scale cultures .....	50
III-2-3 Expression tests of PcATP2/ PcCdc50.1 and PcATP2/ PcCdc50.3 in large-scale cultures. ....	56
III-2-4 Deglycosylation analysis of the PcCdc50.1 and PcCdc50.3 .....	58
III-2-5 Functional complementation assay in <i>S. cerevisiae</i> .....	60
III-2-6 Discussion .....	62

III-3	Detergent solubilisation of PcATP2, PcCdc50.1 and PcCdc50.3.....	64
III-3-1	Screening detergents.....	65
III-3-2	Improving PcATP2/Cdc50.1 and PcATP2/PcCdc50.3 solubilisation: membrane stripping and addition of cholesteryl hemisuccinate .....	67
III-3-3	Discussion .....	71
III-4	Introducing the GFP for the study of the PcATP2/PcCdc50 complex.....	73
III-4-1	Analysis of the cellular localisation of PcATP2 and PcCdc50.1 subunit expressed in <i>S. cerevisiae</i> by confocal microscopy .....	74
III-4-2	Fluorescence-detection size-exclusion chromatography of detergent-solubilized PcATP2 and PcCdc50 subunits.....	78
III-4-3	Determination of the interaction by co-immunoprecipitation .....	82
III-4-4	Discussion .....	85
III-5	Purification and functional characterization of PcATP2/PcCdc50.1 complex.....	87
III-5-1	Purification of PcATP2/PcCdc50.1.....	87
III-5-2	Towards the functional characterization of purified PcATP2/PcCdc50.1 complex in detergent micelles.....	91
1.	Construction of non-functional mutants of PcATP2.....	91
2.	Phosphorylation assay of purified PcATP2.....	93
3.	ATPase activity of purified PcATP2.....	95
III-5-3	Discussion .....	97
III-6	<i>Pichia Pastoris</i> : an expression host .....	100
III-6-1	Vectors construction and clones selection.....	101
III-6-2	Expression tests in <i>P. pastoris</i> .....	105
III-6-3	Discussion .....	105
IV.	Summary and prospects.....	106
V.	Material and methods.....	111
V-1	Material.....	111
V-1-1	Chemicals products .....	111
V-1-2	Buffers and culture Media.....	112
V-2	Methods .....	114
V-2-1	Cloning strategy and vectors design for expression.....	114
1.	Optimisation of the gene sequence .....	114
2.	Construction of the expression vectors for <i>S. cerevisiae</i> .....	115
3.	Construction of the expression vectors for <i>Pichia pastoris</i> .....	124
4.	Bacterial strains .....	127
5.	General molecular biology .....	127
V-2-2	Expression in the yeast <i>Saccharomyces cerevisiae</i> .....	130



1.	<i>Saccharomyces cerevisiae</i> strain .....	130
2.	Transformation by the lithium acetate method.....	131
3.	Functional complementation (cold-sensitive assay) .....	131
4.	Protein expression in <i>S. cerevisiae</i> .....	131
5.	Membrane preparation.....	132
6.	Deglycosylation of PcCdc50.1 and PcCdc50.3 subunits .....	134
V-2-3	Expression in the yeast <i>Pichia pastoris</i> .....	134
1.	<i>Pichia pastoris</i> strain .....	134
2.	Transformation by electroporation.....	135
3.	Clones selection.....	135
4.	Protein expression and membrane preparation .....	136
V-2-4	Protein detection.....	137
1.	Determination of total protein concentration .....	137
2.	SDS PAGE and western blot.....	137
3.	General procedure for membrane protein solubilisation .....	138
4.	Fluorescence size exclusion chromatography (FSEC).....	139
5.	Co-immunoprecipitation .....	139
6.	Purification of PcATP2-GFP/PcCdc50.1 complex by affinity chromatography.....	140
a.	Expression and purification of nanobodies targeting the GFP (nanoGFP):.....	140
b.	NanoGFP coupling to agarose beads:.....	141
c.	3C protease production.....	142
d.	Purification of the PcATP2/PcCdc50.1 complex .....	143
V-2-5	Activity assays of the purified PcATP2/PcCdc50.1 complex.....	144
1.	ATPase activity assay .....	144
2.	Phosphorylation assay.....	145
V-2-6	Fluorescence Microscopy of <i>S. cerevisiae</i> cells expressing PcATP2-GFP and Cdc50.1-GFP	145
VI.	Bibliography.....	147
Article	.....	174
Résumé en français	.....	176

# Abbreviations

---

ADP: adenosine diphosphate

AP5-A: Di-adenosine pentaphosphate

ATP: adenosine triphosphate

BAD: Biotin Acceptor Domain

BCA: Bicinchoninic acid

BSA: Bovine Serum Albumin

C<sub>12</sub>E<sub>8</sub>: octaethylene glycol monododecyl ether

CHS: cholesteryl hemisuccinate

CIP: Calf Intestinal Phosphatase

CYMAL-5: 5-Cyclohexyl-1-Pentyl- $\beta$ -D-Maltoside

DDM: n-Dodecyl- $\beta$ -D-maltopyranoside

DM: n-Decyl- $\beta$ -D-maltopyranoside

DNA: deoxyribonucleic acid

dNTPs: deoxynucleotides triphosphates

DOPC: 1,2-dioleoyl-sn-glycero-3-phosphocholine

DTT: dithiothreitol

EB: ethidium bromide

ECL: enhanced chemiluminescent

EDTA: Ethylene diamine tetraacetic acid

eGFP: enhanced Green Fluorescent Protein

ER: endoplasmic reticulum

FosC12: n-dodecyl phosphocholine 12

FSEC: fluorescence-detection size exclusion chromatography

GlcNAc: N-acetylglucosamine  
HEPES: N-(2-Hydroxyethyl) piperazine-N'-(2-ethanesulfonic acid)  
His: Histidine  
HRP: horseradish peroxidase  
IMC: inner membrane complex  
LB: Luria-Bertani medium  
LDAO: Lauryldimethylamin-oxid  
LDH: lactate dehydrogenase  
LMNG: Lauryl maltose neopentyl glycol  
Mw: molecular weight  
NADH: Nicotinamide adenine dinucleotide acid  
NaPi: sodium phosphate buffer  
Ni-NTA: Ni<sup>2+</sup>-nitrilotriacetic acid  
NPP: new permeation pathways  
OD: optical density  
OG: n-Octyl-β-D-glucopyranoside  
OTG: n-Octyl-β-D-thioglucopyranoside  
PBS: Phosphate Buffer Saline  
PCR: Polymerase Chain Reaction  
PEG: polyethylene glycol  
PEP: phosphoenol pyruvate  
PGK: phosphoglycerate kinase  
Pi: inorganic phosphate  
PI4P: Phosphatidylinositol 4-phosphate  
PIC: Protease Inhibitor Cocktail  
PIP<sub>2</sub>: Phosphatidylinositol 4,5-bisphosphate  
PfCRT: *Plasmodium falciparum* Chloroquine Resistance Transporter

PK: pyruvate kinase

PMSF: Phenylmethanesulfonyl fluoride

POPC: 1-palmitoyl-2oleoyl-sn-glycero-3-phosphocholine

POPE: 1-palmitoyl-2oleoyl-sn-glycero-3-phosphoethanolamine

POPS: 1-palmitoyl-2oleoyl-sn-glycero-3-phosphoserine

PVDF: Polyvinylidene difluoride

PVM: parasitophorus vacuole membrane

SDS: sodium dodecylsulfate

SDS-PAGE: polyacrylamide gel electrophoresis (with SDS)

SERCA: sarco-endoplasmic reticulum Ca<sup>2+</sup> ATPase

sGFP: superfolded Green Fluorescent Protein

RDT: Rapid Diagnosis Test

SSD: Salmon sperm DNA

TCA: Trichloroacetic acid

TEV: Tobacco Etch Virus

TGN: Trans-Golgi Network

TM: transmembrane segment spanning

Tris: Tris(hydroxymethyl)aminomethane

UDM: n-Undecyl-β-D-maltopyranoside

w/v: weight/volume

w/w: weight/weight

# I. Introduction

---

## I-1 Malaria

### I-1-1 General information on the disease

Malaria is a parasitic disease caused by different species of the genus *Plasmodium* and transmitted by the bite of a female mosquito of the genus *Anopheles*. This disease is considered as a global health problem, as it occurs in 91 tropical and subtropical countries worldwide (fig 1). Malaria is mostly prevalent in countries with particular climate conditions necessary for the habitat of the mosquito *Anopheles*: high temperatures, high humidity and seasonal rainfalls. However, the incidence of this disease is also influenced by different factors related to the man's activities as agriculture, migration movements or even wars. Indeed, in many areas, the high incidence of malaria is closely related with the socio-economic environment of the country, so under-developed countries are more susceptible to have a higher incidence. Other elements that can affect the incidence of malaria are the susceptibility of the parasite against treatments, the population density of the mosquito vector, and longevity or insecticide susceptibility, among others (Autino et al. 2012; Machault et al. 2011).

In 2016, there was about 216 million cases of malaria reported worldwide with 90% accounted for the African regions, 7% to the South-East Asia regions, and 2% to the Eastern Mediterranean regions. 15 countries carry 80% of the global burden among them, 14 situated in sub-Saharan Africa and India. With regard to the mortality, malaria caused 450 000 deaths, 91% occurring in African regions and 6 % in the South-East of Asia (World Health Organization 2017b). Importantly, about 70% of the total deaths were children under the age of 5, estimating that one child died every two minutes (World Health Organization 2016). In fact, the populations with a high risk acquiring malaria are those ones with a low immunity, like children under 5 years old, pregnant women or travellers visiting endemic countries (World Health Organization 2018).

Due to the efforts to control malaria and to the economic development, between 2000 and 2015 the incidence rate decreased globally 41%, the mortality rate decreased

globally of 62%, and 17 countries eliminated malaria completely reporting zero indigenous cases<sup>1</sup> for 3 years or more (fig 1). Although malaria's incidence and mortality have globally declined over the past 18 years, this decline has started to stall since 2014 (World Health Organization 2017b). There are still many efforts to do on the prevention part, including the access to the public health services.

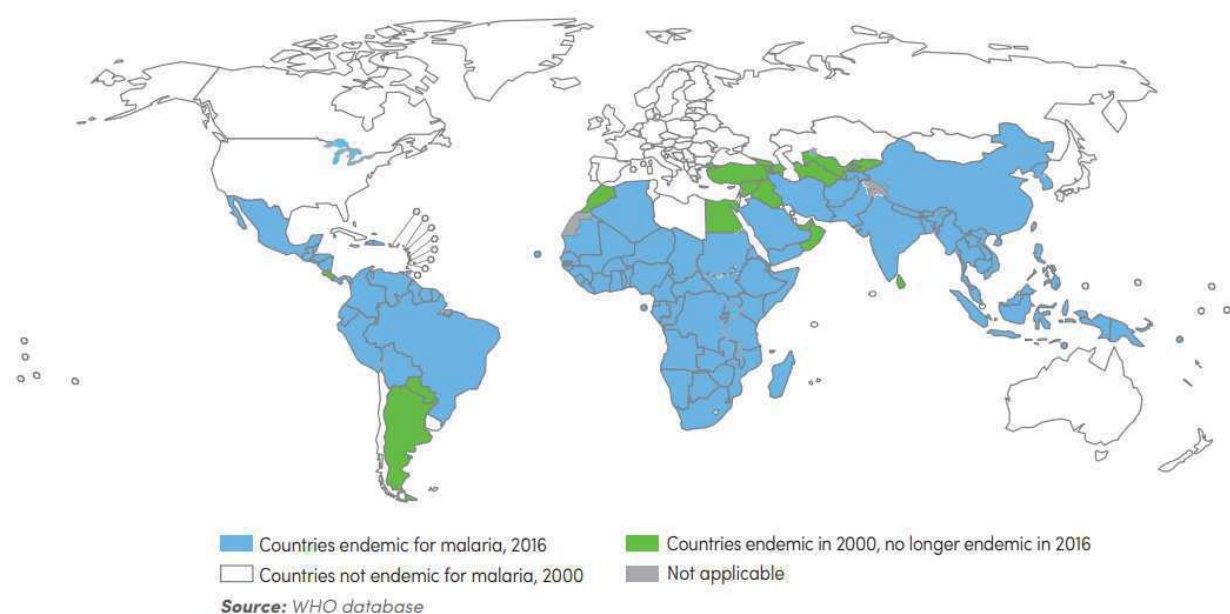


**Figure 1: Evolution of the malaria endemic countries between 2000 and 2016** (World Health Organization 2017a).

In 2000, 108 countries were reported endemic for malaria, and in 2016, 91 countries still remained endemic. Kyrgyzstan and Sri Lanka were certified malaria free in 2016, countries with zero indigenous cases over the past 3 consecutive years are eligible to request certification of malaria free status from WHO (World Health Organization 2017b).

## I-1-2 Plasmodium parasites and their complex life cycle

*Plasmodium* species, the parasites responsible of malaria belong to the *Apicomplexa* phylum. About 200 *Plasmodium* species exist and can infect mammals, birds and reptiles. Five species of *Plasmodium* infect humans: *P. falciparum*, *P. vivax*, *P. malariae*, *P. ovale* and *P. knowlesi*. The two most prevalent parasites are *P. falciparum* and *P. vivax*, *P. falciparum* is responsible of ~99% of malaria cases in Africa, while *P. vivax* is

<sup>1</sup> Indigenous cases: malaria acquired by mosquito transmission in an area where malaria is regular occurrence. <https://wwwn.cdc.gov/nndss/conditions/malaria/case-definition/2010/>

responsible for 64% of malaria cases in the Americas, 30% in South East Asia, and 40% in the Eastern Mediterranean regions (World Health Organization 2017b)

*Plasmodium* parasites are obligate intracellular parasites and, like other parasites of the *Apicomplexa* phylum, the infective forms are characterized by an apical complex (fig 2). In this apical complex region, we find the polar rings (the organizing center of microtubules). In addition, we find the apical secretory organelles, rhoptries and micronemes, which release their contents sequentially during parasite motility and host cell invasion (Baum et al. 2008; Counihan et al. 2013). They also possess an inner membrane complex (IMC) or pellicular cisterna (Harding and Meissner 2014), made of flattened membrane sacs (alveoli), supported by the thin filaments of the subpellicular network. A unique mitochondrion is found just under the IMC, closely linked to a vestigial plastid related to the plant chloroplast, the apicoplast, which is surrounded by four membranes (Mcfadden et al. 1997). The food vacuole is formed during the intraerythrocytic stage of the parasite when haemoglobin is proteolyzed.

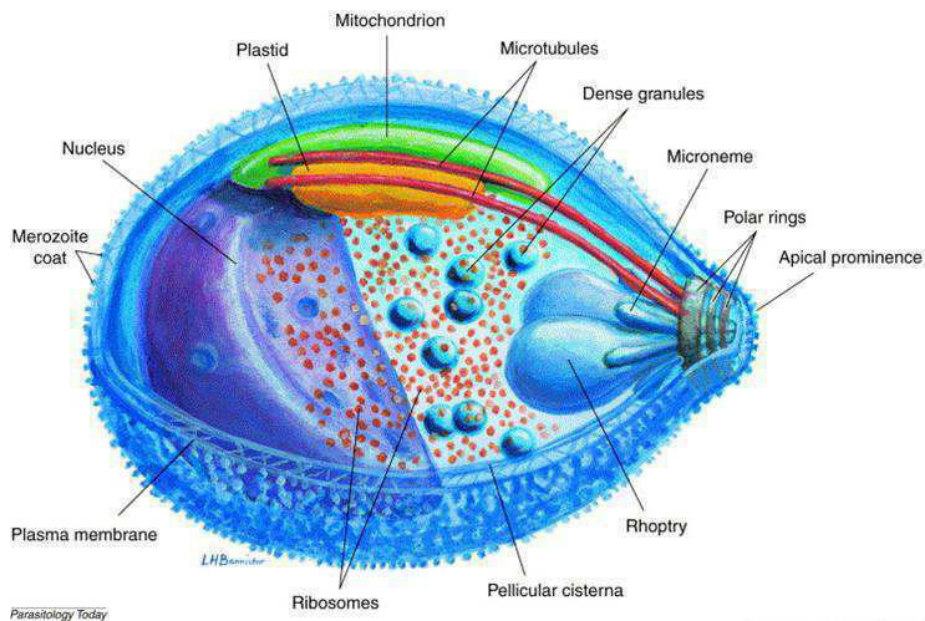


**Figure 2: Schematic organisation of a *Plasmodium falciparum* merozoite.**

*Three-dimensional organisation of a P. falciparum merozoite. The characteristic organelles of a merozoite are represented with the apical complex composed of the polar rings, the two rhoptries, the micronemes and the dense granules. Under the plasma membrane is found the pellicular cisterna attached by the filament of the subpellicular network. The unique mitochondrion is closed to the pellicular cisterna and linked to the apicoplast, a plastid related to chloroplasts. (Bannister et al. 2000)*

The malaria disease was already known during the Antiquity; however, its causative agent, the *Plasmodium* parasite, was only discovered in 1880 by Alphonse Laveran, a French military doctor who received the Nobel Prize for his discovery in 1907 (Sherman 2005; Cox 2010). The transmission of the parasite by the mosquito was described by Ronald Ross, a surgeon-major in the Indian medical service, working first on human malaria and later, on bird malaria. He was awarded the Nobel Prize in 1902 (Sherman 2005).

The life cycle of *Plasmodium* parasite is divided in two parts, one occurring in the animal host and the other in the insect vector, the female mosquito of the *Anopheles* genus (Sherman 2005; Heussler et al. 2016) (Fig 3). The *Plasmodium* parasite is first transmitted into the host by an infected female mosquito during blood meal. At this moment, less than 25 sporozoites are released from the mosquito's salivary glands into the skin of the host. Not all the sporozoites succeed to migrate from the skin to the blood vessel (Amino et al. 2006). However, once in the bloodstream, it takes less than an hour for the sporozoites to reach the liver and invade the hepatocytes. The liver stage of the parasite, after hepatocyte invasion, lasts from 2 to 10 days. During this time, the parasite multiplies asexually, releasing between 10 000 and 40 000 merozoites per hepatocyte. Then, the merozoites leave the hepatocyte inside a membranous bud called the meroosome and enter the blood system. In two *Plasmodium* species, *P. vivax* and *P. ovale*, a proportion of liver-stage parasites, named hypnozoites, can remain dormant in the hepatocytes for months or several years without clinical manifestations (Richter et al. 2010). Thereby, they can initiate a cycle of asexual reproduction in the absence of a new mosquito bite. Within 2 hours after reaching the blood circulatory system, the merozoites invade red blood cells (erythrocytes or reticulocytes, depending on the *Plasmodium* species), starting another cycle asexual reproduction or schizogony. After invasion of the red blood cell, the merozoite goes through different stages or forms inside the host, evolving from an initial state called "ring stage" to the trophozoite and, then, to the schizont. Each mature schizont gives a new generation of merozoites that are released into the blood system after the lysis of the red blood cell. These merozoites can invade other red blood cells and repeat more schizogony cycles, resulting in up to a 10-fold increase of the parasite population. Most of clinical symptoms in malaria are caused after red blood cell destruction. After a new invasion of a red blood cell, some parasites switch to a sexual differentiation leading to male and female gametocytes.



These gametocytes are released into the blood system and ingested by a female mosquito during blood feeding. In the mosquito, the male gametocyte divides into eight flagellated microgametes that escape from the red blood cell in a process called exflagellation (Sinden et al. 2010). Then, the microgamete fertilizes one female macrogamete to form the ookinete, which due to its motility, moves through the cells of the stomach wall and differentiates into an oocyst. Into the oocyst, sporozoites are formed after asexual multiplication; then, the oocyst bursts and the released sporozoites migrate to the mosquito salivary glands. Finally, when the female mosquito takes a new blood meal, it injects the sporozoites in the new host, completing, therefore, the cycle.

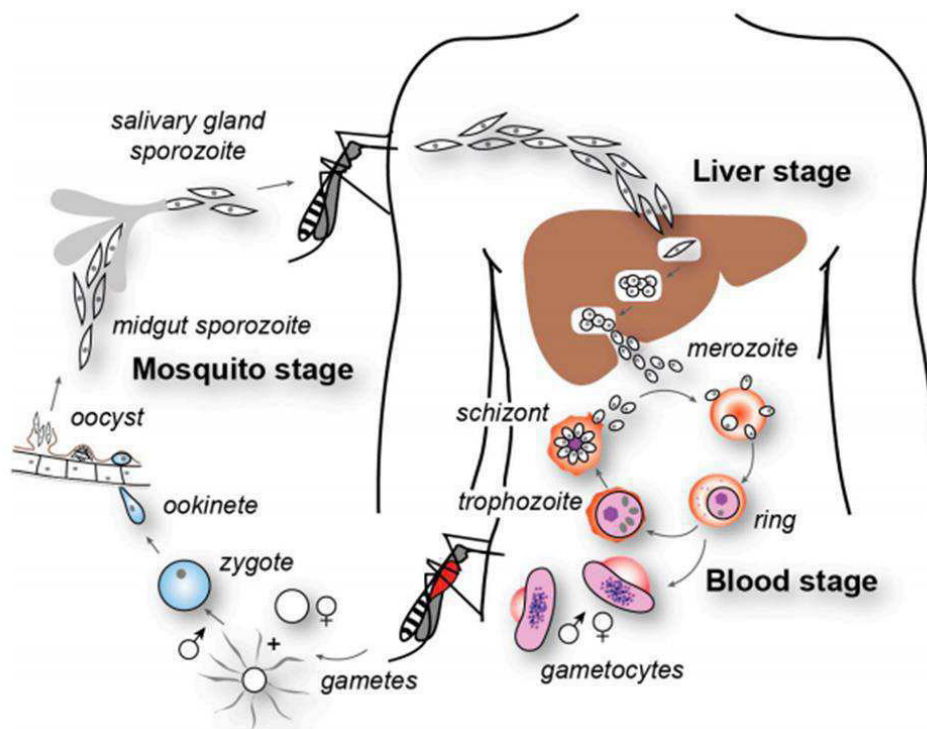


**Figure 3: Scheme of the life cycle of *Plasmodium falciparum*.**

*The female Anopheles mosquito injects sporozoites in the host during a blood meal. The sporozoites move to the liver and invade hepatocytes, in which they asexually multiply to produce merozoites that are released into the blood stream from the merozoite. Merozoites invade erythrocytes and go through different stages: an initial ring stage followed by a trophozoite form, and, finally, the mature schizonts that evolve to merozoites. Merozoites, released by the lysis of the erythrocyte, can reinvade new red blood cells and perform new schizogony cycles. Some merozoites after erythrocyte's invasion differentiate into either male or female gametocytes that, after being released to the blood systems, are ingested by a mosquito. Into the mosquito's gut, the mature male microgamete fertilizes the mature female macrogametes, leading to the fertilized zygote forms known as ookinetes due to their high motility. Ookinetes develop into an oocyst where the sporozoites are formed by asexual reproduction. Finally, these sporozoites are released and migrate to the*

salivary glands, where they will be transmitted to a new host after a new blood feeding. (Cowman, Berry, and Baum 2012)

In some cases, the malaria infection is not due to the bite of a mosquito. The parasite can be also transmitted from mother to child during pregnancy or even after a blood transfusion with infected blood (Abdullah and Karunamoorthi 2016; Poespoprodjo et al. 2010).

## I-1-3 Treatments and resistance

### 1. Symptoms and diagnosis

#### **Symptoms:**

After infection by the bite of the female mosquito, the incubation period between the infection and the apparition of the symptoms varies between 9 to 30 days depending on the *Plasmodium* species. *P. falciparum* has the shortest period and *P. malaria* the longest one (Bartoloni and Zammarchi 2012). This period can vary depending on several factors, such as the immunity of the person, the use of chemoprophylactic drugs or the parasite density inoculated. The clinical symptoms are fundamentally associated to the erythrocytic stage of the parasite. The release of the red blood material and accumulated wastes from the parasite after erythrocyte's rupture and merozoite release, induces a reaction by the immune system, resulting in periods of high fever. Usually, the infection leads to a so-called uncomplicated malaria, defined by non-specific symptoms such as fever, chills, sweat, body-aches, headache, cough, diarrhoea, nausea and vomiting, which can be related to other infections like flu, rendering complicated the diagnosing. The fever is irregular and appears after each of the schizogony cycles. Thrombocytopenia is also common in uncomplicated malaria. Importantly, the delay in the diagnosis, lack of treatment, and the immunological background of the host can lead to a severe form of malaria.

Severe malaria can lead to different complications as cerebral malaria, respiratory failure, pulmonary oedema, kidney injuries, hypoglycaemia or severe anaemia (Trampuz et al. 2003). One feature of severe malaria caused by *P. falciparum* is the sequestration of infected erythrocytes in the microvasculature contributing to metabolic acidosis and organ damages. Indeed, cerebral malaria, the most severe neurological complication of *P. falciparum* malaria, is caused by the sequestration of infected erythrocytes within

cerebral blood vessels (Idro, Jenkins, and Newton 2005). Clinical symptoms of severe malaria are, among others, prostration, impaired consciousness, coma, convulsion, jaundice, anuria and hypoglycaemia. Moreover, severe malaria is propitious for invasive bacterial infections in children. In addition, HIV infection is a major risk after severe malaria development (Ashley, Pyae Phyo, and Woodrow 2018; Bartoloni and Zammarchi 2012; Cowman et al. 2016).

In the case of non-immune pregnant women, malaria can cause a severe pathology for the mother (like pulmonary oedema and hypoglycaemia) and can lead to stillbirth or premature labour. For women with a certain degree of immunity, the infection with malaria normally results in anaemia for the mother and a low birth weight for the child. Sequestration of parasites in the placenta can also occur (Cowman et al. 2016).

### **Diagnosis:**

The diagnosis is mostly based on a parasitological test by microscopic examination or Rapid Diagnosis Tests (RDT) of a blood sample. In addition, and if the resources are available, the parasite's nucleic acid can be detected by PCR. It is very important to do the tests and have a diagnosis as fast as possible, especially for children and non-immunized population for whom the infection can be rapidly fatal (Moody 2002; Wongsrichanalai et al. 2007; Mathison and Pritt 2017).

The microscopy analysis is based on a stained blood film to directly visualise the parasites and to quantify the parasitemia ("M15-A Laboratory Diagnosis of Blood-Borne Parasitic Diseases; Approved Guideline" 2000). This widely used technique is called the "gold standard" to diagnose *Plasmodium* infection, and it requires trained people. Fluorescence microscopy is also used but it needs a specific microscope and trained people and, sometimes, it is not accessible in endemic areas.

RDT are based on the detection of parasite-specific antigens or enzymes that are genus or species-specific. This test gives a result in 15-30 min and requires no laboratory or trained people. They are immune chromatographic tests that use monoclonal antibodies targeting three parasite's enzymes. In *P. falciparum*, they target the histidine rich protein HRP-2, a water-soluble protein present during the asexual and the early gametocyte, stages of the parasite and presented at the surface of the erythrocyte. The HRP-2 antigen can be found even after successful treatment so it will not inquire on the disease's

evolution. The parasite's lactate dehydrogenase, pLDH, from the glycolytic pathway is also used and it is a pan-species marker. The parasite's enzyme aldolase is also used as pan-species marker and it is mostly used in combination with HRP-2 detection (Wilson 2012).

The parasite's nucleic acid detection by PCR is also used as diagnosis tool since it is a very sensitive technique which can detect very low parasitemia. Detection of the 18S rRNA and the circumsporozoite gene allows to identify the different *Plasmodium* species (Vasoo and Pritt 2013). The downside of this technique is that it can detect also dead parasites after successful treatment, so it is not suited for monitoring the level of parasitemia after treatments.

## **2. Protection: chemoprophylaxis, vaccines and vector control**

In order to decrease the incidence of malaria, prevention measures were applied. This includes chemoprophylaxis, control of the mosquito vector, and, most importantly, the development of vaccines.

Chemoprophylaxis: For pregnant women and children, an intermittent preventive treatment consists on a minimum dose of sulfadoxine–pyrimethamine (SP) (Ashley, Pyae Phy, and Woodrow 2018). In the areas with seasonal malaria, children receive a combination of SP and amodiaquine. In the case of travellers, the preventive treatment is the combination of atovaquone and proguanil, sold under the name Malarone®. Doxycycline, mefloquine and primaquine are also used for traveller's prophylaxis.

Control of mosquito vectors and/or bite prevention: The insecticide dichlorodiphenyltrichloroethane (DDT) was discovered at the beginning of the 1940s and was a powerful tool for eliminating the mosquito vector until mosquitoes started to develop resistance against this molecule. Nowadays, in high transmission areas, the most effective measures for controlling the malaria vector, and, therefore, infection are the combination of long-lasting insecticidal nets and indoor residual spraying (Ashley, Pyae Phy, and Woodrow 2018).

Vaccination: To radically eliminate malaria it is mandatory to design an effective vaccine to provide immunity to high risk population as children and pregnant women. Different vaccines are currently under development, targeting different stages of the parasite's life cycle (Coelho et al. 2017). To this day, the most developed one is the RTS,S/ AS01

vaccine that is already in phase IV of clinical trials (Gosling and von Seidlein 2016). This vaccine contains the central repeat region of the *P. falciparum* circumsporozoite protein (CSP) fused to the Hepatitis B surface antigen, HBS. Other vaccines are composed by whole attenuated parasites by either radiation (PfSPZ) (Greenwood 2017; Mordmüller et al. 2017), genetic attenuation (GAP) or chemical attenuation (CVac). Vaccines targeting the blood stage include the vaccine containing the *Plasmodium* Apical Membrane Antigen (AMA1) together with the rhoptry neck protein 2 (RON2), or the one containing the parasite's Reticulocyte Binding Protein Homolog 5 (PfRH5) (Douglas et al. 2015). All these vaccines contain essential components of the merozoite's invasion machinery and, therefore, they are designed to block infection. Some vaccines are designed to block the transmission by the mosquito, targeting antigens present in the sexual stage parasite inside the mosquito. After vaccination, the antibodies generated by the host's immune response are taken by the mosquito during blood feeding and, therefore, they can reach their target. Finally, and since placental malaria caused by *P. falciparum* is a major cause of maternal, foetal and infant mortality, important efforts have been made to understand the mechanisms of this type of infection, representing a promising path for vaccine development (Fried and Duffy 2015).

### 3. Treatments

One of the first isolated molecules with antimalarial properties was the quinine, a molecule extracted from the tree *Cinchona succirubra* in 1817 by the French pharmacists Pelletier and Caventou (Lee 2002). Quinine remained the mainstay of malaria treatment until the 1920s when more effective synthetic anti-malarials became available like chloroquine. Quinine is still used in combination with antibiotics mainly for uncomplicated malaria and pregnant women (Achan et al. 2011). Chloroquine attained a worldwide use as antimalarial drug at the end of the 1940s due to its low toxicity, efficacy and affordable price (Slater 1993). It was commonly used together with the insecticide DDT, and its use has had a huge impact on malaria elimination in low transmission-rate countries. However, from the 1960s onwards, use of chloroquine progressively succumbed to the appearance and spread of resistant strains of *Plasmodium* around the world (Trape 2001) that stalled the elimination of malaria (Fidock et al. 2004). Nowadays, chloroquine still maintains some efficacy in areas where patients have acquired partial immunity to malaria (Petersen, Eastman, and Lanzer

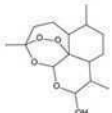
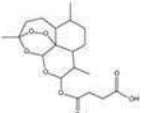
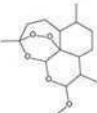
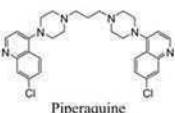
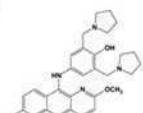
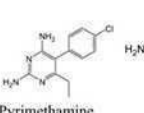
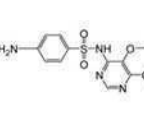
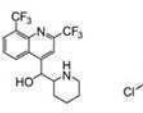
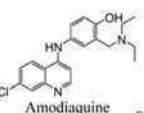
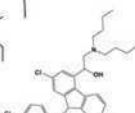
2011). Currently, the most effective treatment for malaria are artemisinin-based combination therapies (ACTs), that combine a semi-synthetic derivative of artemisinin, a chemical compound isolated from the Chinese wormwood *Artemisia annua*, with a partner drug. Artemisinin was first isolated in the 1970s by Chinese scientists and more particularly by Youyou Tu who was awarded the Nobel Prize in 2015 (Youyou 2015). At present, the most common derivatives of artemisinin are artesunate, artemether, arteether and dihydroartemisinin (Meshnick 2002).

Antimalarial drugs in the current arsenal have been classified in three broad categories according to their chemical structure and mechanism of action (Arrow, Panosian, and Gelband 2004). (1) Aryl aminoalcohol compounds: quinine, quinidine, chloroquine, amodiaquine, mefloquine, halofantrine, lumefantrine, piperaquine and tafenoquine; (2) Antifolate compounds: pyrimethamine, proguanil, chlorproguanil and trimethoprim; and (3) Artemisinin compounds: artemisinin, dihydroartemisinin, artemether and artesunate. Atovaquone is an antimalarial on its own class, commonly combined with proguanil (Malarone®) (Flannery, Chatterjee, and Winzeler 2013).

The ACTs consist in using two compounds that, theoretically, interact with two different targets in the parasite. This strategy aims at decreasing the appearance of resistant strains to this treatment since the probability of generating resistance to both compounds at the same time while preserving parasite's fitness is very low. In addition, ACTs combine a compound with short half-life and rapid action (artemisinin and derivatives) with slowly-eliminated compounds which remain active much longer (amino alcohol compounds) (Eastman and Fidock 2009; Ashley, Pyae Phyo, and Woodrow 2018). The current ACTs used as first-line treatment of uncomplicated malaria are (table 1): artemether/lumefantrine, artesunate/amodiaquine, artesunate/mefloquine, artesunate/sulfadoxine/pyrimethamine, dihydroartemisinin /piperaquine. As to severe malaria, the treatment consists in artesunate, quinine or artemether. Finally, in the case of pregnancy, the treatment consists in a combination quinine/clindamycin or, in some cases, chloroquine.

Several antibacterial drugs (e.g., tetracycline, clindamycin) have also anti-malarial activity although, in general, their action is slow, so they are recommended only in combination with other antimalarial drugs.

**Table 1: Artemisinin-based combination therapies with their target and the associated resistance to the partner drug (Ouji et al. 2018)**

ACTs	Dihydroartemisinin - piperazine	Artesunate-pyronaridine	Artesunate-sulfadoxine-pyrimethamine	Artesunate-mefloquine	Artesunate-amodiaquine	Artemether-lumefantrine	
<b>Brand name (suppliers)</b>	Eurartesim® (Sigma-Tau) Artekin® (Holleykin) Diphos® (Genix Pharma)	Pyramax® Shin Poong Pharmaceutical Co. Ltd.	Artesunate + Sulfadoxine + Pyrimethamine Tablets (Advacare PHARMA) Malosunate® (Anhui)	ASM FDC (DNDI/Cipla Ltd)	ASAQ Winthrop® (Sanofi)	Coartem® Riamet® (Novartis)	
<b>Artemisinin derivative</b>	 Dihydroartemisinin		 Artesunate			 Artemether	
<b>Partner drug</b>	 Piperazine	 Pyronaridine	 Pyrimethamine	 Sulfadoxine	 Mefloquine	 Amodiaquine	 Lumefantrine
<b>Target of the partner drug</b>	Hemozoin synthesis	Hemozoin synthesis	DHPS - DHFR	Hemozoin synthesis	Hemozoin synthesis	Hemozoin synthesis	
<b>Resistance mechanism of the partner drug</b>	<i>Plasmepsin 2-3</i> amplification	Not identified	Modification of the drug target	Amplification of <i>Pfmdr1</i> copy number	<i>Pfprt</i> and <i>Pfmdr1</i> mutations	Amplification of <i>Pfmdr1</i> copy number	

#### 4. Mechanisms of action of antimalarial drugs and resistance to them

To develop new antimalarial drugs outwitting the capacity of the parasite to develop resistance against them, it is very important to have a deep knowledge of the mechanisms of action of the current drugs and also to understand the mechanisms that the parasite develops to fight back while keeping its physiological roles (also called, fitness cost).

The physical chemistry properties of chloroquine allow this drug to concentrate in the interior of the acidic food vacuole, since once on its interior the drug is protonated and cannot cross back the membrane. The food vacuole is involved in the enzymatic digestion of the host haemoglobin and, at the same time, in detoxifying the group heme resulting from haemoglobin digestion, which is dimerized to  $\beta$ -haematin and crystallizes as the chemically inert malaria pigment, hemozoin (Rosenthal 2005). Chloroquine interferes with the heme dimerization process and therefore, avoids heme detoxification. The most common way for the parasite to develop resistance to this drug is by simply expelling it out from the food vacuole. In *P. falciparum*, this is achieved

through different mutations in the gene that encodes the essential food vacuole transporter PfCRT (initially named chloroquine resistant transporter because the physiological substrates were unknown), giving it the capacity to recognize chloroquine and to transport it outside the food vacuole (Sidhu, Verdier-Pinard, and Fidock 2002). In addition, in chloroquine-resistant strains, point mutation in the encoding gene of another food-vacuole transporter, the *P. falciparum* multidrug-resistant transporter, PfMDR1 is also implicated in chloroquine resistance (Schlitzer 2007; Duraisingh and Cowman 2005).

Antifolate drugs interfere with the folic acid synthesis by inhibiting the parasite's enzymes dihydrofolate reductase-thymidilate synthase (DHFR) and dihydropteroate synthase (DHPS). Mutations in both genes allow the parasite to acquire resistance to those drugs (Antony and Parija 2016).

Atovaquone interferes with the mitochondrial electron transport leading to the inhibition of cellular respiration. Atovaquone's resistance is accomplished by the parasite by single-point mutations in the gene encoding the cytochrome b (Antony and Parija 2016).

The mechanism of action of artemisinin is still under considerable debate. It was first proposed that the main mechanism of action of artemisinin is to create toxic free radicals in the parasite's cytoplasm. Other proposed mechanisms involve targeting the heme polymerization (as chloroquine does) or inhibiting the respiratory chain of the parasite's mitochondrion (Cui and Su 2009). A few years ago, Krishna and co-workers (Eckstein-Ludwig et al. 2003) proposed that PfATP6, the unique endoplasmic reticulum Ca<sup>2+</sup> ATPase homolog of *P. falciparum*, was indeed the target of artemisinin; however, a direct interaction of PfATP6 and artemisinin was discarded in our laboratory using recombinantly-produced PfATP6 (Arnou et al. 2011; Cardi et al. 2010). Instead, recent studies have provided solid evidences that artemisinin and derivatives are potent inhibitors of the *P. falciparum* phosphatidylinositol-3-kinase (PfPI3K) (Mbengue et al. 2015). In addition and although the resistance mechanism is still not fully understood, a mutation in the propeller domain of the gene encoding the Kelch protein 13 (K13) was associated with artemisinin resistance (Mbengue et al. 2015). The function of this protein is still unknown but it shares homologies with the human Keap1 protein,



involved in the cell response to oxidative stress. K13 is localised in the reticulum endoplasmic of the parasite (Ouji et al. 2018).

Although the mechanism of action of quinine is still unknown, the main resistance is due to an increased number of the gene copies encoding PfMDR1, also implicated in the resistance to other amino alcohol (Schlitzer 2007). In addition, resistance to this drug is linked to simultaneous mutations in different membrane transporters as PfMDR1, PfCRT, and the sodium/hydrogen exchanger, PfNHE1 (Cheruiyot et al. 2014),

The antibiotics used in combination with other antimalarial drugs are prokaryotic protein-synthesis inhibitors and their target is localized in the apicoplast (Fidock et al. 2004).

Finally, a new class of antimalarial drug molecules, the spiroindolones, were shown to target the *P. falciparum* Na<sup>+</sup>/K<sup>+</sup> ATPase pump, PfATP4 (Rottmann et al. 2010; Natalie J. Spillman et al. 2013).

## **I-2 Membrane transport proteins from *Plasmodium falciparum***

The appearance and spreading of *P. falciparum* strains resistant to practically all the antimalarial drugs urge the development of new treatments, which implies more efforts towards the identification and validation of essential proteins of the parasite that can be used as drug targets. Membrane transport proteins (MTP) encoded by the parasite represent an important, yet little explored, potential source of new drug targets. In fact, in humans, MTPs are considered as one of the most important pharmacological targets due to their essential role in many physiological processes (Giacomini et al. 2010; Rask-Andersen, Almén, and Schiöth 2011). The intracellular mode of living of *Plasmodium* species requires precise mechanisms to import nutrients and precursors to fuel metabolic pathways, in addition to highly efficient systems to expel metabolites; and MTPs are the main proteins responsible of these tasks. In addition, and as indicated earlier, they are directly involved in the drug-resistance mechanisms against current drugs. Therefore, to identify future candidates for drug targeting, it is very important to study in detail the different membrane transporters encoded by the parasite, to know at which stage of its life cycle they are expressed, where they are localised within the cell, what are their functional characteristics (this include the identification of their

physiological substrate), and how the absence or functional depletion of a particular transporter may affect the viability of the parasite.

The genome of the *P. falciparum* strain 3D7 is composed of ~23 megabases distributed on 14 chromosomes. It is one of the most A+T rich genome, accounting for 80% of its composition. The sequencing of the entire genome in 2002 (Gardner et al. 2002) allowed the identification of about 5 268 protein-coding genes. Among these genes, *P. falciparum* encodes ~ 140 MTPs distributed in 28 families and superfamilies, and representing about 2.5% of the encoded proteins (Martin et al. 2005; Weiner and Kooij 2016). For most of them, the functional annotation is still not completed, and many cases it has been deduced from homology to genes of other organism, already characterized. Databases like the PlasmoDB (<http://plasmodb.org/plasmo/>) offers a remarkable tool to study *Plasmodium*-encoded proteins, where available information of every single gene is presented in a very comprehensible manner. In addition, the TransportDB2 database (<http://www.membranetransport.org/transportDB2/index.html>) contains the largest dataset for MTPs, and includes phylogenetic classification and functional annotations.

### **I-2-1 Membrane transporters in the infected erythrocyte**

As explained earlier, MTPs are necessary for the physiology and the development of the parasite within the erythrocyte. They mediate the uptake of nutrients through the different membrane compartments of the parasitized cell, as well as the generation and maintenance of the electrochemical gradients across the membranes and the removal of the metabolic wastes, including xenobiotics. MTPs are also associated to the resistance to antimalarial drugs and can be themselves drugs targets (Kirk & Lehane, 2014; Staines et al., 2010).

After invading the erythrocyte, *P. falciparum* starts developing inside the host, where it multiplies different organelles such as the nucleus, the endoplasmic reticulum, the Golgi apparatus, the food vacuole, the mitochondrion or the apicoplast; all of them surrounded by lipid membranes (see scheme fig 4)(Staines et al., 2010). In addition, *P. falciparum* radically modifies the properties of its host cell plasma membrane by exporting and inserting in it its own proteins (Maier et al. 2009). The subcellular localisation of a few number of MTPs have been determined by fluorescent tagging in the cell using antibodies (Martin, Ginsburg, & Kirk, 2009), in situ tagging with the GFP or

hemagglutinin tags. However, for a large proportion of them, the localisation still needs to be determined. Most of the information we have with respect MTPs localization in the different membranes comes from functional studies or indirect assays.

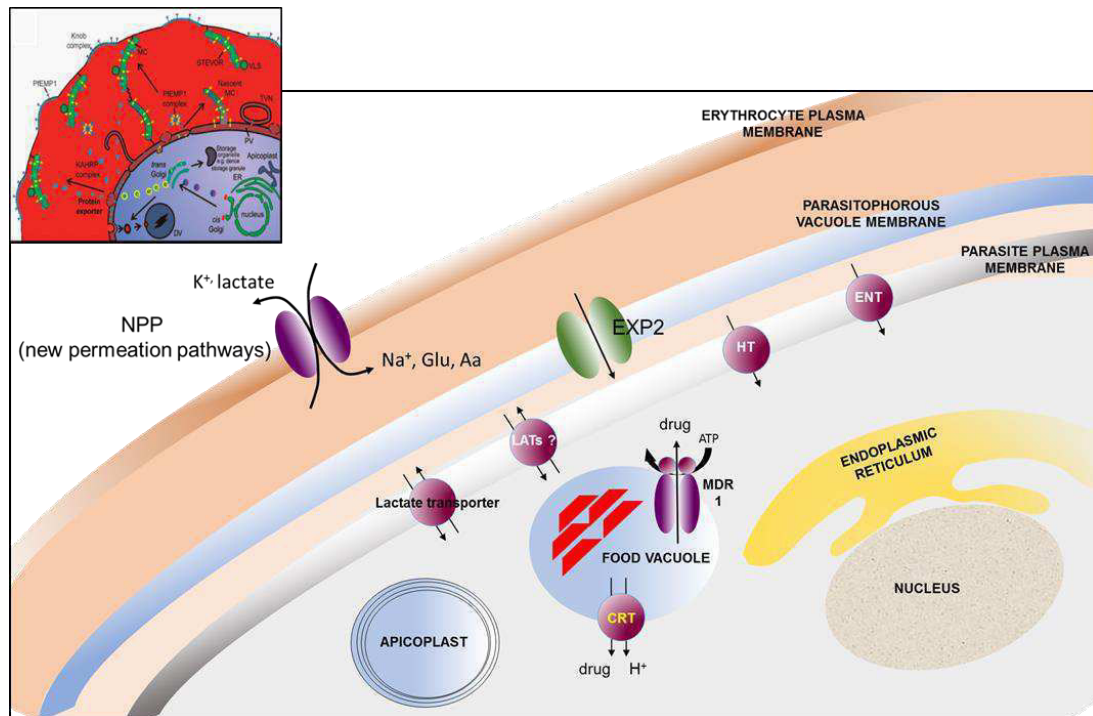


**Figure 4: Membrane transport proteins within the infected erythrocyte.**

*Schematic representation of membrane transport within the infected erythrocyte. Erythrocyte plasma membrane: transport of the essential nutrients and ions into the infected erythrocyte via the NPP. Parasitophorous vacuole membrane: protein translocon EXP2. Parasite plasma membrane: are found here the hexose transporter (PfHT), the nucleoside transporter PfENT1, amino acid transporter(s) (LATs) still unknown. Food vacuole membrane: are found here the drug transporters PfMDR1 and PfCRT (chloroquine transport). Picture in the upper left corner: schematic representation of the different organelles and membranes found in the infected erythrocyte (Tilley et al. 2007)*

Several *P. falciparum*-encoded MTPs are involved in the establishment of new permeability pathways (NPP) in the plasma membrane of the erythrocyte (fig 4). The identity of all the MTPs participating in the NPP is not known yet, and some transporters from the host's erythrocyte participate as well. The NPPs role is to transport nutrients like sugar, amino acids, nucleosides and vitamins into the erythrocyte's cytoplasm. They also are involved in maintaining the ionic composition of the erythrocyte's cytoplasm, and in extruding wastes from the metabolic reactions like lactate (Kiaran Kirk and Lehane 2014). The parasitophorous vacuole membrane (PVM) is known to be highly permeable to many and quite different solutes, ions and even small peptides and proteins (Spielmann et al. 2012). It is suggested that the *Plasmodium*-encoded protein

translocon EXP2 is the main responsible of this large permeability and poor specificity (De Koning-Ward et al. 2009). Moreover, this year, a cryo-electron microscopy (cryo-EM) structure of the PTEX was revealed, showing seven EXP2 protomers (of one TM) forming a funnel through the PVM; thus helping to understand the PTEX mechanism for protein translocation (Ho et al. 2018). The uptake of sugars, nucleosides and amino acids through the parasite's plasma membrane is catalysed by different secondary transporters as the hexose transporters (PfHT), the nucleoside transporters (PfENT) or neutral amino acid transporters (LATs) (fig 4) (Kieran Kirk and Lehane 2014).

### **I-2-2 Genetic studies on the membrane transporters**

Different genetic manipulation tools have been recently used to study the role of MTPs in the *Plasmodium* life cycle. The importance of some *Plasmodium* MTPs has been uncovered after disrupting the target genes and observing a deleterious effect upon parasite's survival. A transposon mutagenesis approach on *P. falciparum* showed that 2680 out of 5399 genes (87%), were essential for optimal growth during *in vitro* asexual blood stages (M. Zhang et al. 2018). A similar screening, although doing a full knockout of 2,578 genes of *P. berghei*, reported 1,652 essential genes needed for the parasite to grow in mice (Bushell et al. 2017), therefore estimating that almost two-thirds of the parasite genes are required for normal asexual growth during *in vivo* blood stage. Concerning MTPs, the former study showed that 26 out of 79 MTPs, are essential for the parasite and another 19 from these 79 are required for normal growth (Bushell et al. 2017). Among these essential transporters, there is a considerable number of MTPs belonging to the P-type ATPase family (Weiner and Kooij 2016), implicated on both maintaining ion homeostasis and lipid translocation in membranes. For instance, PfATP4, the *P. falciparum* Na<sup>+</sup>/H<sup>+</sup> pump is required to maintain Na<sup>+</sup> homeostasis in the parasite and, therefore, it is not surprising to find that PfATP4 deletion resulted in a growth defect of the parasite (M. Zhang et al. 2018). Moreover, PfATP4 was identified as the target of the antimalarial drugs spiroindolones (Rottmann et al. 2010), and one of these molecules has already reached clinical trials (Natalie Jane Spillman and Kirk 2015). Another example of an essential P-type ATPase is the *Plasmodium* homolog of the sarcoplasmic/endoplasmic reticulum calcium pump, PfATP6, which regulates the intracellular Ca<sup>2+</sup> concentration of the parasitized cell (Kieran Kirk 2015). As in other organisms, ion-transporting P-type ATPases encoded by malaria parasites are already

considered as potential drug targets (Yatime et al. 2009; Natalie Jane Spillman and Kirk 2015). Importantly, besides these already characterized P-type ATPases, these studies have also shown that four putative aminophospholipid transporters belonging to the P4 subfamily of P-type ATPases are also essential or important for the parasite's normal development (Kenthirapalan et al. 2016; M. Zhang et al. 2018; Bushell et al. 2017). These transporters are still only poorly known and, therefore, their functional characterisation will give insights into their role for the parasite and into their potential as drug target.

### **I-2-3 Heterologous expression of *Plasmodium* membrane transporters**

*Plasmodium* MTPs have important physiological roles for the parasite but our understanding of the *Plasmodium* membrane proteome is still quite limited: many essential *Plasmodium* MTPs are still waiting to be functionally characterized to understand their role within the parasite's life cycle (and, of course, to assess their suitability for drug targeting). Unfortunately, biochemical characterization of individual transporters in *Plasmodium*-infected erythrocyte cultures or in other "in vivo" *Plasmodium* cultures is always complicated due to the low amount of protein under study, it has nevertheless been successful in a recent study with PfATP4 (Rosling et al. 2018). The production of *Plasmodium* MTPs in heterologous hosts is a valuable tool to assess in detail their functional properties, since it is possible to produce sufficient amount of protein for the desired experimental technique and, in addition, no other proteins from the parasite are present that, presumably, might interfere with the results. Different organisms can be used and the choice depends on the type of protein that will be produced, the resources and experience of the laboratory, and what kind of analysis will be performed with the recombinant MTP. Moreover, one of the difficulties to heterologously produce proteins from *P. falciparum* is that its genome contains a very high proportion of A+T bases (Weber 1987), hardly compatible with commonly used heterologous hosts. Consequently, to overexpress *P. falciparum* proteins it is necessary to use synthetic cDNA, where both the whole sequence and the individual codons are optimised for the chosen expression host.

Different expression systems have been already used to produce *Plasmodium* proteins (reviewed by Birkholtz et al. 2008): *E. coli*, *S. cerevisiae*, *Pichia pastoris*, insect cells, mammalian cells, *X. laevis* oocytes, single-celled amoeba *Dictyostelium discoideum*, *T. gondii* and even cell-free system. Interestingly, the most popular expression systems to

produce and study *Plasmodium* MTPs are the *X. laevis* oocytes and yeast (K Kirk et al. 2005). Using *Xenopus* oocytes has been the method of choice for characterizing *Plasmodium* MTPs, particularly because the oocytes appear to be more tolerant than other eukaryotic cells to the peculiar codon preferences of *Plasmodium* genes (Penny et al. 1998). The oocyte system has been shown to provide a useful method for the characterisation of several *Plasmodium* MTPs (Natalie Jane Spillman and Kirk 2015) like the Equilibrative Nucleoside Transporters 1 and 4, PfENT1 and PfENT4 (Frame et al. 2012; Carter et al. 2000; Parker et al. 2000), the Hexose Transporter PfHT (Woodrow, Penny, and Krishna 1999; Woodrow, Burchmore, and Krishna 2000), the *Plasmodium* aquaglyceroporin PfaQP (Hansen et al. 2001), the *Plasmodium* Ca<sup>2+</sup>/H<sup>+</sup> exchanger PfCHA (Rotmann et al. 2010), PfMDR1 (Sanchez et al. 2008), the *Plasmodium* Folate Transporters 1 and 2, PfFT1 and PfFT2 (Salcedo-Sora et al. 2011), the *Plasmodium* inorganic phosphate transporter PfPiT (Saliba et al. 2006), PfCRT (Martin et al. 2009) and the *Plasmodium* Formate-Nitrite Transporter PffNT (Marchetti et al. 2015). Functional characterization of PfATP6 expressed in oocytes has also recently provided further evidence that artemisinin is not interacting with PfATP6 (David-Bosne et al. 2016). Notably, recent expression of PfCRT expressed in *E. coli* has provided one of the first evidences that PfCRT is a H<sup>+</sup>-coupled transporter able to transport peptides of different sizes generated after haemoglobin digestion (Juge et al. 2015). The well-known yeast expression hosts *Saccharomyces cerevisiae* and *Pichia pastoris* have also been used to characterise a number of *Plasmodium* MTPs, for instance, the *Plasmodium* Ca<sup>2+</sup>/H<sup>+</sup> exchanger PfCHA (Salcedo-Sora, Ward, and Biagini 2012; Guttery et al. 2013), PfATP6 (Cardi et al. 2010; Arnou et al. 2011), PfCRT (Baro, Pooput, and Roepe 2011), PfMDR1 (Amoah, Lekostaj, and Roepe 2007), PffNT (Wu et al. 2015), or the *P. falciparum* homolog of the tryptophan transporter Tat2p of *S. cerevisiae* (Tindall et al. 2018). We also find recent examples of *Plasmodium* MTP expression using cell-free expression, for example for the *Plasmodium* lactate transporter PffNT (Holm-Bertelsen et al. 2016; Lim et al. 2010).

Finally, it is very important to note here that among all these heterogously expressed transporters, to date, only three were purified and functionally or structurally characterized: PfaQ (Hedfalk et al. 2008), providing the first atomic-resolution 3D structure of a *Plasmodium* membrane protein, PfCRT (Tan et al. 2006b; Juge et al. 2015) and PfATP6 (Cardi et al. 2010; Arnou et al. 2011; David-Bosne et al. 2013).

## I-3 P4-ATPases

### I-3-1 P-type ATPases

#### 1. General information and subfamilies

P-type ATPases are primary MTPs that use the energy of the hydrolysis of ATP to pump their substrates against their concentration gradient. One of their characteristics is that, during the catalytic cycle, they are transiently phosphorylated at a conserved aspartate residue (Palmgren and Nissen 2011).

P-type ATPases are classified within five subfamilies:

P1-ATPases, comprising two groups:

- P1A: represented by the bacterial  $K^+$  transporters.
- P1B: They are “heavy metal” transporters and are present in all organisms. They transport  $Cu^+$ ,  $Ag^+$ ,  $Cu^{2+}$ ,  $Zn^{2+}$ ,  $Co^{2+}$ ,  $Pb^{2+}$ ,  $Cd^{2+}$ .

P2-ATPases, divided into three groups:

- P2A, which includes the sarco (endo)plasmic reticulum  $Ca^{2+}$  ATPases SERCA ( $Ca^{2+}/H^+$ ), the most studied P-type ATPases from functional and structural points of view.
- P2B: PMCA plasma membrane calcium ATPase; calmodulin binding ATPases, they have one  $Ca^{2+}$  binding site.
- P2C: comprising the  $Na^+/K^+$  and the gastric  $H^+/K^+$  ATPases. These P-type ATPases are associated to a  $\beta$  subunit.

P3-ATPases, which include the  $H^+$  pumps found at the plasma membrane of plants and fungi.

P4-ATPases. Members of this subfamily transport phospholipids rather than ions, and they are only found in eukaryotes. As the P2C members, P4-ATPases are also associated to a  $\beta$  subunit.

P5-ATPases. This subfamily has still unknown substrates. There are two subgroups: P5A, whose members are localized in the ER, and P5B which includes transporters found in lysosomes (humans), vacuole (yeast) or plasma membrane (*C. elegans*).

## 2. Structural characteristics:

Different structures of the sarcoplasmic reticulum  $\text{Ca}^{2+}$  ATPase (SERCA) have defined the molecular architecture of this family, providing a deep understanding of the relations between structure and activity during the transport cycle (for review see (Møller et al. 2010)). Structurally, P-type ATPases are organized into three cytoplasmic domains (A, P, and N) and two membrane-embedded domains (T and S) (fig 5). The transported substrates bind in the middle of the T-domain and alternate between being exposed to the cytoplasm and the extracytoplasmic side. The S-domain is an auxiliary domain with high rigidity that provides structural support to the T-domain and can have specialized functions such as providing substrate-coordinating side chains for additional substrate binding sites (Toyoshima and Nomura 2002). P-type ATPases also have a large cytoplasmic part composed of three domains, named P, N and A. (fig 5). The phosphorylation domain (P domain) contains the conserved sequence DKTG where the initial aspartate is transiently phosphorylated during the transport cycle. In this P domain we also find two other conserved motifs: the TGDN and the GDGXND that are involved in the coordination of the  $\text{Mg}^{2+}$  associated to the bound ATP in the N domain. The nucleotide-binding domain (N domain) binds ATP and allows the phosphorylation of the P domain. The N domain is inserted in the P domain and it is the most variable part of P-type ATPases. The actuator domain (A domain) is constituted by the loop between TMs 2 and 3 and a region in the N-terminal of the protein. The A domain contains the TGES motif conserved among all P-type ATPases, and implicated in the dephosphorylation of the aspartate of the P domain. This domain is flexible and acts as a “phosphatase”. Several P-type ATPases contain also a regulation domain (R domain) (Ekberg et al. 2010), located at the C-terminal, the N-terminal or both extremities of the pump. This R domain can act as an auto-inhibitory element by interacting with a still unknown region of the pump (Azouaoui et al. 2017; Zhou, Sebastian, and Graham 2013a).



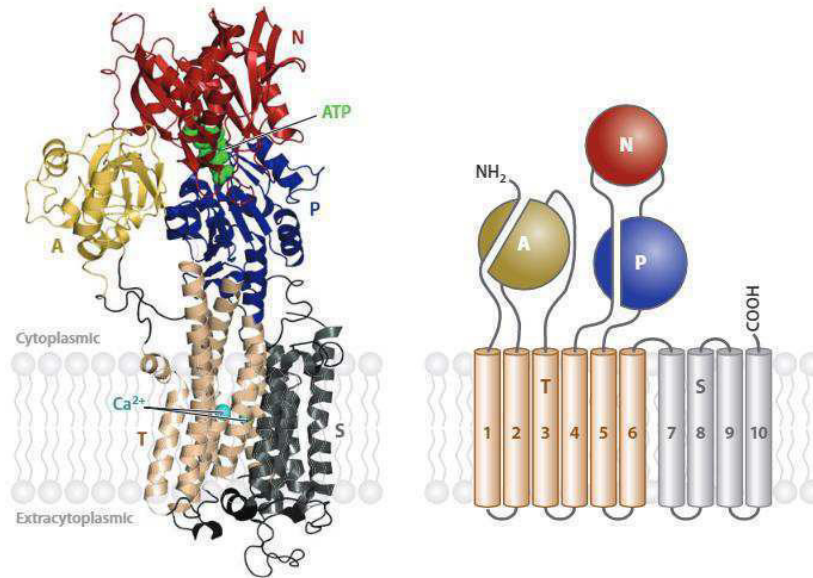


**Figure 5: Schematic overview of a P-Type ATPase: the example of SERCA1a.**

*Schematic overview of the structural organization of P-type ATPases. Left: Ribbon model of the crystal structure of the sarco(endo)plasmic reticulum  $\text{Ca}^{2+}$  ATPase SERCA1a with its two types of ligand bound: one ATP and two  $\text{Ca}^{2+}$  (PDB Accession number 1T5S). Right: Structural organization of P-type ATPase domains. The domains described in the text are indicated with capital letters (A, N, P, T, S). From reference (Palmgren and Nissen 2011).*

Some P-type ATPases possess associated subunits needed during biogenesis, trafficking or function (Kühlbrandt 2004; Palmgren and Nissen 2011). For example, the renal  $\text{Na}^+/\text{K}^+$  ATPase has an integral membrane protein  $\beta$ -subunit with only one TM and a large cytoplasmic domain. It is suggested that this  $\beta$ -subunit is required for targeting the complex to the final membrane destination during biogenesis, and also it has shown that it can modulate the affinity of the pump for the  $\text{K}^+$  substrate (Geering 2001). In some cells, the  $\text{Na}^+/\text{K}^+$  ATPase and its  $\beta$ -subunit can interact with a  $\gamma$ -subunit, a peptide from the FXYD family, also containing one TM (Geering et al. 2003). Similarly, in the muscle, SERCA1a is regulated by sarcolipin (Montigny, Decottignies, et al. 2014; Barbot et al. 2016), a small peptide. Likewise, in the heart, SERCA2a can be regulated by phospholamban, a 52-amino acid transmembrane peptide (MacLennan, Asahi, and Tupling 2003).

### 3. Catalytic cycle of P-Type ATPases

As commented earlier, different atomic-resolution 3D structures of SERCA have provided a framework of different structural conformers of the protein along the

catalytic cycle. This information, together with a remarkable amount of functional and computational data, has permitted a good understanding of the catalytic cycle of this pump in particular and, of P-type ATPases in general (Møller et al. 2010).

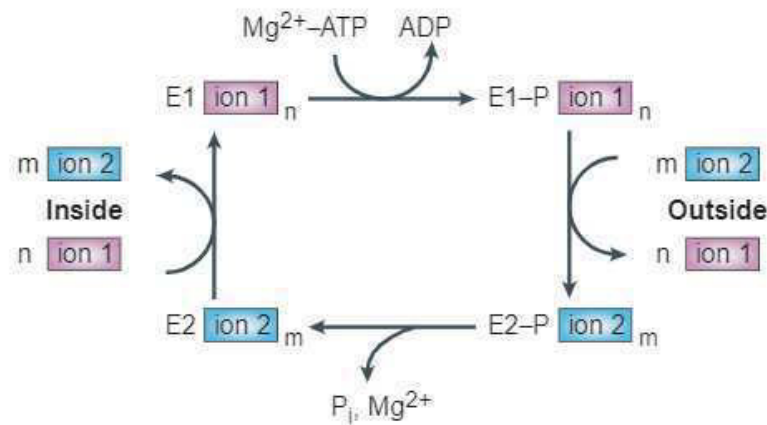


**Figure 6: Scheme of the catalytic cycle of P-type ATPases** (Kühlbrandt 2004).

*Ion 1 (inside the cell) binds to a high-affinity site in the E1 conformation of the ATPase. Ion binding leads to phosphorylation of the enzyme by  $Mg^{2+}$ -ATP, leading to the phosphorylated E1-P conformation. Transition to the phosphorylated E2-P conformation leads to a reduced affinity for ion 1, which is released outside of the cell. Ion 2 then binds (from outside) and the enzyme dephosphorylates, releasing ion 2 inside the cell. Another ion 1 will subsequently start another cycle.  $n$  and  $m$  are the numbers of ions transported (between 1 and 3).  $P_i$ : inorganic phosphate.*

Taking as example an ion exchanger pump like the  $Na^+/K^+$  P-type ATPase (Kühlbrandt 2004), the transport cycle begins when ion 1 binds the high-affinity fixation site of the pump through a channel open towards the cytoplasmic side and replaces the ion 2 that has been transported from the other side of the membrane and now is released into the cytoplasmic side. The protein is thus in the E1 conformation. The ion 1 induces a rearrangement of the P domain, which brings a  $Mg^{2+}$  binding-site close to the conserved aspartate of this domain, which is then phosphorylated by the ATP previously bound in the N domain. This leads to the E1-P conformation that releases ADP. This conformation is a “high energy” conformation and, therefore, the addition of ADP will lead to the inverse reaction and the formation of ATP. In the E1-P conformation, the ion 1 has no longer access to the cytoplasm. At this moment, there is a spontaneous transition from the E1-P conformation to the E2-P conformation (or “low energy” conformation). This transition brings the TGES sequence of the A domain close to the phosphorylated aspartate and opens the channel to the extracellular side. In SERCA, this transition is the

rate-limiting step of the transport cycle. Then, ion 1 is released in the extracellular side of the membrane and ion 2 binds in the same binding site, since now this site has evolved to a high-affinity fixation site for ion 2. Upon ion 2 binding, the channel gets occluded from the extracellular side, and the P domain changes conformation and gets dephosphorylated, resulting into the dephosphorylated E2 conformation. Finally, domain A moves away from P domain and the protein goes back to the E1 conformation.

## I-3-2 P4-ATPases

### 1. Overview of the P4-ATPases

P4 ATPases (also known as flippases) constitute a particular subfamily of the P-type ATPase family and are present only in eukaryotic organisms. Unlike the rest of P-type ATPase members that pump ions, P4-ATPases mediate the translocation of phospholipids from the exoplasmic to the cytoplasmic leaflet of biological membranes (fig 7) (López-Marqués, Holthuis, and Pomorski 2011). This process enables eukaryotic cells to create and maintain non-random lipid distribution between the two leaflets of the membrane. They mostly transport PS, PE, PC and lysophospholipids, although recently they were shown to transport glycosphingolipids (Roland et al. 2018).

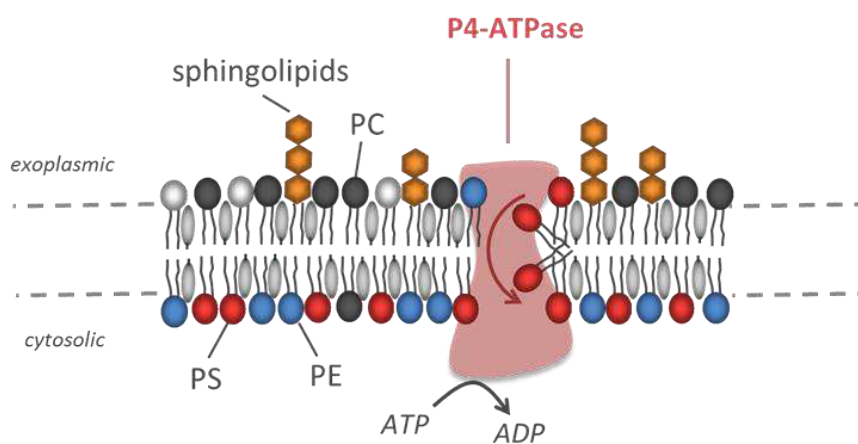


**Figure 7: Schematic flipping of a phospholipid by a P4-ATPase.**

*The P4-ATPases drive the active transport of phospholipids from the external leaflet to the internal leaflet of the membrane.*

The activity of P4-ATPases has a direct relation with important cellular functions. For instance, the imbalance in phospholipid number between the two leaflets determines the curvature of the phospholipid bilayer inducing membrane invagination, thus facilitating endocytic or secretory vesicle budding, a key step for protein trafficking and membrane biogenesis. In addition, they play an important role in cell signaling, since the

exposition of PE in the external leaflet of the cell is a signal that triggers apoptosis and blood clotting. In plants, the transport of lysophospholipids mediated by P4-ATPases is suggested to have an important role in cell signaling (Lisbeth R. Poulsen et al. 2015). In addition, P4-ATPases are also implicated in cell polarity and migration both, in yeast (Koji Saito et al. 2007) and in humans (Kato et al. 2013). Also, P4-ATPases are implicated in the virulence of pathogens as *Cryptococcus* (Huang et al. 2016; Shor et al. 2016), and they mediate the transport of drugs in the *Leishmania* parasite (Pérez-Victoria et al. 2003). In humans, mutations in certain P4-ATPases may lead to intrahepatic cholestasis e.g. mutations in ATP8B1 (van der Mark, Oude Elferink, and Paulusma 2013).

P4-ATPases are predicted to have 10 TMs and they are associated to a  $\beta$  subunit from the CDC50/LEM family (fig 8). The subunits possess two TMs with a large exoplasmic loop containing 4 conserved cysteines that form two intramolecular disulfide bridges. In addition, this extracellular domain is glycosylated, which is important during biogenesis and for the interaction with the P4-ATPase (Jonathan A Coleman and Molday 2011). Cdc50 proteins are able to interact with more than one type of P4 ATPase: for example the *S. cerevisiae* Cdc50 protein Lem3p can interact with two P4-ATPases, Dnf1 and Dnf2 (Koji Saito 2004; Furuta et al. 2007). Moreover, different studies have revealed the crucial role of Cdc50 for proper protein folding and membrane localization of the P4-ATPase/Cdc50 functional complex (Van Der Velden et al. 2010; López-Marqués et al. 2010; S. Chen et al. 2006). There are few exceptions of P4-ATPases that do not have a Cdc50-associated subunit; among them, Neo1p in *S. cerevisiae* or the human ATP9A and ATP9B (López-Marqués, Holthuis, and Pomorski 2011; van der Mark, Oude Elferink, and Paulusma 2013).

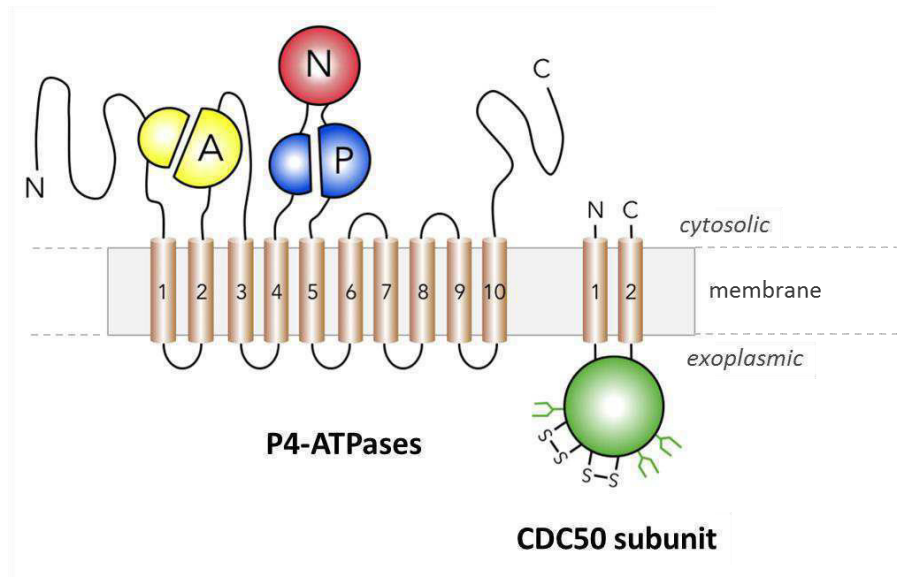


**Figure 8: Predicted topology of P4-ATPases and CDC50 subunits.**

*P4-ATPases possess 10 TMs and 3 cytoplasmic domains as in most P-Type ATPases. The associated CDC50 subunit possess 2 TMs and a large exoplasmic loop with two disulfide bridges and potential glycosylation sites.*

## 2. Regulation of the P4-ATPases

As mentioned earlier, P-type ATPases are highly regulated through different mechanisms. Drs2p, the *S. cerevisiae* P4-ATPase requires the presence of PI4P for its activation (Jacquot et al. 2012), possibly upon interaction in the RMKKQR motif located at the C-terminal end (Natarajan et al. 2009). In addition, both the N- and the C-terminal ends of Drs2p exert an autoinhibitory effect on enzyme's activity (Azouaoui et al. 2017). Moreover, the C-terminal end of Drs2p has a potential binding site for Gea2p, a protein known to regulate Drs2p activity during the formation of clathrin vesicles. Other *S. cerevisiae* P4-ATPases, Dnf1p and Dnf2p, contain the phosphorylation site RXSLD, recognized by the Fpk1p kinase. The Fpk1p kinase is activated in response to the sphingophospholipids composition in membranes. Finally, the activity of the human flippases ATP11A and ATP11C seem to be down-regulated by exposure to calcium (Segawa et al., 2016).

## 3. Transport mechanism of P4-ATPases: two different models.

It is likely that all P-type ATPases share the main conformational changes along the transport cycle despite having differences on their primary sequence and on their substrates. In this view, the catalytic cycle of P4-ATPases should be similar to the one

described for SERCA. There are experimental evidences showing similar functional characteristics between P2 and P4-ATPases. For instance, a similar transient auto-phosphorylation step (as studied using  $[\gamma\text{-}^{32}\text{P}]\text{ATP}$ ), similar requirement for  $\text{Mg}^{2+}$  and similar sensitivity to inhibitors that mimic the phosphate group (Montigny et al. 2016). In P4-ATPases, phospholipids are transported from the extracellular (or luminal) side to the cytoplasmic side of the membrane, therefore it is the phospholipid substrate who induces the dephosphorylation of the enzyme (E2-P to E2 transition, see fig 6). However, since P4-ATPases do not require any other species to activate phosphorylation, it is generally thought that the phospholipid substrate is the only species transported.

Accepting the above similarities between the catalytic cycles of P2 and P4 ATPases, the main difference between them is the nature of transported substrate, cations for P2 and phospholipids for P4. In the absence of a high-resolution 3D structure of a P4-ATPase, two putative transport models have been proposed for P4-ATPases: the two-gates model, in which the phospholipid is transported through the interior of the transporter and the hydrophobic gate model where the phospholipid travels at the protein-membrane interface (fig 9) (Lopez-Marques et al. 2014; Montigny et al. 2016).

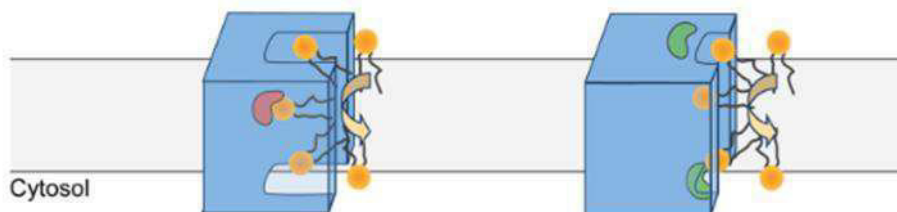


**Figure 9: Scheme of the proposed pathways for phospholipid transport.**

*On the left: the two gates model with the phospholipid going through the transporters itself during translocation. On the right, the hydrophobic gate model, in with the fatty acid chains of the phospholipid substrate remain in the membrane during translocation. (Lopez-Marques et al. 2014).*

In the two-gates model, (Baldrige and Graham 2013) the phospholipid molecule is first recognized in the exoplasmic leaflet of the membrane by residues forming a so-called “entry gate” that drives the phospholipid to a protein groove delineated by TMs 1, 3 and 4. After translocation, the phospholipid will be delivered to the membrane’s cytosolic leaflet through a new “exit gate”. In this model, the phospholipid molecule is

completely surrounded by the protein during translocation (fig 9, left). The second model: the hydrophobic gate model is formulated based on homology modelling between P2 and P4 ATPases, which revealed the presence of a large groove formed by TMs 1, 2, 4, and 6, forming a network of hydrophobic residues around I364 (TM4) (Vestergaard et al. 2014). These residues form the so-called 'hydrophobic gate'. Thus, the up and down movements of TM4 during the catalytic cycle would move the hydrophobic gate from one leaflet to the other leaflet of the membrane, and along this groove, there will be water filled pockets where the phospholipid head group would bind. In this way, the fatty acid chains of the phospholipid substrate would always remain in the membrane during translocation (fig 9, right).

### **I-3-3 P4-ATPases and Cdc50 proteins in *Plasmodium* parasites**

The genome of *P. falciparum* contains approximately 140 MTPs (Martin, Ginsburg, and Kirk 2009) and among them, 13 P-type ATPases. 5 out of these 13 P-type ATPases have been classified as P4 ATPases: ATP2 (PF3D7\_1219600), ATP7 (PF3D7\_0319000) and ATP8 (PF3D7\_1223400), as well as two combined transporters GC $\alpha$  (PF3D7\_1138400) and GC $\beta$  (PF3D7\_1360500), which contain a P4-ATPase fused to a guanylyl cyclase. Note that the first reports on *Plasmodium* P4-ATPases appeared in the mid-1990s where the *P. falciparum* ATP2 (PfATP2) was first identified as a P-type ATPase based on sequence analysis and similarity with Drs2p, the *S. cerevisiae* P4-ATPase (Trottein and Cowman 1995; Krishna et al. 1994). But at the time of those studies both PfATP2 and Drs2p were thought to be Ca<sup>2+</sup>ATPases. Several years later, in 2003, Pasini and co-workers (Pasini et al. 2013) showed that the ortholog gene encoding for ATP2 in *P. berghei* was refractory to gene deletion and thus considered as essential during the blood stage. In agreement with this and using gene-deletion tools in murine malaria models and in *P. falciparum* cultures, three recent publications have confirmed the essentiality of ATP2 for *Plasmodium* (Kenthirapalan et al. 2016; Bushell et al. 2017; M. Zhang et al. 2018). As for the other P4-ATPases, the results are not clear; Kooij and colleagues (Kenthirapalan et al., 2016) found that ATP7, ATP8 and GC $\alpha$  are all essential for the parasite; while Bushell and collaborators (Bushell et al., 2017) reported that ATP7 is dispensable whereas knocking down ATP8, GC $\alpha$  and GC $\beta$  lead only to a growth defect of the parasite (fig 10, panel A). Interestingly, a phylogenetic analysis showed that ATP2 and ATP8 are very well conserved not only in the *Apicomplexa* phylum, but also they seem to have

orthologs in men, whereas ATP7 is largely apicomplexan-specific (Weiner and Kooij 2016). An *in situ* fluorescent tagging of intra-erythrocytic parasites revealed that ATP2 and ATP8 are localized at the parasite–host interface, and ATP7 and GC $\alpha$  in intra-parasitic structures and surrounding membranes (fig 10, panel B) (Kenthirapalan et al. 2016).

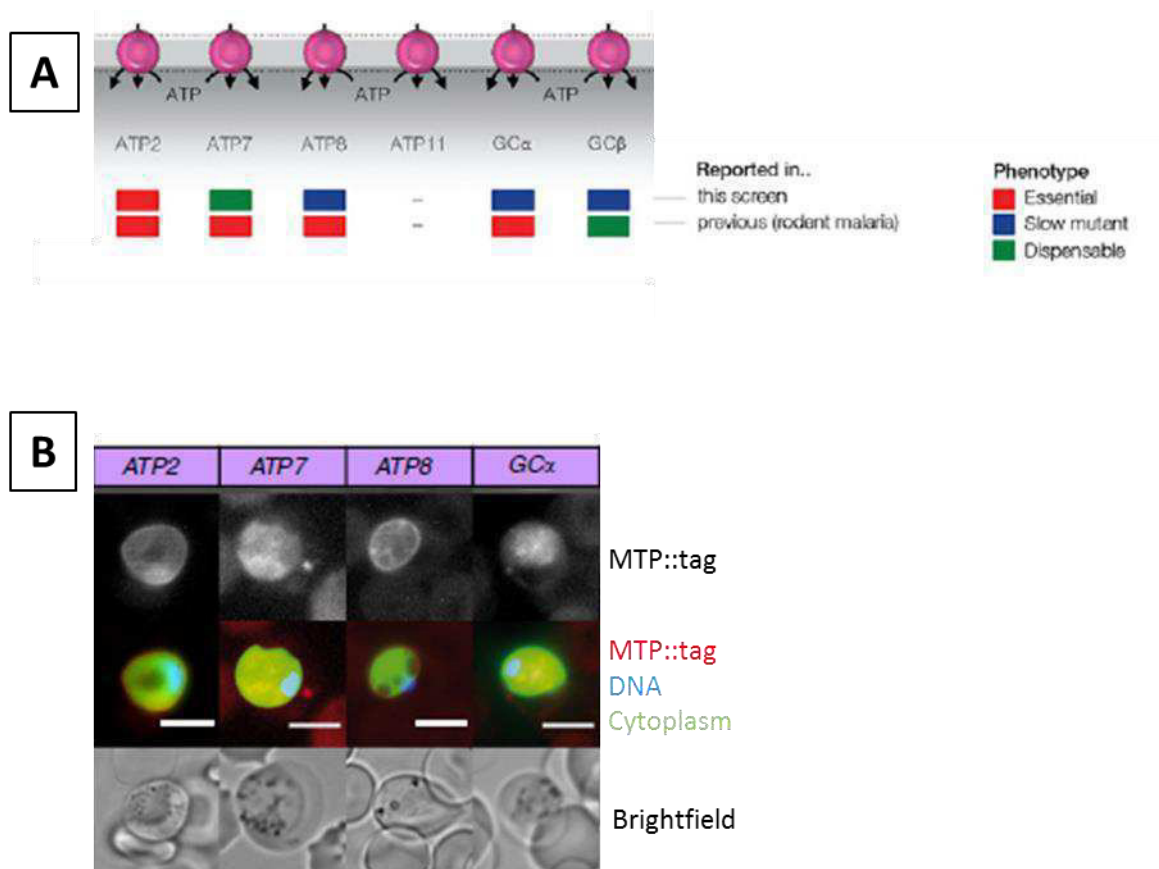


**Figure 10: Knockout phenotypes and localisation of putative P4-ATPases of *P. berghei*.**

Panel A: Knockout phenotypes of putative *P. berghei* P4-ATPases. Modified from (Bushell et al. 2017) The phenotypes are from this study (top) and from published *P. berghei* studies (bottom). Dispensable, slow, and essential phenotypes are indicated by coloured boxes. ATP11 from *P. falciparum* has no homolog in the *P. berghei* genome. Panel B: Endogenous fluorescent tagging of four putative P4-ATPases refractory to gene deletion in the erythrocyte stage. Red: endogenous tagged MTP; Blue: DNA; Green: cytoplasm. scale bars 5 $\mu$ m modified from (Kenthirapalan et al. 2016).

At the moment *Plasmodium* P4-ATPases, including ATP2, have no functional annotation and they are still considered as putative transporters. Besides their importance for the parasite, ATP2 has brought further attention from a therapeutic perspective. A recent study has shown that amplification events of the gene encoding ATP2 were induced after culturing the parasite with two antimalarial drugs present in the “malaria box”



(Cowell et al. 2018; Spangenberg et al. 2013) strongly suggesting that ATP2 can be the target of these two compounds.

With respect to Cdc50 proteins encoded by malaria parasites, in this thesis we have found that the genome of *P. falciparum* contains 3 putative CDC50/Lem3 family members, well conserved as well among the *Apicomplexa* phylum. From our knowledge, there is not a single publication focusing on these putative proteins and, therefore, there is no information about their functional role and possible association with a *Plasmodium* P4-ATPase. Notably, a recent study using saturation mutagenesis has revealed that all three putative CDC50/Lem3 proteins are also essential for *P. falciparum* during intre-erythrocytic stage (M. Zhang et al. 2018).

## I-4 Project

Although genetic studies have revealed the importance of *Plasmodium*-encoded P4-ATPases during malaria infection, particularly ATP2, none of these proteins has been functionally characterized and therefore, there is no information linking their activity with their important biological role for the parasite's survival. Indeed, many important processes during the complex life cycle of the parasite can be imagined to include the participation of P4-ATPases. For instance, during the intracellular stages of *Plasmodium*, the dynamic and transit of phospholipids is fundamental in order to build intracellular organelles and to remodel the host's membrane. In addition, lipidomic analyses of different intraerythrocytic stages of *P. falciparum* have revealed continuous changes in membrane's lipid composition during parasite's maturation (Tran et al. 2016). *Plasmodium* parasites have a limited capacity of synthesizing fatty acids, the precursors of phospholipids; consequently the majority of lipids are obtained from the host cell membrane or from the serum. Therefore, the malaria parasite must have strong mechanisms to maintain and modify the lipid composition of the different membrane compartments and, eventually, phospholipid transporters like P4-ATPases can play important roles.

To advance in the knowledge of these putative and yet important transporters during the malaria parasite life cycle, in this thesis we undertook the challenge to clone these *Plasmodium* P4-ATPases and express them in the yeast *S. cerevisiae* with the long-term goal to study the function and the structure of these putative lipid flippases. In addition,

we also aimed at investigating the possible association of these transporters with a Cdc50 partner and therefore we also conducted the co-expression of *Plasmodium* P4-ATPases with the different Cdc50 proteins encoded by *Plasmodium*. As discussed before, the production and purification of recombinant protein is a powerful tool to study in detail the functional properties of orphan proteins and, ultimately, its 3D atomic structure. In our project, two different options were considered before starting: (1) study the three main putative flippases ATP2, ATP7 and ATP8 from *P. falciparum*, or (2) focus on only one, ATP2, together with other well-conserved ATP2 orthologs from other *Plasmodium* species. In this thesis we have chosen the option (2): to work only with ATP2 and orthologs. This choice was initially made on the basis of the amino acid identity with the well-characterized P4-ATPase of *S. cerevisiae*, Drs2p, and, also, on the basis of the high sequence identity between *Plasmodium* ATP2 orthologs (about 60%). Remarkably, during the initial months on this thesis, different publications appeared demonstrating by genetic manipulation tools that ATP2 is indeed the only P4-ATPase essential for the parasite (Kenthirapalan et al. 2016; Bushell et al. 2017; Cowell et al. 2018; M. Zhang et al. 2018).

## II.Objectives

---

As ATP2 is an essential protein for the parasite survival, understanding what is its role within the parasite and in which transport process actually ATP2 intervenes is desirable. In order to understand the precise role of ATP2 within the cell, it is important to have knowledge on the functional and structural properties of this transporter. And as ATP2 is a putative P4-ATPase, it is important to first check:

- If ATP2 is actually a lipid flippase, as predicted.
- If it can associate to one or several putative Cdc50 subunits.
- What is (are) the physiological substrate(s) transported?

To try to address these questions we undertook the cloning of ATP2 and Cdc50 subunits and their co-express in the yeast *S. cerevisiae*.

## III. Results and discussion

---

This project has aimed to initiate the biochemical characterization of P4-ATPases or lipid flippases encoded by the malaria parasites of the genus *Plasmodium*. As mentioned in the introduction, none of these transporters has been functionally characterized to this day and therefore, they still remain putative transporters. Despite this, genetic studies in *Plasmodium* have revealed the importance of these P4-ATPases for the survival of the parasite as well as their potential importance as drug targets. This thesis has therefore focused on the expression in yeast of one of these putative *Plasmodium*-encoded flippases, ATP2, in complex with its putative associated Cdc50 subunits. We describe here our strategies and results for protein co-expression, solubilisation by detergent and purification, and the first trials for its functional characterization.

### III-1 Analysis of ATP2 and Cdc50 sequences present in the genome of *Plasmodium* species

As mentioned in the introduction, P4-ATPases are implicated in important physiological processes in many organisms, including yeast, plants or humans (Lopez-Marques et al. 2014). Many different studies have identified conserved residues and protein motifs within P4-ATPases sequence with important roles in phospholipid transport and/or P-type ATPase activity (J. A. Coleman et al. 2012; Perandr es-L opez et al. 2018; Gantzel et al. 2017; Montigny et al. 2016). The purpose of this section is to identify these essential residues and motifs in *Plasmodium* ATP2 orthologs and in other homologs encoded by parasites of the Apicomplexa phylum in order to analyse the degree of conservation among them.

The alignment of ATP2 orthologs from *P. falciparum* (PF3D7\_1219600), *P. vivax* (PVX\_123625) and the malaria mouse models, *P. berghei* (PBANKA\_1434800) and *P. chabaudi* (PCHAS\_1436800) (fig 11), indicates a high conservation of this transporter among *Plasmodium* species, as judged by an average of 60 % amino acid identity between all of them. This degree of conservation might reflect the fact that ATP2 is an essential protein in several species of *Plasmodium* (Cowell et al. 2018; Bushell et al. 2017; M. Zhang et al. 2018). Importantly, well-conserved P4-ATPases homologous to

ATP2 are also present in other disease-causing parasites belonging, like *Plasmodium*, to the Apicomplexa phylum: the *Toxoplasma gondii* (TGME49\_247690), the *Cryptosporidium parvum* (cgd7\_1760) or the *Babesia microti* (BMR1\_01G011915) P4-ATPases (fig 11). All these Apicomplexan P4-ATPases are still putative and uncharacterized like the *Plasmodium* P4-ATPases. Their conservation among these Apicomplexan parasites might support the idea that these proteins perform important functional roles during the intracellular life-cycle of these parasites.

As expected, all the sequences contain the typical P-type ATPase motifs, like the DGET motif in the A domain (intracellular loop between TMs 2 and 3), containing a key glutamate involved in the dephosphorylation of the enzyme (fig 11, panel A), or the DKTGT motif in the P domain (intracellular loop between TMs 4 and 5), where the initial aspartate is transiently phosphorylated during the transport cycle (fig 11, panel B).

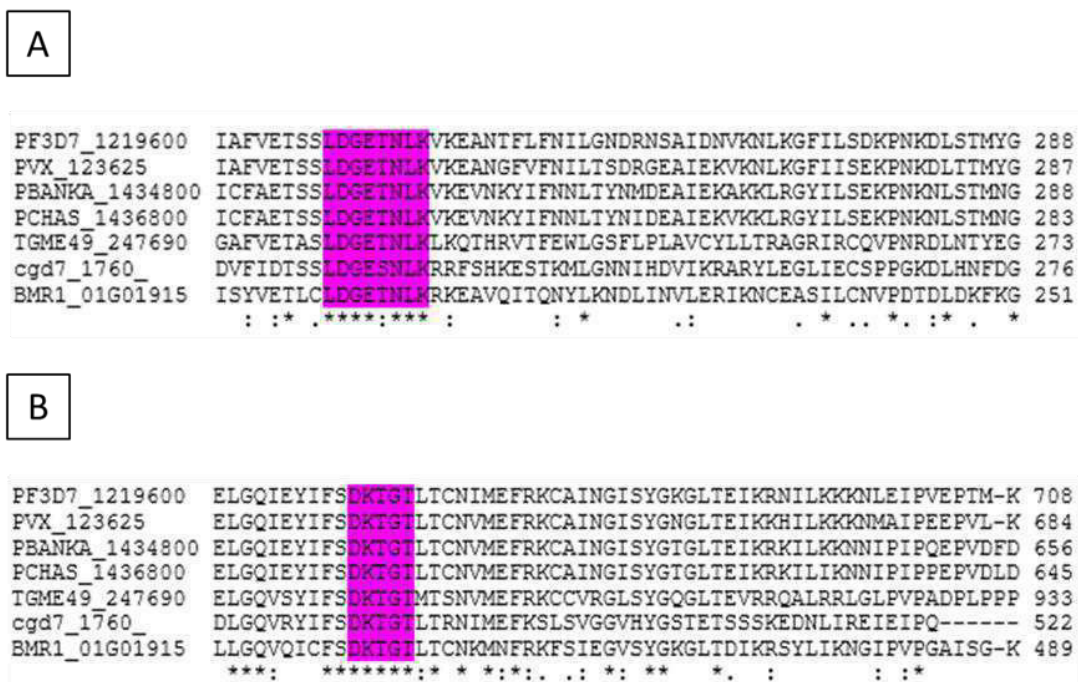


**Figure 11: Conservation of P-type ATPase consensus motifs in ATP2 homologs encoded by apicomplexan parasites.**

Multiple alignment of ATP2 homologs of *Plasmodium* and Apicomplexan parasites. Panel A: Detail of the A domain (the intracellular loop between TMs 2 and 3) of P4-ATPases. The highlighted consensus DGET sequence found here (TGES instead of DGET in most other P-type ATPases) contains the conserved glutamate involved in dephosphorylation. Panel B: Detail of the P domain (intracellular loop between TMs 4 and 5). The highlighted DKTGT sequence found here contains the aspartate transiently phosphorylated. The alignments were performed with the multiple sequence alignment CLUSTALW resource (Thompson, Higgins, and Gibson 1994) for the following proteins: *P. falciparum* PF3D7\_1219600; *P. vivax* PVX\_123625; *P. berghei* PBANKA\_1434800; *P. chabaudi* PCHAS\_1436800; *Toxoplasma gondii* TGME49\_247690; *Cryptosporidium parvum* cgd7\_1760; *Babesia microti* BMR1\_01G011915.

The length of the N-terminal tail of P4-ATPases, and of P-type ATPases in general, is quite variable. In this region preceding TM1, we find several conserved residues, the replacement of which in the *Leishmania* P4-ATPase miltefosine transporter, results in a decrease of translocation activity (fig 12, panel A). These residues are suggested to be implicated in the stability of the protein and in the conformational transition and hydrolysis of the phosphorylated state of the protein (Perandr s-L pez et al. 2018).

Interestingly, other conserved motifs and essential amino acids conserved in P4-ATPases are also present in these Apicomplexan sequences. We found important conserved residues known in other P4-ATPases to be implicated in substrate recognition and binding affinity. This is the case of a conserved isoleucine in TM1 (fig 12, panel A) that corresponds to L127 in the human flippase, hATP8B1; the congenital mutation L127P found in this transporter causes progressive familial intrahepatic cholestasis type 1 (PFIC1) (Klomp et al. 2004). The homologous replacement by proline of I91, the homologous residue of L127 of the bovine flippase bATP8A2, leads to a lower expression of the protein and a decrease of the maximal rate of ATP hydrolysis (or  $V_{max}$ ) in the presence of the phospholipid substrates PS and PE (Gantzel et al. 2017). Moreover, a conserved isoleucine in TM3 is also present in these putative P4-ATPases (fig 12, panel B). The congenital mutation of the corresponding residue in hATP8B1, I344F, is responsible of a pathology called benign recurrent intrahepatic cholestasis type 1 (BRIC1) (Klomp et al. 2004). Mutation of the homologous residue in bATP8A2, L308, to a phenylalanine leads to a reduced affinity for PS and PE, although does not impair protein expression (Gantzel et al. 2017). These Apicomplexan P4-ATPases also contain the highly conserved PICL (or PISL) motif in TM4, a region suggested to have an essential role in substrate recognition and translocation in P4-ATPases (fig 12, panel B). Indeed, residues I364 in bATP8A2 and I508 in Drs2p of this conserved motif are involved in substrate recognition and selectivity (Montigny et al. 2016). In the sarco/endoplasmic reticulum  $Ca^{2+}$ ATPase (SERCA), the isoleucine in this PICL motif is always a glutamate that coordinates a  $Ca^{2+}$  ion in the so-called second binding site of the protein (Olesen et al. 2007).



The FYKN motif in TM5 present in these Apicomplexan sequences is also well conserved in P4-ATPases. Indeed, mutations of the lysine residue of this motif in bATP8A2 (K873) result in a reduction in the dephosphorylation rate of the enzyme and a reduced affinity for PS (J. A. Coleman et al. 2012). The same study with bATP8A2 has suggested that the conserved FE residues in the extracellular loop between TMs 5 and 6 (fig 13) participate in substrate selectivity, probably because they are located in the hypothetical entry gate of the lipid substrate. Finally, a conserved asparagine found in TM6 (fig 13) is also present in SERCA and participates in the coordination of Ca<sup>2+</sup> in the second binding site. Its functional involvement in P4-ATPases has not studied yet (Montigny et al. 2016).

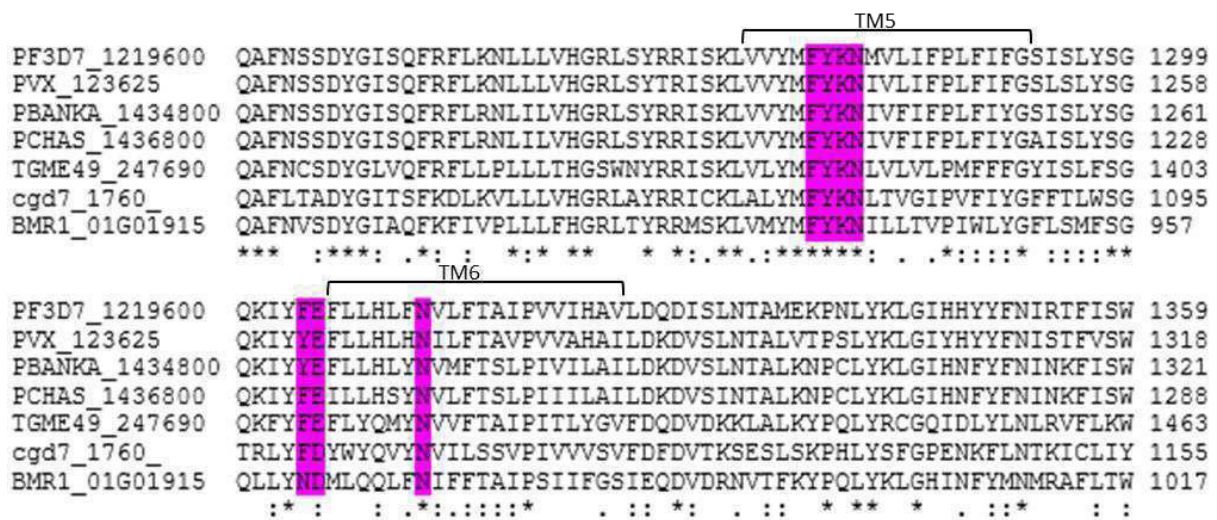


**Figure 13: Detail of the multiple alignments of ATP2 homologs of *Plasmodium* and apicomplexan parasites.**

Residues highlighted in pink are involved in the recognition and affinity for the phospholipid substrate in other P4-ATPases. The FYKN motif in TM5 (J. A. Coleman et al. 2012), the FE residues before the TM6 and the conserved asparagine in the TM6 (Montigny et al. 2016). Alignments were performed using the multiple sequence alignment resource CLUSTALW (Thompson, Higgins, and Gibson 1994) for *P. falciparum* PF3D7\_1219600; *P. vivax* PVX\_123625; *P. berghei* PBANKA\_1434800; *P. chabaudi* PCHAS\_1436800; *Toxoplasma gondii* TGME49\_247690; *Cryptosporidium parvum* cgd7\_1760; *Babesia microti* BMR1\_01G01915.

After a BLAST search, we found in the genome of *P. falciparum* three putative Cdc50 (or LEM) proteins. As for *P. falciparum* ATP2, we also found well-conserved orthologs of these putative Cdc50 proteins in other *Plasmodium* species such as *P. vivax* and the mouse malaria parasites, *P. berghei* and *P. chabaudi*. The amino acid identity between them is about 50 to 60 %, indicating a high degree of conservation between *Plasmodium* species, similar to the one for ATP2.





*parvum* (cgd5\_360) and *Babesia microti* (BMR1\_03g01157) (fig 14). The length of the N-terminal here also varies between sequences (fig 14), however all of them possess two predicted TMs. We clearly observed that the four cysteines potentially involved in the two disulfide bridges found in Cdc50 proteins are very well conserved among these sequences (Puts et al. 2012). Previous studies have shown that these potential disulfide bridges are important for association of the Cdc50 protein with the P4-ATPase and for the functional behaviour of the enzyme complex (Puts et al. 2012). Surprisingly, there is no predicted glycosylation sites in these Cdc50.1 sequences, despite the fact that in some organisms, glycosylation of Cdc50 seems to be essential for protein maturation and for heterodimerization with the P4-ATPase partner (Montigny et al. 2016; Jonathan A Coleman and Molday 2011).

Analysis of the alignments of Apicomplexan ATP2 and Cdc50.1 subunits indicated a good degree of conservation of these proteins among the phylum (fig 11, fig 12, fig 13 and fig 14) and as expected, the conserved cysteines in the Cdc50 sequences, known to be important for the stability and the functional activity of these proteins, were very well conserved. Based on these observations we decided to initiate the cloning and heterologous expression in yeast of PfATP2 in complex with the three putative Cdc50 subunits encoded by *P. falciparum*. Since we did not know which one (if any) of the putative Cdc50 proteins would associate with PfATP2, our approach consisted in making different expression vectors containing combinations of PfATP2 and the various PfCdc50 sequences in order to identify the eventual partner of PfATP2 during co-expression. To increase our chances of success, and given the high amino acid identity (~ 60 %) of *Plasmodium* ATP2 orthologs, we also proceeded to the cloning of the ATP2 orthologs from *P. berghei* and *P. chabaudi*, as well as all their predicted Cdc50 orthologs found in each species. Table 2 displays the three flippases and the nine Cdc50 subunits studied in this thesis, with their corresponding accession numbers from PlasmoDB (EuPathDB project), and the nomenclature we used along this thesis.

### **III-2 Expression of ATP2 and potentially associated Cdc50 subunits in *S. cerevisiae***

Our laboratory possesses a long-standing expertise for producing P-type ATPases in the yeast *S. cerevisiae*, for functional characterization and structural determination

(Azouaoui et al. 2014; Jidenko et al. 2006; Marchand et al. 2008). Proteins successfully expressed include the rabbit Ca<sup>2+</sup> ATPase SERCA1a (Lenoir et al. 2002), the Ca<sup>2+</sup> ATPase of *P. falciparum* PfATP6 (Cardi et al. 2010; David-Bosne et al. 2013), and P4-ATPase/Cdc50 complexes, Drs2p/Cdc50p (Azouaoui et al. 2014; Jacquot et al. 2012) from *S. cerevisiae* and ATP8B1/CDC50A from men (still unpublished). Among the multiple advantages of *S. cerevisiae* as heterologous host for membrane protein production (Routledge et al. 2016), it is worth mentioning that this organism is easy to handle and transform with plasmids. In addition, large volumes of *S. cerevisiae* culture can be grown, being more affordable than other eukaryote expression system as mammalian cell lines or insect cells (Lyons et al. 2016).

**Table 2: PlasmoDB accession numbers of ATP2 and Cdc50 proteins encoded by *P. falciparum*, *P. berghei* and *P. chabaudi*.**

	<i>P. falciparum</i>	<i>P. berghei</i>	<i>P. chabaudi</i>
P4-ATPase	PF3D7_1219600 PfATP2	PBANKA_1434800 PbATP2	PCHAS_1436800 PcATP2
Cdc50 subunits	PF3D7_1133300 PfCdc50.1	PBANKA_091510 PbCdc50.1	PCHAS_093090 PcCdc50.1
	PF3D7_1029400 PfCdc50.2	PBANKA_051340 PbCdc50.2	PCHAS_051350 PcCdc50.2
	PF3D7_0719500 PfCdc50.3	PBANKA_061700 PbCdc50.3	PCHAS_061870 PcCdc50.3

The cDNA encoding all ATP2 and Cdc50 variants was synthesized. Each cDNA, designed by Genscript, was optimized to theoretically attain the maximum level of protein expression in *S. cerevisiae* (see the Material and Methods section V-2-2-1). Previous work in our laboratory with PfATP6, the Ca<sup>2+</sup>-ATPase of *P. falciparum* (Cardi et al. 2010; David-Bosne et al. 2013) as well as in other laboratories (H. Zhang, Howard, and Roepe 2002) has concluded that it is mandatory to use cDNA sequences previously optimized to express membrane transport proteins from *Plasmodium* species (particularly from *P. falciparum*) in *S. cerevisiae*. In particular, the A/T-rich genome of *P. falciparum* can lead to premature transcriptional termination (Graber et al. 1999). Three optimized ATP2 cDNA sequences were ordered to Genscript: PfATP2 from *P. falciparum*, PbATP2 from *P.*

*berghei* and PcATP2 from *P. chabaudi* (Table 2). Similarly, the cDNA encoding the three putative Cdc50 subunits from each species were also ordered, giving a total of nine Cdc50 sequences (Table 2).

### III-2-1 Construction of expression plasmid vectors

The vector used in our laboratory for single-expression and co-expression of *Plasmodium* ATP2 and Cdc50 subunits orthologs was the pYeDP60 (described in the material and methods, and originally provided by Denis Pompon (Pompon et al 1996)). The optimized ATP2 cDNA sequences ordered to Genscript were cloned by the company in the pYeDP60 vector with the TEV cleavage site and the Biotin Acceptor Domain (BAD) at the 3' end of each sequence (fig 15, panel A). The optimized Cdc50 cDNA sequences provided by Genscript were originally cloned between the EcoRI and BamHI sites in a pUC57 vector. We therefore subcloned each Cdc50 subunit into the EcoRI/BamHI sites of the pYeDP60 vector, adding a decahistidine tag (His<sub>10</sub>) and the TEV protease cleavage site at the 3' end of each sequence (fig 15, panel B). We also cloned the ATP2 sequences in the pYeDP60 vector with the BAD and the TEV protease cleavage site at the 5' end. The reason of changing the position of the tag was to know whether the presence of this tag at either the N- or the C-terminal end could affect the expression (or even the function) of ATP2. With the *P. falciparum* and *P. chabaudi* sequences, we had no trouble with the different cloning steps. Unfortunately, we were unable to construct the N-terminal tagged version of PbATP2, due to difficulties in replicating in *E. coli* the cDNA encoding this protein (table 3). Even the vector provided by Genscript was difficult to replicate in the *E. coli* strains used regularly for cloning. We changed the *E. coli* strain for DNA amplification from XL1-Blue to EPI400. This new *E. coli* strain has been modified to achieve a low plasmid-DNA replication rate, and it is normally used to amplify potentially toxic plasmids or large plasmids with a high tendency to form secondary structures. Unfortunately, this strategy did not work for us, either. At this point, we chose to stop working with *P. berghei* sequences and focus only on *P. falciparum* and *P. chabaudi* sequences.

Once the single-expression vectors were obtained, we undertook the construction of the different co-expression vectors. The sequences of the Cdc50 subunits in the pYeDP60 vectors were amplified together with the GAL10/Cyc1 promoter, the TEV protease cleavage site, the His<sub>10</sub> tag, and the PGK terminator (fig 15, panel B). This cassette was

then introduced into the corresponding single-expression vectors containing the ATP2 sequence tagged with the BAD at either, the 5' or the 3' terminal end (fig 15 panel C). Table 3 summarizes all the expression vectors constructed for the initial screening of expression.

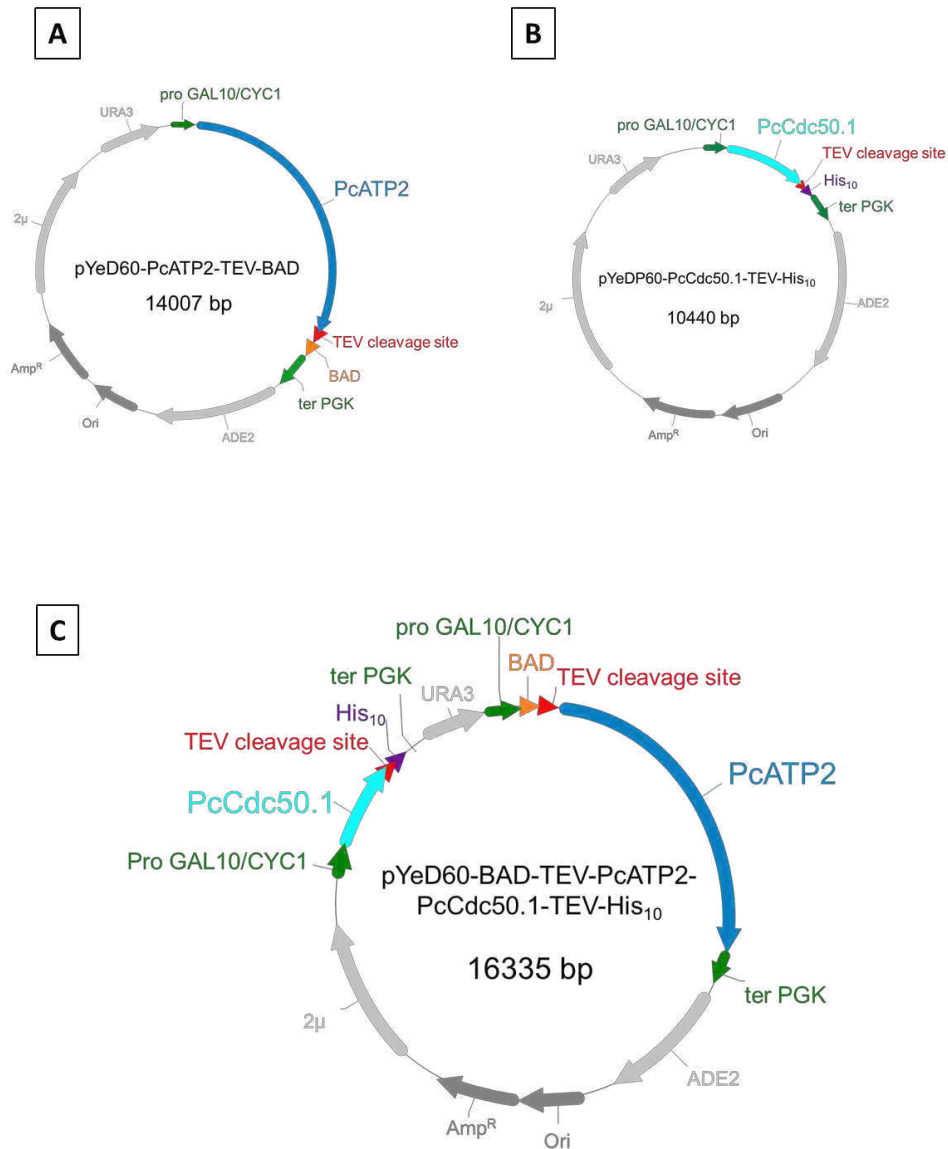


**Figure 15: The different types of plasmid constructs used to express the *Plasmodium* ATP2 orthologs alone or in complex with the Cdc50 subunits in *S. cerevisiae*.**

Panel A: The yeast expression vector encoding *PcATP2* alone, *pYeD60-PcATP2-TEV-BAD*. Panel B: The yeast expression vector encoding the *PcCdc50* subunits *pYeDP60-PcCdc50.1-TEV-His<sub>10</sub>*. Panel C: The yeast co-expression vector *pYeD60-BAD-TEV-PcATP2-PcCdc50.1-TEV-His<sub>10</sub>* encoding both *PcATP2* and *PcCdc50.1*. Replication and selection in *E. coli*: origin of replication, ori; ampicillin-resistance  $\beta$ -lactamase gene, Amp<sup>R</sup>. Replication and selection in the yeast *S. cerevisiae*: origin of replication, 2 $\mu$ ; auxotrophy selection marker for adenine, ADE2; auxotrophy marker for uracil, URA3. Expression: Galactose hybrid promoter GAL10/Cyc1 (*pro GAL10/CYC1*), and terminator PGK (*ter PGK*). ATP2 orthologs are cloned in frame with the sequence of the TEV protease cleavage site followed by a BAD either at the N- or at the C-terminal end of the protein. For the *Cdc50* subunits a TEV protease cleavage site followed by a 10xHis tag is fused at the C-terminal end of the protein.

**Table 3: Summary of the different single and co-expression vectors encoding the ATP2 and Cdc50 orthologs from *Plasmodium*.**

Constructs included in the box with white background were tested for expression. The empty grey boxes are the vectors we never succeed to obtain. For clarity the position of the TEV cleavage site is not written in the table. BAD: Biotin Acceptor Domain; His<sub>10</sub>: 10 x Histidine tag.

	ATP2 single-expression vectors	Cdc50 single-expression vectors	Co-expression vectors
<i>P. falciparum</i>	PfATP2-BAD	PfCdc50.1-His <sub>10</sub>	PfATP2-BAD /PfCdc50.1-His <sub>10</sub>
			BAD-PfATP2 /PfCdc50.1-His <sub>10</sub>
	BAD-PfATP2	PfCdc50.2-His <sub>10</sub>	PfATP2-BAD /PfCdc50.2-His <sub>10</sub>
			BAD-PfATP2 /PfCdc50.2-His <sub>10</sub>
	BAD-PfATP2	PfCdc50.3-His <sub>10</sub>	PfATP2-BAD /PfCdc50.3-His <sub>10</sub>
			BAD-PfATP2 /PfCdc50.3-His <sub>10</sub>
<i>P. berghei</i>	PbATP2-BAD	PbCdc50.1-His <sub>10</sub>	
		PbCdc50.2-His <sub>10</sub>	
		PbCdc50.3-His <sub>10</sub>	
<i>P. chabaudi</i>	PcATP2-BAD	PcCdc50.1-His <sub>10</sub>	PcATP2-BAD /PcCdc50.1-His <sub>10</sub>
			BAD-PcATP2 /PcCdc50.1-His <sub>10</sub>
	BAD-PcATP2	PcCdc50.2-His <sub>10</sub>	PcATP2-BAD /PcCdc50.2-His <sub>10</sub>
			BAD-PcATP2 /PcCdc50.2-His <sub>10</sub>
	BAD-PcATP2	PcCdc50.3-His <sub>10</sub>	PcATP2-BAD /PcCdc50.3-His <sub>10</sub>
			BAD-PcATP2 /PcCdc50.3-His <sub>10</sub>

### III-2-2 Expression tests in small-scale cultures

Once all the expression vectors were verified by DNA sequencing, they were transformed into the *S. cerevisiae* strain W3031b GAL4-2 by the lithium acetate method (see section V-2-2-2)

Transformed *S. cerevisiae* harbouring the vectors encoding the two *Plasmodium* ATP2 orthologs, alone or with one of the three putative Cdc50 subunits were tested in small-scale cultures to first assess protein expression. The cells were grown during 30 h at 28°C, and after dropping the temperature of the culture to 18°C, the expression was induced by the addition of galactose in the medium. After 18 h of induction, the cells were collected and broken. Total membranes were prepared and protein expression in these membranes was analysed by western blot. In parallel, *S. cerevisiae* total membranes, expressing no protein or co-expressing the yeast flippase Drs2p and its corresponding Cdc50 subunit, were used as negative and positive controls, respectively. The two ATP2 orthologs and Drs2p were detected using a biotin probe (avidin coupled to HRP) that recognizes biotinylated proteins; the biotin acceptor domain (BAD) fused to the flippases, at either the N-terminal or the C-terminal end, is actually directly biotinylated by the yeast (Cronan 2005). Cdc50 subunits were detected using the His probe (Ni<sup>2+</sup>-NTA coupled to HRP), that recognizes the His<sub>10</sub> tag fused at the C-terminal end of the protein.

Initial controls are here first described. As seen on figure 16 panel A, a negative control experiment with the biotin probe and total membranes from cells transformed with an empty pYeDP60 vector, shows the different biotinylated proteins of *S. cerevisiae* present in the membrane (fig 16, panel A, lane 1). We observed the following biotinylated proteins: the acetyl-CoA carboxylase (Acc1p, ~250 kDa), the urea carboxylases (Dur 1/2p, ~200 kDa), the pyruvate carboxylase isoforms 1 and 2 (Pyc 1/2p ~130 kDa), and the complex acyl-RNA (Arc 1p ~42 kDa). All of them are membrane-associated proteins. In a positive control experiment using membranes expressing Drs2p (fig 16, panel A, lane 2), the efficiency of the biotin probe to detect BAD fusion proteins was confirmed as previously observed (Jacquot et al. 2012; Jidenko et al. 2006). Figure 16 panel B then shows a similar western blot but now revealed with a His probe to detect His<sub>10</sub> tagged proteins. For the empty vector membrane preparation (fig 16, panel B, lane 1), three non-specific bands were found, at around 100 kDa, 75 kDa and below 50 kDa,

respectively, while our positive control (of membranes expressing Cdc50p) showed in addition a band corresponding to the fully glycosylated Cdc50p subunit, in agreement with previous works (Azouaoui et al. 2014) (fig 16, panel B, lane 2). Thus, the galatose-inducible expression system is working in our hands too.

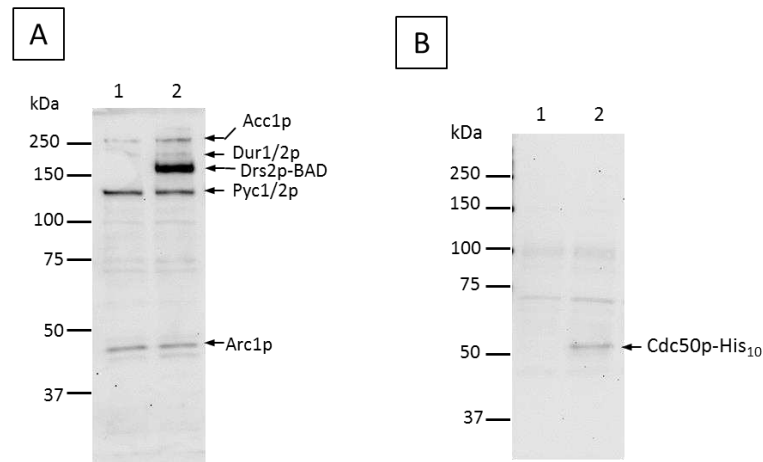


**Figure 16: Western blot analysis of total membrane from *S. cerevisiae* all expressing no protein or co-expressing Drs2p/Cdc50p.**

*Panel A: Western blot revealed with a biotin probe to detected biotinylated proteins. Lane 1, membranes of *S. cerevisiae* transformed with an empty vector (negative control) showing the endogenous biotinylated proteins of *S. cerevisiae*; lane 2: membranes obtained after co-expressing Drs2p-BAD/Cdc50p-His<sub>10</sub> (positive control). Panel B: Western blot revealed with a His probe to detect His<sub>10</sub> tagged proteins. Lane 1 membranes of *S. cerevisiae* transformed with an empty vector showing the background obtained with the His probe; lane 2: membranes obtained after co-expressing Drs2p-BAD/Cdc50p-His<sub>10</sub>. 20µl at 0.04 OD unit of cells, of each membrane sample, were loaded on the gel. Theoretical masses: Acc1p, acetyl-CoA carboxylase ≈250 kDa; Dur 1/2p, urea carboxylase ≈200 kDa; Drs2p-BAD, ≈ 153 kDa; Pyc 1/2p, pyruvate carboxylase isoform 1 and 2 ≈130 kDa; Arc 1p, complex acyl-RNA ≈ 42 kDa; Cdc50p≈ 52kDa (fully glycosylated).*

In the experiments testing PfATP2 expression (fig 17), we were expecting a protein band at about 190 kDa (the expected size of PfATP2 is about 180 kDa and the size of the BAD tag is about 10 kDa). In our experiment, however, we could not detect a band at the expected size, neither after expression of PfATP2 expressed alone (fig 17, lanes 1 and 2), or after its co-expression with any of the three PfCdc50 subunits (fig 17, lanes 3 to 8).



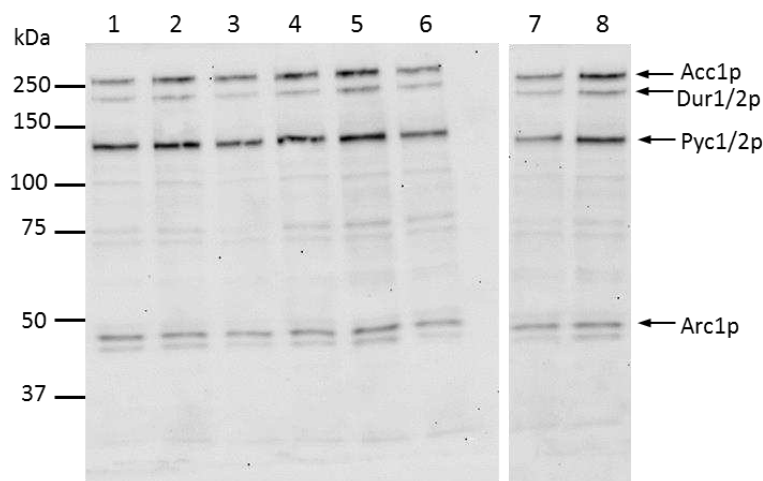


**Figure 17: Expression of *P. falciparum* ATP2, PfATP2 in total membranes obtained from small-scale cultures of *S. cerevisiae*.**

Expression for the various vectors containing the putative flippase PfATP2 labelled at the N- or C-terminal end with the biotin acceptor domain (BAD), and with or without each of the three putative PfCdc50 subunits. The western blots are revealed with a biotin probe to detect the BAD domain fused to PfATP2. 20  $\mu$ l of each membrane sample was loaded in the gel corresponding to 0.04 OD unit of cells. Lane 1: PfATP2-BAD; lane 2: BAD-PfATP2; lane 3: PfATP2-BAD/PfCdc50.1-His<sub>10</sub>; lane 4: BAD-PfATP2/PfCdc50.1-His<sub>10</sub>; lane 5: PfATP2-BAD/PfCdc50.2-His<sub>10</sub>; lane 6: BAD-PfATP2/PfCdc50.2-His<sub>10</sub>; lane 7: PfATP2-BAD/PfCdc50.3-His<sub>10</sub>; lane 8: BAD-PfATP2/PfCdc50.3-His<sub>10</sub>. Theoretical masses: Acc1p, acetyl-CoA carboxylase  $\approx$ 250 kDa; Dur 1/2p, urea carboxylase  $\approx$ 200 kDa; Pyc 1/2p, pyruvate carboxylase isoform 1 and 2  $\approx$ 130 kDa; Arc 1p, complex acyl-RNA  $\approx$  42 kDa; PfATP2-BAD,  $\approx$  190 kDa.

In the same total membrane preparation, we also analysed the expression of the different PfCdc50 subunits. The fig 18 panel A displays the experiments of the three PfCdc50 subunits expression in the absence of PfATP2. The expected sizes for PfCdc50.1, PfCdc50.2 and PfCdc50.3 are about 45 kDa, 60 kDa and 55 kDa, respectively. While no expression was detected for PfCdc50.1 (fig 18, panel A, lane 1), bands corresponding to the expected sizes of PfCdc50.2 and PfCdc50.3 were clearly detected in the blots (fig.18, panel A, lanes 2 and 3). A difference in the intensity of these two bands was observed, indicating a better yield of PfCdc50.2 expression with respect to PfCdc50.3. Co-expressing the three PfCdc50 subunits with PfATP2 tagged with the BAD at either, the N- or the C-terminal end, did not substantially change the pattern of the single expression tests of the three Cdc50 proteins (fig 18, panel B). That is, no expression of PfCdc50.1 was observed, while PfCdc50.2 and PfCdc50.3 expressed in an apparent similar yield than the single-expression tests. Moreover, the different localization of the BAD tag fused to PfATP2 had no effect in neither PfATP2 nor Cdc50 subunits expression. Nevertheless, given that PfATP2 is not expressed in any of the experiments presented

here, it is somehow logical to find that there is no change in the expression of the subunits between the single expression and the co-expression experiments.

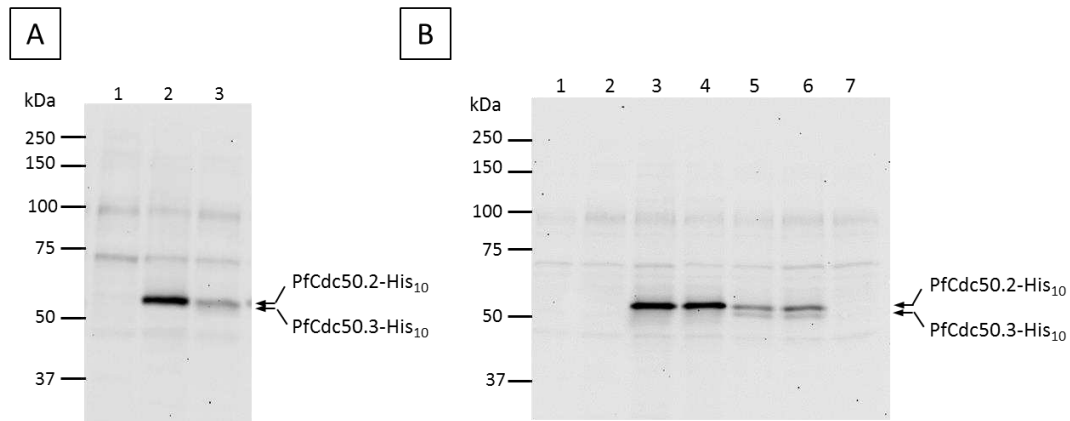


**Figure 18: Expression of the *P. falciparum* putative subunits PfCdc50.1, PfCdc50.2 and PfCdc50.3 in total membranes obtained from small-scale cultures of *S. cerevisiae*.**

Western blots revealed with a His probe for detection of the His<sub>10</sub>-labelled subunits. Panel A: single-expression of the three putative Cdc50 subunits. Lane 1: PfCdc50.1; lane 2: PfCdc50.2; lane 3: PfCdc50.3. Panel B: Co-expression of the Cdc50 subunits with the flippase PfATP2 labelled at the N- or C-terminus with the BAD. 20µl of each membrane sample at 0.04 OD unit of cells were loaded on the gel. Lane 1: PfATP2-BAD/PfCdc50.1-His<sub>10</sub>; lane 2: BAD-PfATP2/PfCdc50.1-His<sub>10</sub>; lane 3: PfATP2-BAD/PfCdc50.2-His<sub>10</sub>; lane 4: BAD-PfATP2/PfCdc50.2-His<sub>10</sub>; lane 5: PfATP2-BAD/PfCdc50.3-His<sub>10</sub>; lane 6: BAD-PfATP2/PfCdc50.3-His<sub>10</sub>; lane 7: PfATP2-BAD. Theoretical masses: Cdc50p ≈ 45 kDa; PfCdc50.1 ≈ 44 kDa; PfCdc50.2 ≈ 60 kDa; PfCdc50.3 ≈ 55 kDa.

The same expression analysis was carried with the *P. chabaudi* ATP2 and Cdc50 subunits orthologs. PcATP2 with the BAD tag has a theoretical molecular mass of about 180 kDa (PcATP2 weights 170 kDa and the BAD 10 kDa). Lanes 1 and 2 of the SDS-PAGE gel of figure 19 correspond to the expression alone of PfATP2-BAD and BAD-PfATP2, respectively. In both constructs we observe protein expression (fig 19, lanes 1 and 2). Notably, despite having the same molecular mass, PcATP2 runs differently depending on the position of the BAD tag. The presence of two bands in the BAD-PcATP2 construct can indicate a proteolysis event of the protein is occurring at the C-terminal end. Moreover, no apparent difference in the expression yield of PcATP2 was observed after changing the position of the BAD tag. Co-expressing PcATP2 with the different PcCdc50 subunits showed no significant differences with respect to the PcATP2 level of expression in the absence of these subunits (fig 19, lanes 3 to 8). One band is still observed in the C-terminal tagged PcATP2 and two bands for the N-terminal tagged PcATP2. A different

pattern is observed when BAD-PcATP2 is co-expressed with the PcCdc50.3 subunit (fig 19, lane 8) the lowest band corresponding to BAD-PcATP2 is the main PcATP2 band observed in the gel. In conclusion, PcATP2 electrophoretic mobility and possible proteolytic cleavage changes upon the position of the BAD tag and the presence of a particular Cdc50 subunit.

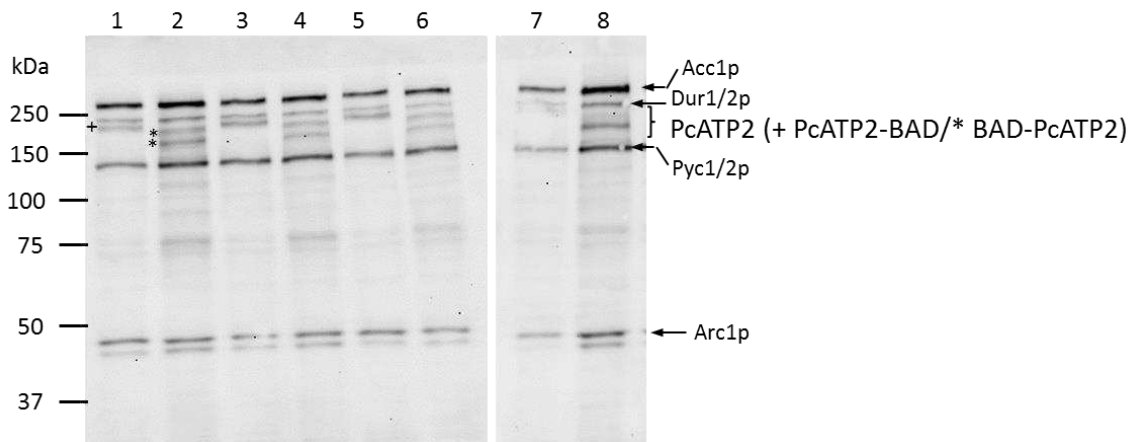


**Figure 19: Expression of *P. chabaudi* ATP2 in total membranes obtained from small-scale cultures of *S. cerevisiae*.**

Expression of the various flippases PcATP2 labelled at the N- or C-terminus with the BAD, alone or in the presence of each of the three putative Cdc50 subunits. 20 $\mu$ l of each membrane sample at 0.04 OD unit of cells were loaded in the gel. Lane 1: PcATP2-BAD; lane 2: BAD-PcATP2; lane 3: PcATP2-BAD/PcCdc50.1-His<sub>10</sub>; lane 4: BAD-PcATP2/PcCdc50.1-His<sub>10</sub>; lane 5: PcATP2-BAD/PcCdc50.2-His<sub>10</sub>; lane 6: BAD-PcATP2/PcCdc50.2-His<sub>10</sub>; lane 7: PcATP2-BAD/PcCdc50.3-His<sub>10</sub>; lane 8: BAD-PcATP2/PcCdc50.3-His<sub>10</sub>. Theoretical masses: Acc1p, acetyl-CoA carboxylase  $\approx$ 250 kDa; Dur 1/2p, urea carboxylase  $\approx$ 200 kDa; Drs2p,  $\approx$  153 kDa; Pyc 1/2p, pyruvate carboxylase isoform 1 and 2  $\approx$ 130 kDa; Arc 1p, complex acyl-RNA  $\approx$  42 kDa; PcATP2-BAD  $\approx$  180 kDa.

Next, we performed the single-expression tests of the *P. chabaudi* Cdc50 subunits. The expected size of PcCdc50.1 is 45 kDa, 61 kDa for PcCdc50.2, and 51 kDa for PcCdc50.3. As seen in the western blot, the three subunits were expressed and localized in total membranes (fig 20, panel A). PcCdc50.1 (fig 20, panel A, lane 1) migrated faster than expected ( $\sim$ 37 kDa), a likely artefact of the SDS-PAGE gels commonly seen for membrane proteins. Moreover, PcCdc50.2 appeared to be less expressed than the other two, and PcCdc50.3 showed two bands in the gel with, apparently, similar intensity (fig 20, panel A lanes 2 and 3). The upper band of PcCdc50.3 suggested a glycosylated form of this subunit (see the section III-2-4). When the PcCdc50 subunits were co-expressed with PcATP2 (fig 20, panel B, lanes 1 to 7), we found a very low expression yield of

PcCdc50.2 compared to the two others. Moreover, the level of expression of the subunits appeared to be higher when PcATP2 was tagged at the N-terminal end (fig 20, panel B, lanes 2, 4 and 6).

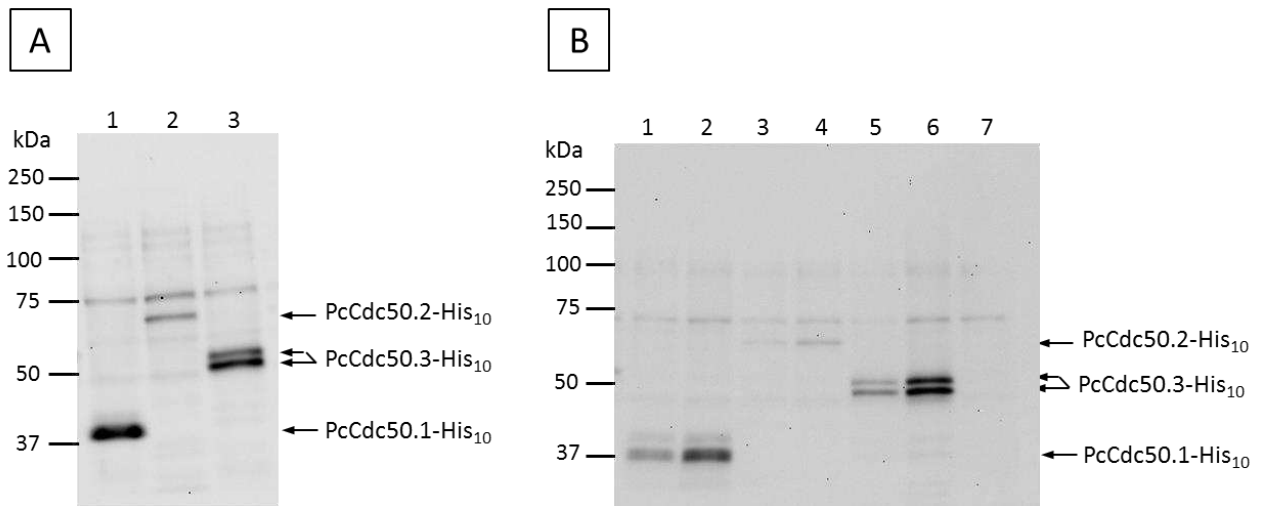


**Figure 20: Expression of *P. chabaudi* putative subunits PcCdc50.1, PcCdc50.2 and PcCdc50.3 in total membranes obtained from small-scale cultures of *S. cerevisiae*.**

Panel A: single-expression of the three putative Cdc50 subunits. Lane 1: PcCdc50.1; lane 2: PcCdc50.2; lane 3: PcCdc.3. Panel B: Co-expression of each of the three putative Cdc50 subunits with PcATP2 tagged at the N- or C-terminal end with the BAD. 20 $\mu$ l of each membrane sample at 0.04 OD units of cells were loaded on a gel. Lane 1: PcATP2-BAD/PcCdc50.1-His<sub>10</sub>; lane 2: BAD-PcATP2/PcCdc50.1-His<sub>10</sub>; lane 3: PcATP2-BAD/PcCdc50.2-His<sub>10</sub>; lane 4: BAD-PcATP2/PcCdc50.2-His<sub>10</sub>; lane 5: PcATP2-BAD/PcCdc50.3-His<sub>10</sub>; lane 6: BAD-PcATP2/PcCdc50.3-His<sub>10</sub>; lane 7: PcATP2-BAD. Theoretical masses: PcCdc50.1  $\approx$  45 kDa; PcCdc50.2  $\approx$  61 kDa; PcCdc50.3  $\approx$  51 kDa.

These small-scale expression tests of ATP2 and related Cdc50 subunits from the two *Plasmodium* species therefore allowed a quick screening of protein expression for the different constructs (single-expression of ATP2 or co-expression with the Cdc50 subunits) and gave the first hint of which one of the Cdc50 subunits can be associated to ATP2. Based on the results obtained in these experiments, we chose to continue working with two co-expression constructs of *P. chabaudi* proteins, BAD-PcATP2/PcCdc50.1-His<sub>10</sub> and BAD-PcATP2/PcCdc50.3-His<sub>10</sub> for expression in large-scale cultures and study of the localization of PcATP2 and the two subunits PcCdc50.1 and PcCdc50.3 in different membrane fractions.

### III-2-3 Expression tests of PcATP2/ PcCdc50.1 and PcATP2/ PcCdc50.3 in large-scale cultures.

Large-scale cultures were done in 500 mL of rich media in fernbach culture flasks (see section V-2-2-4). The cells were grown for 36 h, then galactose was added and the induction of protein expression was performed for 18 h at 18°C. After collecting and breaking the cells, sequential centrifugation steps (see section V-2-2-5 for full description) allowed to obtain the heavy membranes fraction (or P2 pellet fraction), known to be enriched in plasma membrane and mitochondrial membranes, and the light membrane fraction (or P3 pellet fraction), enriched in Golgi and endoplasmic reticulum membranes (Jidenko et al. 2006). As for the small-scale cultures, cells transformed with the empty vector or co-expressing Drs2p/Cdc50p were grown in parallel and membranes were prepared in the same way.

The corresponding P3 membranes of both controls were analysed by western blot (fig 21, panels A and B, lanes 1 and 2) to reveal background levels and show positive controls for Drs2p and Cdc50p. In the two co-expression experiments of *Plasmodium* ATP2/Cdc50 complexes (fig 21, panels A and B), PcATP2 and both PcCdc50 subunits were found in the P2 and P3 membranes, as expected. In the co-expression of BAD-PcATP2/PcCdc50.1-His<sub>10</sub> (fig 21, panel A), the apparent distribution of both ATP2 and the subunit is practically one half in the P2 and the other half in the P3 fraction. We can notice that, in this case, the lowest band of PcATP2 is much stronger than the upper band, a slightly different behaviour of what we saw in total membranes from small-scale cultures where the two bands of PcATP2 displayed similar intensity (fig 19, lane 4). On the other hand, in the experiments of BAD-PcAPT2/PcCdc50.3-His<sub>10</sub> co-expression (fig 21, panel B), the flippase and the subunit were mostly localized in the P2 membrane fraction. As in the total membrane preparation from small-scale cultures, a second band of PcCdc50.3, presumably a glycosylated form of this subunit, is also present in the western blot, at an apparent similar intensity as the eventual unglycosylated form (fig 21, panel B). It is worth mentioning that for Cdc50p, the predominant band is the glycosylated one (fig 21, panels A and B lane 2).

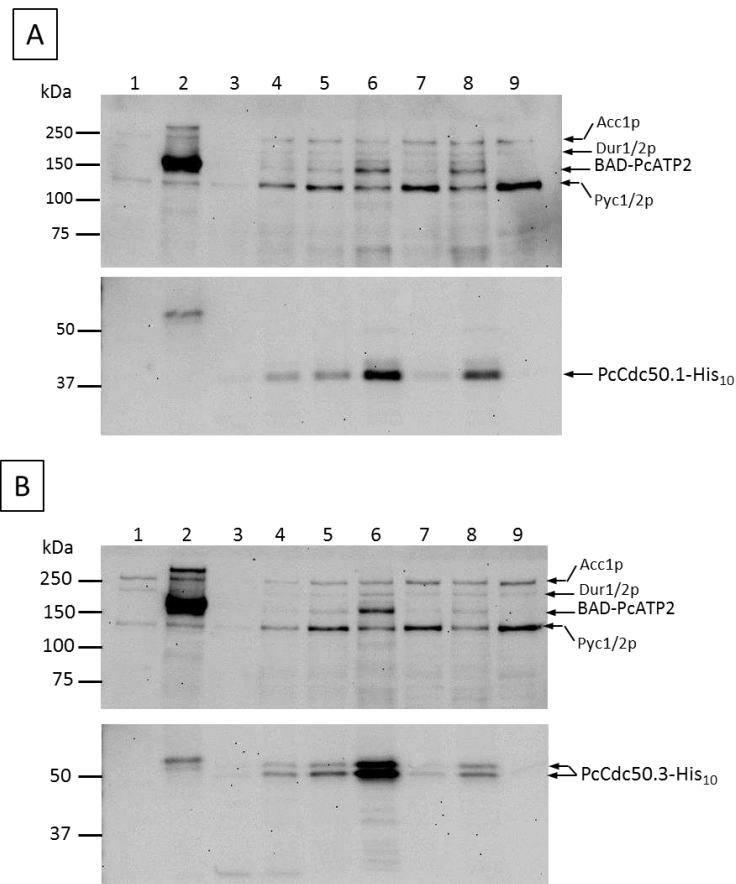


**Figure 21: Western blot analysis of the various yeast membrane fractions obtained after co-expressing BAD-PcATP2/PcCdc50.1-His<sub>10</sub> or BAD-PcATP2/PcCdc50.3-His<sub>10</sub>.**

1 $\mu$ g of total protein is loaded in each line. The top of the membrane is revealed with a biotin probe to detect the flippase and the bottom with a His probe to detect the subunit. Panel A: co-expression BAD-PcATP2/PcCdc50.1-His<sub>10</sub>. Lane 1: *S. cerevisiae* P3 membranes transformed with the empty vector; lane 2: P3 membranes with *Drs2p/Cdc50p*; lane 3: crude extract; lanes 4 and 5: respectively pellet 1 (P1) and supernatant 1 (S1) obtained after the first centrifuge at 1000 x g; lanes 6 and 7: respectively pellet 2 (P2) and supernatant 2 (S2) obtained after the centrifugation at 20000 x g; lanes 8 and 9: respectively pellet 3 (P3) and supernatant 3 (S3) obtained after the centrifugation at 125000 x g. Panel B: co-expression BAD-PcATP2/PcCdc50.3-His<sub>10</sub>. Lane 1: *S. cerevisiae* P3 membranes transformed with the empty vector; lane 2: P3 membranes with *Drs2p/Cdc50p*; lane 3: crude extract; lanes 4 and 5: respectively pellet 1 (P1) and supernatant 1 (S1); lanes 6 and 7: respectively pellet 2 (P2) and supernatant 2 (S2); lanes 8 and 9: respectively pellet 3 (P3) and supernatant 3 (S3).

The results obtained in these two co-expression experiments using large-scale cultures and membrane fractionation shows that PcATP2 and the two PcCdc50 subunits can be localized in both P2 and P3 membrane fractions. Interestingly, PcATP2 distribution between P2 and P3 membrane fractions switches depending on the Cdc50 subunit that is co-expressed with it (fig 21). In addition, the distribution of PcATP2 between the two fractions is identical as the distribution of its co-expressed subunit (Fig 21); in other words, they co-localize in the same membrane fraction. These observations strongly

suggest the possibility that PcATP2 can be associated with both subunits, a situation already seen with other lipid flippases (López-Marqués et al. 2010). It has been reported that over-expressed membrane proteins localized in the P2 membrane fraction are less prone to solubilisation with detergent than the same proteins in the P3 fraction. This suggests that some of the proteins found in P2 might be poorly folded and, therefore, less likely to be active (Lenoir et al. 2002). Since in the P3 membrane fraction the proportion of PcATP2/PcCdc50.1 was higher than the one of PcATP2/PcCdc50.3, this would indicate that in our expression system, PcCdc50.1 is a better partner to form the complex with PcATP2 than with PcCdc50.3. This hypothesis still needs to be experimentally tested.

### III-2-4 Deglycosylation analysis of the PcCdc50.1 and PcCdc50.3

Following the analysis of the expression of PcATP2 and PcCdc50 subunits, we assessed the glycosylation state of the PcCdc50 subunits expressed in *S. cerevisiae*. We used the online tool NetNGlyc (<http://www.cbs.dtu.dk/services/NetNGlyc/>) to predict the possible N-glycosylation sites of both subunits containing the motif Asp-Xaa-(Ser/Thr). We found no potential sites for N-glycosylation in the sequence of PcCdc50.1, however one glycosylation site was found in the sequence of PcCdc50.3. Indeed, the FNDDT motif found in Cdc50p, the yeast Cdc50 subunit known to be glycosylated, is also conserved in other subunits from other organisms (L. R. Poulsen et al. 2008; García-Sánchez et al. 2014), including PcCdc50.3, which contains the potential glycosylation site N260 (fig 22).

```

PcCdc50.3 TKA---SDVSQCFPIVTNK-----EGKVLHPCGLVARSI FNDDTFTLYKDINLREK--- 274
PfCdc50.3 TKD---NEVSQCGPITKNH-----EGKILHPCGLIARSI FNDDTFSVYMDRELHNM--- 306
PbCdc50.3 TNP---SDISQCFPIITNK-----EGKILHPCGLVARSV FNDDTFTLYKDVNLKEK--- 268
Cdc50p    KKD---DLDTSCSPIRS-R-----EDKIYPCGLIANSMFNDDTFSQVLSGIDD-T--- 212
Lem3p    SYETVHDATGINCKPLSKNA-----DGKIYPCGLIANSMFNDDTFPLQLTNVGDTS--- 254
ALIS1    -DE---NQIDACKPEDDF-----GGQPIVPCGLIAWSLFNDDTYVLSRNN----- 191
ALIS2    -EY---SHTSSCEPEESS-----NGLPIVPCGLIAWSMFNDDTFTFSRER----- 187
ALIS3    -YE---NQISACKPEDDV-----GGQPIVPCGLIAWSLFNDDTYALSRNN----- 190
CDC50A   ALL---NPSKECEPYRRNE-----DKPIAPCGAIANSMFNDDTLELFLIGNDSYP--- 194
CDC50B   ALR---HPVNECAPYQRSA-----AGLPIAPCGAIANSLFNDDSFSLWHQRQPGGP--- 185
LdRos3   AIS-----KMCAPFRFPGEATGDSVSGYYPNCGAYPWAMFNDDISLYRTDGTLICDGS 193
          * *                .      ***      : : * * * :

```

**Figure 22: Conserved glycosylation site of the Cdc50 subunits encoded by different organisms.**

The consensus N-glycosylation motif Asp-Xaa-(Ser/thr) is highlighted in blue. PcCdc50.3 from *P. chabaudi*; PfCdc50.3 from *P. falciparum*; PbCdc50.3 from *P. berghei*; Cdc50p and Lem3p from *S. cerevisiae*; ALIS1, ALIS2 and ALIS3 from *A. thaliana*; CDC50A and CDC50B from humans; LdRos3 from *L. donovani*. Multiple alignment done with CLUSTALW (Thompson, Higgins, and Gibson 1994).

To test this hypothesis we used the amidase PNGase F and the N-glycosylase EndoH to confirm this predicted glycosylation site. The reactions of deglycosylation were performed on membranes co-expressing PcATP2/PcCdc50.1 and PcATP2/PcCdc50.3. As control, we used membranes co-expressing Drs2p/Cdc50p. Cdc50p (fig 23, lanes 7 to 9), which on the western blot display two major bands, the fully glycosylated form above 50 kDa and the core Cdc50p above 37 kDa. After incubation with PNGase F or EndoH, the glycosylated band disappeared and the core Cdc50p was predominantly found. In the deglycosylation experiments of PcCdc50.1 (fig 23, lanes 1 to 3), there was no difference in the western blot after the addition of the enzymes; as expected since this subunit does not contain predicted glycosylated sites and it always runs in the SDS-PAGE as a single band. In contrast, for the PcCdc50.3 subunit, two bands were originally present (fig 23, lane 4), but after digestion with either PNGase or EndoH, the upper band disappeared, and the lowest band remained (fig 23, lanes 5 and 6), demonstrating that, as predicted, PcCdc50.3 can indeed be glycosylated when expressed in yeast.

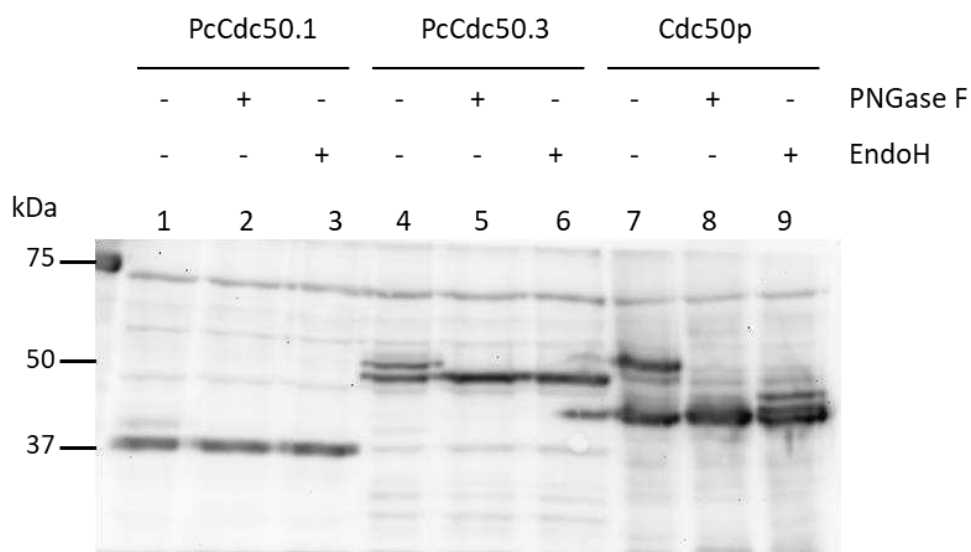


**Figure 23: Deglycosylation assays of PcCdc50.1 and PcCdc50.3 co expressed with PcATP2.**

*Deglycosylation was achieved with the PNGase F or the EndoH enzymes. 10 µg total proteins of P3 membranes deglycosylated (+) or not (-) were deposited in the experiments with PcAT2/PcCdc50 subunits and 5 µg total proteins of P3 membranes deglycosylated (+) or not (-) in the control experiment with Drs2p/Cdc50p. The western blot was revealed with the His probe. Lanes 1 to 3: P3 membranes co-expressing PcATP2/PcCdc50.1; lanes 4 to 6: P3 membranes co-expressing PcATP2/PcCdc50.3; lanes 7 to 9: P3 membranes co-expressing Drs2p/Cdc50p.*



### III-2-5 Functional complementation assay in *S. cerevisiae*

In order to qualitatively assess the functionality of PcATP2 and PcCdc50 subunits expressed in *S. cerevisiae*, a functional complementation assay was performed using the *S. cerevisiae* strains *W3031b Gal4-2 Δcdc50* where Cdc50p is disrupted from the genome (Montigny, Azouaoui, et al. 2014; Koji Saito 2004). This strain is unable to grow at the restrictive temperature of 20°C due to the functional absence of the Drs2p/Cdc50p complex (K. Saito 2004). The wild-type phenotype can be rescued after transforming the yeast with a vector containing the missing copy of these genes or, eventually, with a gene (or genes) with the ability to do a similar functional work as the Drs2p/Cdc50p complex (Azouaoui et al. 2014; L. R. Poulsen et al. 2008). The different single-expression vectors (pYeDP60-BAD-TEV-PcATP2, pYeDP60-PcCdc50.1-TEV-His<sub>10</sub>, and pYeDP60-PcCdc50.3-TEV-His<sub>10</sub>) and co-expression vectors (pYeDP60-BAD-TEV-PcATP2-PcCdc50.1-TEV-His<sub>10</sub> and pYeDP60-BAD-TEV-PcATP2-PcCdc50.3-TEV-His<sub>10</sub>) were transformed into the *Δcdc50* strain.

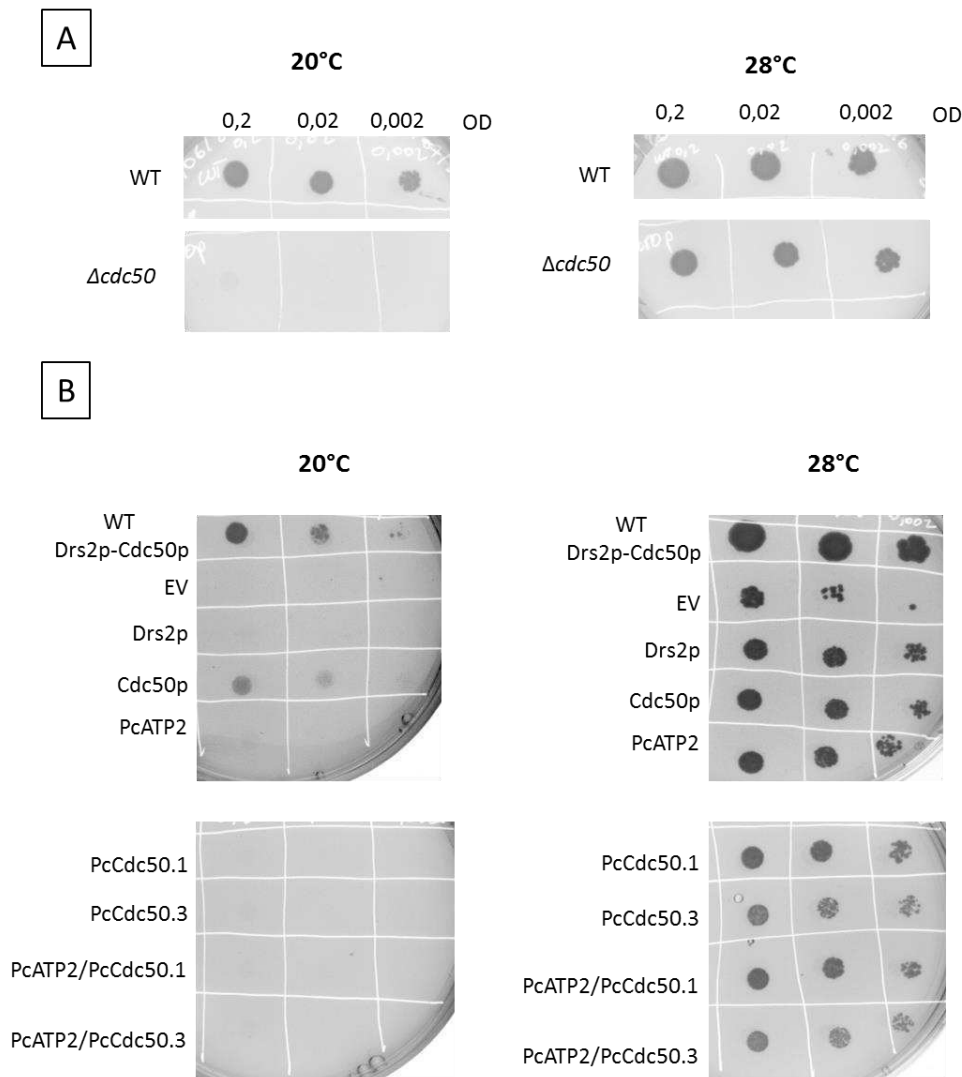


**Figure 24: Functional complementation in  $\Delta cdc50$  temperature-sensitive *S. cerevisiae* strain**

Panel A: Test of the phenotype of the wild type strain W3031b Gal4-2 (WT) and the temperature-sensitive W3031b Gal4-2  $\Delta cdc50$  growing at both 28°C and 20°C on S6AU plates. Panel B:  $\Delta cdc50$  cells were transformed with the empty vector (EV), single-expression vector encoding *DRS2* or *CDC50*, single-expression vector encoding *PcATP2*, *PcCdc50.1* or *PcCdc50.3* and co-expression vectors encoding *PcATP2/PcCdc50.1* or *PcATP2/Cdc50.3*. Wild type strain (WT) expressing *Drs2p/Cdc50p* was used as control. Serial dilutions of yeast cells were spotted on plates and incubated at 28°C or at the restrictive temperature of 20°C on S5AF plates. *PcATP2* was tagged with a BAD tag at the N-terminus and the *PcCdc50* with a *His<sub>10</sub>* tag at the C-terminus.

First, the cold sensitive phenotype of the non-transformed  $\Delta cdc50$  strain was verified by growing it at 20°C and 28°C on S6AU plates. The non-transformed wild type strain was used as control (fig 24, panel A). As expected  $\Delta cdc50$  cells did not grow at 20°C when transformed with the empty vector or with the vector expressing only *Drs2p* (fig 24, panel B). The wild-type phenotype was rescued after transforming this strain with the

vector encoding the Cdc50p sequence (Azouaoui et al. 2014). However, neither the single-expression of PcATP2 nor the single-expressions of both subunits PcCdc50.1 and PcCdc50.3, did rescue the normal growing phenotype (fig 24, panel B), suggesting that the *Plasmodium* subunits do not functionally associate with Drs2p to rescue the function of the Drs2p/Cdc50p complex. Moreover, co-expressing PcATP2/PcCdc50.1 or PcATP2/PcCdc50.3 in this strain did not rescue the wild-type phenotype either (fig 24, panel B)

### III-2-6 Discussion

The heterologous expression of proteins and, especially membrane transport proteins, can be challenging. In our case, we undertook the co-expression of two integral membrane proteins supposed to form a complex and originating from *Plasmodium* species. The different sequences were codon optimized as shown to be necessary for the expression in yeast. Indeed, the high A/T rich sequences found in *P. falciparum* can lead to premature transcriptional end of the proteins (Graber et al. 1999). The strategy used for co-expression was set up in the laboratory for the expression of the yeast P4-ATPase Drs2p/Cdc50p. It has been previously used for co-expression of the Na<sup>+</sup>/K<sup>+</sup> ATPase, a P2C ATPase, with its beta subunit (Strugatsky et al. 2003). However, we could not detect an expression of PfATP2 in any of the constructs used, while some expression was observed for PfCdc50.2 and PfCdc50.3 (fig 20). In addition, neither the position of the BAD tag in PfATP2 nor the co-expression with any of the three Cdc50 subunits helped to detect the expression of PfATP2 in *S. cerevisiae*. On the other hand, expression of the *P. chabaudi* ATP2 was detected in total membranes, displaying a slightly different pattern in the gel depending on the position of the BAD tag (fig 19). In addition, a change in the intensity of the SDS-PAGE bands corresponding to PcATP2 tagged at the N-terminal end was observed when it was co-expressed with PcCdc50.3 (fig 19, lane 8). The intensity of the lowest band was higher than the upper band only in the co-expression experiment (fig 21). Moreover, two PcCdc50 subunits showed an apparent higher expression level when co-expressed with PcATP2 with the tag in the N-terminal end (fig 20). This result suggests that PcATP2 can have some role in helping to fold and stabilize the PcCdc50 subunit, as similar results were previously documented for human CDC50A and CDC50B subunits (van der Velden et al. 2010). The level of expression obtained is not very high

but it is in the range obtained in the laboratory for other P-type ATPases as SERCA1a from rabbit and PfATP6 from *P. falciparum*.

Consequently, for large-scale cell-culture followed by membrane fractionation, we focused on co-expressions of the *P. chabaudi* variants PcATP2/PcCdc50.1 and PcATP2/PcCdc50.3. Analysis of the different membrane fractions showed that PcATP2 and PcCdc50 subunits were found in both the P2 and the P3 membrane fractions, with preference towards the P2 fraction (fig 21). Interestingly, PcATP2 distribution between P2 and P3 membrane fractions changes depending on the co-expressed subunit, following the same distribution between P2 and P3 as the co-expressed partner (fig 21) suggesting that PcATP2 can be associated with both subunits in any of the membrane compartments of *S. cerevisiae*. Moreover, a higher proportion of both PcATP2 and PcCdc50.1 when co-expressed is found in the P3 fraction compared to PcATP2 and PcCdc50.3 co-expression. Since previous experimental data shows that well-folded and functional overexpressed proteins are most likely to be located in the P3 fraction (Jidenko et al. 2006), our results suggest that *S. cerevisiae* expressed PcATP2 is more prone to associate with PcCdc50.1 than to PcCdc50.3, forming, eventually, a more stable complex. Interestingly, a predicted glycosylation site was found in the sequence of PcCdc50.3 and not in the sequence of PcCdc50.1. It is known for other subunits as Cdc50p, bCDC50A or LiRos3 that glycosylation is important for the stability of the complex, and perhaps for the activity of the flippase (Jacquot et al. 2012; Jonathan A Coleman and Molday 2011; García-Sánchez et al. 2014). Long N-glycosylations are not commonly found in proteins from *Plasmodium* parasites. In contrast, yeast has the capacity of N-glycosylate with two N-acetylglucosamines that incorporate mannose and glucose residues (Aebi 2013). Proteins from *Plasmodium* normally contain more truncated or short glycosylations (Cova et al. 2015). In addition, as the two forms of PcCdc50.3 (glycosylated and unglycosylated) are apparently present at similar level, at this stage we cannot make any conclusion about the role of PcCdc50.3 glycosylation for the association with PcATP2. Perhaps, this could be answered by removing the glycosylation site and analysing PcATP2 expression.

The fact that PcATP2 alone or co-expressed with either PcCdc50.1 or PcCdc50.3 does not rescue Drs2p/Cdc50p function in *S. cerevisiae*  $\Delta cdc50$  strain could be attributed to different reasons. In one hand, the *Plasmodium* co-expressed proteins in *S. cerevisiae*

perhaps are not functional. On the other hand, it is possible that PcATP2, although having an amino acid identity with Drs2p of ~ 36%, recognizes different substrates and, therefore, functional rescue would never occur with this particular strain.

### III-3 Detergent solubilisation of PcATP2, PcCdc50.1 and PcCdc50.3

Solubilisation with detergent is an important step for the isolation of membrane proteins if possible in a stable and active form for subsequent purification and functional studies. In our laboratory we have established different protocols to screen detergents for membrane protein solubilisation, and we have set up different methodologies to assess the stability and functional behaviour of solubilized P-type ATPases (Lenoir, G., Dieudonné, T., **Lamy, A.**, Lejeune, M., Vázquez-Ibar, J.-L., & Montigny, C. (2018). Screening of detergents for stabilization of functional membrane proteins. *Current Protocols in Protein Science*, 93, e59. doi: 10.1002/cpps.59 ) (Lenoir et al. 2018). Detergents are normally categorized in four classes: non-polar, anionic, cationic and zwitterionic. This classification is based on the nature of the head group and the length of the hydrocarbon chain (Le Maire, Champeil, and Møller 2000). Non-polar detergents with mid-length hydrocarbon chains (non-toxic and referred as mild detergent) are often used in solubilisation and stabilization of membrane proteins. In such attempts, it is always necessary to find a correct ratio of detergent versus protein because a sufficient amount of detergent around the hydrophobic core is required to prevent aggregation of the protein, but too large excess can lead to delipidation and destabilisation of the protein. It is also very important to carefully choose and control the temperature and composition of the solubilisation buffer because the presence of osmolytes such as glycerol or salts as well as changes of temperature can influence the critical micellar concentration (CMC) of the detergent and, therefore, the amount of detergent available for membrane solubilisation.

In order to find the optimal conditions for solubilisation of PcATP2 and its potentially associated subunits, PcCdc50.1 and PcCdc50.3, we undertook detergent screening assays. In addition to test different detergents, we also tested other parameters like changing the protein versus detergent ratio, solubilisation time, temperature, or pH; we also tested the effect of additives as the cholesteryl hemisuccinate (CHS), phospholipids

and salts. We also tested to wash both the P2 and the P3 membrane fractions (or membrane stripping) prior to solubilisation.

### III-3-1 Screening detergents

As commented earlier, our lab has found for other P-type ATPases, like SERCA1a, PfATP6 or Drs2p, that recombinantly-produced membrane proteins present in the P3 membrane fraction are easier to solubilize with detergent, having at the same time a better chance to be functional (Lenoir et al. 2002; Jacquot et al. 2012). Since, in our case, a considerable amount of PcATP2, PcCdc50.1 and PcCdc50.3 is found in the P2 fraction, in addition to the P3 fraction, we also tried to solubilize these P2 membranes hoping to recover active protein from this fraction too. Eleven detergents from different classes were used in this initial screening: DM, UDM, DDM, OG, OTG, C<sub>12</sub>E<sub>8</sub>, LMNG, LDAO, CHAPS, FosC12, and CYMAL-5 (see section V-2-4-3). We performed solubilisation tests of P2 and P3 membrane fractions co-expressing PcATP2/PcCdc50.1 or PcATP2/PcCdc50.3. The first experimental conditions for solubilisation were, a protein:detergent ratio of 1:10 (w/w), pH 7.8, 4°C and overnight incubation (about 15 h). After incubation, solubilized and non-solubilized fractions were separated by ultracentrifugation and every fraction was analysed by western-blot. Figure 25 shows the results of PcATP2/PcCdc50.1 solubilisation with six of the above detergents. Panel A displays the experiments done with P2 membrane fractions: no solubilisation can be observed with the detergents DM, UDM, DDM, LMNG and C<sub>12</sub>E<sub>8</sub>, neither for PcATP2 nor for PcCdc50.1 which are only found in the pellet after ultracentrifugating the detergent-containing solubilisation medium. Identical negative results were obtained with the other detergents tested: OG, OTG, LDAO, CYMAL-5 (not shown). In contrast, FosC12 (Fig 25, panel A) was able to solubilize the PcCdc50.1 subunit as well as PcATP2, to some extent. However, PcATP2 was hardly detected in the total extract solubilized fraction (TE) and in the solubilised supernatant (fig 25, Panel A), an indication that probably PcATP2 is not stable in FosC12. Solubilisation of the P3 membranes (fig 25, panel B), gave the same results as for the P2 membranes: no solubilisation of PcATP2 or PcCdc50.1 except when FosC12 was used. Solubilisation of PcCdc50.1 was not complete with FosC12, and PcATP2 was not detectable neither in the total extract nor in the supernatant, suggesting again that PcATP2 is not stable in FosC12.

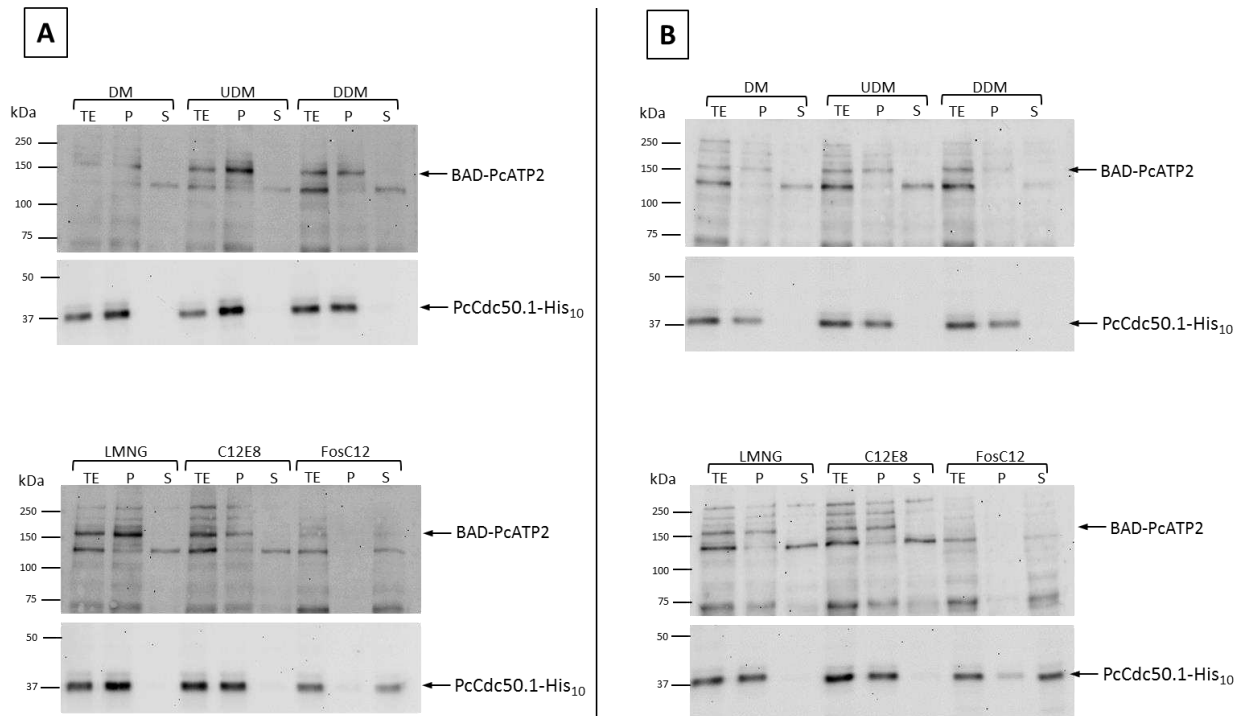


**Figure 25: Western blot analysis of the solubilisation of P2 and P3 membrane fraction co-expressing PcATP2 and PcCdc50.1.**

*1*µg of total protein was loaded in each line. The top of the blot was revealed with a biotin probe to detect BAD-PcATP2 and the bottom with a His probe to detect PcCdc50.1-His<sub>10</sub>. The “solubilisation medium” contained 2 mg/mL of total protein and 20 mg/mL of detergent, at pH 7.8 and 4°C for overnight incubation. Panel A: Solubilisation of P2 membranes. Panel B: solubilisation of P3 membranes. TE: total extract before ultra-centrifugation; P: pellet after ultracentrifugation (non-soluble material); S: supernatant (solubilized material); detergents: DM; DDM; UDM; LMNG; C12E8; FosC12.

The solubilisation attempts gave similar results for PcATP2/PcCdc50.3 as PcATP2/PcCdc50.1. In both P2 and P3 membrane fractions, no solubilisation of PcATP2 or PcCdc50.3 was observed with any detergent except with FosC12 (fig 26). Again, the detection of PcATP2 in the presence of FosC12 was difficult and sometimes the corresponding band of PcATP2 was not visible in either the total extract or the supernatant. It is noticeable that the glycosylated form of PcCdc50.3 (upper band, fig 26), was much less solubilised with FosC12 than the unglycosylated form (fig 26). As we do not know the effect of the glycosylation on PcCdc50.3 folding and trafficking, or on the interaction with PcATP2, we can just speculate that this form tends to aggregate and is therefore found in the pellet after ultracentrifugation.

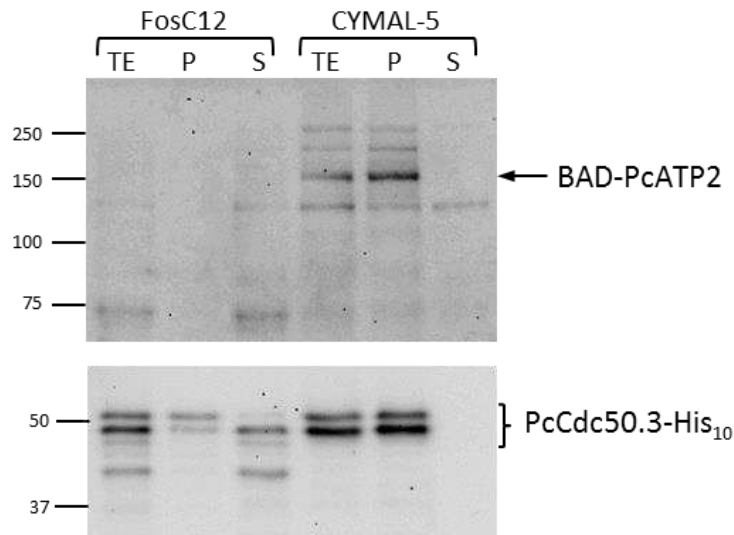


**Figure 26: Western blot analysis of solubilisation of P2 membranes co-expressing PcATP2 and PcCdc50.3.**

1 $\mu$ g of total protein was loaded in each line. The top of the membrane was revealed with a biotin probe to detect BAD-PcATP2 and the bottom with a His probe to detect PcCdc50.3-His<sub>10</sub>. Solubilisation was performed with 2 mg/mL of total protein and 20 mg/mL detergent, at pH 7.8 and 4°C, overnight. TE: total extract before ultracentrifugation; P: pellet after ultracentrifugation (non-soluble material); S: supernatant (solubilized material); detergents: FosC12; CYMAL-5.

Clearly, the solubilisation conditions used in these first tests were unable to efficiently solubilize PcATP2 and the two Cdc50 subunits in both the P2 and the P3 membrane fractions. Solubilisation with FosC12 resulted into some solubilized PcATP2; however, the signal in the western blot was weak or not detectable, even in the total solubilized extract, suggesting a very poor stability of PcATP2 in FosC12.

### III-3-2 Improving PcATP2/Cdc50.1 and PcATP2/PcCdc50.3 solubilisation: membrane stripping and addition of cholesteryl hemisuccinate

We then included a step of membrane stripping prior to solubilisation to remove as much as possible the biotinylated membrane-associated proteins of *S. cerevisiae* (Fig 16). The purpose was to improve sensitivity in the western blot and therefore better visualize the presence of PcATP2, and also to make future purifications (with a streptavidin resin, see below) easier by decreasing the amount of biotinylated proteins of no interest (which might compete with the BAD tagged P4-ATPase for the resin). In addition, with this stripping step we can remove not only biotinylated proteins, but also other proteins that will eventually increase the efficiency of the detergents to solubilize



our proteins. We tested different buffers during membrane stripping using high concentration of salt, NaCl or KCl. In parallel, solubilisation was also tested without the stripping step to assure that the conditions used did not affect the solubilisation. The membranes were stripped for 30 min at 4°C with different stripping buffers. The results were similar between the different conditions, the presence of concentrations up to 0.5 M of NaCl or KCl did not change the solubilisation efficiency observed in the previous experiments. In addition, no difference in solubilisation before or after the stripping was observed either (data not shown), indicating that this stripping step was not affecting the solubilisation.

We also tested whether the presence of the cholesterol derivative CHS affected the solubilisation efficiency of the detergents used, and whether CHS improved the stability of the proteins in the soluble mixed micelles. It has indeed been described for some membrane proteins that the addition of CHS is important for solubilisation and also for activity (Sonoda et al. 2010). As *P. falciparum* parasites possess cholesterol in their membranes (Wunderlich et al. 1991), the addition of CHS might be helpful for the stability of PcATP2 and/or the two Cdc50 subunits in mixed micelles (it is important to remark here that *S. cerevisiae* has no cholesterol on its membrane, but ergosterol).

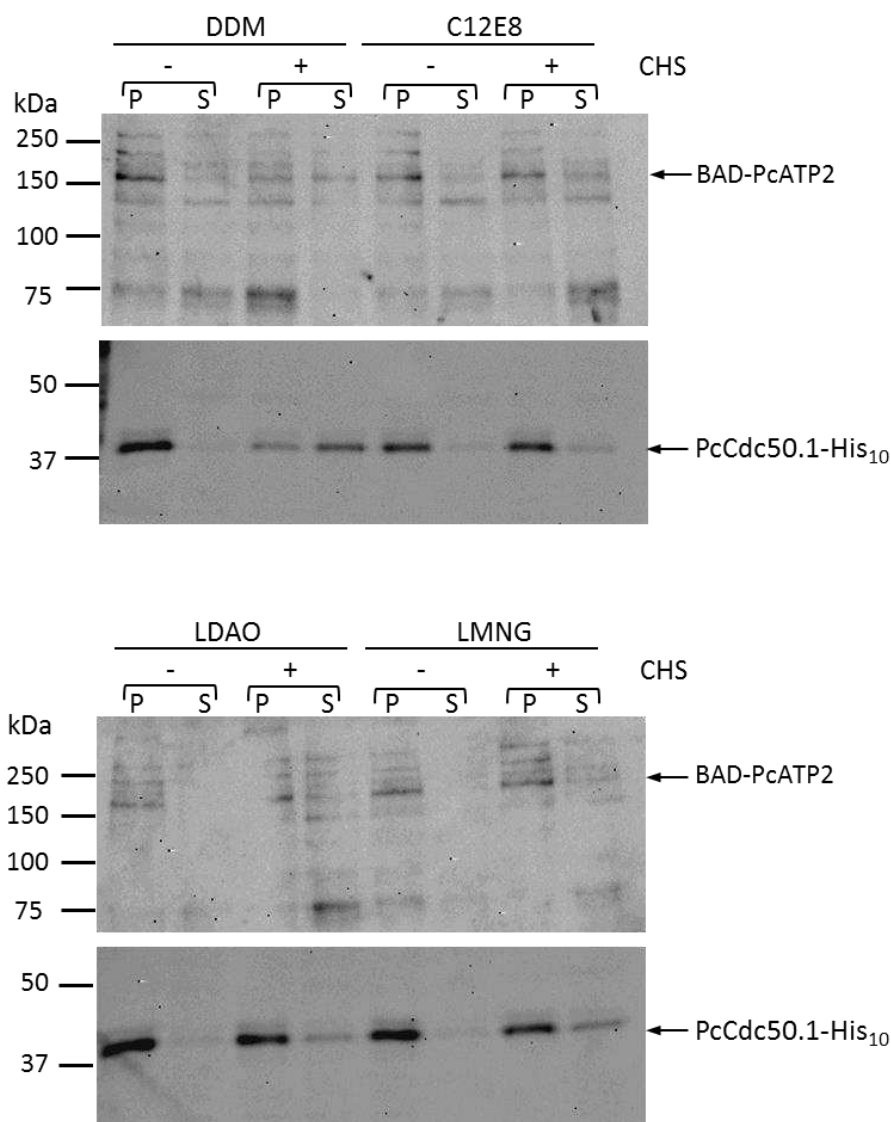


**Figure 27: Western blot analysis of the solubilisation of P3 membrane co-expressing PcATP2/PcCdc50.1 in the presence of CHS.**

*2 µg of total protein were loaded in each line. The top of the blot was revealed with a biotin probe to detect BAD-PcATP2 and the bottom part with a histidine probe to detect the PcCdc50.1-His<sub>10</sub> subunit. The P3 membranes were first stripped to remove membrane associated proteins and solubilisation was performed with 2 mg/mL of total proteins in 10 mg/mL detergent +/- 2 mg/mL CHS for 1h, at pH 7.8 and 20°C. TE: total extract before ultracentrifugation; P: pellet after ultracentrifugation (non-soluble material); S: supernatant (solubilized material).*

Consequently, membrane stripping and addition of CHS were tested in the new solubilisation assays; combining this with different times and temperatures. After several attempts, we found that the most efficient conditions for solubilisation were the following ones: incubation for 1 h at 20°C, 2 mg/mL of total protein concentration of membranes, and 10 mg/mL and 2 mg/mL of detergent and CHS, respectively. As in the previous experiments, solubilisation tests of P2 membrane fractions co-expressing

PcATP2/PcCdc50.1 or PcATP2/PcCdc50.3 did not show substantial solubilisation. A very weak solubilisation was observed for the PcCdc50 subunits but nothing for PcATP2 (not shown). Solubilisation tests of P3 membrane fractions co-expressing PcATP2/PcCdc50.1 are shown in figure 27. Partial solubilisation of PcATP2 and PcCdc50.1 was observed with the detergents DDM, C12E8, LDAO and LMNG, but only in the presence of CHS. C12E8, LMNG and LDAO were able to solubilize about 10-20% of the total amount of both PcATP2 and PcCdc50.1. On the other hand, DDM in the presence of CHS solubilized about 50% of both PcATP2 and PcCdc50.1, representing a remarkable improvement with respect the previous tests and a very promising result.

As the experiments using DDM and CHS with PcATP2/PcCdc50.1 showed positive results, we assessed also the solubilisation of co-expressed PcATP2/PcCdc50.3. In addition, we tested a second protein/detergent ratio by increasing the amount of DDM and CHS to increase the yield of solubilised PcATP2 and PcCdc50.1. In this second condition, membranes containing 2 mg/mL of total protein were solubilized with 20 mg/mL of DDM and 4 mg/mL of CHS. The figure 28 panel A shows the effect of these new solubilisation conditions for membranes expressing PcATP2/PcCdc50.1. First, despite using the same experimental conditions as in the results of figure 27, a slightly lower solubilisation efficiency of PcATP2 and PcCdc50.1 was obtained this time; actually we never succeeded to reach a 50% solubilisation efficiency as in figure 27 with DDM/CHS. Similar results were obtained when more DDM/CHS was added (fig 28, panel A). Solubilisation of membranes co-expressing PcATP2/PcCdc50.3 gave also similar results (fig 28, panel B); PcATP2 and PcCdc50.3 were partially solubilised in the two conditions tested. Interestingly, we noticed that only the non-glycosylated form of PcCdc50.3 was solubilised in these conditions (fig 28), as previously observed with FosC12 (fig 26).

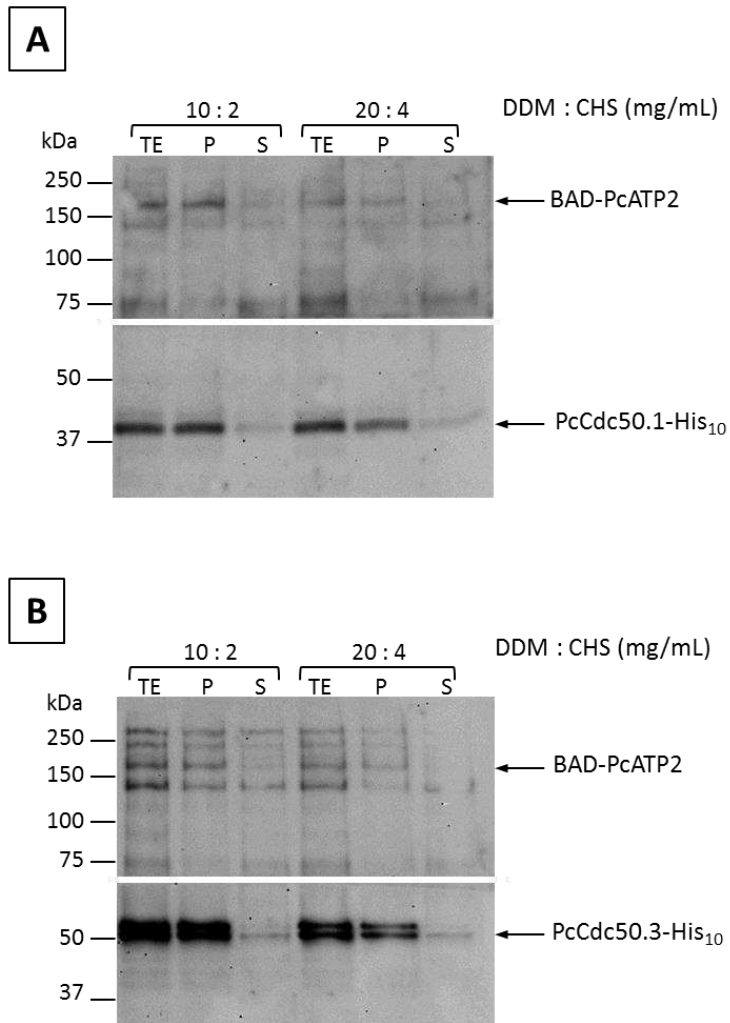


**Figure 28: effect of DDM/CHS concentration upon the solubilisation of PcATP2/PcCdc50.1 or PcATP2/PcCdc50.3 in P3 membranes.**

2 $\mu$ g of total protein were loaded in each line. The top of the blot is revealed with a biotin probe to detect BAD-PcATP2 and the bottom with a histidine probe to detect PcCdc50.1-His<sub>10</sub> or PcCdc50.3-His<sub>10</sub>. Solubilisation of 2mg/ml of total protein in 10 mg/mL of DDM/ 2 mg/mL of CHS or in 20 mg/mL of DDM/ 4 mg/mL of CHS for 1h at 20°C. Panel A: solubilisation of PcATP2/PcCdc50.1. Panel B: solubilisation of PcATP2/PcCdc50.3. TE: total extract before ultracentrifugation; P: pellet after ultracentrifugation (non-soluble material); S: supernatant (solubilized material).

### III-3-3 Discussion

This chapter describes the experimental work done in order to find the best conditions to extract from the membrane and solubilize in detergent PcATP2 and the PcCdc50 subunits expressed in both the P2 and the P3 membrane fractions of *S. cerevisiae* cells. As explained before, different parameters can have an effect on the solubilisation and on the stability of the protein (and in our case, the putative complex). First, a battery of ten detergents were not able to solubilize any protein in both P2 and P3 membrane fractions. Only FosC12, an ionic detergent, was able to solubilize a fraction of PcATP2

and the two PcCdc50 subunits. The stability of PcATP2 in FosC12 was questioned due to the difficulty to detect the protein by western blot in the supernatant after centrifugation or even in the total solubilized extract. As the detection of PcATP2 with the biotin probe was difficult during these solubilisation trials, we added a membrane stripping step to remove as much as possible the others biotinylated proteins and therefore try to obtain a better contrast in the western blot. In parallel, the addition of CHS was tested to improve solubilisation as well as stabilisation of the protein in the detergent micelles, as previously shown for some mammalian membrane proteins as GPCR or the GABA type A receptor (O'Malley et al. 2007; X. Zhang and Miller 2015). In fact, it was also shown in the case of the Na<sup>+</sup>/K<sup>+</sup> ATPase, that a cholesterol binding to the protein enhances the stability of the transporter (Habeck et al. 2017). Moreover, as the membranes of *Plasmodium* parasites contain cholesterol (Tokumasu et al. 2014), the presence of ergosterol in the yeast membranes might be not sufficient for the stabilising the heterologously expressed protein. Not only the addition of CHS was assessed but also different solubilisation times and pHs. In summary, we were able to obtain a partial solubilisation of PcATP2 and the two PCdc50 subunits from the P3 membrane fraction, and only in the presence of CHS. The best experimental conditions were a ratio detergent/CHS of 5:1 and a ratio protein/detergent of 1:5, and when the solubilisation was performed at 20°C for 1h. Variations of the pH and/or protein/detergent ratio did not provide any difference on the solubilisation efficiency, even using higher concentrations of detergent, which did not destabilize the protein. Moreover, the stripping buffers containing different amounts of NaCl or KCl had no effect on the solubilisation efficiency. If we analyse carefully the solubilisation of each protein, we can notice that the percentage of solubilized PcATP2 is similar to that of the PcCdc50 subunit co-expressed with it (fig 27). This observation and the fact that PcATP2 is also present in the same membrane fraction, and similarly distributed between the two P2 and P3 membrane fractions as its PcCdc50 co-expressed subunit, strongly suggest that PcATP2 is able to associate in the membrane with its Cdc50 subunit, either PcCdc50.1 or PcCdc50.3. In addition, the PcATP2/PcCdc50.1 or PcATP2/PcCdc50.3 heterodimer seems to be also present in detergent micelles after solubilisation, since both proteins are solubilized together and in similar proportion (fig 28). Interestingly, we were unable to solubilize the glycosylated form of PcCdc50.3 (fig 28), and only the unglycosylated form of this subunit was solubilized together with PcATP2. In fact, it is usually the

glycosylated form of most Cdc50 subunits of other organisms the one needed for the stabilisation of the P4-ATPase partner (Azouaoui et al. 2014; Jonathan A Coleman and Molday 2011). Obviously, our experimental data is not sufficient at this point to explain the effect of this glycosylation upon the interaction with PcATP2 and why it is not solubilised.

### **III-4 Introducing the GFP for the study of the PcATP2/PcCdc50 complex**

This section will focus on the study of the potential association between PcATP2 and the two PcCdc50 subunits when co-expressed in yeast. As shown before, the level of expression of PcATP2 is fairly low, the yield of its solubilisation is also low, and difficulties for detecting PcATP2-BAD arise from the presence of yeast endogenously biotinylated proteins. We therefore decided to introduce the Green Fluorescent Protein (GFP) in our expression system. The use of the GFP fluorescence, which is a very sensitive tool, should more easily allow the detection of both proteins and, in particular provide new tools to study the association of PcATP2 with its PcCdc50 subunits. With this objective, we made new plasmid vectors by introducing the GFP at the C-terminal end of PcATP2, between the TEV cleavage site and the BAD tag, obtaining the pYeDP60-PcATP2-TEV-GFP-BAD expression vector (fig 29, panel A). In addition, a 3C protease cleavage was inserted at the C-terminal end of the PcCdc50 subunits immediately before the GFP and the TEV cleavage site, yielding the pYeDP60-PcCdc50.1-3C-GFP-TEV-His<sub>10</sub> and the pYeDP60-PcCdc50.3-3C-GFP-TEV-His<sub>10</sub> expression vectors (fig 29, Panel A). From these vectors, the different co-expressions vectors were made, containing either, PcATP2 with the GFP or the PcCdc50 subunits with the GFP (fig 29, Panel B).

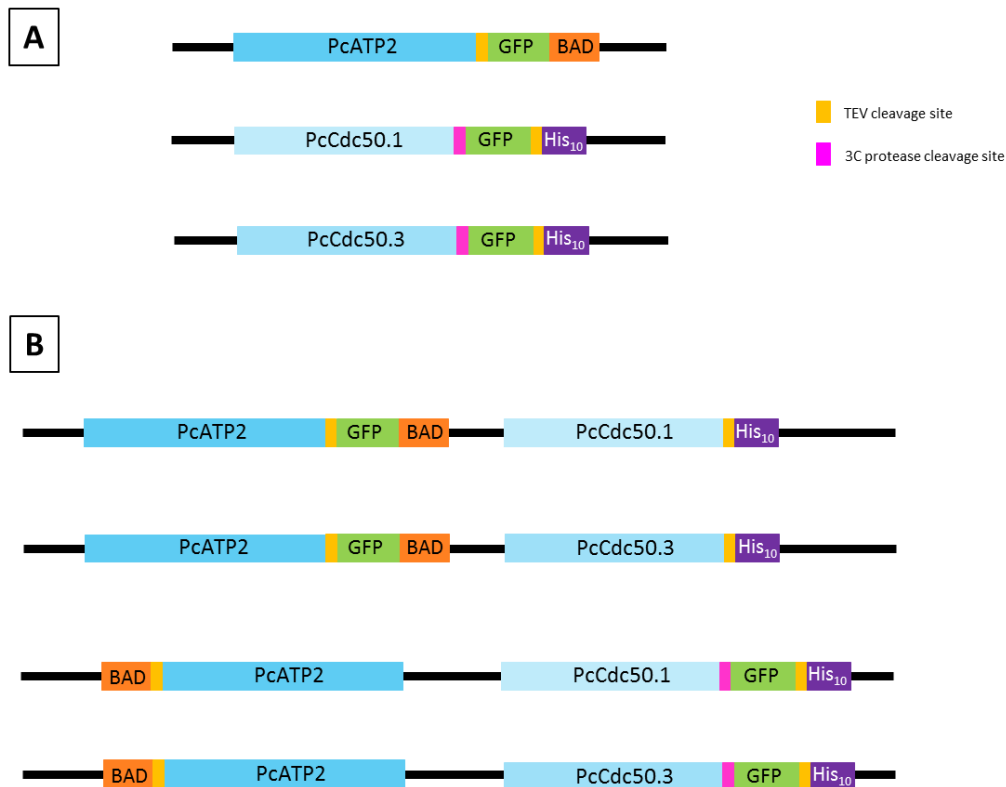


**Figure 29: Single expression and co-expression pYeDP60 vectors encoding PcATP2/PcCdc50 subunits with a GFP tag.**

The sequence of the GFP was cloned at the C-terminal end of PCATP2 or PcCdc50 subunits. Panel A: single-expression vectors, *pYeDP60-PcATP2-TEV-GFP-BAD*, *pYeDP60-PcCdc50.1-3C-GFP-TEV-His<sub>10</sub>*, *pYeDP60-PcCdc50.3-3C-GFP-TEV-His<sub>10</sub>*. Panel B: co-expression vectors, *pYeDP60-PcATP2-TEV-GFP-BAD-PcCdc50.1-TEV-His<sub>10</sub>*, *pYeDP60-PcATP2-TEV-GFP-BAD-PcCdc50.3-TEV-His<sub>10</sub>*, *pYeDP60-BAD-TEV-PcATP2-PcCdc50.1-3C-GFP-TEV-His<sub>10</sub>* and *pYeDP60-BAD-TEV-PcATP2-PcCdc50.3-3C-GFP-TEV-His<sub>10</sub>*.

The presence of GFP at the C-terminal end of either PcATP2 or the PcCdc50 subunits allowed additional strategies for the study these proteins: (1) their localisation in the yeast *S. cerevisiae* by confocal microscopy, (2) their stability and heterodimeric association by fluorescence-detection size exclusion chromatography (FSEC), and (3) co-immunoprecipitation experiments aimed at revealing PcATP2/PcCdc50 association using nanobodies targeting the GFP.

### III-4-1 Analysis of the cellular localisation of PcATP2 and PcCdc50.1 subunit expressed in *S. cerevisiae* by confocal microscopy

We were interested in studying the possibly different localisation of PcATP2 and PcCdc50 subunits in the yeast *S. cerevisiae* after these proteins were expressed alone or co-expressed. A small-scale expression (as described previously in the section V-2-2-4) was performed to obtain cells expressing the GFP-tagged PcATP2 or the GFP-tagged

PcCdc50.1, either alone or co-expressed with their counterpart. Then, a small drop of cells resuspended in PBS was deposited on an agarose pad, a thin piece of agarose on top of a glass slide, to immobilize the cells (see section V-2-6).

Cells co-expressing Drs2p-GFP/Cdc50p were used as reference in these experiments since we already know that these two proteins can be nicely expressed using the same expression system. Previous intracellular localisation studies of Drs2p in *S. cerevisiae* showed that Drs2p in the presence of Cdc50p is localised in the trans Golgi network (TGN), characterized by the formation of punctual compartments close to the plasma membrane (S. Chen et al. 2006; Filigheddu et al. 2007). Our experiments agreed well with those previous studies, and we indeed observed that Drs2p-GFP was localised in small compartments close to the plasma membrane (white arrows in fig 30) which could be assigned as the TGN. We also found in others cells (without white arrows fig 30) an accumulation of these compartments containing Drs2p-GFP (fig 30). In this regard, it is also known that *S. cerevisiae* builds proliferated membranes in its cytoplasm during over-expression of recombinant membrane proteins, probably to accommodate these newly synthesized proteins (Bleve, Di Sansebastiano, and Grieco 2011; Wittekindt, Wurgler, and Sengstag 1995). From our confocal microscopy images (figure 30) , it is however difficult to determine the exact type of compartment implicated; in addition, it is also true that these membranes can also contain a proportion of unfolded or not-well folded proteins (Bleve, Di Sansebastiano, and Grieco 2011; Wright et al. 1988)



**Figure 30: Confocal microscopy image of *S. cerevisiae* cells co-expressing Drs2p-GFP-BAD/Cdc50p.**

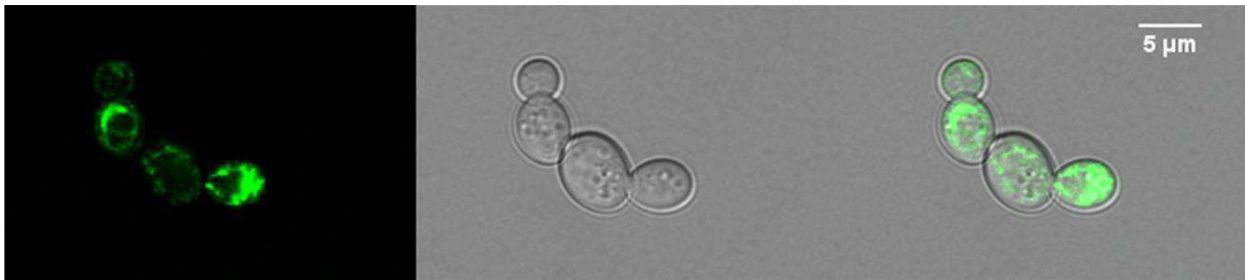
*Pictures were taken with a Leica SP8 confocal microscope, using the 63x oil objective, excitation wavelength 488 nm. Picture on left: GFP emission; Picture on the middle: brightfield; Picture on the right: merge pictures.*

The images obtained from cells expressing PcATP2-GFP-BAD alone or co-expressed with PcCdc50.1, are shown in figure 31. PcATP2-GFP-BAD expressed alone was found in large compartments but not as close to the plasma membrane as Drs2p-GFP (fig 31, panel A).



On the other hand, in cells co-expressing PcATP2-GFP-BAD/PcCdc50.1, PcATP2-GFP was localized in smaller compartments surrounding the nucleus (fig 31, panel B). We therefore observed a slightly difference in PcATP2-GFP localisation after co-expressing with PcCdc50.1. Fluorescence was spotted in smaller compartments and closer to the nucleus in cells co-expressing both proteins.

**A**



**B**

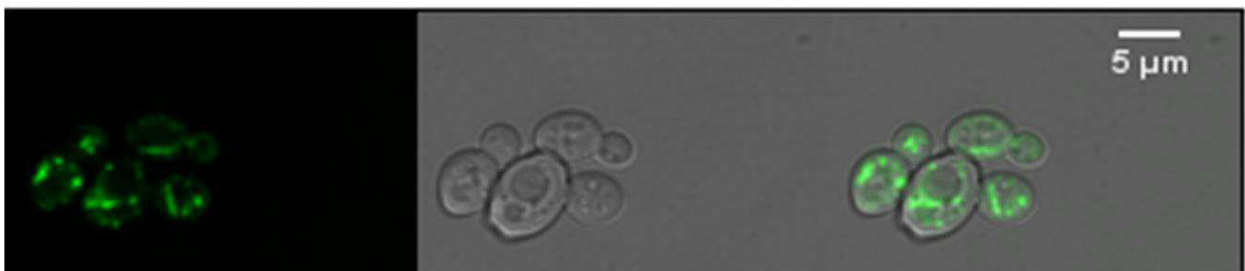


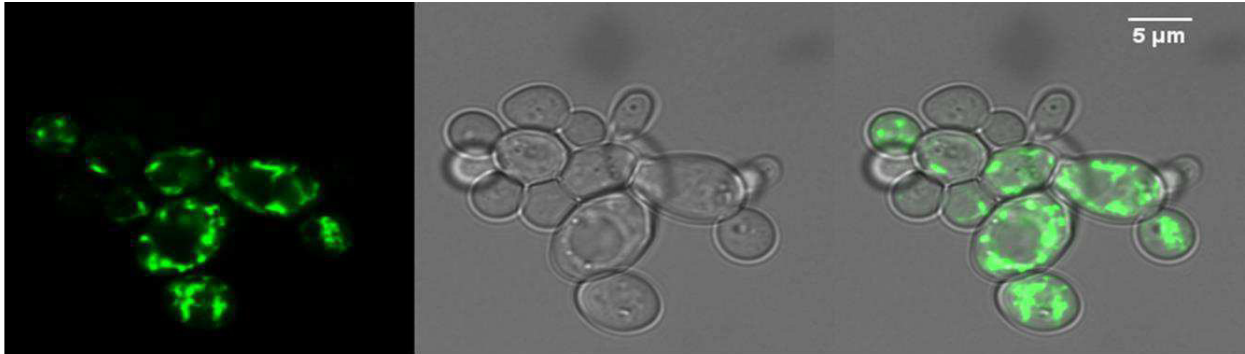
**Figure 31: Confocal microscopy images of *S. cerevisiae* cells expressing PcATP2-GFP-BAD alone or co-expressed with PcCdc50.1.**

*Pictures were taken with a Leica SP8 confocal microscope, using the 63x oil objective, excitation wavelength 488 nm. Panel A: PcATP2-GFP-BAD. Panel B: PcATP2-GFP-BAD-Cdc50.1-His<sub>10</sub>. Pictures on left: GFP emission; Pictures on the middle: brightfield; Pictures on the right: merge pictures.*

The previous experiments suggested a small effect of PcCdc50.1 on PcATP2-GFP localization. We then performed similar experiments but moving the GFP tag from PcATP2 to PcCdc50.1. The fluorescent images of cell expressing PcCdc50.1-GFP-His<sub>10</sub> alone (fig 32, panel A) show most of the fluorescence localized in large compartments but not close to the plasma membrane. When PcCdc50.1-GFP-His<sub>10</sub> was co-expressed with PcATP2, the fluorescence was localized in smaller dot-like compartments closer to the plasma membrane: again, the distribution of the GFP fluorescence in the cytoplasm of *S. cerevisiae* changes when PcATP2 and PcCdc50.1 are co-expressed. In this case, changes in compartment's shape and intracellular localization of PcCdc50.1-GFP after

co-expressing with PcATP2 are even easier to visualise than those obtained when GFP is fused to PcATP2 (Figures 31 and 32).

**A**



**B**



**Figure 32: Confocal microscopy images of *S. cerevisiae* expressing PcCdc50.1-GFP-His<sub>10</sub> alone or co-expressed with PcATP2.**

*Pictures were taken with a Leica SP8 confocal microscope, using the 63x oil objective, excitation wavelength 488 nm. Panel A: PcCdc50.1-GFP-His<sub>10</sub>. Panel B: PcATP2/PcCdc50.1-GFP. Pictures on left: GFP emission. Pictures on the middle: brightfield. Pictures on the right: merge pictures.*

It is however clear that irrespective of the protein to which GFP is bound, the subcellular localizations of PcATP2 or PcCdc50.1 after their co-expression with the respective partner do not seem to be identical. However, these experiments are unable to inform about the folding state of PcATP2 and PcCdc50.1, either alone or in the presence of each other. Rather, these experiments are only suggesting again that these two proteins interact in the membrane, probably during biogenesis, and that this interaction induces a change in the final membrane compartment destination of both proteins as judged by the small changes in the localisation and the shape of the GFP fluorescence between single and co-expression experiments (fig 31 and 32). To be certain of the localization and the type of membranes in which the proteins are found we need to use specific

fluorescent markers of the different intracellular compartments; however, this was not the original purpose of these experiments.

### **III-4-2 Fluorescence-detection size-exclusion chromatography of detergent-solubilized PcATP2 and PcCdc50 subunits**

Size-exclusion chromatography (SEC) coupled to fluorescence detection (or FSEC) has been used for a few years now to study the stability of heterogously expressed GFP-tagged membrane proteins in detergent (Errasti-Murugarren, Rodríguez-Banqueri, and Vázquez-Ibar 2017; Drew et al. 2008; Kawate and Gouaux 2006). FSEC permits an accurate evaluation of the degree of monodispersity in detergent of GFP-tagged membrane proteins before their purification by simply analyzing the shape and retention time of the chromatogram using the fluorescence of the GFP as readout (Kawate and Gouaux 2006). In addition, the high sensitivity of fluorescence allows to minimize the amount of sample required for each chromatogram. We therefore used this technique to investigate the behaviour of PcATP2, PcCdc50.1 and PcCdc50.3 after detergent solubilisation. As in the confocal microscopy studies, we aimed at evaluating the possible association between PcATP2 and the PcCdc50 subunits by analysing possible differences in the elution profiles of PcATP2 or PcCdc50 subunits expressed alone or co-expressed. We simultaneously aimed at analysing possible changes in the behaviour of the fluorescently labelled protein upon the presence or the absence of its partner. P3 membranes expressing PcATP2-GFP-BAD, PcCdc50.1-GFP-His<sub>10</sub> or PcCdc50.3-GFP-His<sub>10</sub> alone or co-expressed with the corresponding partner were solubilised at 2 mg/mL of total protein concentration with 10 mg/mL of DDM and 2 mg/mL of CHS during 1h at 20°C. After ultracentrifugation, the supernatant was injected into a SEC column and elution of GFP-fused proteins was monitored with the fluorescence detector. To analyse better the different results, the measured fluorescence was normalized in order to compare the shape and retention times of the different chromatograms.

In the chromatogram of detergent-solubilized PcATP2-GFP-BAD expressed alone (fig 33, panels A and B, dotted line) we first observed a small proportion of aggregated proteins present in the void volume, indicating that PcATP2-GFP-BAD has a small tendency to aggregate in these experimental conditions. Then, at around 11 mL of elution, we observed the peak corresponding to PcATP2-GFP-BAD elution in mixed micelles (fig 33,

grey shadows). The apparent  $M_w$  of PcATP2-GFP-BAD elution is much higher than the theoretical molecular weight ( $M_w$ ) of the protein (210 kDa), a common feature seen in this technique for detergent-solubilized membrane proteins, due to the large volume of the mixed detergent/cholesterol/lipid micelle surrounding the protein and the shape of the micelle. Indeed a detection corresponding to empty micelles of DDM/CHS can be observed at about an apparent  $M_w$  of 150 kDa (fig 33). This is due to light scattering and is actually the second peak observed between 15-16 mL of elution. The profile of PcATP2-GFP-BAD elution peak shape is somehow wide, indicating perhaps that the solubilized protein/micelle complex is not completely homogenous. When PcATP2-GFP-BAD is co-expressed with PcCdc50.1-His<sub>10</sub> (fig 33, panel A, continuous line), the proportion of aggregated proteins in the void volume is essentially similar. The peak corresponding to PcATP2-GFP-BAD elution is hardly shifted, and the presence of the subunit does not have a significant impact on the shape of the peak.

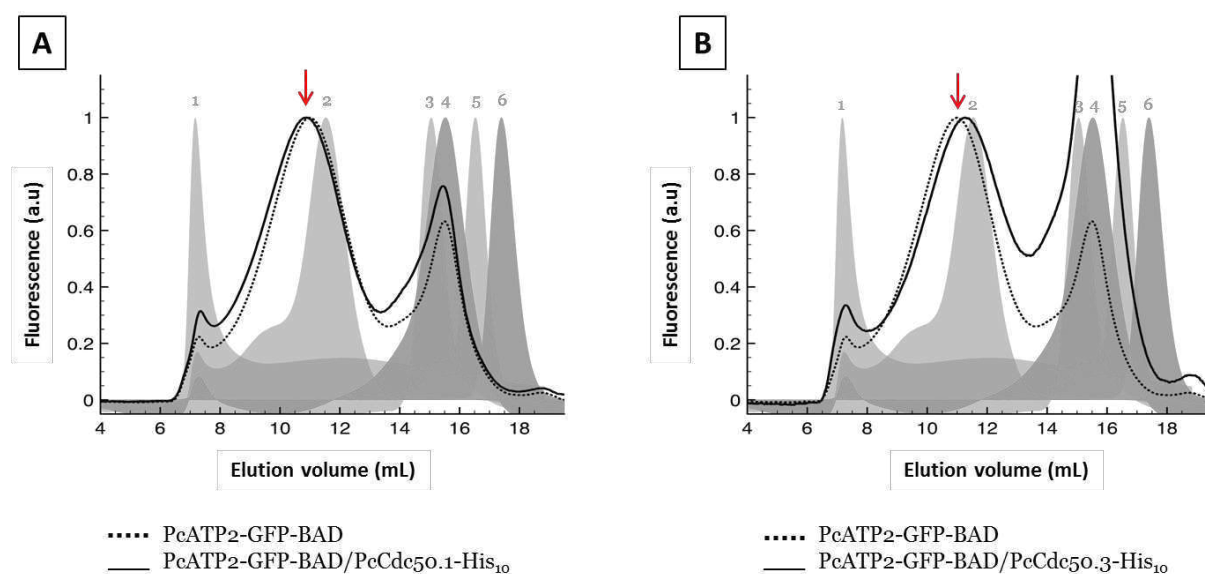


**Figure 33: Fluorescence-detection Size Exclusion Chromatography of solubilized P3 membranes expressing PcATP2-GFP-BAD alone or co-expressed with PcCdc50 subunits.**

2 mg/mL of P3 membranes were solubilized with 10 mg/mL of DDM and 2 mg/mL of CHS during 1h at 20°C. The supernatant obtained was loaded into a Superose 6 10/300 GL column coupled to an AKTA purifier and the JASCO FP 4025 fluorescence detector. Panel A: FSEC profile of the single-expression PcATP2-GFP-BAD and the co-expression PcATP2-GFP-BAD/PcCdc50.1-His<sub>10</sub>. Panel B: FSEC profile of the single-expression PcATP2-GFP-BAD and the co-expression PcATP2-GFP-BAD/PcCdc50.3-His<sub>10</sub>.  $M_w$  standard in grey shadows: 1: blue dextran (void volume); 2: Thyroglobulin  $M_w$  669 000; 3: Aldolase  $M_w$  158 000; 4: DDM/CHS micelles  $M_w$  124 000; 5: Ovalbumin  $M_w$  43 000; 6: sGFP  $M_w$  30 000.

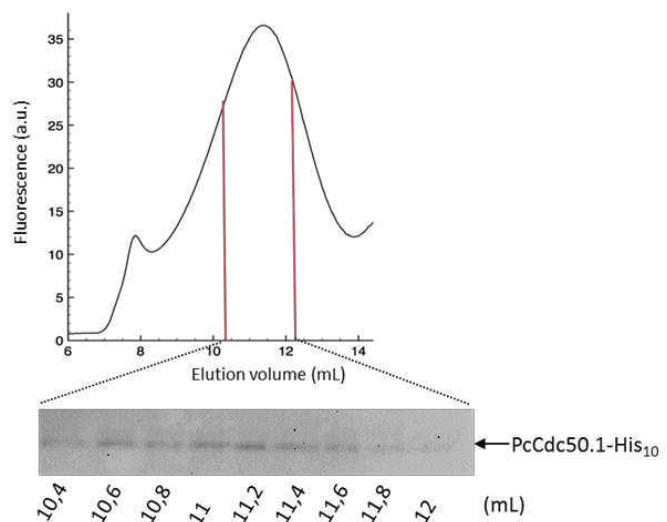
A quite different result is obtained when PcATP2-GFP-BAD is co-expressed with PcCdc50.3 (fig 33, panel B, continuous line), in this case a small shift towards the right is

observed (smaller Mw) but is more an artefact due to the saturating signal of the second peak.

To support the potential interaction between PcATP2 and PcCdc50.1, we collected fractions of the peak corresponding to PcATP2-GFP-BAD when co-expressed with PcCdc50.1-His<sub>10</sub>. These fractions were analysed by western blot to detect the presence of PcCdc50.1-His<sub>10</sub> (fig 34). PcCdc50.1-His<sub>10</sub> was detected in the nine deposited fractions at a level more or less in line with the intensity of the PcATP2-GFP-BAD elution pattern, suggesting its co-elution with PcATP2.

**Figure 34: Western blot analysis of the PcATP2-GFP-BAD elution peak co-expressed with PcCdc50.1.**

*Fractions of 200 µl were collected from the elution peak of PcATP2-GFP-BAD and the presence of the PcCdc50.1-His<sub>10</sub> was analysed by western blot. 9 fractions were deposited from 10.4 mL to 12 mL of elution. The western blot is detected by the His probe*



We also used FSEC to study elution of GFP-tagged PcCdc50 subunits in the absence or presence of PcATP2. The difference in size between the subunits alone, 75 kDa for PcCdc50.1-GFP-His<sub>10</sub> and 81 kDa for PcCdc50.3-GFP-His<sub>10</sub> and the BAD-PcATP2/PcCdc50-GFP-His<sub>10</sub> complexes, 255 kDa for BAD-PcATP2/PcCdc50.1-GFP-His<sub>10</sub> and 261 kDa for BAD-PcATP2/PcCdc50.3-GFP-His<sub>10</sub>, allows even clear potential separating in the FSEC chromatogram. Elution of PcCdc50.1-GFP-His<sub>10</sub> expressed alone, displayed a quite heterogeneous profile (fig 35, panel A, dotted line). A small amount of aggregated protein was seen in the void volume (fig 33), followed by a very wide peak corresponding to high Mw (probably, the peak around 13-14 mL of elution corresponds to the least aggregated forms of PcCdc50.1-GFP-His<sub>10</sub> in the mixed micelles). This result clearly suggests that the PcCdc50.1 subunit expressed alone was not stable in detergent or, perhaps, not well folded in the yeast membrane when PcATP2 is absent. The chromatogram of the second subunit PcCdc50.3-GFP-His<sub>10</sub> expressed alone (fig 35, panel B, dotted line) showed a similar profile as for PcCdc50.1-GFP-His<sub>10</sub>. We then did the

chromatograms of the GFP-tagged PcCdc50 subunits when co-expressed with PcATP2, expecting to see a main peak at around 11 mL corresponding to the complex, as the one seen previously for the complexes PcATP2-GFP-BAD/PcCdc50.1-His<sub>10</sub> or PcATP2-GFP-BAD/PcCdc50.3-His<sub>10</sub> (fig 33). However, we observed a completely different behaviour when PcCdc50.1-GFP-His<sub>10</sub> was co-expressed with PcATP2. The profile drastically changed with respect to the single-expression chromatogram (fig 35, panel A, continuous line); the elution peak of PcCdc50.1-GFP-His<sub>10</sub> was shifted to the right at about 14 mL, becoming narrow and sharp. This result is a clear indication of the positive effect of PcATP2 for the stabilisation of PcCdc50.1 either at the level of the membrane during biogenesis or after detergent solubilisation (or both). This stabilization effect of the flippase has been observed before in the human CDC50A and CDC50B subunits (van der Velden et al. 2010). Contrarily, when PcCdc50.3-GFP-His<sub>10</sub> was co-expressed with PcATP2, the elution profile of the subunits appeared quite similar to the single-expression chromatogram, although slightly shifted to the left (fig 35, panel B). Clearly, the presence of PcATP2 did not rescue PcCdc50.3-GFP from being aggregated.

In all FSECs experiments we normalized all the chromatograms in order to compare the shape of the elution profiles between the different experiments. However, quantitatively, the fluorescence signal obtained for the PcCdc50-GFP-His<sub>10</sub> subunits was about 10 times higher compared to the fluorescence signal obtained for PcATP2-GFP-BAD. This indicates that PcCdc50-GFP-His<sub>10</sub> expression yield is about ten times higher than that of PcATP2-GFP-BAD. Thereby, this implies that the maximum signal expected for the BAD-PcATP2/PcCdc50.1-GFP-His<sub>10</sub> complex in the chromatogram of figure 35 would be about 0.1 and, therefore, it would be completely hidden by the shoulder of the main elution peaks of both subunits.

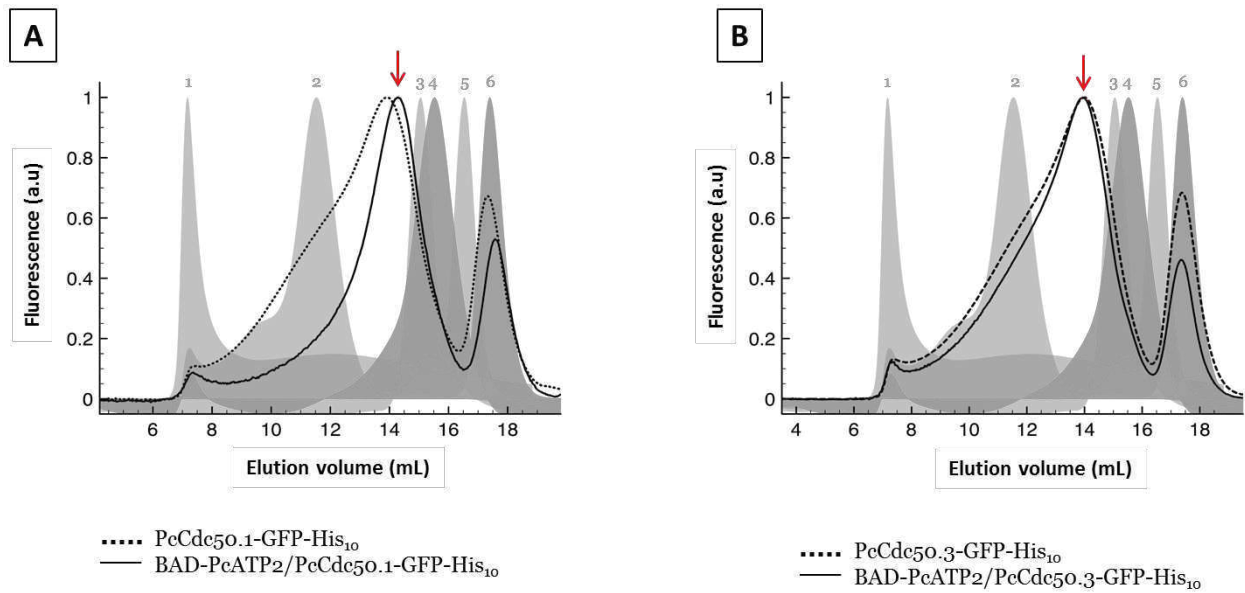


**Figure 35: Fluorescence-detection Size Exclusion Chromatography of solubilized P3 membranes expressing GFP-tagged PcCdc50 subunits alone or co-expressed with PcATP2.**

5 mg/mL of P3 membranes were solubilized with 20 mg/mL of DDM and 4 mg/mL of CHS during 1h at 20°C. The supernatant obtained was loaded into a Superose 6 10/300 GL column coupled to an AKTA purifier and the JASCO FP 4025 fluorescence detector. Panel A: FSEC profile of the single-expression PcCdc50.1-GFP-His<sub>10</sub> and co-expression BAD-PcATP2/PcCdc50.1-GFP. Panel B: FSEC profile of the single-expression PcCdc50.3-GFP and co-expression BAD-PcATP2/PcCdc50.3-GFP. Mw standard in grey shadow: 1: blue dextran (void volume); 2: Thyroglobulin Mw 669 000; 3: Aldolase Mw 158 000; 4: DDM/CHS micelles Mw 124 000; 5: Ovalbumin Mw 43 000; 6: sGFP Mw 30 000.

### III-4-3 Determination of the interaction by co-immunoprecipitation

In order to demonstrate the association between PcATP2 and the PcCdc50 subunits in a more direct way, we decided to do a co-immunoprecipitation assay. Our approach consisted in immobilizing on agarose beads detergent-solubilized PcATP2-GFP co-expressed with the PcCdc50 subunits. After extensive washing of the proteins bound to the beads and their elution, the eluted PcATP2-GFP will contain its corresponding co-expressed subunit if the two proteins are forming a heterodimer (and if this heterodimer is conserved in detergent micelles). To immobilize PcATP2-GFP we used agarose beads coupled to anti-GFP nanobodies (or nanoGFP). Nanobodies are small single-domain antibodies from camelids of about 12-15 kDa. Their small size, their remarkable stability in solution and the possibility to produce large amounts of them in recombinant hosts like *E. coli*, make them very useful tools in protein research, for instance, in immunoprecipitation studies or as co-crystallization helpers (Traenkle et al. 2016; Rothbauer et al. 2008). NanoGFP recognize specifically the GFP with a binding affinity in the nanomolar range (Kubala et al. 2010). In these experiments we used the

co-expression constructs PcATP2-GFP-BAD/PcCdc50.1-His<sub>10</sub> and PcATP2-GFP-BAD/PcCdc50.3-His<sub>10</sub>. In addition and, as negative controls, the same co-expression constructs without the GFP were also tested, (BAD-PcATP2/PcCdc50.1-His<sub>10</sub> and BAD-PcATP2/PcCdc50.3-His<sub>10</sub>), providing the non-specific binding background of the detergent-solubilized membranes to the nanoGFP-coupled beads. The positive control used to verify the association flippase/subunit was the co-expression Drs2p-GFP-BAD/Cdc50p-His<sub>10</sub>. As in the FSEC studies, P3 membrane fractions at 2 mg/mL of total protein concentration were solubilised with 10 mg/mL of DDM and 2 mg/mL of CHS during 1 h at 20°C. After ultracentrifugation, the supernatant recovered was incubated with the beads coupled to the nanoGFP. After the washing steps, the proteins bound to the resin were eluted with a low pH buffer and samples were analysed by western blot.

As expected, the elution of the co-immunoprecipitation experiment with co-expressed Drs2p-GFP-BAD/Cdc50p-His<sub>10</sub> (fig. 36, panel A, lane 9), shows that Cdc50p-His<sub>10</sub> is co-eluted with Drs2p-GFP-BAD, proving the feasibility of this assay to detect a P4-ATPase/Cdc50 association. Next, in the negative controls using co-expressed BAD-PcATP2/PcCdc50.1-His<sub>10</sub> (fig 36, panel A, lane 8) and BAD-PcATP2/PcCdc50.3-His<sub>10</sub> (fig. 36, panel B, lane 8), no PcCdc50 subunit is detected in the elutions, indicating that no specific interactions between either, the BAD or the His<sub>10</sub> tag, and the nanoGFP-coupled beads did occur. In these experiments, BAD-PcATP2 is revealed with an antibody against the GFP, and therefore the BAD-PcATP2 cannot be detected (fig 36, panel A and B, lanes 8). Nevertheless, further verification of the absence of BAD-PcATP2 in these samples was done using the biotin probe in the western blot (data not shown).

In the experiments corresponding to the co-expression of PcATP2-GFP/PcCdc50.1-His<sub>10</sub> (fig 36, panel A, lanes 1 to 4), the presence of PcATP2 is difficult to see in the detergent-solubilized supernatant (sample before adding to the nanoGFP-coupled beads); however, the band corresponding to PcATP2-GFP-BAD (about 210 kDa, fig 36, panel A lane 4) is clearly detected in the elution fraction. In addition, the band corresponding to PcCdc50.1-His<sub>10</sub> is also detected in the same elution fraction (fig 36, panel A, lane 4). Given that the control experiments demonstrated that non-specific binding of PcCdc50.1-His<sub>10</sub> with the nanoGFP-coupled beads does not occur, this result strongly support the existence of the heteromeric complex between PcATP2 and PcCdc50.1.



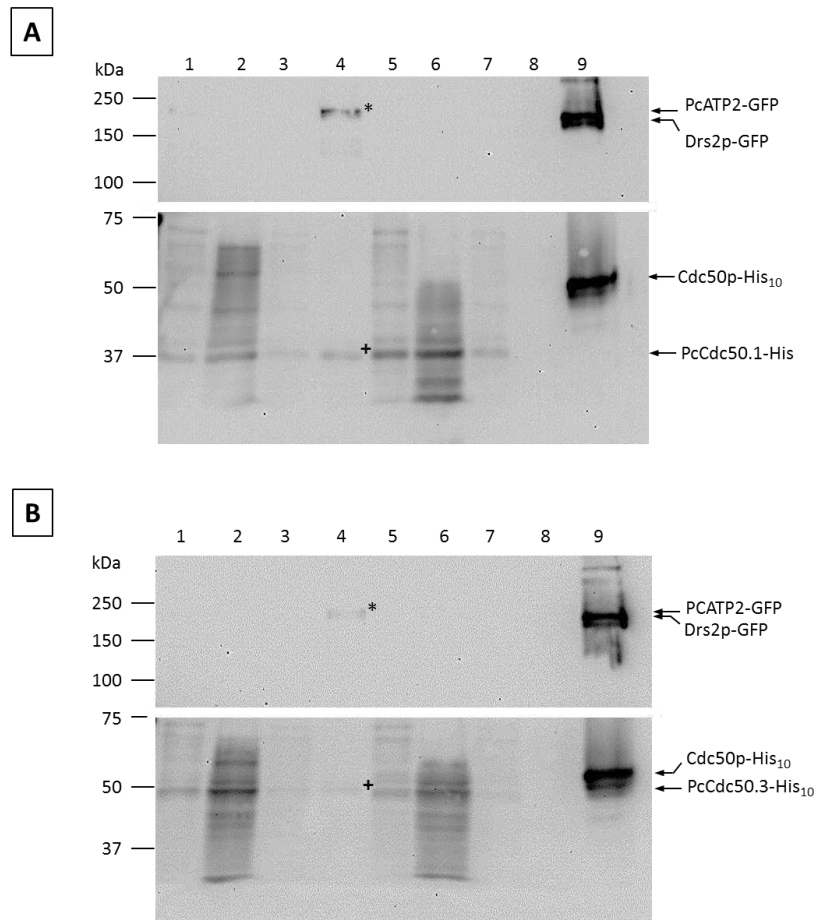


**Figure 36: Western blot analysis of co-immunoprecipitation of PcATP2-GFP-BAD/PcCdc50.1-His<sub>10</sub> and PcATP2-GFP-BAD/PcCdc50.3-His<sub>10</sub>.**

The top of the blot was revealed with an antibody against the GFP to detect the PcATP2-GFP-BAD and the bottom with a histidine probe to detect the PcCdc50-His<sub>10</sub>. Panel A: co-immunoprecipitation of PcATP2-GFP-BAD and PcCdc50.1-His<sub>10</sub>. Lanes 1 to 4: PcATP2-GFP-BAD/PcCdc50.1-His<sub>10</sub> respectively: supernatant, flowthrough, washings, elution; Lanes 5 to 8: negative control BAD-ATP2/Cdc50.1-His<sub>10</sub>; fraction corresponding respectively to, supernatant, flowthrough, washings, elution; Lane 9: eluted Drs2p-GFP-BAD/Cdc50p-His<sub>10</sub>. Panel B: co-immunoprecipitation of PcATP2-GFP-BAD and PcCdc50.3-His<sub>10</sub>. Lanes 1 to 4: PcATP2-GFP-BAD/PcCdc50.3-His<sub>10</sub>; fractions corresponding respectively to, supernatant, flowthrough, washings, elution; Lanes 5 to 8: negative control BAD-PcATP2/PcCdc50.3; fractions corresponding respectively to, supernatant, flowthrough, washings, elution; Lane 9: eluted Drs2p-GFP-BAD/Cdc50p-His<sub>10</sub>.

Similarly, in the experiments with co-expressed PcATP2-GFP-BAD/PcCdc50.3-His<sub>10</sub>, weak but clear bands corresponding to PcATP2-GFP and PcCdc50.3-His<sub>10</sub> can also be seen in the elution fraction (fig 36, panel B, lane 4). Clearly there is a very low amount of protein in this elution fraction compared to the experiment with co-expressed PcATP2-GFP and PcCdc50.1-His<sub>10</sub> (fig 36), even though the experimental conditions were identical. However, the amount of PcATP2-GFP and PcCdc50.3-His<sub>10</sub> present in the P3 membrane fraction is substantially lower than the amount found in P3 membranes co-expressing PcATP2-GFP and PcCdc50.1-His<sub>10</sub>. In addition to this, and as observed in the

previous chapter, the yield of solubilisation of PcATP2-GFP and PcCdc50.3-His<sub>10</sub> in this membrane fraction is also much lower than the one of PcATP2-GFP and PcCdc50.1-His<sub>10</sub>.

With these experiments we confirmed that the agarose beads coupled to the nanoGFP can specifically recognize the GFP fused to PcATP2, since we found no binding of either PcATP2 or PcCdc50 subunits when these proteins were only tagged, respectively, with the BAD or the His<sub>10</sub> tag. More importantly, these experiments fairly demonstrated that PcATP2 is able to associate with both PcCdc50.1 and PcCdc50.3, and, as also seen in the FSEC experiments, that these complexes are not dissociated in detergent micelles.

### III-4-4 Discussion

The introduction of the GFP as a reporter allowed the use of more sensitive techniques to assess the association between PcATP2 and the two PcCdc50 subunits. We have exploited the GFP tag to directly demonstrate their association by FSEC and immunoprecipitation, and to analyse how this association affects the stability of both subunits (as judged by the FSEC elution profiles) after detergent solubilisation. Analysis by confocal microscopy of the intracellular localisation in *S. cerevisiae* of PcATP2-GFP-BAD or PcCdc50.1-GFP-His<sub>10</sub>, either, alone or co-expressed, showed that in both cases the proteins are present in compartments that look like proliferated membranes deriving from the ER (fig 31 and fig 32). Studies of *Plasmodium*-infected erythrocytes suggested that ATP2 of *P. berghei* is targeted to the parasite's plasma membrane (Kenthirapalan et al. 2016). The fact that both proteins are found in these compartments might be due to some of them encountering some problems during biogenesis and protein folding, since unfolded or not well-folded proteins are retained in the ER and redirected to the degradation pathways of the yeast (Ellgaard and Helenius 2003; Blevé, Di Sansebastiano, and Grieco 2011). This would explain the fact that the solubilisation efficiency is only about 20 %-30%, if only properly folded proteins can be solubilized by a mild detergent like DDM (Thomas and Tate 2014). We also observed some small differences in the subcellular localization of PcCdc50.1-GFP-His<sub>10</sub> when co-expressed with PcATP2 (fig 32). However, PcATP2-GFP intracellular localization did not change drastically after co-expressing with PcCdc50.1 (fig 31). This different behaviour was also noticed in the FSEC experiments. The difference in the shape and intensity of the peaks corresponding to PcATP2-GFP-BAD elution, alone or co-expressed with PcCdc50 subunits were not substantially different (fig 33, panel A). In contrast, the elution profile

of PcCdc50.1-GFP changed dramatically from highly polydisperse to monodisperse after co-expressing this subunit with GFP-untagged PcATP2 (fig 35, panel A). From these experiments we can suppose that PcCdc50.1 requires the presence of PcATP2, at least in detergent micelles, to avoid its aggregation. Our experimental data is not sufficient to confirm that PcCdc50.1 is already misfolded in the yeast membranes before detergent solubilisation when expressed alone. However the small changes observed in the confocal microscopy studies between PcCdc50.1-GFP single expression and PcATP2/PcCdc50.1-GFP co-expression suggest some misfolding issues of PcCdc50.1 when expressed alone.

When we tried to analyse directly the association of PcATP2 and PcCdc50 subunits, we found that both subunits were able to associate with PcATP2 as judged from the co-immunoprecipitation assays (fig 36). FSEC analyses were also in agreement with the previous assays, since a small shift in the elution peak of PcATP2-GFP-BAD towards a higher molecular weight was observed when it was co-expressed with either PcCdc50.1 (fig 33, panel A). Moreover, an analysis by western blot of fractions corresponding to the PcATP2-GFP-BAD elution confirms the presence of PcCdc50.1-His<sub>10</sub> (fig 34). However, when we look at the results obtained when the GFP tag was moved from PcATP2 to the PcCdc50 subunits we could not distinguish in the chromatograms of the two co-expression experiments any peak corresponding to the complex PcATP2/PcCdc50. This was most likely due to the different level of expression between PcATP2 and the two PcCdc50 subunits. The total intensity of GFP fluorescence in the FSEC experiments indicated that the PcCdc50 subunits are expressed, at least, ten times more than PcATP2; therefore, the monomeric peak of the GFP-tagged PcCdc50 subunits completely hides the elution of the putative PcATP2/PcCdc50.1-GFP or PcATP2/PcCdc50.3-GFP complexes (fig 35). Interestingly, we observed also by FSEC that PcCdc50.1-GFP-His<sub>10</sub> and PcCdc50.3-GFP-His<sub>10</sub> did not behave similarly in detergent micelles when co-expressed with PcATP2: PcCdc50.1-GFP-His<sub>10</sub> elution profile became monodisperse, and the elution profile of PcCdc50.3-GFP-His<sub>10</sub> remained highly polydisperse (fig 35). Despite the fact that the two PcCdc50 subunits can be associated with PcATP2, the presence of PcATP2 has not the same effect with regard the stability of the two subunits in detergent micelles, suggesting that the association PcATP2/PcCdc50.1 is more stable or less prone to aggregate than the PcATP2/PcCdc50.3 association, at least, when co-expressed in yeast. In agreement with this, we found that both PcATP2 and PcCdc50.3,

when co-expressed, are mostly found in the P2 membrane fraction, a fraction more resistant to solubilisation by mild detergents like DDM than P3 membrane fraction. On the other hand, both PcATP2 and PcCdc50.1 were found in the P3 membrane fraction and solubilized with DDM and CHS. As discussed earlier, glycosylation of PcCdc50.3 might play an essential yet unknown role during association with PcATP2 and/or for stabilizing the complex. However, since the glycosylation form of PcCdc50.3 was not solubilized in none of the membrane fractions, we were unable to test experimentally this hypothesis.

### **III-5 Purification and functional characterization of PcATP2/PcCdc50.1 complex**

All the results obtained support the idea that the PcATP2/PcCdc50.1 complex is the best candidate for purification and functional characterization. Given the low expression yield of this complex together with the relatively low solubilisation efficiency (not higher than 20 %) of the protein fraction present in the P3 membrane fraction, we decided to set up a new affinity purification protocol. PcATP2-GFP/PcCdc50.1-His<sub>10</sub> purification was performed using a home-made affinity resin by covalently coupling agarose beads with nanoGFP nanobodies produced in our laboratory. The resulting purified PcATP2/PcCdc50.1 was functionally tested using two different assays in order to characterize the P-type ATPase-like functional behaviour of PcATP2.

#### **III-5-1 Purification of PcATP2/PcCdc50.1**

The already reported immunoprecipitation assays demonstrated the ability of the nanoGFP nanobodies coupled to agarose beads to trap specifically the PcATP2-GFP/PcCdc50.1-His<sub>10</sub> complex. Therefore, we decided to apply the same strategy to purify this complex using the co-expression vector pYeDP60-PcATP2-TEV-GFP-BAD-PcCdc50.1-TEV-His<sub>10</sub>. Unlike immunoprecipitation assays, purification requires much larger quantities of agarose beads coupled to nanoGFP, therefore we decided to prepare our own affinity resin. NanoGFP was produced in *E. coli* and after purification it was covalently coupled to NHS-activated agarose resin (see section V-2-4-6-b). Using a standard GFP-tagged membrane protein, we calculated that the binding capacity of our agarose beads coupled to nanoGFP was around 300 micrograms of protein per mL of beads. P3 membranes expressing PcATP2-GFP/PcCdc50.1-His<sub>10</sub> were solubilised as

previously described, and the solubilised material was then incubated with the nanoGFP resin. To elute the complex out of the column we incubated the beads with the TEV protease overnight at 4°C. Unfortunately, the analysis of the elution fractions by Coomassie blue staining and western blot showed that the proteins were still bound to the beads after protease incubation, suggesting that the TEV protease digestion did not work (data not shown). To verify the ability of the TEV protease to cleave between the C-terminal end of PcATP2 and the GFP, we performed the cleavage enzymatic assay directly on the P3 membrane fractions co-expressing PcATP2-GFP-BAD/PcCdc50.1-His<sub>10</sub>. It appeared that the TEV protease was able to cleave the His<sub>10</sub> tag of PcCdc50.1 (there is an identical TEV site between the C-terminal end of PcCdc50.1 and the His<sub>10</sub> tag); however, the protease was unable to cleave off the GFP-BAD peptide fused to PcATP2 at the C-terminal end (data not shown). This result explained the incapacity of the TEV digestion to elute the complex from the agarose beads. In view of this, we decided to add extra amino acids (or spacers) between the protease cleavage site and both the C-terminal end of PcATP2 and the N-terminal end of the GFP. At the same time we changed the TEV protease site for the 3C protease cleavage site and put a STOP codon after the GFP, resulting in the new vector: pYeDP60-PcATP2-3C-GFP-PcCdc50.1-TEV-His<sub>10</sub> schematized in figure 37, panel A.

Using this new construct, we carried out a new purification attempt following the same procedure as before. This time, the elution of the PcATP2/PcCdc50.1-His<sub>10</sub> complex was performed by the addition of the 3C protease in the beads to cleave off the GFP fused at the C-terminal end of PcATP2 (fig 37). In the buffer used during this overnight digestion, together with DDM and CHS, we included the phospholipid DOPC to hopefully prevent protein aggregation. The eluted fraction was concentrated, and the different steps of the purification were analysed by Coomassie blue stained SDS-PAGE gel and western blot (fig 37). In the Coomassie blue stained gel (fig 37, panel B) we observed a band between 150 kDa and 250 kDa that corresponds to the size expected for PcATP2 without the GFP, indicating that we were indeed able to elute PcATP2 (hence the complex) from the resin with the 3C protease. We also observed three other bands corresponding to different forms of the well-known 3C protease (monomer at about 48 kDa, dimer around 75 kDa and trimer around 100 kDa), as well a fourth one at 50 kDa which must be a protein contaminant. The amount of protein in the eluted fraction was not sufficient to reveal PcCdc50.1 after Coomassie blue staining (fig 37, panel B, lane E), but we were able to

detect its presence by western blot thanks to the His<sub>10</sub> tag in it (fig 37, panel C, lane E). In this blot we also detect the 3C-Protease because it contains a His-tag as well. After enzymatic digestion and the first elution, we did a second elution using a low-pH buffer to try to remove some of the proteins which may remain attached to the beads after the previous enzymatic digestion. After this low-pH elution we found some digested or non-tagged PcATP2 still attached to the beads (fig 37, panel B, lane Re), and could reveal with an antibody against GFP the residual presence of non-cleaved protein bound to the resin (fig 37, panel C, lane Re). Finally, we also observed a band between 100 and 150 kDa that may correspond to some N-terminal proteolysed form of PcATP2 on the resin. Thus, during the elution we lost a non-negligible portion of the complex due to the fact that the 3C protease does not cleave 100 % of the PcATP2-GFP bound to the beads, and a small proportion of digested PcATP2 remained attached to the beads.

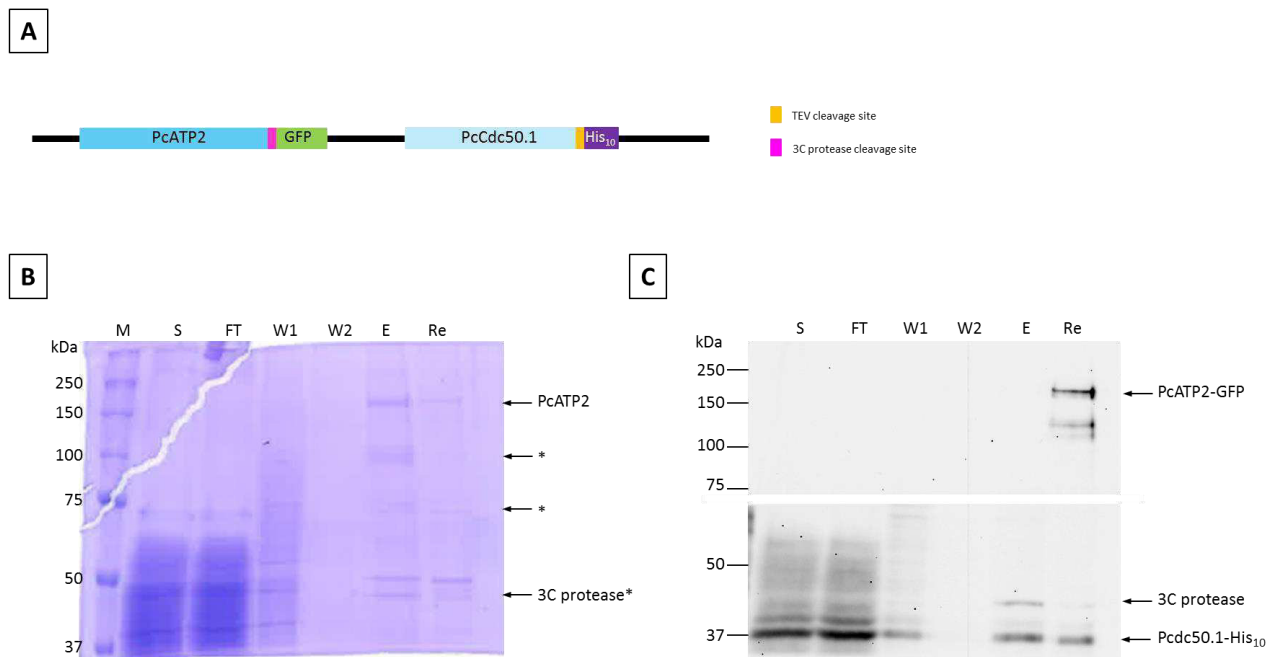


**Figure 37: Purification of PcATP2/PcCdc50.1.**

Panel A: scheme of the new pYeDP60-PcATP2-3C-GFP-PcCdc50.1-TEV-His<sub>10</sub> vector. Panel B: Coomassie blue staining of the different purification steps. Panel C: western blot analysis of the different purification steps, the top of the blot was revealed by an anti-GFP antibody and the bottom by the His probe. S: supernatant after solubilisation and ultracentrifugation; FT: column flow through; W1: washing number 1; W2: washing number 2; E: elution after 3C protease digestion; the two elutions pooled and concentrated 6x; Re: resin after the two elutions, elution of the proteins by acidic buffer. 3C protease~ 47.8kD, PcATP2 ~170 kDa; PcCdc50.1~45 kDa (run at 37 kDa).

We further analysed the protein content bound to the beads before and after elution by enzymatic digestion in another purification experiment of PcATP2-GFP/PcCdc50.1

complex (fig 38). Some beads with bound PcATP2-GFP/PcCdc50.1, right before adding the 3C-protease to elute the complex, were washed with low-pH buffer to analyse the protein content bound to the beads at this stage. We observed clearly in a Coomassie blue staining gel the band corresponding to PcATP2-GFP as well as another band below 150 kDa which could correspond to the N-terminally proteolysed form of PcATP2-GFP (fig 38, lane Re). After elution by 3C-protease digestion, PcATP2 without the GFP tag is again perfectly visible in the gel; indeed we can see clearly the shift due to the cleavage of the tag (fig 38). This eluted fraction also contains the band corresponding to the monomer of the 3C protease (here, the other forms of the 3C protease were not visible for some unknown reasons). As for the previous purification (fig 37), we washed the beads after enzymatic elution with a low-pH buffer and analysed what was left bound to the beads (fig 38, lane Re). Again we saw the presence of both the non-cleaved PcATP2-GFP and the N-terminally proteolysed form. However, in this new experiment we could not detect digested PcATP2. Overall, despite the fact that we cannot recover 100 % of PcATP2-GFP bound to the beads after 3C-protease digestion, we can obtain in the final eluted fraction (fig 38, lane E) an enough quantity of purified complex to initiate its functional characterization using the methodologies available in our laboratory.

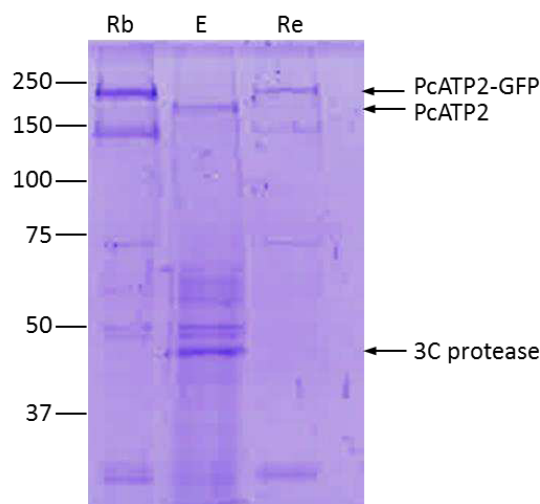


**Figure 38: Analysis of PcATP2/PcCdc50.1 bound to the nanoGFP resin and their elution by Coomassie blue staining.**

*Rb: resin with bound proteins after the washings; E: elution (the two elutions pooled and concentrated 12x); Re: resin after elution of the proteins remained bound with low pH buffer.*

### **III-5-2 Towards the functional characterization of purified PcATP2/PcCdc50.1 complex in detergent micelles.**

Despite the low amount of protein obtained after purification of the PcATP2/PcCdc50.1 complex, we initiated the functional characterization of this complex in detergent micelles using two different functional assays: (1) autophosphorylation of PcATP2 using radioactive ATP ( $[\gamma\text{-}^{32}\text{P}]$  ATP), and (2) ATPase activity of PcATP2 using an enzyme-coupled assay (Sehgal, Olesen, and Møller 2016). To evaluate the specific activity of purified PcATP2 versus a possible background due to protein contaminants, we undertook the construction and expression of two predicted non-functional mutants of PcATP2, the E235Q and the D596N. In other P-type ATPases these mutations are known to impair, respectively, dephosphorylation and phosphorylation of the enzyme during the catalytic cycle.

#### **1. Construction of non-functional mutants of PcATP2**

A unique feature of P-type ATPases during transport is the transient autophosphorylation of the well-conserved aspartate in the P domain followed by its dephosphorylation catalysed by a glutamate residue in the A domain (fig 5). The mutation on these two fundamental residues leads to the loss of enzyme's activity by impairing critical steps of the transport cycle. Logically, these mutants are excellent negative controls to assess the specific ATPase activity of our purified PcATP2/PcCdc50.1 complex. Consequently, we made these two mutants in PcATP2, the E235Q mutation in the A domain impairing the dephosphorylation and the D596N mutation in the P domain impairing the phosphorylation.

The expression of these PcATP2 mutants (E235Q or D596N) was determined by western blot in both the P2 and the P3 membrane fractions and compared to the wild type expression profile figure 39. First, a band at the expected size (PcATP2 + GFP) was observed corresponding to the two mutants, showing that both mutants can be expressed. In addition, as seen at the bottom of the blot, expression of PcCdc50.1 was also observed. The distribution of E235Q or D596N-PcATP2 and PcCdc50.1 between the P2 and P3 membrane fractions is similar as wild-type PcATP2 (fig 39). We however detected some small differences: for wild type we have about 60% of PcATP2 and PcCdc50.1 in the P2 fraction and 40% of both proteins in the P3, whereas in both E235Q and D596N mutants, it seems an equal repartition of the protein between the two



membrane fractions (fig 39). This result might suggest that these non-functional mutants of PcATP2 could be slightly more stable than the wild type.

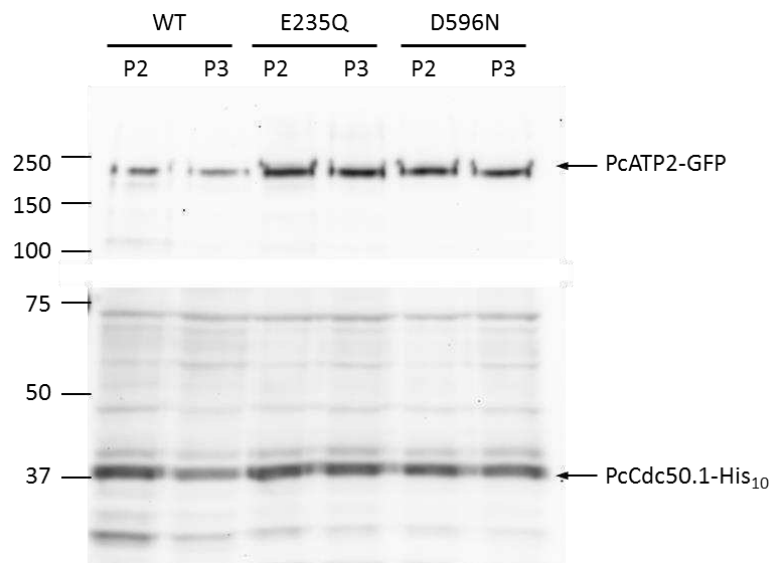


**Figure 39: Western blot analysis of PcATP2/PcCdc50.1 wild type, E235Q-PcATP2/PcCdc50.1 and D596N-PcATP2/PcCdc50.1 co-expression.**

*10µg of total proteins were loaded on the gel. The top of the blot was revealed with an antibody against GFP to detect the flippase, and the bottom was revealed with a histidine probe to detect the subunit. P2 and P3 membranes were analyzed after membrane fractionation. WT: wild type co-expression PcATP2/PcCdc50.1; E235Q: the co-expression PcATP2-E235Q/PcCdc50.1; D596N: the co-expression PcATP2-D596N/PcCdc50.1.*

We then undertook the purification of the D596N-PcATP2 mutant in complex with PcCdc50.1, in order to obtain the control for the phosphorylation assays. The D596N-PcATP2/PcCdc50.1 complex was purified in the same manner as the wild type PcATP2/PcCdc50.1. As before, the different steps of the purification were analysed by Coomassie blue staining SDS-PAGE and western blot. On the figure 40, panel A, the band corresponding to D596N-PcATP2 is visible in the elution fraction at the expected size. As in wild type purification, the three bands corresponding to the electrophoretic mobilities of the 3C protease and the protein contaminant at about 50 kDa were also visible. In the western blot of the different purification steps (fig 40, panel B), we can observe that PcCdc50.1-His<sub>10</sub> is also co-eluted with D596N-PcATP2. As expected, a proportion of the cleaved protein was still bound to the beads after the first elution (fig 40, panel A) and as well as a fraction of non-digested D596N-PcATP2-GFP (fig 40, panel B).

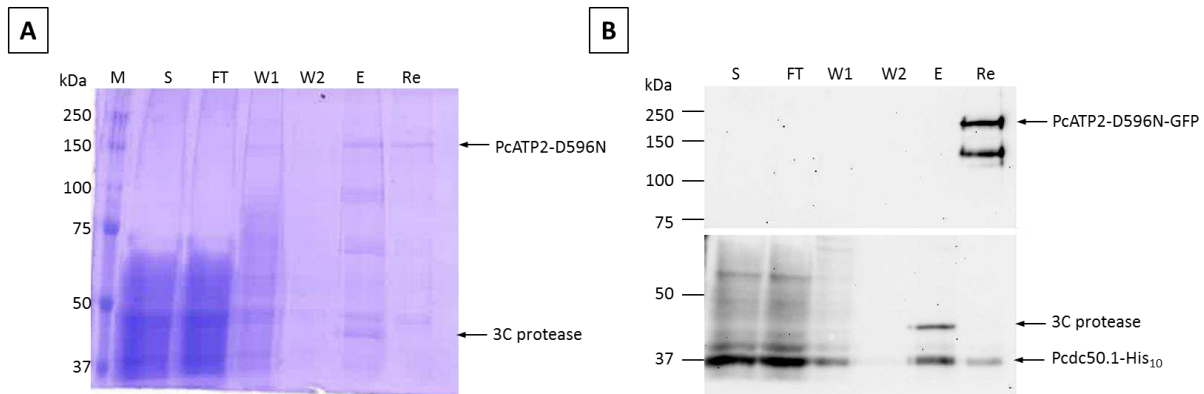


**Figure 40: Analysis of the purification of D596N-PcATP2-GFP/PcCdc50.1-His<sub>10</sub>.**

10 $\mu$ l of each sample were loaded on the gels. Panel A: Coomassie blue staining of the different purification steps. Panel B: western blot analysis of the different purification steps. The top of the gel was revealed with an antibody against the GFP to detect the flippase, and the bottom was revealed with a histidine probe to detect the subunit. S: supernatant after solubilisation and ultracentrifugation; FT: flow through; W1: washing number 1; W2: washing number 2; E: elution, the two elutions pooled and concentrated 12x; Re: resin after elution of the proteins remained bound with low buffer.

These results show that the two mutants of PcATP2, E235Q and D596N, expected to be functionally deficient, can be co-expressed with PcCdc50.1 in *S. cerevisiae*. Moreover, we managed to purify the D596N mutant in complex with PcCdc50.1-His<sub>10</sub> in a yield similar as wild type.

## 2. Phosphorylation assay of purified PcATP2

Purified PcATP2 was subjected to an *in vitro* autophosphorylation assay using radioactive [ $\gamma$ -<sup>32</sup>P] ATP. This is a sensitive technique which does not require a large amount of protein and allows the detection of the phosphorylated intermediate of the protein during the catalytic cycle (fig 6) (Azouaoui et al. 2017). The purified protein is incubated for 2 min with the radiolabelled ATP and the reaction is stopped by the addition of trichloroacetic acid (TCA). The samples are then subjected to SDS-PAGE using an acidic or Sarkadi gel (Sarkadi et al. 1988) because the formed aspartyl phosphate is only stable in acidic conditions and rapidly hydrolyzed in alkaline conditions. After Coomassie blue staining and drying of the gel, the radioactive [ $\gamma$ -<sup>32</sup>P] bound to PcATP2 in the gel was measured by autoradiography in a phosphoimager. This assay was performed on the following purified complexes: wild-type PcATP2/PcCdc50.1-His<sub>10</sub>, D596N-PcATP2 /PcCdc50.1-His<sub>10</sub> and, as positive control, human ATP8B1/CDC50A complex (kindly given by Thibaud Dieudonné) expressed in *S. cerevisiae* as well. As negative control in the assays with the PcATP2/PcCdc50.1

complexes, we added the well-known ATPase inhibitor beryllium trifluoride ( $\text{BeF}_3^-$ ) (Olesen et al. 2007). This molecule is not only an inhibitor of P-type ATPases, but also inhibits other ATP-binding proteins because it competes with ATP for the ATP-binding site of the protein; in our case, situated in the N domain of PcATP2. We also tested whether the presence of two drugs from the malaria box, MMV007224 and MMV665852 (Spangenberg et al. 2013) could affect autophosphorylation of purified PcATP2. A recent study based on chemogenomics has predicted an inhibitory effect of these two drugs on ATP2 (as mentioned in the introduction) (Cowell et al. 2018). Those two drugs were also tested on ATP8B1 autophosphorylation.

On the Coomassie blue stained gel, among other bands, the bands corresponding to wild type PcATP2 and the D596N mutant were visible at the expected size  $\sim 150$  kDa (fig 41, panel A, lanes 1 to 5). We also again observed the different electrophoretic versions of the 3C Protease also seen during our first purification (fig 37). The pyruvate kinase, 57 kDa, was used as loading control of the amount of protein. There was less protein in the lane corresponding to the D596N mutant, and this should be taken into account for the analysis of the phosphorylation. ATP8B1 was also visible at the expected size ( $\sim 140$  kDa).

Panel B in figure 37 then shows the results of a autoradiography of this gel revealing the phosphorylated proteins. In the lanes containing both, wild-type PcATP2 and D596N-PcATP2 (fig 41, panel B, lanes 1 to 5), a main phosphorylated band is observed at a similar mobility that phosphorylated ATP8B1 (fig 41, panel B, lanes 6 to 8), around 140 kDa. This band is not visible in the Coomassie blue staining of the same gel (fig 41, panel A, lanes 6 to 8), and, it is unlikely to correspond to a proteolysed form of PcATP2. In addition, and since the same band is also detected in the lane loaded with D596N-PcATP2, a predicted non-phosphorylatable variant of PcATP2, we can conclude that this band does not correspond to PcATP2, but rather to a phosphorylated protein contaminant, indeed, the presence of  $\text{BeF}_3^-$  causes a small decrease of phosphorylation (fig 41, panel B, line 2). ATP8B1 appears to be well phosphorylated as expected, and no effect of the two antimalarial drugs used were visible with regard to the phosphorylation rate of ATP8B1.

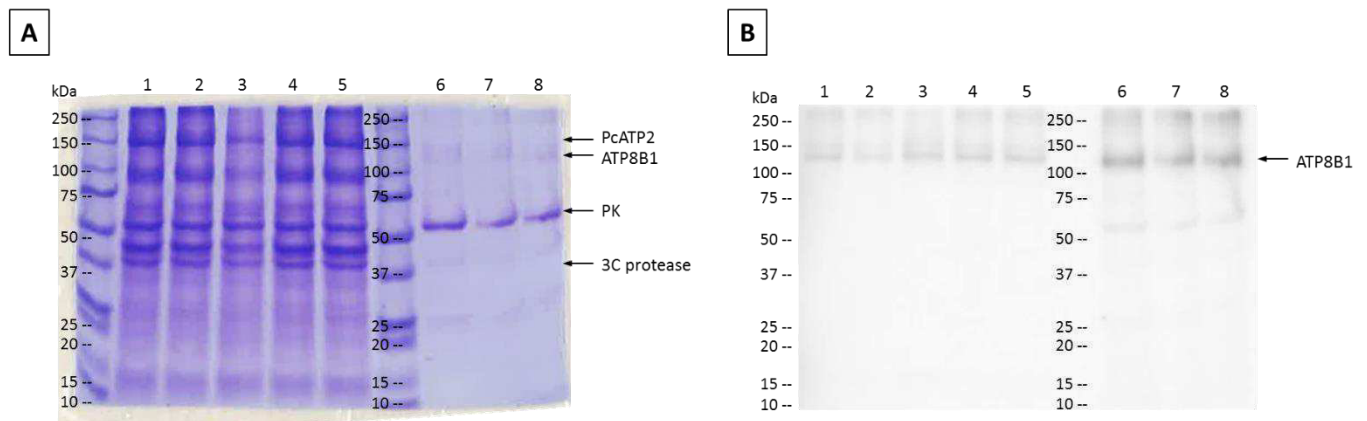


**Figure 41: Phosphorylation assay on purified PcATP2/PcCdc50.1, D596N-PcATP2/PcCdc50.1 and ATP8B1/CDC50A**

Panel A: Coomassie blue staining of the sarkadi gel. Panel B: radioactivity footprint of the phosphorylation by  $[\gamma\text{-}^{32}\text{P}]$  ATP. For the two panels: lane 1: PcATP2/PcCdc50.1; lane 2: PcATP2/PcCdc50.1+  $\text{BeF}_3^-$ ; lane 3: PcATP2-D596N/PcCdc50.1; lane 4: PcATP2/PcCdc50.1+ MMV007224; lane 5: PcATP2/PcCdc50.1+ MMV665852; lane 6: ATP8B1/CDC50A; lane 7: ATP8B1/CDC50A+ MMV007224; lane 8: ATP8B1/CDC50A+ MMV665852; PK: pyruvate kinase, loading control (1,3  $\mu\text{g}$ ).

### 3. ATPase activity of purified PcATP2

In parallel of the autophosphorylation assays, ATPase activity of purified PcATP2 was also tested. ATPase activity is measured thanks to an enzyme-coupled assay, where the hydrolysis of ATP is coupled to the oxidation of NADH, which can be monitored by spectrophotometry (see scheme in fig 58, section V-2-5-1). This ATPase assay not only requires protein autophosphorylation, but also its transit through all the conformational states of the transport cycle (see scheme fig 6, section I-3-1-3), i.e. cycles of phosphorylation and dephosphorylation ((Puts and Holthuis 2009) and scheme fig 6). In addition, some P4-ATPases are highly regulated and require the presence of regulatory factors for functional activation. Indeed, this is the case of the yeast flippase Drs2p, that is inhibited by its N- and C-terminal ends, and it only shows ATPase activity after partial enzymatic cleavage of these ends. (Jacquot et al. 2012; Azouaoui et al. 2017). In addition, Drs2p requires the presence of PI4P to perform ATPase activity (Jacquot et al. 2012; Zhou, Sebastian, and Graham 2013b). Unfortunately, PcATP2 is still a putative transporter and therefore there is no data concerning transportable phospholipid substrate(s) or potential regulatory factors. In this regard, we decided to test the ATPase activity of PcATP2 with the most common phospholipids substrates transported by P4-ATPases: PS, PE and PC (Lopez-Marques et al. 2014). In addition, besides the substrates, we tested the ATPase activity of PcATP2 in the presence of the phospho-inositides PI4P

and PIP<sub>2</sub> as possible regulatory factors. Furthermore, we also tested the effect of adding trypsin to allow a partial enzymatic cleavage of both N- and the C-terminal ends of PcATP2, a strategy which was found to activate Drs2p by removing its auto-inhibitory ends (Azouaoui et al. 2017). A cuvette for spectrophotometry was prepared containing all the necessary enzymes for the ATPase-coupling assay and the purified PcATP2/PcCdc50.1 complex. The reaction was initiated by addition of Mg-ATP and NADH (fig 42). To measure ATPase activity, we follow the decrease in NADH absorbance over the time due to its oxidation to NAD<sup>+</sup>, which does not absorb at this wavelength (see scheme fig 58). We always observe a continuous small decrease of absorbance in the absence of substrates or any treatment (Azouaoui et al. 2017), traditionally attributed to photolysis of NADH, therefore this small and constant decay observed from the beginning of the experiments is considered as background (fig 42). After stabilisation of the NADH absorbance, the different phospholipid substrates, trypsin or the phosphoinositides were sequentially added into the cuvette as indicated in the figure 42. The reaction was finally tentatively stopped by the addition of BeF<sub>3</sub>.

On figure 42, panel A, we observed no change in the slope on the absorbance's decay after the addition of DOPC and POPS, indicating that, in these conditions, PcATP2 does not hydrolyse ATP. The addition of PIP<sub>2</sub> and trypsin did not show any activity either. An inhibitor of the enzyme adenylate kinase, AP5-A, was added in the cuvette to avoid a possible false positive due to the activity of this enzyme, sometimes present as contaminant in this kind of assays. In a second experiment (fig 42, panel B), POPS and POPC were tested again in addition to POPE. Again, no ATPase activity was detected in these conditions even in the presence of trypsin and PI4P.

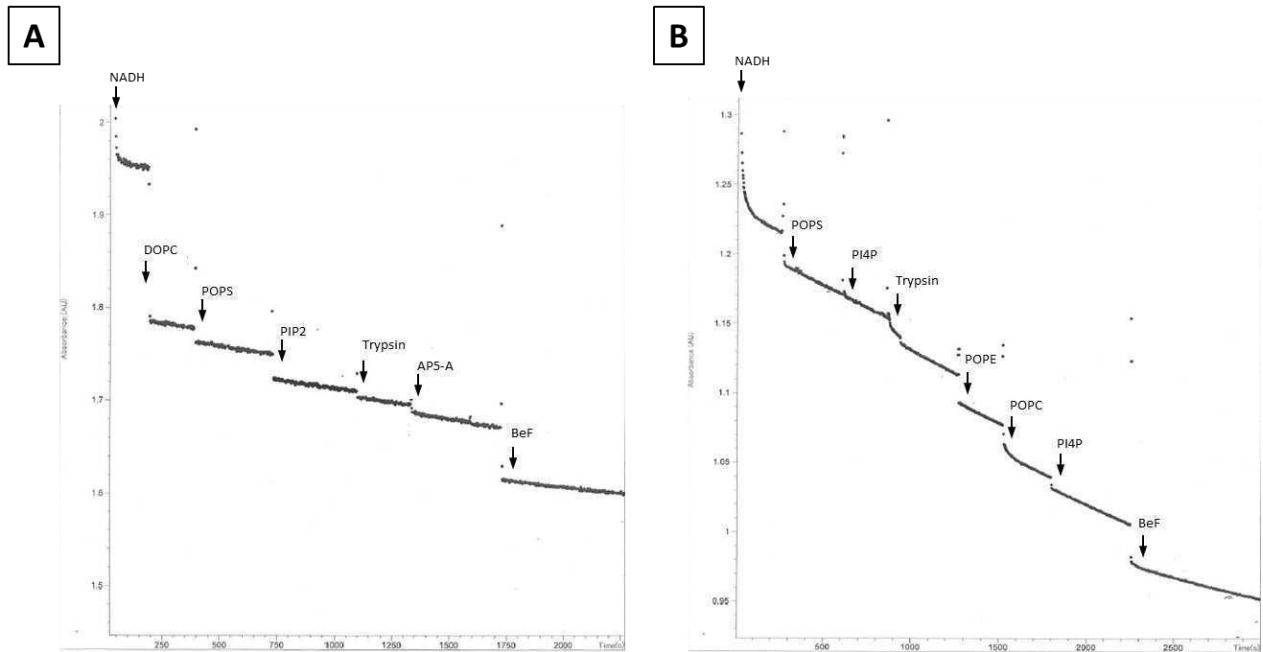


**Figure 42: ATPase activity of purified PcATP2/PcCdc50.1.**

Experiments done at 30 °C in SSR buffer at pH 7.5 supplemented with 0.2 mg/ml of DDM. Others conditions: ~2 µg PcATP2/PcCdc50.1, 1 mM of MgATP, 250 mM of NADH. Different lipids mixed with DDM (0.5 to 1 mg/mL) were added along the reaction and the reaction was stopped by addition of 1 mM BeF<sub>3</sub>. Panel A: additions of 0.1 mg/mL DOPC; 0.2 mg/mL POPS; 0.03 mg/mL PIP2; 120 µg Trypsin final; 1.1 µM AP5-A. Panel B: additions of 0.2 mg/mL POPS; 0.03 mg/mL PI4P; 120 µg Trypsin final; 0.1 mg/mL POPE; 0.2 mg/mL POPC, 0.03 mg/mL PI4P. The continuous decrease in absorbance is considered as background and is due to the photolysis of the NADH.

The negative results obtained in these experiments initially suggested that the purified PcATP2/PcCdc50.1 was simply inactive. However other considerations should be taken into account. For instance, PcATP2 might not be able to recognize the phospholipids chosen as substrates or, even, PIP2 and PI4P do not activate PcATP2. In addition, it is also possible that the presence of DDM is inhibiting PcATP2 or simply that this detergent is not the optimal one to keep the PcATP2/PcCdc50.1 complex stable and functional, as was already shown for SERCA1a (Champeil et al. 2016). There are still many possibilities and conditions that should be explored.

### III-5-3 Discussion

After demonstrating the association of PcATP2 with PcCdc50.1 after detergent solubilisation, we undertook the purification of this complex using a resin coupled to nanoGFP nanobodies. To our knowledge, this is perhaps the first example of the use of a nanobody against the GFP for affinity purification of a membrane protein, since these nanobodies are mostly used for cellular localization or co-immunoprecipitation. This

approach allowed us to purify the complex of PcATP2 with PcCdc50.1. The purified complex obtained was fairly pure except for one non-specific protein contaminant of about 50 kDa (fig 37) and the 3C protease. As a common issue in protein purification, we lost some protein during the enzymatic elution as the cleavage was not 100% efficient. We estimated that after elution, we obtained about 100 µg of purified protein from 4 L of culture and after concentration of the sample we were at 5 µg for 4 L of culture. We actually lost a substantial amount of protein complex in the concentrator, probably because aggregation after concentrating the sample. Therefore, we had to prepare a large quantity of membranes in order to obtain a sufficient quantity of purified PcATP2/PcCdc50.1 complex to perform the functional assays. In addition, to be able to measure the specific activity of purified PcATP2, we made two presumably non-functional mutants of PcATP2: E235Q and D596N. The two mutants were expressed at approximately similar level as wild type, although we found a slightly higher proportion of these mutants in the P3 membrane fraction in comparison to wild type (fig 39), suggesting a small improvement of the expression and, perhaps, the stability of the heterodimer due to these two mutations. The non-phosphorylatable D596N mutant of PcATP2 in complex with PcCdc50.1 was purified in the same way as wild type, obtaining similar yields (fig 40).

Unfortunately, the results obtained in the autophosphorylation experiments showed that purified PcATP2 was unable to autophosphorylate, at least, under our experimental conditions (fig 41, panel B). The observed  $\text{BeF}_3^-$  sensitive phosphorylated band around 140 kDa was a protein contaminant because it appeared in all samples, including the predicted phosphorylation-deficient mutant of PcATP2 (fig 41, panel B). In the same experiment, ATP8B1 did experience phosphorylation, but the two drugs tested predicted to interact with the *P. falciparum* ortholog of PcATP2 had no effect on ATP8B1 phosphorylation (fig 41, panel B). This result can be interpreted in two different ways: (1) these drugs are not able to target ATP8B1, which, in fact, is an interesting result or (2) they do affect ATP8B1 phosphorylation, but by interfering with another step of its catalytic cycle.

The ATPase activity assays of purified PcATP2/PcCdc50.1 gave negative results like the autophosphorylation tests. None of the possible substrates were able to trigger ATPase activity in PcATP2 and the addition of PIP<sub>2</sub>, PI<sub>4</sub>P or trypsin did not activate the protein,

either. Consequently, one of the first conclusions was that the purified complex is simply inactive. If this is the case and the conditions and/or detergent used during membrane solubilisation and protein purification were not the right ones to keep PcATP2 in an active form, we have to make adjustments in the purification process. With regard the detergent used to solubilize the PcATP2/PcCdc50.1 complex, DDM is a mild detergent considered sometimes as a “quality control” detergent to solubilize eukaryotic membrane proteins expressed in heterologous hosts (Privé 2007). In fact, it is considered by many researches that if DDM can solubilize a membrane protein, there is a good probability that this protein is properly folded. In any case, our experience in the laboratory with other P-type ATPases like SERCA1a and Drs2p (Lenoir et al. 2018) indicate that the choice of the right detergent and phospholipid additives during protein solubilisation are key not only on the stability of the protein but also on its activity. For example, a detergent like OG was able to solubilize SERCA1a; however within a few minutes the enzyme was completely inactivated (Champeil et al. 2016). In addition, solubilisation using mixtures of detergent and lipids has proved to be quite efficient to stabilize the solubilized protein in detergent/lipid micelles. Successful examples are the mixtures DDM+POPS and LMNG+POPS+PI4P to solubilize and functionally stabilize SERCA1a and Drs2p, respectively (Lenoir et al. 2018; Azouaoui et al. 2014). In the case of PcATP2, we needed to add CHS to solubilize the protein and, in addition, we added DOPC during the purification steps. It will be necessary to screen other phospholipid (or mixtures), some of them potential substrates as well, to improve and optimize the stability of the PcATP2/PcCdc50.1 complex during membrane extraction and purification.

Other considerations to explain the lack of PcATP2 functionally should be taken into account. For instance, PcATP2 might not be able to recognize the phospholipids chosen as substrates in our experiments: PC, PE and PS. Due to the low amount of purified complex obtained during purification we could not test other lipids like lysophospholipids, known substrates of some plant P4-ATPases (Lisbeth R. Poulsen et al. 2015). Moreover, the addition of the phosphoinositides PIP2 and PI4P, and trypsin did not activate PcATP2 ATPase activity as it does with Drs2p. Functional data on Drs2p has revealed that PI4P is necessary to activate the ATPase activity of the enzyme together with a partial trypsin cleavage of the N- and C-terminal extensions of the protein (Azouaoui et al. 2017). Therefore, the auto-inhibitory effect of the N- and C-terminal



ends of Drs2p can be partially suppressed after PI4P binding. Our laboratory and collaborators has recently identified from the 3D structure of Drs2p a new PI4P binding site at the C-terminal end of Drs2p (Guillaume Lenoir, personal communication). Interestingly, the alignment of PcATP2 with Drs2p reveals that this new identified domain involved in PI4P binding is also well conserved in PcATP2 (and other *Plasmodium* ATP2 orthologs as well) unlike the other binding sequence RMKKQR previously determined (Natarajan et al. 2009), suggesting that the C-terminal end of PcATP2 could play a similar regulatory role as the C-terminal end of Drs2p. These observations lead us to speculate that probably the addition of PI4P and trypsin are necessary to activate PcATP2, so we should put our focus on finding the right substrates and/or improving the purification protocol in order to have an active protein. Overall, there are still many experimental conditions that need to be explored with regard the purification and functional characterization of the PcATP2/PcCdc50.1 complex; however, our main handicap is the amount of protein complex we can obtain using *S. cerevisiae* as expression host. In this respect, we decided to clone and express PcATP2 and PcCdc50.1 in a new yeast expression host: *Pichia pastoris*.

### **III-6 *Pichia Pastoris*: an expression host**

The amount of PcATP2 in complex with PcCdc50.1 that we were able to purify from *S. cerevisiae* was quite low, mostly due to the low expression yield and the poor efficiency to solubilize the expressed protein in detergent. We then decided to use another expression host like the yeast *Pichia pastoris*, also an organism largely used for membrane protein production, including MTPs from *Plasmodium* (Tan et al. 2006a; Amoah, Lekostaj, and Roepe 2007). Given the results with *S. cerevisiae*, we focused only in the PcATP2 co-expression with PcCdc50.1 or PcCdc50.3. The same codon-optimized cDNA sequences used for *S. cerevisiae* were kept for *P. pastoris* as codon usage is similar. *P. pastoris* has the specificity that it can grow at high-density levels, and protein expression is controlled under the strong methanol-inducible promoter AOX1. In addition, it is also relatively easy to do molecular and genetic manipulations with this yeast (Cregg 1993).

### III-6-1 Vectors construction and clones selection

As for the experiments in *S. cerevisiae*, the strategy consisted in constructing the co-expression vectors PcATP2/PcCdc50.1 and PcATP2/PcCdc50.3. The two vectors used for the cloning were the pJIN vectors, pJIN77 and pJINC8H, kindly provided by Dr Alex Peralvarez-Marin (Autonomous University of Barcelona, Barcelona, Spain), which are derived from the pPICZ vector (Invitrogen). The pJIN77 vector contains the sequence of the enhanced GFP (or eGFP) followed by a 6 x His tag (His<sub>6</sub>) at the 3' end of the cloning site. Between the sequence of the protein of interest and the sequence of the eGFP, there is a thrombin cleavage site. The pJINC8H contains the sequence of an 8 x His tag (His<sub>8</sub>) at the 3' of the cloning site. In both vectors, the sequence of the protein of interest is cloned between the EcoRI and NotI restriction sites. First, we constructed the single-expression vectors. The sequence of PcATP2 was cloned in the pJIN77 vector resulting in the expression vector: pJIN77-PcATP2-thrombin-eGFP-His<sub>6</sub>. Likewise, the sequences of the PcCdc50 subunits were cloned into the pJINC8H vector obtaining the pJINC8H-PcCdc50.1-His<sub>8</sub> and the pJINC8H-PcCdc50.3-His<sub>8</sub> expression vectors. To make the co-expression vectors, we inserted the sequence of the PcCdc50-His<sub>8</sub> subunits in the pJIN77-PcATP2-thrombin-eGFP-His<sub>6</sub> vector, using the unique BamHI restriction site of the pJIN vectors. This BamHI site is located after the AOX1 terminator, so in order to clone the whole cassette containing the AOX1 promoter, PcCdc50 subunit, His<sub>8</sub> tag and AOX1 terminator in the vector containing PcATP2, we had to introduce a second BamHI site in the pJINC8H-PcCdc50 vectors, just at the 5' end of the AOX1 promoter. Finally, we obtained the co-expression vectors pJIN-PcATP2-thrombin-GFP-His<sub>6</sub>-PcCDC50.1-His<sub>8</sub> (fig 43) and pJIN-PcATP2-thrombin-GFP-His<sub>6</sub>-PcCDC50.3-His<sub>8</sub>.

The strain SMD1168H ( $\Delta pep4$ ) of *P. pastoris* was transformed with the co-expression plasmids by electroporation (section V-2-3-4). Unlike *S. cerevisiae*, the plasmids in *P. pastoris* need to be integrated in the yeast genome by homologous recombination in the *AOX1* loci. It is always recommended to linearize the vector to facilitate the integration of the vector, however after the introduction of the subunits, we left the co-expression plasmid without unique restriction sites. Therefore, we did the transformation with a high amount of circular plasmid DNA, as also recommended by Invitrogen.

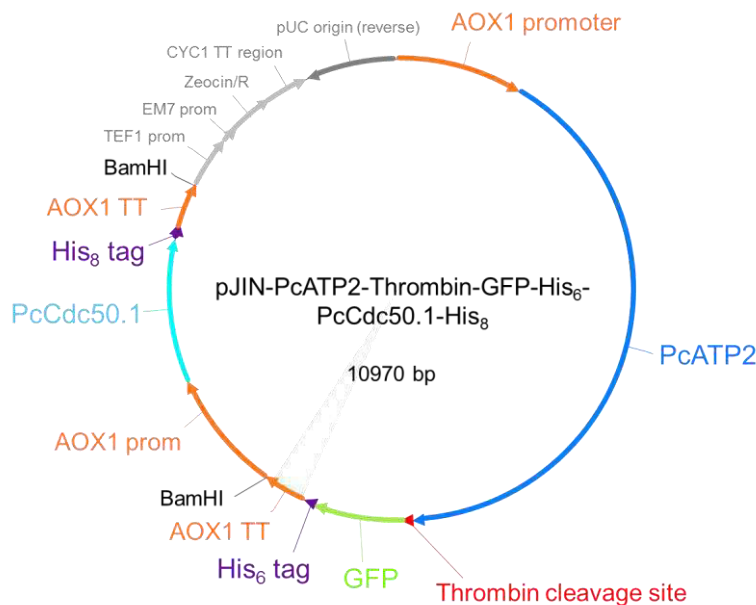


**Figure 43: scheme of the co-expression vector pJIN-PcATP2-Thrombin-GFP-His<sub>6</sub>-PcCdc50.1-His<sub>8</sub> used in *Pichia pastoris***

*Replication and selection in E. coli: origin of replication pUC, Zeocin resistance gene and EM7 promoter for the expression of the Zeocin resistance gene in E. coli. Replication and selection in the yeast Pichia pastoris: Zeocin resistance gene and TEF1 promoter for the expression of the Zeocin resistance gene in P. pastoris. Expression: AOX1 promoter and AOX1 transcription termination. The sequence of the flippase is cloned in frame with the thrombin cleavage site, the GFP and a His<sub>6</sub> tag. The sequence of the Cdc50 is cloned in frame with a His<sub>8</sub> tag.*

After transformation, we started the selection of clones using the Zeocin-resistant phenotype. This gene is present in the expression vectors and is integrated in the yeast genome together with the gene or genes of interest. Therefore, positive-transformed clones were selected on YPDS plates supplemented with Zeocin. To verify that the whole vector was inserted in the yeast genome, Zeocin-resistant clones were subjected to a PCR on colony in order to find the DNA sequences of PcATP2 and PcCdc50.1 or PcCdc50.3. We amplified a fragment of about 1 kb of PcATP2 and a fragment of about 0.4 kb of PcCdc50.1 (fig 44). 40 clones transformed with either pJIN-PcATP2-thrombin-GFP-His<sub>6</sub>-Cdc50.1-His<sub>8</sub> or pJIN-PcATP2-thrombin-GFP-His<sub>6</sub>-Cdc50.3-His<sub>8</sub> were tested in this screen. In addition, non-transformed cells were used as negative control and the same co-expression vectors, pJIN-PcATP2-thrombin-GFP-His<sub>6</sub>-Cdc50.1-His<sub>8</sub> or the pJIN-PcATP2-thrombin-GFP-His<sub>6</sub>-Cdc50.3-His<sub>8</sub>, as positive controls. As we can see on figure 44, in 20 clones tested, almost all of them displayed PcATP2 (fig 44, panel A) and PcCdc50.1 (fig 44, panel B) amplification. Similar results were obtained for the remaining 20 clones transformed with PcATP2 and PcCdc50.1, and the 40 clones

transformed with PcATP2/PcCdc50.3. The PCR on colony demonstrated that a partial sequence of PcATP2 and the two PcCdc50 subunits seems to be integrated in the yeast genome in, practically, all the Zeocin-resistant clones. At this stage, however, we decided not to restrict the number of clones in the subsequent screening.

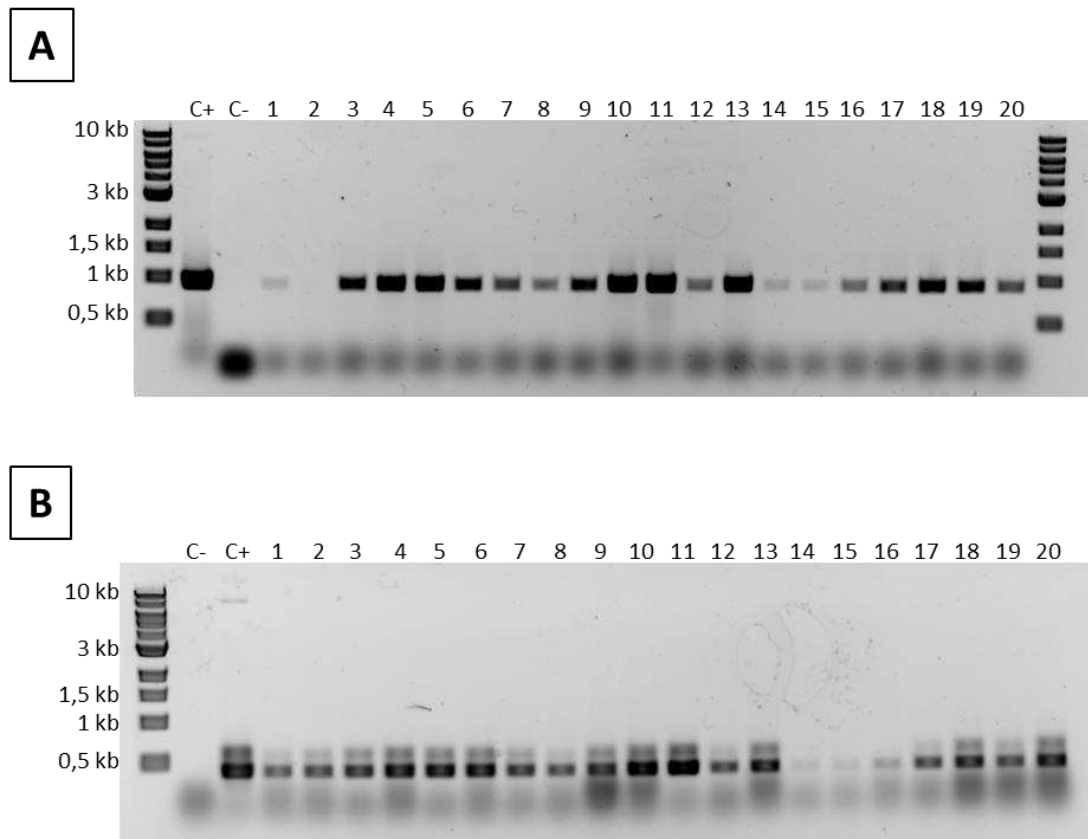


**Figure 44: Selection of *Pichia pastoris* clones containing PcATP2/PcCdc50.1 by “on colony” PCR.**

After breaking the cells by boiling, a PCR was done in order to amplify a fragment of PcATP2 or PcCdc50.1. The PCR product was analysed in a 1% agarose gel stained with ethidium bromide. Panel A: PCR amplification of a fragment of ATP2 (about 1kb). Panel B: PCR amplification of a fragment of Cdc50.1 (about 400 bp). Positive control C+: PCR amplification using pJIN-ATP2-Thrombin-GFP-His<sub>6</sub>-Cdc50.1-His<sub>8</sub> vector; negative control C-: non transformed *P. pastoris* SMD1168H; 1 to 20: tested clones.

We then proceeded to a next screening based on protein expression of each single selected clone, exploiting the fluorescence of the eGFP fused to the C-terminal end of PcATP2. All the clones were plated in solid media and protein expression was induced by methanol in the same plate. Therefore, the comparison of the intensity level of the GFP (thus, the level of expression of PcATP2) can be easily analysed in all the clones, in order to select those ones showing the best expression. An overnight culture in YPD rich

media was done and the clones were re-suspended in Minimal Methanol (MM) induction media. Then, drops of each clone were plated on MM plates and incubated at 28°C for 48 h. Non-transformed cells were used as negative control and cells transformed with the empty vector pJIN77 containing only the eGFP, were used as positive control. Figure 45 shows the results obtained for 20 Zeocin-resistant clones transformed with PcATP2/PcCdc50.1. On the left of figure 45 a picture of the plate was taken to verify the growing of the different clones. Except clone 11, all the others grew similarly. The right picture of the figure 45, displays the fluorescence of the same colonies. The negative control (C-) showed a small fluorescence intensity, corresponding to the background given by the yeasts. On the other hand, the positive control (C+) showed the fluorescence intensity obtained for the expression of the soluble eGFP and indicated as well that the assay was working. Out of the 20 tested clones, only a few of them showed a fluorescent intensity substantially higher than the background, for example, clones 9 and 14. Consequently, these two clones were selected for further protein expression analysis using small-scale cultures followed by membrane preparation and western blot analysis.

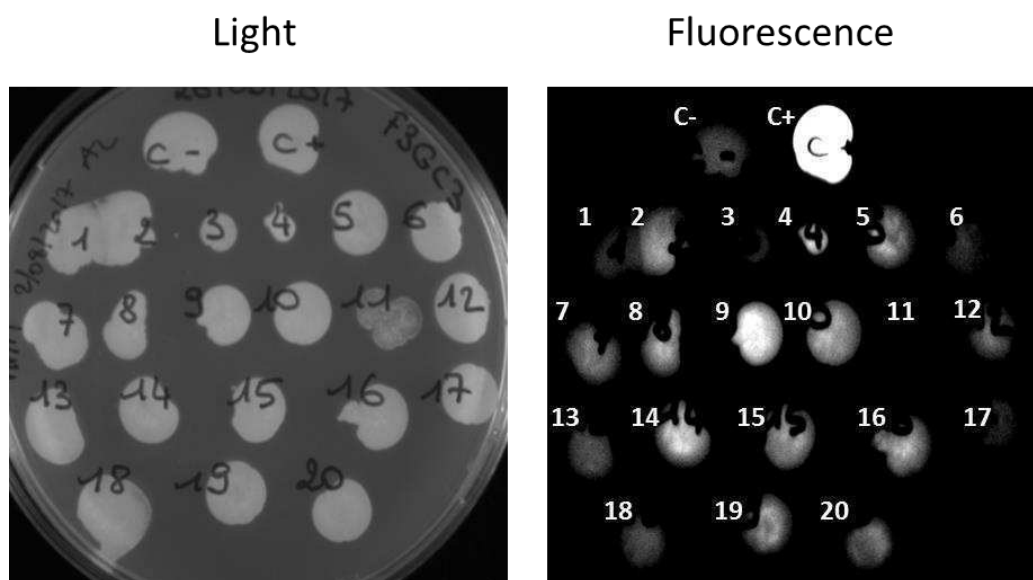


**Figure 45: Plate induction test to select *P. pastoris* clones expressing PcATP2-GFP and PcCdc50.1.**

*The cells were grown in YPD rich media, and then plated on MM agar plates for induction of the expression. They were left at 28°C for 48 h with a second addition of methanol after 24 h. left: image of the clones, to compare their growing. Right: fluorescence. image C-: negative control; the SMD1168H strain non-transformed; C+: SMD1138H strain expressing the eGFP; 1 to 20: the tested clones of PcATP2/PcCdc50.1.*

### III-6-2 Expression tests in *P. pastoris*

After the plate-induction assay (fig 45), a few clones harbouring PcATP2/Cdc50.1 were selected and cultured in small-scale cells cultures, to test PcATP2 and PcCdc50.1 expression. However, analysis by western blot of these samples showed no expression of either PcATP2-GFP or PcCdc50.1-His<sub>8</sub> in any of the selected clones (data not shown). Indeed, although the plate-induction assay reported GFP fluorescence in the selected clones, in subsequent western blots we could not detect any band with the anti-GFP antibody, not even free GFP sometimes observed in GFP-fused proteins. We thought that, maybe, the cell breaking protocol used in this assay was poorly efficient. We therefore tested different protocols to break the cells (section V-2-3-4). But unfortunately, analysis by western blot of membranes obtained from all different protocols again did not show expression of either PcATP2-GFP or PcCdc50.1-His<sub>8</sub> (data not shown).

### III-6-3 Discussion

Up to this day, our trials for expression in the yeast *P. pastoris* were not conclusive. We were able to selected clones on Zeocin plates assuming that these clones integrated the Zeocin resistant marker of the vector. Then we performed PCR on colony to amplify a portion of the PcATP2, PcCdc50.1 or PcCdc50.3 genes, and a positive amplification was obtained for the majority of the clones. In the same way, plate induction selection showed the presence of the GFP suggesting that GFP can be produced. Unfortunately, the expression analysis showed no detection of PcATP2 or PcCdc50 subunit on western blot, revealing troubles in the expression or in the cloning of the genes. We followed the strategy suggested by Invitrogen to transform non-linearized plasmid DNA. Our results suggest that, perhaps, by using our protocol, only a portion of the plasmid vector got inserted in the genome of *P. pastoris*. Alternatively, it is also possible that the homologous recombination did not occur, resulting in the generation of false positives.

## IV. Summary and prospects

---

To our knowledge, this thesis reports the first biochemical attempts to study *Plasmodium* P4-ATPases (or lipid flippases) and their Cdc50-associated subunits. Indeed, at the time this thesis began, almost nothing was known about *Plasmodium* P4-ATPases, except a predicted functional annotation based on sequence homology to P-type ATPases and P4-ATPases (Trottein and Cowman 1995; Martin, Ginsburg, and Kirk 2009). Among the five putative P4-ATPases encoded by *P. falciparum*, we decided to focus our efforts on PfATP2 based on its amino acid homology to Drs2p, the yeast P4-ATPase and a paradigm for the P4-ATPase family. We first found that the amino acid identity between different *Plasmodium* ATP2 orthologs was fairly high (~60%), a first indication of a possible essential role of this transporter for the parasite. We also were able to identify in the sequence alignment of *Plasmodium* ATP2 orthologs and *Apicomplexa* ATP2 homologs, well-conserved residues known from previous works to be critical for the stability and the functional activity of P4-ATPases (fig 11, fig 12, and fig 13). Our initial plan to focus only on PfATP2 was actually right since over the last two years different genetic approaches have agreed that ATP2 in *P. falciparum* (and its ortholog in *P. berghei*) is the only parasite-encoded P4-ATPase essential for parasite's survival (Kenthirapalan et al. 2016; Bushell et al. 2017; M. Zhang et al. 2018). Furthermore, PfATP2 was also identified as a potential drug target of two antimalarial molecules included in the malaria box (Cowell et al. 2018). Since P4-ATPases are normally associated to a  $\beta$ -subunit protein from the Cdc50/LEM family, we also identified from a BLAST search three putative Cdc50 proteins encoded by *P. falciparum*, with also a good degree of conservation among *Plasmodium* species and *Apicomplexa* (fig 14), together with the typical conserved features of Cdc50 proteins. Notably, a saturation mutagenesis analysis have recently reported that all three putative Cdc50 proteins are essential for the parasite, just like PfATP2 (M. Zhang et al. 2018). Obviously, all this information reinforced our interest for functional characterization of ATP2 and its possible association with one of the three putative Cdc50 proteins encoded by *Plasmodium* species (including the functional consequences of this). Logically, the long-

term goal of our studies was to better understand the essential functional role of ATP2 within the parasite.

Besides the experimental difficulty of handling *Plasmodium*-infected erythrocyte cultures, the usually obtained yield of membrane protein expression in such systems was quite low for most of our experimental needs. In this scenario, heterologous expression is an excellent choice to produce a sufficient amount of the target protein to undertake a deep functional characterization or, eventually, structural determination (Birkholtz et al. 2008). The most used methods to study and functionally characterize *Plasmodium* MTPs are the expression in *X. laevis* oocytes or in yeast (Kiaran Kirk 2004; Amoah, Lekostaj, and Roepe 2007). Our laboratory has a long-standing expertise to produce membrane transporters and, more specifically, P-type ATPase transporters in the yeast *S. cerevisiae*, as for example the Ca<sup>2+</sup> ATPase from *P. falciparum*, PfATP6, that was expressed and functionally purified in our laboratory (Cardi et al. 2010; Arnou et al. 2011; David-Bosne et al. 2013). Moreover, our laboratory recently established an experimental strategy to, coordinately, overexpress in *S. cerevisiae* P4-ATPases and its associated Cdc50 subunits (Azouaoui et al. 2016). Using this strategy, we undertook the heterologous co-expression in *S. cerevisiae* of ATP2 and related Cdc50 subunits from three *Plasmodium* species: *P. falciparum*, *P. berghei* and *P. chabaudi*. We succeeded to heterologously co-express the *P. chabaudi* ATP2 (PcATP2) and its three Cdc50 subunits (PcCdc50.1, PcCdc50.2 and PcCdc50.3), but because of the low expression yield of PcCdc50.2, we finally decided to focus on the co-expression of PcATP2/PcCdc50.1 and PcATP2/PcCdc50.3.

Analysis of protein expression in two membrane fractions of *S. cerevisiae* gave us the first indications that PcATP2 might interact with both Cdc50 subunits, although with a different behavior. While both co-expressed PcATP2 and PcCdc50.1 were localized in the P3 membrane fraction and solubilized with DDM/CHS, co-expressed PcATP2 and PcCdc50.3 were mostly confined in the P2 membrane fraction, showing also a high resistant to be solubilized with mild detergents (fig 21 and 28). Interestingly, we found that PcCdc50.3, but not PcCdc50.1, was glycosylated by the yeast (fig 21). In addition, the non-glycosylated form of PcCdc50.3 was the only one to be solubilized with detergent (fig 28). This made us to think that it is perhaps the glycosylated form of PcCdc50.3 the one that has the largest affinity for PcATP2, since a large proportion of



PcATP2 co-expressed with PcCdc50.3 was not solubilized with detergent like the glycosylated form of PcCdc50.3. It seems that the yeast host-cell processes the glycosylated form of PcCdc50.3 in a different way than for PcCdc50.1, dragging also PcATP2 to a membrane compartment resistant to solubilization by DDM/CHS. It will be really interesting to investigate in *Plasmodium* if glycosylation of PcCdc50.3 also occurs, and if this has a role on PcATP2 interaction and membrane localization within the *Plasmodium*-infected host. Indeed, N-glycosylation is not very common in *Plasmodium* parasites and mostly occurs in the erythrocyte's plasma membrane (Cova et al. 2015).

Given the low expression yield of PcATP2 in all conditions tested, we decided to introduce the GFP as reporter at the C-terminal end of PcATP2 or the PcCdc50 subunits. This allowed us to use more sensitive techniques to explore the interaction of PcATP2 with the Cdc50 subunits, either in yeast cells or after detergent solubilisation. Fluorescence microscopy analysis of *S. cerevisiae* cells revealed that PcATP2-GFP expressed alone or co-expressed with PcCdc50.1, is localized in compartments that resemble proliferated membranes deriving from the ER (fig 31). The question is if these proliferated membranes are indeed intermediate compartments of the yeast's degradation pathways. This could explain the fact that the solubilisation efficiency of PcATP2/PcCdc50.1 with a mild detergent like DDM is low due to, perhaps, partial misfolding. Nevertheless, and despite the low solubilisation yield, we were able to demonstrate by co-immunoprecipitation using nanobodies against the GFP (nanoGFP) that, after detergent solubilisation, PcATP2 interacts with PcCdc50.1 and also, with PcCdc50.3 (fig 36). Analysis by FSEC of the detergent-solubilized complexes using the GFP fused to PcATP2 as reporter indicated that the solubilized fractions of PcATP2/PcCdc50.1 or PcATP2/PcCdc50.3 were probably not aggregated (fig 33), validating the experiments of co-immunoprecipitation. Moreover, using FSEC but tagging the Cdc50 subunits with the GFP, we also observed that the presence of PcATP2 is mandatory to avoid PcCdc50.1 aggregation, at least, after detergent solubilisation (fig 35). In contrast, the presence of PcATP2 did not rescue PcCdc50.3 from being aggregated. These experiments also showed that the PcATP2 expression yield was approximately ten times lower than the one of the two subunits. Therefore, even with this different expression level, PcATP2 was still able to help on keeping PcCdc50.1 proper folding, most likely during biogenesis in the yeast cell.

Next, we proceeded to purify the PcATP2-GFP/PcCdc50.1 complex using the nanoGFP coupled to agarose beads for affinity purification. We decided to set up this new purification approach due to the low yield of detergent-solubilized PcATP2/PcCdc50.1, incompatible in our hands with other techniques like His-tag purification or Streptavidin-biotin affinity purification. We succeed on purifying the PcATP2/PcCdc50.1 complex but, although both proteins were visible on Coomassie blue staining SDS-PAGE and western blot (fig 37), the total amount of complex recovered was quite low (about 100 micrograms from 4 liters of culture). In addition, when we tried to concentrate the eluted protein sample, a substantial amount of the sample got trapped in the concentrator filter, probably due to aggregation. Nevertheless, we analyzed the functional state of the PcATP2/PcCdc50.1 complex that had remained in solution, by assaying its ATPase activity and its autophosphorylation ability with  $\gamma$ -<sup>32</sup>P-ATP, as well as its ATPase activity. Unfortunately, the results from ATPase activity were all negative and the autophosphorylation assays did not give any conclusive results either. There are many factors that can explain the lack of functional activity of the purified PcATP2/PcCdc50.1 complex. Perhaps the most obvious is the low stability of the complex after eluting from the column and its tendency to aggregate when trying to concentrate. For future purifications, it can be worth to avoid the concentration step by eluting the complex in smaller volumes. Moreover, the detergent used for solubilisation may not be the most suitable for the activity of the protein, something already documented for other membrane proteins. It would be interesting to assess the stability of the complex by FSEC after solubilisation with other detergents like C12E8, LMNG or LDAO, which gave some positive results during solubilisation trials when combined with CHS. Stabilization with phospholipids during purification is also a common strategy on membrane protein purification. We added DOPC during purification; however, other phospholipids (or mixtures) should be tried as well; as for example, PE or PS. (Champeil et al., 2016)

In summary, in the yeast *S. cerevisiae*, we succeeded in producing and purifying the putative P4-ATPase, ATP2 from the *Plasmodium chabaudi* in complex with its associated Cdc50 subunit. Our studies also identified that the two subunits PcCdc50.1 and PcCdc50.3 can interact with PcATP2, although PcCdc50.1 seems to be the preferential associated subunit, at least, when expressed in *S. cerevisiae*. Despite the low expression yield and poor solubilisation, we succeeded in purifying PcATP2 in complex with

PcCdc50.1. The purified complex appears not to be functional in the conditions used but it gives a good starting point for further optimization towards its biochemical and functional characterization.

During this thesis and in order to improve the expression of PcATP2, we made the plasmid expression vectors encoding PcATP2 with PcCdc50.1 or PcCdc50.2 to use the yeast *Pichia pastoris* as expression host. Unfortunately, we were unable to obtain clones of *P. pastoris* co-expressing PcATP2 and PcCdc50.1 or PcCdc50.3. We needed to transform the cells with circular plasmid encoding both proteins and although this protocol has worked before for other constructs, we did not succeed on the proper integration of our proteins into the yeast genome. Certainly, it will be necessary to introduce a new restriction site in the plasmid vector to linearize the vector and, consequently, to increase the chance for homologous recombination in the *Pichia* genome (Bornert et al. 2012; Strugatsky et al. 2003).

We also started to test other strategies to improve the expression yield of PfATP2 in *S. cerevisiae*, such as codon harmonization (Angov 2011). This strategy implies the incorporation of low-frequency codons in suitable positions within the protein sequence aiming to slow down the translation of the protein in the chosen positions that eventually will help to achieve a better folding of the proteins. One of the most sensitive parts of proteins during translation is the N-terminal region. It is relatively frequent to find low-frequency codons within the first 30-50 codons of proteins and, indeed, this is the case of PcATP2. Therefore, we replaced four codons in the N-terminal region of our optimized cDNA encoding PcATP2 to match with the codon-frequency used by the parasite on its genome. The results showed that this change in the cDNA of PcATP2 did not improve the expression level of ATP2. We are now planning to apply the codon harmonization strategy to the rest of the protein, particularly in the intracellular region between TMs 4 and 5 (approximately 700 residues) where the P and the N domain are located.

# V. Material and methods

---

## V-1 Material

### V-1-1 Chemicals products

The restriction enzymes, the Alkaline Phosphatase, Calf Intestinal Phosphatase (CIP), the Phusion® high fidelity DNA polymerase and the 1kb DNA ladder were supplied by New England Biolabs. The dNTPs come from Eurobio. The Luria-Bertani (LB) medium supplemented or not with agar is from Fisher Scientific. The yeast culture media come from BD. The reagents for the different buffers, the SigmaFast™ Protease Inhibitor Cocktail (PIC) tablets (EDTA-free,) the Bicinchoninic acid (BCA), the CuSO<sub>4</sub> solution, the ethidium bromide (EB), the salmon sperm DNA (SSD) and the Tween®20 are from Sigma-Aldrich. The Polyvinylidene difluoride (PVDF) membrane immobilon®-P is from Merck. The ECL Western Blotting detection kit is from GE healthcare. The Bovine Serum Albumin (BSA) is from Carl Roth. The Vivaspin® ultrafiltration units are from Sartorius. The n-Decyl-β-D-maltopyranoside (DM), n-Undecyl-β-D-maltopyranoside (UDM), C12E8 are from Calbiochem. The n-Dodecyl-β-D-maltopyranoside (DDM), the Lauryl maltose neopentyl glycol (LMNG), the n-dodecyl phosphocholine 12 (FosC12) are from Anatrace. The n-Octyl-β-D-glucopyranoside (OG), the n-Octyl-β-D-thioglucopyranoside (OTG) and the Cholesteryl Hemisuccinate (CHS) are from Sigma-Aldrich. The Lauryldimethylamin-oxid (LDAO) and the 5-Cyclohexyl-1-Pentyl-β-D-Maltoside (CYMAL-5) are from Fluka. The 1,2-dioleoyl-sn-glycero-3-phosphocholine (DOPC) is from Avanti Polar Lipids. The TALON® metal affinity resin is from Clontech, and the NHS-Activated Sepharose 4 Fast Flow and the Streptavidin Sepharose high performance resins are from GE healthcare. The HisProbe™-HRP conjugate is from ThermoFisher. The mouse IgG1K Anti-GFP primary antibody is from Roche. The Goat Anti-Mouse IgG-HRP conjugate secondary antibody is from Bio-Rad. The Avidin peroxidase probe and the Phenylmethanesulfonyl fluoride (PMSF) are from Sigma-Aldrich. The 30% Acrylamide/Bis Solution (29:1) is from Bio-Rad.

## V-1-2 Buffers and culture Media

### **Buffers and solutions:**

Phosphate Buffer Saline (PBS) (10X): 27 mM KCl, 1.4 M NaCl, 0.13 M Na<sub>2</sub>HPO<sub>4</sub> and 18 mM KH<sub>2</sub>PO<sub>4</sub> (pH 7,4)

PLATE buffer: 40% PEG 4000, 100 mM lithium acetate, 10 mM Tris-HCl pH 7.5 and 1 mM EDTA

TEPI buffer: 50 mM Tris-HCl pH 6; 8, 5 mM EDTA; 20 mM NaN<sub>3</sub>; 1 mM PMSF and 1X PIC

TEKS buffer: 50 mM Tris-HCl pH 7.5, 1 mM EDTA, 0.1 M KCl and 0.6 M sorbitol

TES buffer: 50 mM Tris-HCl pH 7.5, 1 mM EDTA and 0.6 M sorbitol

Solubilisation buffer: 20 mM Tris-HCl pH 7.8, 10% glycerol, 150 mM NaCl and 1X PIC

Re-suspension buffer: 20 mM Tris-HCl pH 7.8, 150 mM NaCl, 1X PIC and 10% (v/v) glycerol

Membrane washing buffer: 50 mM MOPS-Tris pH 7, 0.5 M KCl, 20% (v/v) glycerol, 1 mM CaCl<sub>2</sub>, 1 mM β-mercaptoethanol, 1 mM PMSF; 1X PIC

2XU loading buffer: 100 mM Tris-HCl pH 6.8; 1.4 M β-mercaptoethanol; 5% (w/v) SDS, 1 mM EDTA, 8 M urea and 0.01% (w/v) bromophenol blue

2X Sarkadi loading buffer: 300 mM Tris-HCl pH 6.8, 4% (w/v) SDS, 8 M urea, 20% (v/v) glycerol, 20 mM EDTA, and 1.4 M β-mercaptoethanol

Electrophoresis running buffer: 25 mM Tris, 0.25 M Glycine, 0.1% SDS

Transfer buffer: 27.6 mM Trizma base, 192 mM Glycine, 10% (v/v) Methanol

10% DDM/2% CHS stock solution: 200 mM Tris pH 8, 10 % (w/v) DDM, 2% (w/v) CHS

FSEC equilibration buffer: 20 mM Tris-HCl pH 7.8, 150 mM NaCl, 10% (v/v) Glycerol, 0.1 mg/mL DDM, 0.02 mg/mL CHS

SSR buffer: 100 mM KCl, 50 mM MOPS-TRIS pH7, 5 mM MgCl<sub>2</sub>, 20% (v/v) glycerol

### ***Escherichia coli* culture media:**

SOB: 2% (w/v) Bacto Tryptone , 0.5% (w/v) Yeast Extract, 10 mM NaCl, 2.5 mM KCl, 10 mM MgCl<sub>2</sub> and 10 mM MgSO<sub>4</sub>

***Saccharomyces cerevisiae* culture media:**

S6A/S6AU minimal medium: 0.1% (w/v) Bacto Casamino Acids, 0.7% (w/v) Yeast Nitrogen Base (without amino acids and with ammonium sulfate), 2% (w/v) glucose, 20 µg/mL adenine, +/- 20 µg/mL uracil, +/- 2% (w/v) agar

S5A medium: 0.1% (w/v) Bacto Casamino Acids, 0.7% (w/v) Yeast Nitrogen Base (without amino acids and with ammonium sulfate), 2% (w/v) galactose, 20 µg/mL adenine.

S5AF medium: 0.1% (w/v) Bacto Casamino Acids, 0.7% (w/v) Yeast Nitrogen Base (without amino acids and with ammonium sulfate), 2% (w/v) galactose, 1% (w/v) fructose, 20 µg/mL adenine, +/- 2% (w/v) agar

YPGE2X-rich medium: 2% (w/v) Bacto Peptone, 2% (w/v) Yeast Extract, 1% (w/v) glucose and 2.7% (w/v) ethanol

SD media: 0.17% Yeast Nitrogen Base (without amino acids and without ammonium sulfate), 5% (w/v) ammonium sulfate, 2% (w/v) glucose, 55 µg/mL uracil, 55 µg/mL adenine, 1X drop out solution (10 µg/ml L- histidine, 60 µg/mL L- leucine, 40 µg/mL L- lysine and 40 µg/mL L- tryptophan), +/- 2% (w/v) agar

***Pichia pastoris* culture media:**

YPD: 1% (w/v) Yeast Extract, 2% (w/v) Peptone, 2% (w/v) dextrose , +/- 100 µg/ml Zeocin, 2% (w/v) agar.

YPDS agar plates: 1% (w/v) Yeast Extract, 2% (w/v) Peptone, 2 % dextrose, 1M sorbitol, +/- 100 µg/ml Zeocin, 2% agar

Minimal Glycerol medium (MG): 1.34% Yeast Nitrogen Base (YNB), 1% glycerol, 4.10<sup>-5</sup> % biotin.

Minimal Methanol medium (MM): 1.34% (w/v) YNB, 4.10<sup>-5</sup> % biotin, 0.5% (v/v) methanol.

## V-2 Methods

### V-2-1 Cloning strategy and vectors design for expression

#### 1. Optimisation of the gene sequence

The heterologous expression of lipid flippases from *Plasmodium* species and associated Cdc50 subunits was done in the yeast *Saccharomyces cerevisiae*. The genome of *Plasmodium falciparum* has a highly rich A-T content of about 82% (Weber 1987), hampering the heterologous expression in yeast (Cardi et al. 2010; Amoah, Lekostaj, and Roepe 2007). In addition, A-T rich regions can lead to premature transcriptional termination in the yeast (Graber et al. 1999). Therefore, the cDNA encoding these transporters was codon-optimized for *S. cerevisiae* expression. We ordered to Genscript synthetic cDNAs encoding the three ATP2 orthologs from *P. falciparum*, *P. berghei* and *P. chabaudi*, and the three Cdc50 subunits encoded per specie. All the cDNAs were optimized by the provider using OptimumGene™, a proprietary gene-optimization algorithm. The GC content was adjusted to ~ 35% (the optimum being between 30% and 70%), and the codon adaptation index (CAI) to ~0.82, considering an optimum CAI of ~0.8 (the CAI allows the measure of synonymous codon usage bias). The ATP2 sequences were directly cloned between the EcoRI/NotI sites in the pYeDP60 vector (fig 15, panel A) while the Cdc50 subunits were cloned in the pUC57 vector by the provider (fig 46).

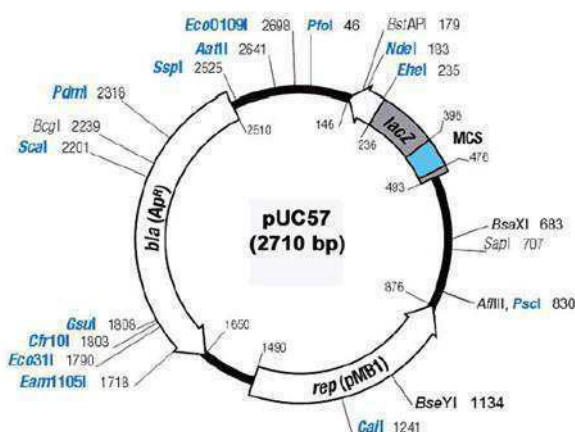


**Figure 46: pUC57 vector.**

The pUC57 vector is used for the cloning and replication in *E. coli*. The sequences of the putative Cdc50 subunits were cloned in the multi cloning site region and flanked by the restriction sites EcoRI and BamHI.

## 2. Construction of the expression vectors for *S. cerevisiae*

Over the last years, our laboratory has optimized the plasmid vector pYeDP60 for the expression of P-type ATPases and, more recently, for the co-expression of P4-ATPase/Cdc50 complexes in the yeast *Saccharomyces cerevisiae* (fig 15, panel C) (Montigny, Azouaoui, et al. 2014). The pYeDP60 shuttle vector (fig 47) contains the sequences needed for amplification in *Escherichia coli*: the bacterial origin of replication Ori, and for clone selection, the ampicillin resistance gene that encodes the  $\beta$ -lactamase. This vector also contains sequences for the amplification and selection in yeast, as the yeast  $2\mu$  origin of replication, and the Adenine and Uracil auxotrophy selection markers. For protein expression, the genes of interest are cloned under the control of a hybrid Gal10/Cyc1 promoter (Guarente, Yocum, and Gifford 1982) which contains the regulatory part of the Gal1/Gal10 promoter (Gal4p fixation site) for induction, and the TATA box of the CyC1 promoter (cytochrome c gene) for a strong transcription. Downstream of the gene of interest, we have the phosphoglycerate kinase (PGK) terminator.

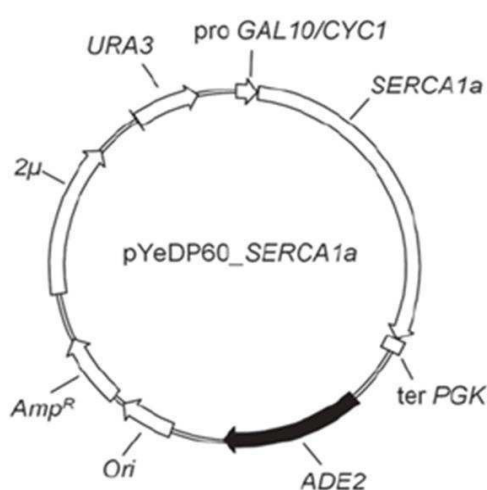


**Figure: Features of the pYeDP60 containing the gene of the SERCA1a.**

Amplification in *E. coli*: Ori: bacterial origin of replication; Amp<sup>R</sup>: ampicillin resistance gene. Amplification and selection in yeast, 2 $\mu$ : yeast origin of replication; Yeast selection markers: ADE2: Adenine auxotrophy selection markers, URA3: Uracil auxotrophy selection marker. For the expression. pro GAL10/CYC1: a hybrid Gal10/Cyc1 promoter; ter PGK: the phosphoglycerate kinase terminator. (Montigny, Azouaoui, et al. 2014)

### Construction of the single expression vectors:

As mentioned before, the optimized sequences of the three ATP2 orthologs (PfATP2, PbATP2 and PcATP2) were directly cloned by Genscript in the pYeDP60 vector between the EcoRI and NotI restriction sites, in upstream position of the tobacco etch virus (TEV) protease cleavage site coding sequence and the biotin acceptor domain (BAD) coding



sequence, allowing therefore the tagging in the C-terminal end of the flippase. These vectors were dubbed:

pYeDP60-PfATP2-TEV-BAD  
 pYeDP60-PbATP2-TEV-BAD  
 pYeDP60-PcATP2-TEV-BAD.

We also constructed the vectors with the tagging at the N-terminal of the flippases. In this case, the flippase sequences were amplified by PCR to add the PmeI and SacI restrictions sites at the 5' and 3' ends, respectively, using the following primers:

For PfATP2:

5'-cacag**tttaaac**ggtggtgagaatctttatcttcagggcggtggtggtggtATGTCTTTGGTCTACAGAAAG-3'  
 (forward, insertion of the **PmeI site**)

5'-agcatg**gagctct**caaatcatattatcttgtttct-3' (reverse, insertion of a STOP codon and a **SacI site**)

For PcATP2:

5'-cacag**tttaaac**ggtggtgagaatctttatcttcagggcggtggtggtggtATGCCAAAACATATTAAGGGT-3'  
 (forward, insertion of the **PmeI site**)

5'-agcatg**gagctct**cagatcaacttatcctgtttct-3' (reverse, insertion of a STOP codon and a **SacI site**)

A gradient of temperature was performed to find the best annealing temperature for this PCR. The PCR conditions are indicated in the following table.

PCR mix(50 µl)		PCR cycles	
Sterile milliQ H <sub>2</sub> O	31, 5 µL	Lid: 110°C	
5X Phusion HF buffer	10 µL	98 °C	30''
dNTP (2mM)	5 µL	98 °C	30''
Primer Forward (20µM)	1, 25 µL	55 +/- 5°C	30''
Primer Reverse (20µM)	1, 25 µL	72 °C	6'
DNA	0,5 µL	4 °C	∞
Phusion HF	0,5 µL		

The PCR fragments obtained were subcloned into the pJet1.2/blunt plasmid vector. The resulting vector and the pYeDP60-BAD-TEV-Drs2p were then digested by PmeI and SacI

to clone the ATP2 orthologs in place of the DRS2 sequence in the pYeDP60 with the tag sequence in the 5' end (fig 48, panel A). The resulting vectors were dubbed:

pYeDP60-BAD-TEV-PfATP2

pYeDP60-BAD-TEV-PcATP2.

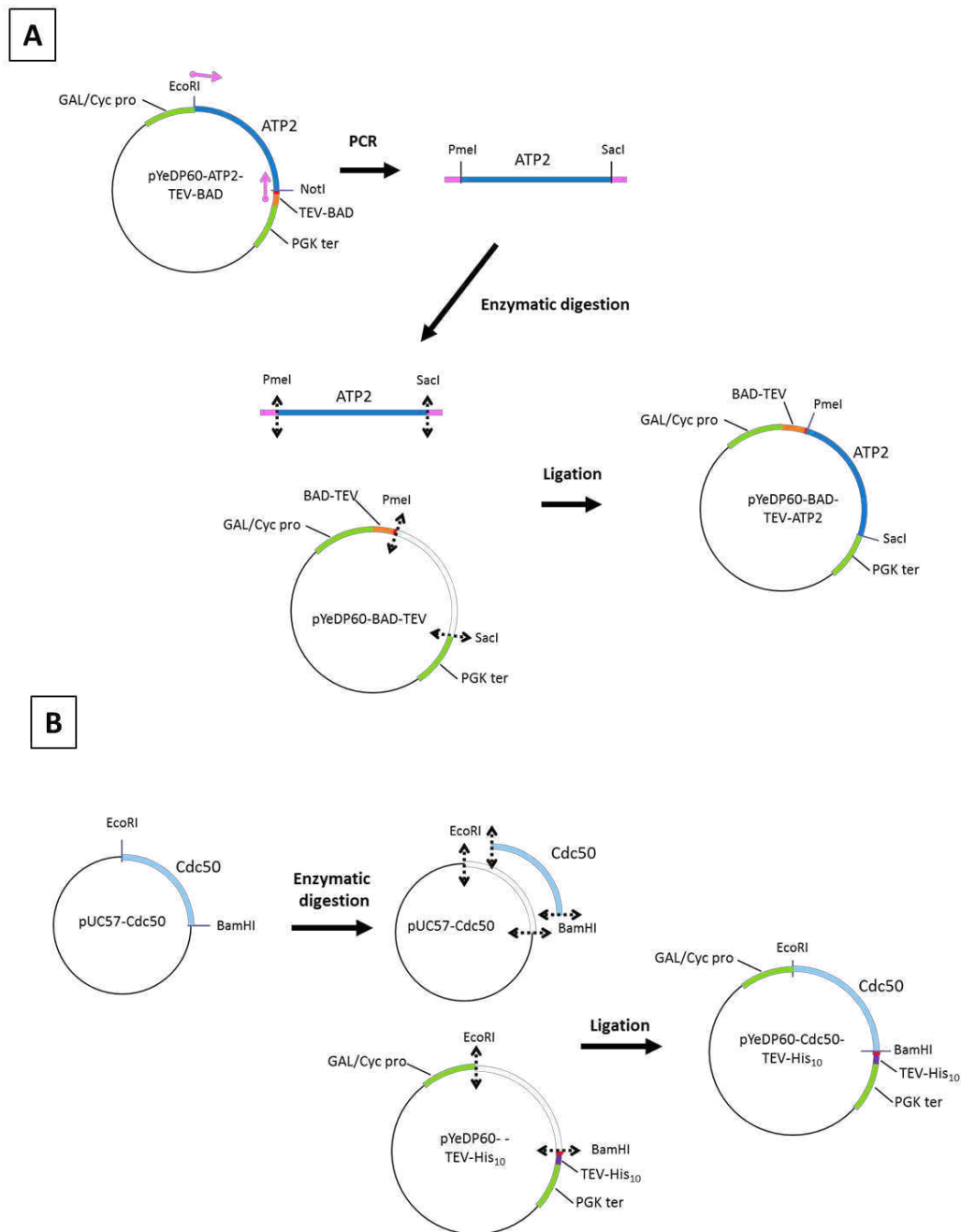


**Figure 48: Construction of the pYeDP60 single expression vectors.**

*Panel A: Construction of pYeDP60-BAD-TEV-ATP2 single expression vectors with the tag positioned at the N-terminal end of ATP2. The sequences of ATP2 were amplified by PCR to introduce the restriction sites PmeI and Sacl. After a subcloning step in a pJET2.1/blunt shuttle vector, the sequence was then cloned into the pYeDP60 vector with the BAD tag and the TEV protease cleavage site at the N-terminal of each ATP2*

orthologs. Panel B: Construction of the pYeDP60-Cdc50-TEV-His<sub>10</sub> single expression vectors with the tag positioned at the C-terminal end. The sequences of the *Plasmodium* Cdc50 subunits were obtained after digesting the pUC57 vectors supplied by Genscript and then cloned into the pYeDP60 with the TEV protease cleavage site and a decahistidine tag at the C-terminal end these Cdc50 sequences.

The nine Cdc50 subunits sequences were subcloned in the pUC57 vector by Genscript between the EcoRI and BamHI restriction sites. These vectors and pYeDP60-Cdc50p-TEV-His<sub>10</sub> were then digested by EcoRI and BamHI to clone each of the nine coding sequences of *Plasmodium* Cdc50 subunits in the place of the CDC50 sequence of pYeDP60, containing the TEV protease cleavage site and a decahistidine tag at the 3' end (fig 48, panel B). The new vectors were dubbed:

*P. falciparum*:

pYeDP60-PfCdc50.1-TEV-His<sub>10</sub>  
pYeDP60-PfCdc50.2-TEV-His<sub>10</sub>,  
pYeDP60-PfCdc50.3-TEV-His<sub>10</sub>

*P. berghei*:

pYeDP60-PbCdc50.1-TEV-His<sub>10</sub>  
pYeDP60-PbCdc50.2-TEV-His<sub>10</sub>  
pYeDP60-PbCdc50.3-TEV-His<sub>10</sub>

*P. chabaudi*:

pYeDP60-PcCdc50.1-TEV-His<sub>10</sub>  
pYeDP60-PcCdc50.2-TEV-His<sub>10</sub>  
pYeDP60-PcCdc50.3-TEV-His<sub>10</sub>

### **Construction of the co-expression vectors:**

To construct the co-expression vectors, the two cassettes containing the Gal10/Cyc1 promoter, the coding sequence for each ATP2 ortholog or the corresponding Cdc50 subunit and the terminator were cloned in the same vector. First, the fragment containing the cassette GAL10/Cyc1 promoter-Cdc50-TEV-His<sub>10</sub>-PGK terminator from each single expression vectors pYeDP60-Cdc50-TEV-His<sub>10</sub> was amplified by PCR in order to insert a SbfI restriction site at both the 5' and the 3' ends. The primers used for this reaction were:

5'-cacac**ctgcagg**tgcatgtataactcaca-3' (forward, **SbfI site**)

5'-cacac**ctgcagg**gctatgacatgattacgc-3' (reverse **SbfI site**)

Conditions for PCR amplification are indicated in the table below.

PCR mix (50 $\mu$ l)		Cycles PCR		
Sterile milliQ H2O	31,5 $\mu$ L	Lid: 110°C		
5X Phusion HF buffer	10 $\mu$ L	98 °C	30''	
dNTP (2mM)	5 $\mu$ L	98 °C	30''	× 30
Primer Forward (20 $\mu$ M)	1,25 $\mu$ L	55 °C	30''	
Primer Reverse (20 $\mu$ M)	1,25 $\mu$ L	72 °C	3'	
DNA	0,5 $\mu$ L	4 °C	$\infty$	
Phusion HF	0,5 $\mu$ L			

The PCR fragments obtained were cloned into the pJet1.2/blunt plasmid vector. Then, the resulting pJet-cassette-Cdc50 vectors and the ATP2 single expression vectors pYeDP60-PfATP2-TEV-BAD, pYeDP60-PcATP2-TEV-BAD, pYeDP60-BAD-TEV-PfATP2 and pYeDP60-BAD-TEV-PcATP2 were digested by SbfI. As SbfI is a unique restriction site in the flippase single-expression vectors, these vectors were dephosphorylated in order to avoid any self-ligation. Then, the Cdc50 cassettes were ligated with the corresponding digested ATP2 single-expression pYeDP60 vectors (fig 49). Since the Cdc50 cassettes could be inserted in the two senses, we had to select the vector with the Cdc50 cassette in the same sense that the flippase sequence. The vectors obtained were dubbed:

*P. falciparum* co-expression vectors:

pYeDP60-PfATP2-TEV-BAD-PfCdc50.1-TEV-His<sub>10</sub>

pYeDP60-PfATP2-TEV-BAD-PfCdc50.2-TEV-His<sub>10</sub>

pYeDP60-PfATP2-TEV-BAD-PfCdc50.3-TEV-His<sub>10</sub>

pYeDP60-BAD-TEV-PfATP2-PfCdc50.1-TEV-His<sub>10</sub>

pYeDP60-BAD-TEV-PfATP2-PfCdc50.2-TEV-His<sub>10</sub>

pYeDP60-BAD-TEV-PfATP2-PfCdc50.3-TEV-His<sub>10</sub>,

*P. chabaudi* co-expression vectors:

pYeDP60-PcATP2-TEV-BAD-PcCdc50.1-TEV-His<sub>10</sub>  
 pYeDP60-PcATP2-TEV-BAD-PcCdc50.2-TEV-His<sub>10</sub>  
 pYeDP60-PcATP2-TEV-BAD-PcCdc50.3-TEV-His<sub>10</sub>,  
 pYeDP60-BAD-TEV-PcATP2-PcCdc50.1-TEV-His<sub>10</sub>  
 pYeDP60-BAD-TEV-PcATP2-PcCdc50.2-TEV-His<sub>10</sub>  
 pYeDP60-BAD-TEV-PcATP2-PcCdc50.3-TEV-His<sub>10</sub>.

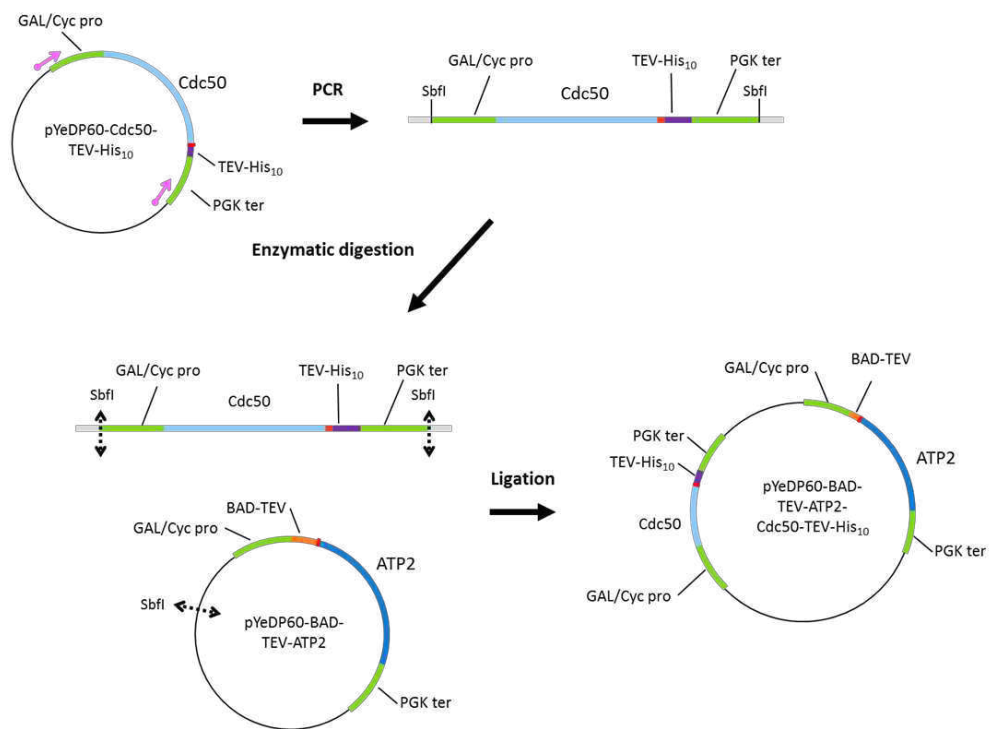


**Figure 49: Construction of the co-expression vectors: Example of the pYeDP60-BAD-TEV-ATP2-Cdc50-TEV-His<sub>10</sub>.**

*The cassette containing the GAL10/Cyc1 promoter-Cdc50 subunit-TEV-His<sub>10</sub>-PGK terminator was amplified by PCR while introducing SbfI restriction sites at both extremities. Then, the cassette was cloned into the pYeDP60-BAD-TEV-ATP2 at the unique SbfI site.*

### Introduction of the superfolder Green Fluorescent Protein (sGFP)

To introduce the sGFP (referred simply as GFP before) between the 3' end of the ATP2 orthologs and the BAD tag, the cDNA coding the sGFP was PCR amplified from the pTTQ18-SteT-3C Protease-GFP-His plasmid (Rodríguez-Banqueri et al. 2016), using primers to introduce a NotI site at the 5' end and a XmaI site at the 3' end of the sGFP. In

the forward primer we added the TEV cleavage site sequence because in the pYeDP60 it is located after the NotI site and we will lose it after digestion with NotI.

5'-**GCGGCCGCGGAGAATCTTTATTTTCAGGGCGAAAGCAAAGGAGAAGAAC**-3' (forward, **NotI site** and TEV cleavage sequence)

5'-**GCCCCGGGGGTACCTGTAATCCCAGCAGC**-3' (reverse, XmaI site)

The PCR product was then cloned into the pJet1.2/blunt plasmid vector. Then, from the pJet-TEV-sGFP digested by NotI and XmaI, the sequence TEV-sGFP was cloned between the C-terminal end of the flippase and the BAD tag (fig 50) in the single-expression vector pYeDP60-PcATP2-TEV-BAD and the co-expression vector pYeDP60-PcATP2-TEV-BAD-Cdc50-TEV-His<sub>10</sub> giving the new vectors:

pYeDP60-PcATP2-TEV-GFP-BAD

pYeDP60-PcATP2-TEV-GFP-BAD-Cdc50-TEV-His<sub>10</sub>

We also introduced at the C-terminus of ATP2, the sGFP but with a 3C protease cleavage site and a STOP codon, at the N-terminal and C-terminal ends of the sGFP, respectively. The cDNA encoding the 3C protease cleavage site and the sGFP was PCR amplified using again the pTTQ18-SteT-3C Protease-GFP-His vector with primer to introduce a NotI site at the 5' and a XmaI site at the 3'.

5'-**ATGCGGCCGCCCTGGAGGTGCTGTTCCAG**-3' (forward, **NotI site** )

5'- **TCCCCGGGGTTAGGTACCTGTAATCCCAGC**-3' (reverse, **XmaI site** and STOP codon)

The PCR product was then cloned into the pJet1.2/blunt plasmid vector. Then the pJet-3C-GFP (NotI/XmaI) was digested by NotI and XmaI and the 3C-sGFP sequence was cloned between the C-terminal end of the flippase and the BAD tag in the single-expression vector pYeDP60-PcATP2-TEV-BAD and the co-expression vector pYeDP60-PcATP2-TEV-BAD-Cdc50-TEV-His<sub>10</sub>, giving the new vectors (fig 37, panel A):

pYeDP60-PcATP2-3C-GFP

pYeDP60-PcATP2-3C-GFP-Cdc50-TEV-His<sub>10</sub>

To introduce the 3C-GFP at the C-terminal of the Cdc50 subunit, the sequence was amplified from the pTTQ18-SteT-3C Protease-GFP-His, introducing a BamHI site at each extremity:

5'-CCGGGATCCGGTATGAAAAACGCAAAGCA-3' (forward, **BamHI** site)

5'-CCGGGATCCGGTACCTGTAATCCCAGCAGCATTAC-3' (reverse, **BamHI** site)

From the pJet-3C-GFP (BamHI), the sequence was cloned between the C-terminal end of the Cdc50 subunit and the decahistidine tag (fig 50) of the single expression vectors pYeDP60-PcCdc50.1-TEV-His<sub>10</sub>, pYeDP60-PcCdc50.3-TEV-His<sub>10</sub>, the co-expression vectors pYeDP60-BAD-TEV-PcATP2-PcCdc50.1-TEV-His<sub>10</sub> and pYeDP60-BAD-TEV-PcATP2-PcCdc50.3-TEV-His<sub>10</sub>; giving the new vectors:

pYeDP60-PcCdc50.1-3C-GFP-His<sub>10</sub>

pYeDP60-PcCdc50.3-3C-GFP-His<sub>10</sub>

pYeDP60-BAD-TEV-PcATP2-PcCdc50.1-3C-GFP-His<sub>10</sub>

pYeDP60-BAD-TEV-PcATP2-PcCdc50.3-3C-GFP-His<sub>10</sub>

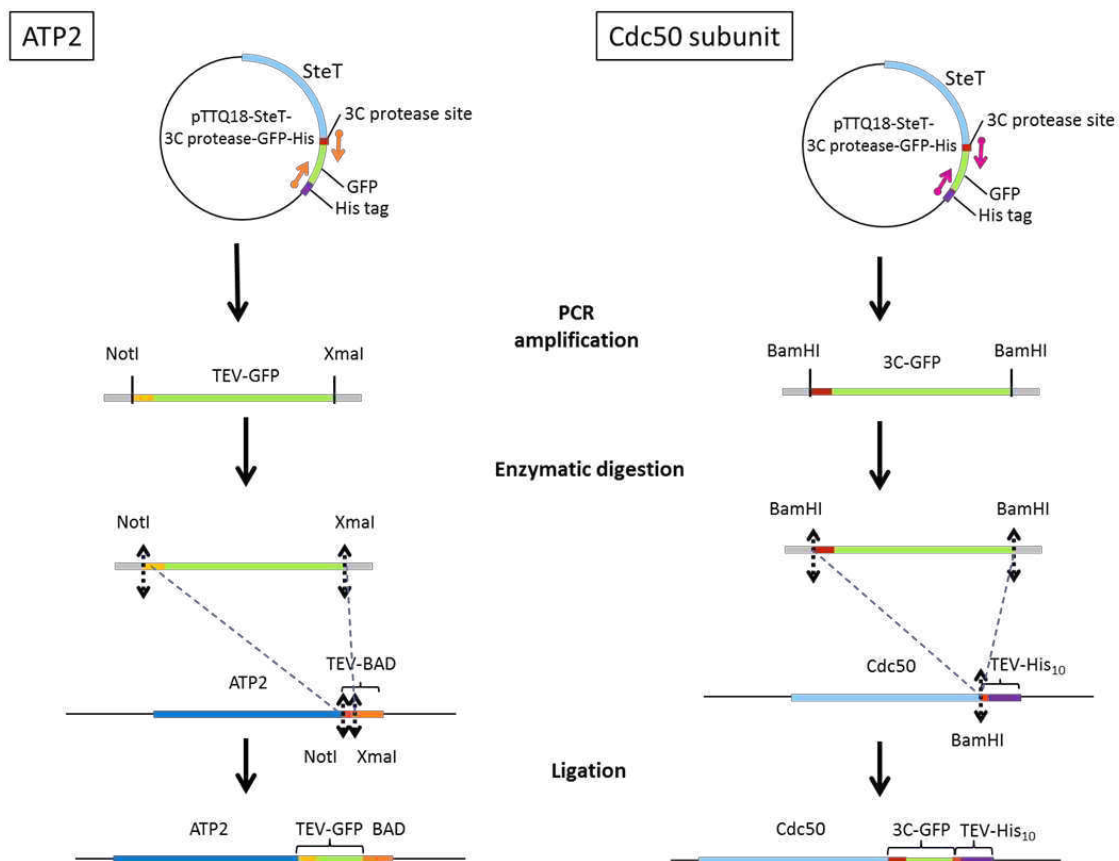


**Figure 50: Insertion of a sGFP at the C-terminal end of each ATP2 or Cdc50 subunit.**

The sequence containing the 3C protease cleavage site and the sGFP was amplified by PCR introducing NotI and XmaI restriction sites for ATP2, and BamHI sites for the Cdc50 subunits. The sequences were then cloned at the C-terminal end of each protein in the corresponding single-expression or co-expression vectors.

## Construction of the predicted non-functional mutants of PcATP2: E235Q-PcATP2 and D596N-PcATP2

We wanted to introduce two single point mutations in the predicted A and P domains of PcATP2 to obtain the non-functional mutants: E235Q-PcATP2 and D596N-PcATP2. The position of these residues was determined from protein sequences alignments with the DGET and DKTG conserved motifs of P4-ATPases. The QuikChange II XL site-directed mutagenesis kit from Agilent technologies was used following all the recommendations given by the supplier. The whole vector was amplified using primers containing the mutation at the desired position. The mutation was done in the pJet-PcATP2 (EcoRI/NotI) vector. The primers used were the following:

E235Q mutation:

5'-GCCGAAACATCATCCTTAGATGGTCAAACCAACTTG-3' (forward, GAA→CAA)

5'-CAAGTTGGTTTGACCATCTAAGGATGATGTTTCGGC-3' (reverse)

D596N mutation:

5'-GGTCAAATCGAATACATCTTTTCAAATAAAGACCGGT-3' (forward, GAT→AAT)

5'-ACCGGTCTTATTTGAAAAGATGTATTCGATTTGACC-3' (reverse)

The PCR conditions used were:

PCR Mix (50 µl)		Cycles PCR	
Sterile milliQ H2O	38µL	Lid: 110°C	
10 X reaction buffer	5 µL	95 °C	1'
dNTPs Mix	1 µL	95 °C	50''
Primer For (20µM)	0,5 µL	60°C	50''
Primer Rev (20µM)	0.5 µL	68 °C	7'30
DNA template (10 ng/µl)	1 µL	68°C	7'
Quick solution	3 µL	4°C	∞
Pfu Ultra HF DNA pol (2,5U/µL)	1 µL		

Once the pJet-E235Q-PcATP2 and pJet-D596N-PcATP2 vectors were obtained (fig 51), the mutated PcATP2 sequences were cloned, using EcoRI and NotI, in the pYeDP60-PcATP2-3C-GFP. Next, the cassette Cdc50.1 was then cloned into the previous vector from the pJet-cassette-PcCdC50.1 using SbfI as explained before (Fig 49). Finally, we obtained two vectors:



pYeDP60-PcATP2\_E235Q-3C-GFP-PcCdc50.1-TEV-His<sub>10</sub>

pYeDP60-PcATP2\_D596N-3C-GFP-PcCdc50.1-TEV-His<sub>10</sub>

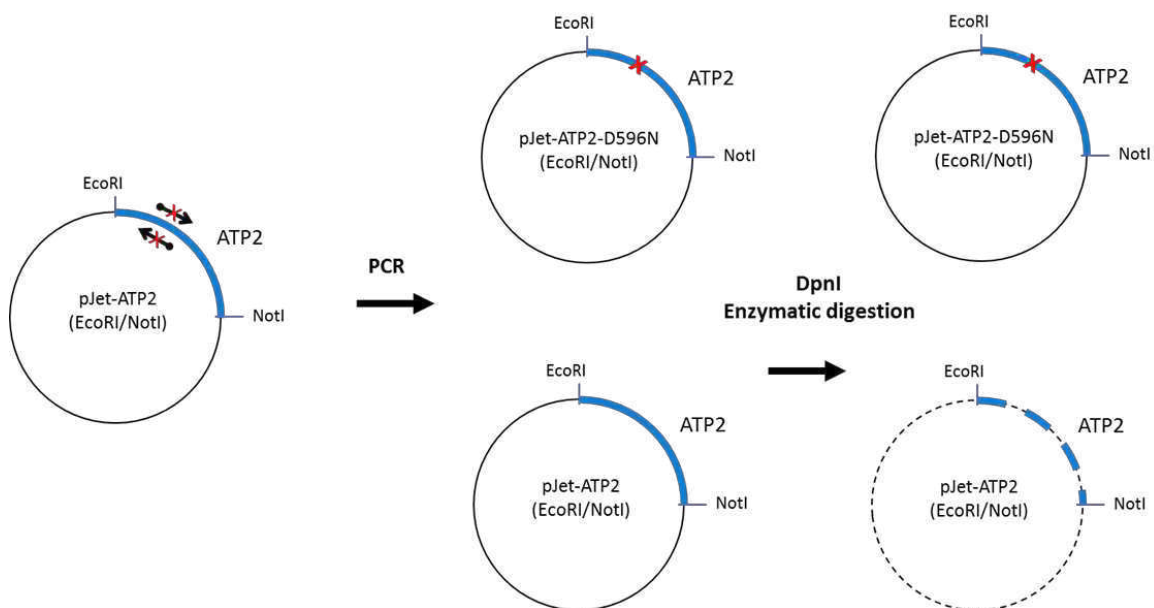


**Figure 51: Obtention of D596N-PcATP2 using the Quickchange mutagenesis kit.**

Two complementary primers containing the desired mutation were used to amplify by PCR the whole vector pJet-PcATP2 (EcoRI/NotI). The PCR products were digested with DpnI which digests the matrix plasmid vector allowing the transformation of *E. coli* cells with only the mutated plasmid vector.

### 3. Construction of the expression vectors for *Pichia pastoris*

For the expression in *Pichia pastoris* we used two vectors kindly provided by Dr Alex Peralvarez-Marin (Autonomous University of Barcelona, Barcelona, Spain) named pJIN vectors and derived from the pPICZ plasmids from Invitrogen. Those vectors contain sequences for the replication and selection in *E. coli*: the pUC origin of replication and the Zeocin resistance gene (fig 52). In *P. pastoris*, plasmids containing both the gene of interest and the Zeocin resistance gene are integrated in the genome of the yeast by recombination, Zeocin is then used to select the transformed yeast clones. For the expression, the genes of interest are under the control of the strong Alcohol oxidase I (AOX1) promoter, allowing the induction by addition of methanol in the culture media. In the pJIN vectors, the myc epitope fused to the C-terminal end of the cloned protein was removed and replaced by an octahistidine tag (pJINC8H) or by a eGFP followed by a thrombin cleavage site and a hexahistidine tag (pJIN077) (fig 52). Both vectors contain the EcoRI/NotI restriction sites for the cloning of the genes of interest.

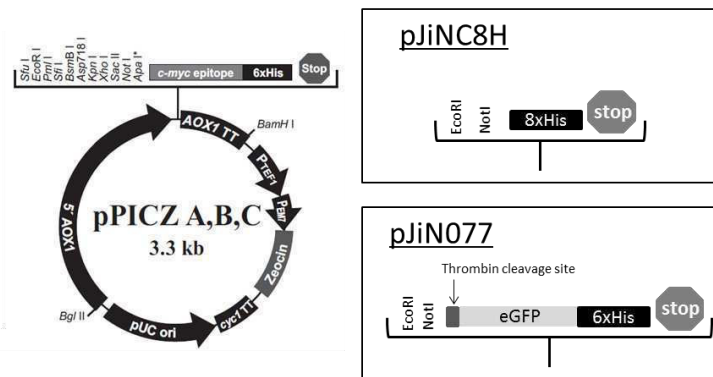


**Figure 52: Features of the pPICZ vector from Invitrogen.**

The original pPICZ from Invitrogen was modified by replacing the myc epitope by a His8 tag (pJINC8H) or by an eGFP-thrombin-His6 tag (pJIN077). Replication and selection in *E. coli*. pUC ori: the origin of replication; Zeocin: resistance marker; EM7 promoter and TEF1 promoter for the expression of the Zeocin resistance gene in *E. coli* and in *P. pastoris*, respectively. Expression in yeast: AOX1: Alcohol oxidase I promoter; AOX1TT: Alcohol oxidase I terminator.

### Construction of the single expression vectors:

The PcATP2 sequence was cloned from the pYeDP60-PcATP2-TEV-BAD into the pJIN077 to obtain the pJIN-PcATP2-Thrombin-eGFP-His<sub>6</sub> vector using directly EcoRI/NotI restriction sites (fig 53, panel A). For the PcCdc50.1 and PcCdc50.3 subunits, I had first to amplify the coding sequence by PCR to introduce the NotI site in the C-terminus of each Cdc50 sequence. The PCR fragment was cloned into the pJet1.2/blunt and the PcCdc50 subunits sequences were cloned into the pJINC8H using EcoRI/NotI restriction sites to obtain the pJIN-PcCdc50.1-His<sub>8</sub> and the pJIN-PcCdc50.3-His<sub>8</sub> vectors (fig 53, panel B).

### Construction of the co expression vectors:

We used the same strategy as for the pYeDP60 co-expression vectors and cloned each gene under the control of its own promoter and terminator in the same expression vector. The pJIN vectors contain a unique BamHI restriction site after the AOX1 terminator (fig 53). In order to clone the cassette promoter-PcCdc50-His<sub>8</sub>-terminator in the pJIN-PcATP2-Thrombin-eGFP-His<sub>6</sub>, I had first to introduce a second BamHI site before the AOX1 promoter in the pJIN-Cdc50 vectors. Here I also used the QuikChange II XL site-directed mutagenesis kit using the primers (forward) 5'-GGGATTTTGGTCATGAGATCGGATCCAACATCCAAAGACG-3' and (reverse) 5'-CGTCTTTGGATGTTGGATCCGATCTCATGACCAAATCCC-3', using the pJIN-PcCDC50.1-Thrombin-His<sub>8</sub> and the pJIN-PcCDC50.3-Thrombin-His<sub>8</sub> as templates. These two vectors

were then digested by BamHI together with the pJIN-PcATP2-Thrombin-GFP-His<sub>6</sub>. The later was also dephosphorylated to avoid self-ligation. The cassette Cdc50 subunit was then cloned in the vector containing PcATP2, so we obtained the co-expression vectors pJIN-PcATP2-Thrombin-GFP-His<sub>6</sub>-PcCdc50-Thrombin-His<sub>8</sub> (fig 53, panel C).

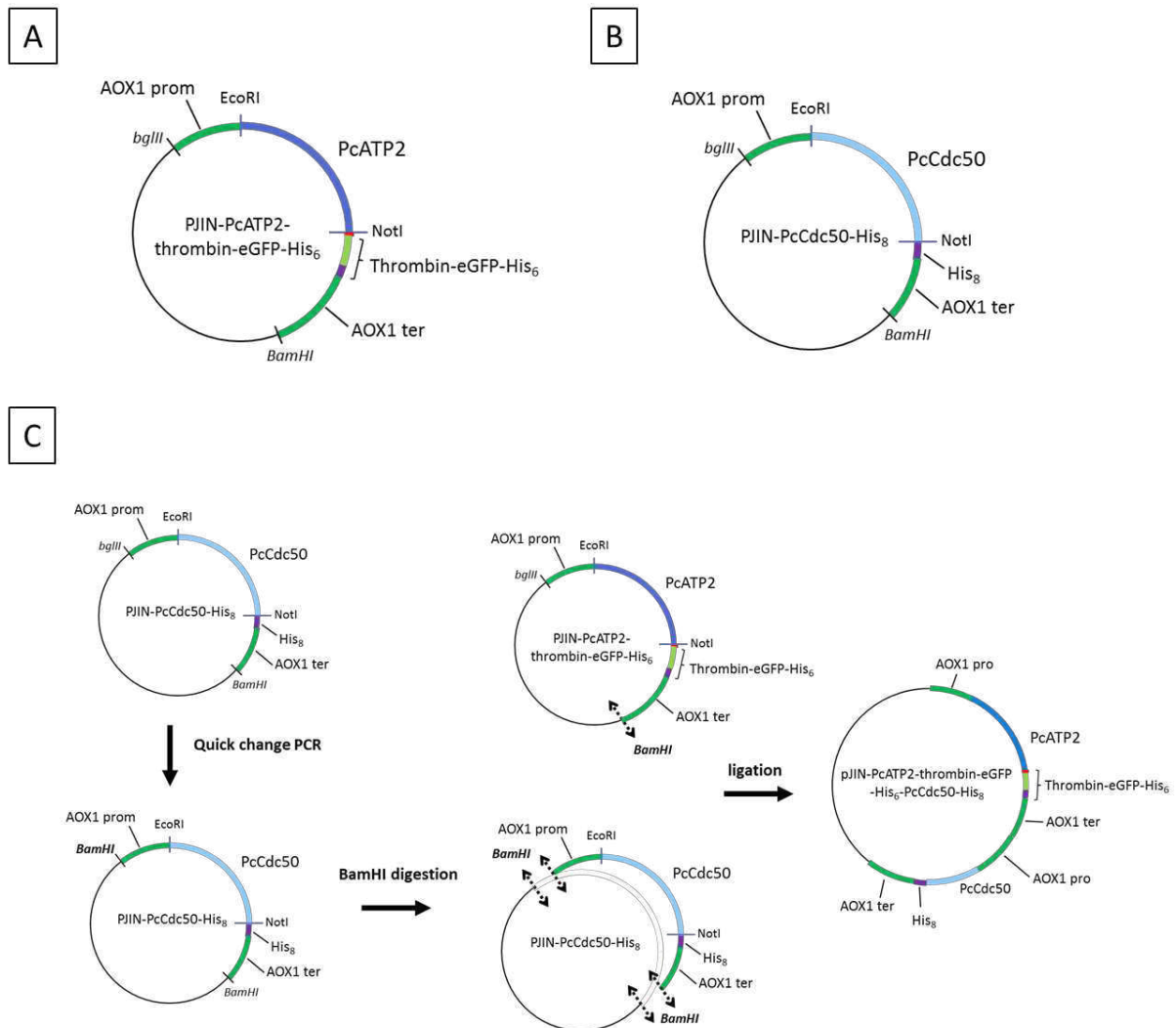


**Figure 53: Cloning strategy to obtain the *P. pastoris* co-expression vectors.**

*Panel A: single-expression vector pJIN-PcATP2-thrombin-eGFP-His<sub>6</sub> containing a unique BamHI restriction site. Panel B: single-expression vector pJIN-PcCdc50-His<sub>8</sub> containing a unique BamHI restriction site. Panel C: strategy to construct the co-expression vector pJIN-PcATP2-thrombin-eGFP-His<sub>6</sub>-PcCdc50-His<sub>8</sub>. The BglIII restriction site in the PcCdc50 expression vector was replaced by a BamHI restriction site using the QuickChange kit. Then, the PcCdc50 expression vector with the two BamHI sites and the PcATP2 expression vector was digested by BamHI and the PcCdc50 encoding gene with the AOX1 promoter and the AOX1 terminator was inserted into the PcATP2 single-expression vector to finally obtain the co-expression vector.*

## 4. Bacterial strains

To clone, amplify the different cDNA constructs in the plasmid vectors, and express some proteins for our work, we used three different strains of *Escherichia coli*, the XL1-blue, the CopyCutter EPI400 and the BL21 (DE3).

The XL1-blue strain (Agilent) is a common strain for cloning and amplifying plasmid DNAs. Its genotype is *recA1 endA1 gyrA96 thi-1 hsdR17 supE44 relA1 lac [F' proAB lacIqZΔM15 Tn10 (Tetr)]*. It is deficient for the endonuclease (EndA), which allows a better quality of plasmids and it is recombination deficient (*recA*) which improves the stability of the construct that is amplified. The *hsdR* mutation avoids the cleavage of the plasmid by the EcoK endonuclease system and this strain is tetracycline resistant.

The CopyCutter EPI400 strain (Epicentre Biotechnologies) is a special strain developed to significantly lower the copy number of the transformed plasmid vectors in order to handle challenging DNA sequences. Its genotype is *F- mcrA D(mrr-hsdRMS-mcrBC) f80dlacZDM15 DlacX74 recA1 endA1 araD139 D (ara, leu)7697 galU galK l- rpsL nupG tonA DpcnB dhfr*. It is possible to increase the copy number by adding a proprietary solution (CopyCutter Induction Solution) during the culture. This strain has a modified *pcnB* gene which controls the copy number of vectors in the cell. The original gene has been replaced by a new *pcnB* gene but under the control of an inducible promoter that is activated by the CopyCutter Induction Solution

The *E. coli* BL21 (DE3) strain was used for the expression of the nanoGFP and the 3C protease. Its genotype strain is *B F- ompT gal dcm lon hsdSB(rB-mB-) λ(DE3 [lacI lacUV5-T7p07 ind1 sam7 nin5]) [malB+]K-12(λS)*. This strain contains the λ prophage DE3 which carries the T7 RNA polymerase and the *lacIq* genes. Plasmids encoding a protein under the control of the T7 promoter have the transcription of the gene completely repressed until isopropylthio-β-D-galactoside (IPTG) is added, inducing the synthesis of the T7 RNA polymerase from a *lac* promoter.

## 5. General molecular biology

### Enzymatic digestion and dephosphorylation:

We usually digested 1 μg of DNA with 1 μL of enzyme, which corresponds to 10-20 units. All the enzymes were used with the CutSmart buffer (NEB), a unique buffer which can be

used for the majority of the enzymes. The digestions were carried out at 37°C for 1 hour. In the case of a digestion with a unique restriction site in the vector, dephosphorylation of the 5' end was also performed to avoid vector self-ligation during the ligation. For this, after the restriction enzymes digestion, 1 µL of calf intestine phosphatase (CIP) was added and incubated at 37°C for 30 min.

### Purification of DNA fragments:

After digestion and dephosphorylation (if needed), the different fragments of DNA required for the construction of the vectors were run in a 1% agarose gel electrophoresis at 60 V. The gel was then stained in 2 µg/mL of ethidium bromide (EB) for 10-15 min and then washed in 1 mM MgSO<sub>4</sub> for 10-15 min. The fragments were purified using the Nucleospin® Gel and PCR clean up kit (Macherey Nagel), after DNA extraction from the agarose gels.

### Ligation:

Two protocols were used for cloning the purified fragments. In a first procedure the quick ligation vector, the CloneJET PCR Cloning kit (Thermo Scientific), was used to easily store and amplify fragments typically obtained after PCR (fig 54). Otherwise, a classical ligation procedure was done using the same PCR fragments as inserts. After purification of the DNA fragments, the reaction of ligation was done using ~30-40 ng of the vector and 90-120 ng of the insert with 400 units of the enzyme T4 DNA ligase. The ligation was performed overnight at 16°C.

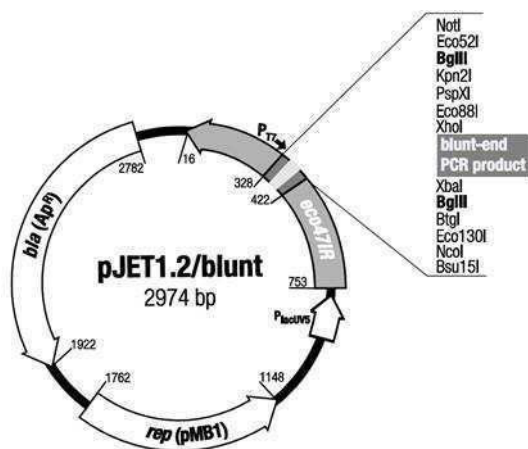


**Figure 54: Features of the pJET1.2/Blunt.**

*The pJET1.2/blunt was used to clone the PCR fragments in order to store and replicate them. It possesses the pMB1 bacterial origin of replication and the ampicillin resistant maker (Ap<sup>R</sup>).*

### Preparation of chemically-competent bacteria and transformation:

We prepared our own *E. coli* competent cells following the protocol of Inoue (Inoue, Nojima, and Okayama 1990). First, an overnight culture was made in 5 mL of Luria-Bertani (LB) media, supplemented with 50 µg/mL of tetracycline for the XL1-blue, at 37°C with 200 rpm shaking. 200 µL of the overnight culture was added to 100 mL SOB media, supplemented or not with tetracycline. The flask was placed in the incubator at 20°C with 200 rpm shaking. Once the cell density reaches an optical density at 600 nm (OD<sub>600nm</sub>) of about 0.6, the culture flasks were placed on ice for 10 min. The cells were centrifuged in 50 mL sterile tubes during 10 min and 4°C at 2500 x *g*, and the cell pellet was re-suspended by gentle shaking in 32 mL of ice-cold TB buffer (10 mM PIPES, 15 mM CaCl<sub>2</sub>, 250 mM KCl, adjusted to pH 6.7 with KOH, and supplemented afterwards with 55 mM of MnCl<sub>2</sub>). Then, the cell suspension was kept on ice for 10 min and centrifuged during 10 min and 4°C at 2500 x *g*. The supernatant was discarded, the cell pellet was gently re-suspended in 8 mL of ice-cold TB buffer and DMSO was added to reach a final concentration of 7%. The cells were left on ice for 10 min and 200 µL aliquots were placed in 1.5 mL Eppendorf tubes. The tubes were flash-frozen in liquid nitrogen and stored at -80°C.

Between 50 µL and 100 µL of chemically-competent cells were incubated with the DNA (0.5 µL of a plasmid miniprep or 10 µL of a ligation) and incubated for 15-30 min on ice. A thermic shock was done at 42°C, for 45 sec for the XL1-blue and BL21, and for 30 sec for the EPI400. Then, the cells were left on ice for 2 min and 800 µL of LB was added. The cells were left at 37°C for 45 min to 1 hour and then plated on LB agar plates supplemented with ampicillin (100 µg/mL) and incubated overnight at 37°C.

### **Plasmid DNA preparation and sequencing:**

In order to select the right vectors after ligation, a 5 mL overnight culture of each clone was done in LB media supplemented with ampicillin. For the CopyCutter EPI400 cells, the replication of the plasmid DNA was induced to obtain a higher copy number and to get enough material for the miniprep. For this, the overnight culture was diluted to an OD<sub>600</sub> of 0.2 in LB supplemented with ampicillin and 1 X CopyCutter solution (from a stock solution of 1000 X). The culture was incubated at 37°C for 4 h with vigorous shaking as the aeration of the culture is critical here to obtain a high density culture at the end. From these cultures, the plasmid DNA was isolated using the Nucleospin® Plasmid kit (Macherey Nagel). The plasmids were then controlled by enzymatic

digestion and samples were sent for sequencing to Eurofins Genomics in order to check the constructs.

## V-2-2 Expression in the yeast *Saccharomyces cerevisiae*

### 1. *Saccharomyces cerevisiae* strain

We used the strain W3031b Gal4-2 (*a, leu2, his3, trp1::TRP1-GAL10-GAL4, ura3, ade2-1, can<sup>r</sup>, cir<sup>+</sup>*) previously described (Lenoir et al. 2002). This strain is auxotrophic for the amino acids leucine and histidine and also for the nitrogen bases adenine and uracil. There are two copies of the gene encoding the Gal4 transcription factor in order to increase the expression of this protein and therefore to increase the expression of our protein. GAL4 is constitutively expressed but the amount of protein is low. In order to significantly increase the level of expression of the gene of interest, a second copy of the Gal4 gene was inserted by homologous recombination in the genome, under the control of the GAL10 inducible promoter. After the addition of galactose in the culture media, the repression of the Gal80p is removed, and more copies of Gal4p are produced to induce the Gal10/Cyc1 hybrid promoter of our pYeDP60 plasmid (fig 55).

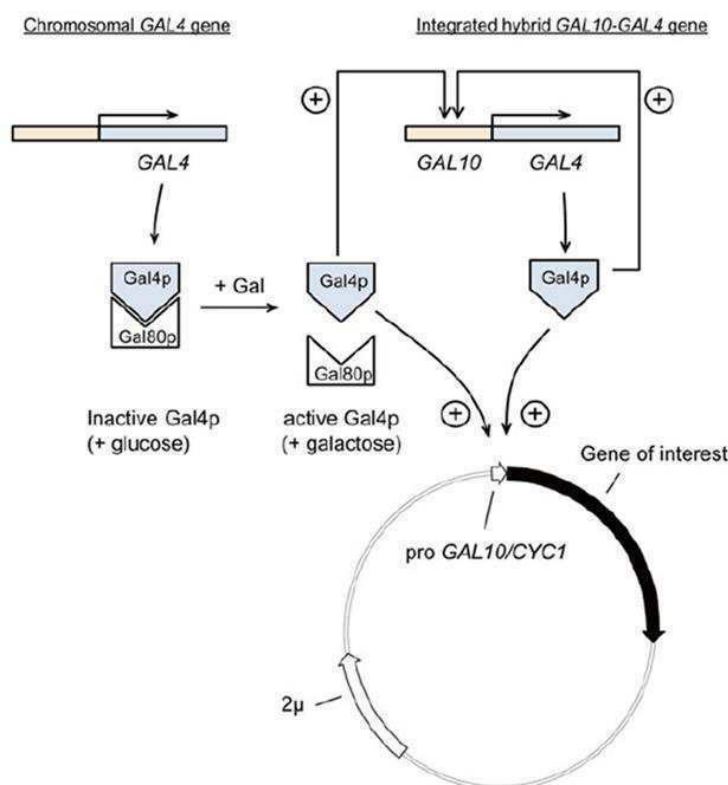


**Figure 55: Expression system of the W303.1b Gal4-2 *S. cerevisiae* strain.**

An additional copy of the *GAL4* gene under the control of the *GAL10* promoter is present in the W3031b Gal4-2 strain.

Gal4p is a transcription factor that induces the activation of the transcription of genes under the control of *GAL* promoters. In the presence of glucose, the Gal80p represses the action of the Gal4p protein. In the presence of galactose and in the absence of glucose, the interaction between Gal4p and Gal80p is disrupted and Gal4p will activate the *GAL* promoters (Azouaoui et al. 2016).

## 2. Transformation by the lithium acetate method

A pre-culture of non-transformed yeast was done in 5 mL of S6AU minimal media for 24 h at 28°C and 200 rpm agitation. Then, a volume of this pre-culture corresponding to 4 optical density units at 600 nm was centrifuged in a sterile 2 mL Eppendorf tube at 800 x *g* for 5 min . The media was removed and 1 µg of plasmid DNA and 100 µg of salmon sperm DNA (denatured at 100°C for 5 min and cooled down on ice) were added. After vortexing the tube, 500 µL of PLATE buffer and 20 µL of 1 M DTT filtered were added. The tube was vortexed again and left overnight at room temperature. The next morning the tube was centrifuged at 350 x *g* for 2 min, the supernatant was removed and the cells were re-suspended in 100 µL of S6A minimal media and plated on S6A agar plates. The plates were left in the incubator at 28°C for 3 to 5 days until the transformed colonies appeared.

## 3. Functional complementation (cold-sensitive assay)

Our lab possesses a *S. cerevisiae* strains where the gene encoding for Cdc50p has been removed: W3031b Gal 4-2  $\Delta cdc50$ . This strain shows a cold-sensitive phenotype, since it is not able to grow at 20°C (C. Y. Chen et al. 1999). A normal growing can be rescued after expressing Cdc50p in the W3031b Gal 4-2  $\Delta cdc50$  strain, or co-expressing Drs2p/Cdc50p, suggesting functional restoration (Azouaoui et al. 2016). In our assay, W3031b Gal 4-2  $\Delta cdc50$  was transformed with pYeDP60 plasmids containing the following proteins: no protein or the empty vector, the single-expression Drs2p-BAD or Cdc50p-His<sub>10</sub> vectors, co-expression Drs2p-BAD/Cdc50p-His<sub>10</sub>, the single expression PcATP2-BAD, PcCdc50.1-His<sub>10</sub>, and PcCdc50.3-His<sub>10</sub>, and the co-expression PcATP2-BAD/PcCdc50.1-His<sub>10</sub> and PcATP2-BAD/PcCdc50.3-His<sub>10</sub>. After transformation, clones of each construct were grown in 5 mL of S6A media during 24 h at 28°C with 200 rpm shaking. Then, the OD<sub>600</sub> of each culture was measured and cultures were diluted to reach OD<sub>600</sub> of 0.2, 0.02 and 0.002. 5µL of each sample dilution were deposited on S5AF agar plates, containing galactose and fructose, and incubated at 28°C from 48 h to 72 h.

## 4. Protein expression in *S. cerevisiae*

### Protein expression in small-scale cultures:

In order to screen the different constructs for protein expression, we did a small-scale expression test in rich media. A pre-culture of 5 mL of S6A media was made for each



construct. The cells were grown for 24 h at 28°C with 200 rpm shaking. After 24 h, the OD<sub>600</sub> of the pre-culture was measured and the culture was diluted to an OD<sub>600</sub> of 0.2 in 20 mL of YPE2X rich media. The culture was incubated for 30 h at 28°C with 150 rpm shaking. After 30 h, the culture was cooled down on ice until it reached 18°C, then 20 g/L of galactose was added to induce expression and the culture was left for 18 h at 18°C with 150 rpm shaking.

### **Protein expression in large-scale cultures:**

For large-scale experiments, we used Fernbach type flasks to grow 500 mL of cells per flask. A first pre-culture was done in 5 mL of S6A media and the cells were grown for 24 h at 28°C with 200 rpm shaking. After this 24 h, the OD<sub>600nm</sub> was measured and the culture was diluted to an OD<sub>600nm</sub> of 0.1 in 50 mL of S6A media. This second pre-culture was incubated at 28°C for 24 h with 200 rpm shaking. After this second incubation, the OD<sub>600nm</sub> was measured and the culture was diluted to an OD<sub>600nm</sub> of 0.05 in 500 mL of YPGE2X media, previously preheated at 28°C. The cells were grown for 36 h at 28°C with 130 rpm shaking. After 36 h, when the yeast has consumed almost all the totality of the glucose present in the media, the culture was cooled down (on ice) to 18°C, and 2% (w/v) of galactose was added (10 g of powder to each 500 mL culture) to induce proteins expression. After 13 h at 18°C with 130 rpm shaking, a second addition of 2% (w/v) galactose was done and the culture was left for five more hours resulting, finally, in 18 h of total induction time. The cells were then centrifuged at 4000 x *g* during 10 min at 4°C and washed several times with water. The cell pellet was weighted and re-suspended in 2 mL of TEKS buffer per gram of cells. After incubation at 4°C for 15 min, the cells were centrifuged and the resulting pellet was flash-frozen in liquid nitrogen, and then stored at -80°C.

## **5. Membrane preparation**

### **Total membrane preparation from small-scale cultures:**

To analyse the expression of the proteins induced in the small-scale cultures, a total membrane preparation was done. First, the OD<sub>600nm</sub> of the culture was measured and in order to have approximately the same amount of cells for each condition, a volume of each culture corresponding to 10 optical density units at 600 nm was centrifuged at 800 x *g* for 10 min and 4°C. Then, the cells were re-suspended in 1 mL of ice-cold TEPI buffer

and transferred into 1.5 mL Eppendorf tubes to be centrifuged at 1000 x *g* for 10 min and 4°C (Beckman allegra X20, rotor 3015). The pellet was re-suspended in 100 µL of ice-cold TEPI and about 100 µL of glass beads (0.5 mm of diameter) were added. The tubes were vortexed for 25 min at 4°C. TEPI buffer was then added up to 1 mL and the tubes were centrifuged at 500 x *g* for 5 min at 4°C. The supernatant was transferred into an ultracentrifuge 1.5 mL Eppendorf tube, and was centrifuged at 100000 x *g* for 90 min at 4°C (benchtop TL-100 Beckman ultracentrifuge with the TLA-45 Beckman rotor). The resulting pellet was re-suspended directly in 200 µL of either 2 X U loading buffer or re-suspension buffer (see section V-1-2).

### **Membrane preparation and fractionation from large-scale cultures:**

The cell-pellet from large-scale cultures harbouring the different plasmid constructs were thawed at room temperature and re-suspended in 1 mL of TES buffer per gram of cell-pellet and supplemented 1 X of Protease Inhibitor Cocktail (PIC) and 1 mM PMSF. The cells were broken with glass beads using a planetary mill (Pulverisette 6 from Fritsch). The cell suspension was poured into an agate grinding bowl with an equal volume of 0.5 mm diameter glass beads and the instrument was set to grind the sample: 450 rpm during 3 min, pause for 30 sec and 450 rpm during 3 min in the reverse sense. The crude extract was recovered and the beads were washed with 1.5 mL of TES buffer supplemented with 1 X PIC and 1 mM PMSF per gram of cell pellet. At this step, the pH of the broken cells was adjusted to 7.5 to prevent the action of endogenous proteases. The crude extract was centrifuged at 1000 x *g* for 20 min and 4°C. After the centrifugation, the first pellet (dubbed P1) contains unbroken cells, cell debris and some glass beads were removed. The resulting supernatant (S1), was centrifuged at 20000 x *g* for 20 min at 4°C to obtain the second pellet (P2) that contains the “heavy membranes”. The supernatant (S2) was centrifuged again at 125 000 x *g* during 1h at 4°C. The resulting pellet (P3) contains the “light membranes” which were re-suspended in 0.2 mL of HEPES-sucrose buffer per gram of cell-pellet. The different membrane pellets were flash-frozen in liquid nitrogen and kept at -80°C (fig 56).

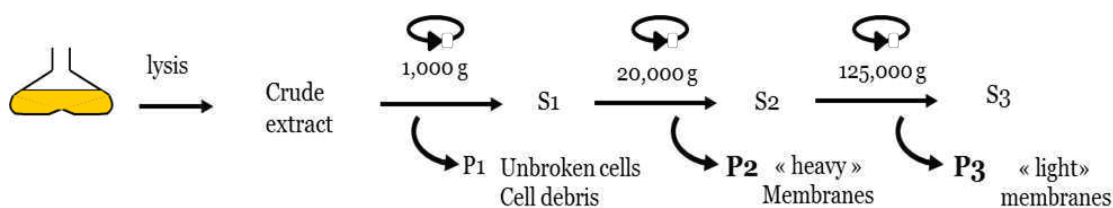


**Figure 56: Membrane fractionation from *S. cerevisiae* cells.**

After cell breaking, the crude extract obtained was subjected to a first low-speed centrifugation in order to remove non-broken cells and cell debris. Then, the S1 supernatant was subjected to a medium-speed centrifugation where we obtained the P2 « heavy membranes » and the S2 supernatant which is subjected to a final ultracentrifugation to obtain the P3 « light membranes » fractions.

## 6. Deglycosylation of PcCdc50.1 and PcCdc50.3 subunits

The two subunits PcCdc50.1 and PcCdc50.3 were tested for deglycosylation by the enzymes PGNase F and EndoH. P3 membranes of *S. cerevisiae* cells co-expressing PcATP2/PcCdc50.1, PcATP2/PcCdc50.3 and Drs2p/Cdc50p were diluted up to 4 mg/mL in HEPES-sucrose buffer. Then, 5  $\mu$ L of this dilution, corresponding to 20  $\mu$ g of total protein, were added to 1  $\mu$ L of the 10 X Glycoprotein denaturing buffer and 4  $\mu$ L of MilliQ water. The denaturation was performed for 10 min at 100°C in a dry bath. Then, the tubes were cooled down on ice for 5 min and centrifuged 10 sec in a mini-centrifuge. In the deglycosylation assays with PGNase F, 10  $\mu$ L of denatured sample were added to 2  $\mu$ L of Glycobuffer 2 (10 X), 2  $\mu$ L of NP-40 buffer, 5  $\mu$ L of milliQ water and 1  $\mu$ L of PGNase F. In the deglycosylation by EndoH, 10  $\mu$ L of denatured sample were added to 2  $\mu$ L of Glycobuffer 3 (10 X), 7  $\mu$ L of MilliQ water and 1  $\mu$ L of EndoH. The tubes were incubated for 1 h at 37°C. The samples were analyzed by western blot.

## V-2-3 Expression in the yeast *Pichia pastoris*

### 1. *Pichia pastoris* strain

We used the *P. pastoris* strain SMD1168H which is derived from the original strain NRRL-Y 11430 (Northern Regional Research Laboratories, Peoria, Ill.), and commercially available by Invitrogen. This strain is  $\Delta$ pep4 which means that it is deficient for proteinase A and carboxypeptidase Y, and has approximately half of proteinase B activity. *Pichia pastoris* is a methylotrophic yeast, so it can metabolize methanol using different alcohol oxidase enzymes, mostly AOX1.

## 2. Transformation by electroporation

To prepare the competent cells, a 100 mL overnight culture of *P. pastoris* SMD1168H in YPD media was made at 30°C with 200 rpm shaking until the cell density reached an OD<sub>600</sub> of 1.3-1.5. The cells were then pelleted at 1500 x *g* for 5 min and 4°C, and then washed in 100 mL of ice-cold sterile water. A second washing step was done in 50 mL of ice-cold sterile water and then the cells were re-suspended in 5 mL of 1 M ice-cold sorbitol. After centrifugation the cells were re-suspended in 500 µL of 1 M ice-cold sorbitol and kept on ice until electroporation, always the same day.

For transformation by electroporation, 80 µL of these cells were incubated with 50 to 100 µg of non-linearized plasmid DNA in a sterile ice-cold 0.2 cm electroporation cuvette for 5 min. The cells were subjected to a pulse of 1.5 kV, 25 µF and 200 Ω (gene pulser, Bio-Rad). Immediately after, 1 mL of 1 M ice-cold sorbitol was added to the cells. The cells were then transferred to a 15 mL falcon tube with 1 mL of YPD and left at 28°C without shaking for 4 to 8 h. 200 µL of cells were plated on YPDS plates supplemented with 100 µg/mL of Zeocin and left at 28°C for 3 to 10 days until colonies appeared.

## 3. Clones selection

### PCR on colony:

Some colonies were picked and re-suspended in 20 µL of milliQ water in small PCR tubes. The cells were then boiled for 5 min at 98°C. To test the incorporation of PcATP2 and PcCdc50.1 on each clone, we amplified both genes by PCR using the following primers. For the PcATP2 we used the primers (forward) 5'-ccgattacggatctctcaat-3' and (reverse) 5'- agcatggagctctcagatcaacttatctgttttct-3'. To amplify a part of the PcCdc50.1 subunit, we used the primers (forward) 5'-gacaaggtatacttctggat-3' and (reverse) 5'-aagactgcgccgcattcttattcttctcataaa-3'. For the reaction, the Quick-Load® *Taq* 2X Master Mix from NEB was used as recommended by the supplier.

### Screening PcATP2 expression following GFP fluorescence:

500 µL of each clone was grown overnight in YPD at 30°C with 250 rpm shaking in 2 mL Eppendorf tubes. Then, the OD<sub>600nm</sub> was measured and the cultures were centrifuged during 5 min at 2000 x *g*. The cells were re-suspended in MM media to a final OD<sub>600nm</sub> of 1. Then, 5 µL drops of these cells were dispensed on top of MM agar plates and left for

drying, before incubation at 28°C for 48 h. After 24h, a few mL of 100% methanol was added at the lid of the plates and left in the incubator for another 24 h of incubation at 28°C.

#### 4. Protein expression and membrane preparation

##### Protein expression in small-scale:

A first culture of 5 mL of selected clones was done in MG media. The cells were grown overnight at 30°C with 200 rpm shaking. The next day the OD<sub>600nm</sub> of the culture was measured, and cells were centrifuged for 5 min at 2000 x *g*. The cell-pellet was re-suspended in an appropriate volume of MM media (induction media) to reach an OD<sub>600nm</sub> of 1 and incubated at 30°C during 24 h with 200 rpm shaking. After 24 h, a second induction was done by addition of 0.5% (v/v) of methanol.

##### Total-membrane preparation from small-scale cultures:

Two different methods were tested to break *P. pastoris* cells as described in the following table:

Protocole 1	Protocole 2
1 mL of cells ( $\approx 10$ OD <sub>600</sub> units)	1 mL of cells ( $\approx 10$ OD <sub>600</sub> units)
Centrifugation at 800 x <i>g</i> for 5 min	Centrifugation at 800 x <i>g</i> for 5 min
Re-suspension of the cells in 1 mL of TEPI buffer and centrifugation at 800 x <i>g</i> for 5 min	Re-suspension of the cells in 1 mL TEPI buffer and centrifugation at 800 x <i>g</i> for 5 min
Re-suspension of the cells in 500 $\mu$ L TEPI buffer	Re-suspension of the cells in 1mL PBS and centrifugation at 800 x <i>g</i> for 5 min
Addition of 500 $\mu$ L of 0.5 mm glass beads	Freeze in liquid nitrogen and thaw. Repeat this 2 times
8 cycles of 1 min vortex/1 min on ice	Re-suspension of the cells in 500 $\mu$ L TEPI buffer
Centrifugation at 200 x <i>g</i> for 5 min	Add 500 $\mu$ L of 0.5 mm glass beads
Take the supernatant and transfer into a 1.5 mL ultracentrifuge Eppendorf tube	8 cycles of 1 min vortex/1 min on ice
Ultracentrifugation at 100 000 x <i>g</i> for 1 h and 4°C	Centrifugation at 200 x <i>g</i> for 5 min
	Take the supernatant and transfer into a 1.5 mL ultracentrifuge Eppendorf tube
	Ultracentrifugation at 100 000 x <i>g</i> for 1 h and 4°C

After the ultracentrifugation, the expression of PcATP2-GFP and PcCdc50.1-His<sub>8</sub> in the membrane preparation was analysed by western blot.

## **V-2-4 Protein detection**

### **1. Determination of total protein concentration**

The concentration of proteins in the samples was measured by the bicinchoninic acid assay (BCA). This assay is compatible with detergents, allowing the use of SDS to solubilize the membrane fractions. In this assay, the first step is the reduction of Cu<sup>2+</sup> to Cu<sup>1+</sup> by the proteins, and then, the cuprous cation is chelated by the BCA forming a purple-coloured product that can be detected by light absorption at 562 nm. The samples were diluted 1/10 in milliQ water and different concentrations of bovine serum albumin (BSA), 0, 1, 2, 3, 4, 5, 6, 7 and 8 mg/mL, were used for the standard curve. 10 µL of the diluted sample was added to 10 µL of milliQ water and 5 µL of 10 % (w/v) SDS. For the standard curve, 10 µL of the different dilutions of BSA were added to 10 µL of a dilution 1/10 of TES buffer or HEPES sucrose buffer and 5 µL of 10% (w/v) SDS. Then, a 50/1 (vol/vol) solution of BCA/CuSO<sub>4</sub> was prepared, and 225 µL of this solution was added to the different samples and standards. 200 µL of each sample or standard was transferred to a 96-well plate and incubated for 30 min at 37°C. The absorbance of each sample was measured at 562 nm using the Epoch microplate spectrophotometer (BioTek Instruments).

### **2. SDS PAGE and western blot**

For protein electrophoresis, 8% SDS PAGE gels were used. Samples at the appropriate total protein concentration were mixed with 2 X U loading buffer to limit membrane protein aggregation (Soulié et al. 1992). The electrophoresis was performed using regular electrophoresis running buffer for 90 min at constant voltage of 110 Volts.

After migration, the gel was stained with a Coomassie-blue staining solution (0.05% (w/v) Coomassie-blue R-250, 40% (v/v) methanol and 10% (v/v) acetic acid) for 30 min at room temperature. The excess of dye was washed with several baths of hot milliQ water. Then, the gel was dried in 10% (v/v) ethanol, 10% (v/v) acetic acid and 5% (v/v) glycerol between two cellophane sheets (Bio-Rad).

For immunoblotting, the proteins in the gel were transferred onto a PVDF (Polyvinylidene difluoride) membrane using a regular transfer buffer during 1 h at constant voltage of 110 Volts, The membranes were then blocked in blocking solution (table 4) for 1 h at room temperature. When the biotin probe (avidin coupled to a peroxydase) was used, the membranes were washed three times for 10 min with PBS-Tween®20 (PBS + 0.02% Tween®20 (v/v)) before the incubation with the probe. The primary antibody (Ab Ir) or the probe was then incubated in blocking solution for 1 h at room temperature, followed by three times 10 min washes with PBS-Tween®20. When needed, the secondary antibody (Ab Iir) was also added in the blocking solution and incubated for 1 h at room temperature. Then, the membranes were washed three times 10 min with PBS-Tween®20 followed by two 10 min washes with PBS. Table 4 displays the different protocols used for the different immunoblots used in this thesis.

**Table 4: summary of the different conditions used for the Western Blot depending on the tag**

Tag	Blocking solution	Primary antibody	Dilution of Ab Ir	Secondary antibody	Dilution of Ab Iir
His tag	2%BSA PBS-tween	His probe	1:2000		
BAD	5% milk PBS-tween	Biotin probe	1:20000		
GFP	5% milk PBS-tween	Mouse Anti-GFP	1:1000	Goat anti-mouse	1:3000

Probe luminescence was triggered using the ECL Western Blotting Detection kit (GE healthcare). The chemiluminescence was recorded with a CCD camera G:BOX (Syngene) using GeneSnap software for the acquisition.

### 3. General procedure for membrane protein solubilisation

In the initial experiments, the solubilisation of membranes (both P2 and P3 membrane fractions) was performed using membranes at total protein concentration of 2 mg/mL, and detergent at 10 mg/mL (1:5 protein/detergent weight ratio) in solubilisation buffer (see section V-1-2). The solubilisation was done overnight at 4°C followed by an ultracentrifugation for 1 h at 125 000 x *g* and 4°C. We performed solubilisation screening testing different detergents, solubilisation times (overnight or 1h), and different temperatures (4 or 20°C). We also tested different pHs: pH 7, pH 8 and pH 7.8.

In addition, we washed the membranes prior the solubilisation to remove membrane-associated proteins using the membrane washing buffer (see section V-1-2) for 30 min at 4°C with gentle rotation. Different ratios of protein/detergent (w/w) were tested: 1:4, 1:5 and 1:10. The addition of the cholesterol derivative, cholesteryl hemisuccinate (CHS) was also tested at a 5:1 (w/w) detergent/CHS ratio.

#### **4. Fluorescence size exclusion chromatography (FSEC)**

The P3 membranes were diluted to 2 mg/mL of total protein concentration and solubilized with 10 mg/mL of DDM and 2 mg/mL of CHS in solubilisation buffer during 1 h at 20°C. After solubilisation, the samples were centrifuged at 125 000 x *g* during 1 h at 4°C to remove large aggregates and non-solubilised membranes. 200 µL of the supernatant was injected into a Superose 6 10/300 GL (GE healthcare) column equilibrated with FSEC equilibration buffer (see sections V-1-2). The AKTA chromatography system (GE healthcare) was used in combination with a fluorescence detector (JASCO FP 4025). The elution profile of PcATP2-GFP, PcCdc50.1-GFP or PcCdc50.3-GFP was analysed following the fluorescence of the GFP. The instrument was piloted by the software UNICORN.

#### **5. Co-immunoprecipitation**

To study the interaction of PcATP2 with their Cdc50 subunits after detergent solubilisation, a co-immunoprecipitation assay was performed using agarose beads coupled to nanobodies that specifically bind the GFP (GFP-Trap®, ChromoTek). Therefore, these beads allowed to trap the GFP fused to PcATP2 or the Cdc50 subunits. P3 membranes diluted to 2 mg/mL of total protein concentration were solubilized in solubilisation buffer with 10 mg/mL of DDM, 2 mg/mL CHS (ratio protein:detergent:CHS 1:5:1, w/w/w) during 1 h at 20°C. After solubilisation, the membranes were ultracentrifuged at 125 000 x *g* for 90 min at 4°C. 25 µL of the GFP-trap beads slurry was put into a 1.5 mL spin column. The beads were equilibrated by addition of 500 µL of ice cold washing buffer 1 (20 mM Tris-HCl pH 7.8, 150 mM NaCl, 0.2 mg/mL DDM 0.04 mg/mL CHS, 10% (v/v) glycerol) and the column was centrifuged at 100 x *g* for 30 seconds. This equilibration step was repeated twice. After the ultracentrifugation, the detergent-solubilized membranes were added to the beads and incubated for 1 h at 4°C with gentle rotation. After incubation the flow-through was collected by centrifugating the sample at 100 x *g* for 30 seconds. The beads were then washed with 500 µL of ice-cold washing



buffer 1 followed by centrifugation at 100 x *g* for 30 seconds. A second wash was done with 500  $\mu$ L of washing buffer 2 (20mM Tris-HCl pH 7.8, 500 mM NaCl, 0.2mg/mL DDM and 10% (v/v) glycerol). The proteins were finally eluted by adding 50  $\mu$ L of 0.2 M glycine buffer pH 2.5 to the beads and pipetting up and down for 30 seconds. The column was placed on a 1.5 ml Eppendorf tube containing 5  $\mu$ L of 1 M Tris base pH 10.4, and the eluted proteins were collected after centrifugation at 100 x *g* for 30 sec. This elution step was repeated a second time. The samples were then analysed by western blot.

## **6. Purification of PcATP2-GFP/PcCdc50.1 complex by affinity chromatography**

### **a. Expression and purification of nanobodies targeting the GFP (nanoGFP):**

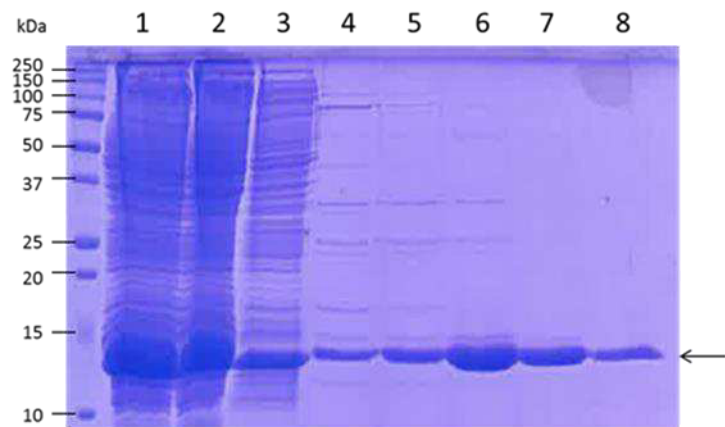
We obtained from Addgene the plasmid vector pOPINE nanoGFP (reference #49172) to express in *E. coli* a C-terminally His-tagged nanobody directed against the GFP (nanoGFP). First, *E. coli* BL21 cells were transformed with the pOPINE nanoGFP plasmid vector and grown overnight at 37°C with 200 rpm shaking in 10 mL LB supplemented with 100  $\mu$ g/mL of ampicillin. 500 mL of LB with ampicillin were inoculated with 4 mL of the overnight pre-culture and the cells were grown at 37°C with 200 rpm shaking. When the OD<sub>600</sub> of the culture reached  $\sim$  0.6, the temperature of the culture and the incubator were reduced down to 20°C. To induce the expression, IPTG was added at a final concentration of 1 mM and the cells were left for 20-24h at 20°C with 200 rpm shaking. The cells were spun down and flash-frozen in liquid nitrogen and stored at -80°C.

For the nanoGFP purification, thawed *E. coli* cells were first re-suspended in 10 mL of lysis buffer (PBS pH 8, 0.5 M NaCl, 5 mM imidazole, 1 mM PMSF and 10  $\mu$ g/ $\mu$ L of lysozyme) and left 1 h at 4°C with gentle rotation. The cells were broken by sonication (Vibra-cell, Bioblock Scientific): 6 cycles of 10 sec on at 40% amplitude and 10 sec off, maintaining the cells always on ice. Broken cells were centrifuged at 20000 x *g* for 20 min at 4°C. Meanwhile, the TALON® cobalt resin (TAKARA) was prepared; 1 mL of the resin was first washed with milliQ water and then equilibrated with 10 resin volumes of equilibration buffer (PBS pH 8, 0.5 M NaCl and 5 mM imidazole). After centrifugation, the supernatant was added to the resin and incubated for 1 h at 4°C with gentle rotation to achieve the binding of the His-tagged nanobodies into the resin. After incubation, the

flow through was recovered and the resin was first washed with 20 resin volumes of equilibration buffer. A second washing was done with 10 resin volumes of equilibration buffer supplemented with 20 mM imidazole and a third washing was done with 10 resin-volumes of equilibration buffer supplemented with 30 mM imidazole. The elution was performed in three steps, two steps where the proteins were eluted with 5 resin-volumes of equilibration buffer supplemented with 150 mM of imidazole and a final step where the remaining proteins were eluted with 5 resin-volumes of equilibration buffer supplemented with 300 mM imidazole. Elution fractions and the different fractions obtained during the purification were analysed in a 14% SDS-PAGE (fig 57). The three elution fractions were pooled and concentrated using a Vivaspin® 20 5000 Mw concentrator (Sartorius) up to a 3 mL of final volume. Concentrated proteins were dialyzed at 4°C to remove the imidazole using a Slide-a-Lyzer (3000 Mw)(ThermoFisher) against, first 500 mL of PBS pH 8 for 5 h and, second, overnight against 500 mL of PBS pH 8. After dialysis, protein concentration was measured and the nanobodies were left at 4°C for several weeks in PBS.

**Figure 57: Purification of the nanoGFP followed by SDS-PAGE and Coomassie blue staining.**

10 µL of each purification fraction were loaded on a 14% SDS-PAGE. Proteins were stained with Coomassie Blue. Lane1: supernatant before incubation with the TALON® resin; lane 2: flow through; lanes 3, 4 and 5: washings of the resin; lanes 6, 7: 150 mM imidazole elution fractions and lane 8: 300 mM elution fraction. The arrow indicates the nanoGFP.



#### **b. NanoGFP coupling to agarose beads:**

We made the nanoGFP sepharose resin by coupling the purified nanoGFP to a NHS-activated agarose beads (GE healthcare). We mostly followed the protocol given by GE and described in Rothbauer et al., (2008). The volume ratio recommended was 0.5:1 nanoGFP/resin. Accordingly, we used 1 mL of NHS-activated agarose beads (2 mL slurry) per mg of purified nanoGFP. 2 ml of NHS-activated slurry (resin + isopropanol) was poured into a plastic column and washed with milliQ water. Just before the reaction,

the resin was washed with 10-15 resin-volumes of 1 mM HCl followed by equilibration with PBS pH 7.5 by adding 10 resin volumes. Thereafter, 1 mg of nanoGFP was added to the 1 mL resin. The volume of the nanoGFP added was kept always between 0.5 to 0.7 mL in order to comply with volume ratio nanoGFP/resin of the reaction. The resin with the nanoGFP was incubated overnight at 4°C under gentle rotation. The next morning, the remaining non-reacted sites of the resin were blocked by the addition of 10-15 resin volumes of 0.1 M Tris-HCl pH 8.5. The resin was incubated in this Tris buffer for 4-5 h at 4°C with gentle rotation. The Tris buffer was removed and the resin was subjected to 3 washing cycles of 3 resin volumes of 0.1 M Tris-HCl, 0.5 M NaCl, pH 8.5 followed by 3 resin volumes of 0.1 M Acetate buffer, 0.5 M NaCl, pH 5.0. Finally, the resin was left in PBS pH 8.0 at 4°C until use.

### c. 3C protease production

An *E. coli* BL21 glycerol stock transformed by a plasmid containing the cDNA encoding the 3C Protease tagged with a 6xHis tag at the N-terminal of the protein was kindly provided by Dr Joe Lyons (Aarhus University, Denmark). The cells from the glycerol stock were first plated on a LB plate supplemented with ampicillin. One *E. coli* colony was inoculated in 10 mL LB supplemented with ampicillin and cells were grown overnight at 37°C with 200 rpm shaking. 2 L of LB supplemented with ampicillin were inoculated with the pre-culture and the cells were allowed to grow at 37°C until they reached a cell density of  $OD_{600nm} = 0.8$ . Then, the cells and the incubator were cooled down to 18°C. Protein expression was induced by the addition of 0.2 mM IPTG in the culture media and the culture was left overnight at 18 °C with 200 rpm shaking.

After pelleting the cells, they were re-suspended in an appropriate volume of Lysis Buffer (50 mM NaPi pH 8.0, 500 mM NaCl, 30 mM Imidazole, 5 mM of  $\beta$ -mercaptoethanol, and no protease inhibitors) in order to obtain a cell density of  $OD_{600} = 10$ . The cells were broken with 0.1 mm glass beads in planetary mill Pulverisette 6 using the same program as for the yeast. Broken cells were centrifuged at 15000 x *g* during 30 min at 4°C. Meanwhile 6 mL of TALON® cobalt beads, previously washed with milliQ water, were equilibrated with 10 resin-volumes of Column Buffer (50 mM NaPi pH 8.0, 500 mM NaCl, 30 mM Imidazole and 5 mM of  $\beta$ -mercaptoethanol). The beads and the supernatant were incubated in a beaker for 1 h at 4°C with soft stirring. After incubation, the beads were washed with 20 column volumes of Column Buffer and the proteins

were eluted with 30 mL (5 column-volumes) of Elution Buffer (50 mM NaPi pH 8.0, 150 mM NaCl, 250 mM Imidazole and 5 mM of  $\beta$ -mercaptoethanol). Eluted proteins were concentrated up to 1 ml using Vivaspin® 20, 30,000 MWCO spin concentrators and further purified by size-exclusion chromatography using a Superose® 6 10/300 GL column equilibrated in 50 mM NaPi pH 8.0, 100 mM NaCl, 1 mM DTT and 0.1 mM EDTA. The purified protein was aliquoted and supplemented with 20 % glycerol and 250 mM NaCl before freezing in liquid N<sub>2</sub> and stored at -80°C.

#### **d. Purification of the PcATP2/PcCdc50.1 complex**

The purification of PcATP2/PcCdc50.1 complex was done using the home-made affinity chromatography column containing the nanoGFP coupled to agarose beads (see nanoGFP coupling to agarose beads). P3 membranes expressing PcATP2/PcCdc50.1 were diluted up to 5 mg/mL of total protein concentration in a buffer containing 20 mM Tris pH 7.8, 150 mM NaCl, 10% (w/v) glycerol, 1X PIC, 20 mg/mL DDM and 4 mg/mL CHS. The solubilisation was performed in a beaker during 1h at 20°C with soft stirring. Then, the sample was ultracentrifuged at 125 000 x *g* during 1h at 4°C. Meantime, in a plastic column, 1 mL of nanoGFP coupled to agarose beads slurry was taken and equilibrated with 10 resin volumes of washing buffer 1 (20 mM Tris pH 7.8, 150 mM NaCl, 10% (w/v) glycerol, 0.2 mg/mL DDM, 0.04 mg/mL CHS and 0.01 mg/mL DOPC). After ultracentrifugation, the detergent-solubilized membranes were incubated with the nanoGFP resin in a beaker for 2 h at 4°C with soft stirring. After incubation, the resin was poured back into the plastic column and the flow-through was recovered. The resin was washed first with 10 resin-volumes of washing buffer 1 and then a second washing was done with 10 resin-volumes of the washing buffer 2 containing a higher amount of salt (20 mM Tris pH 7.8, 500 mM NaCl, 10% (v/v) glycerol, 0.2 mg/mL DDM, 0.04 mg/mL CHS, 0.01 mg/mL DOPC). The resin was then washed with 10 resin volumes of the elution buffer 1 (20 mM Tris pH 7.8, 150 mM NaCl, 10% (w/v) glycerol, 0.2 mg/mL DDM, 0.04 mg/mL CHS, 0.01 mg/mL DOPC and 1 mM DTT). The resin was re-suspended in 1 mL of elution buffer 1 and transferred to a 2 mL Eppendorf tube. 5  $\mu$ g of purified 3C protease was added to the resin and the sample was incubated overnight at 4°C with gentle rotation. After 3C protease digestion, the resin was poured back into the plastic column and the 1 mL of flow-through elution was recovered. The beads were also washed with 0.5 mL of elution buffer 1. A second elution was done with 3 resin volumes

of the elution buffer 2 (20 mM Tris pH 7.8, 500 mM NaCl; 10% (w/v) glycerol; 0.2 mg/mL DDM; 0.04 mg/mL CHS; 0.01 mg/mL DOPC; 1mM DTT). The two elution fractions were combined and concentrated to 250  $\mu$ L using a Vivaspin® 100 concentrator following several centrifugations at 4000 x *g* during 10 min. The different samples from the different steps of the purification were subjected to a SDS-PAGE followed by Coomassie-blue staining analysis and western blot.

## V-2-5 Activity assays of the purified PcATP2/PcCdc50.1 complex

### 1. ATPase activity assay

The ATPase activity of the purified complex was measured by an enzyme coupled system monitored by spectrophotometry. As shown in the figure 58, the hydrolysis of one molecule of ATP leads to the oxidation of one molecule of NADH. As the NADH absorbs at 340 nm, NADH oxidation can be monitored by following the decrease in absorbance at 340 nm that, logically, correlates with ATP hydrolysis.

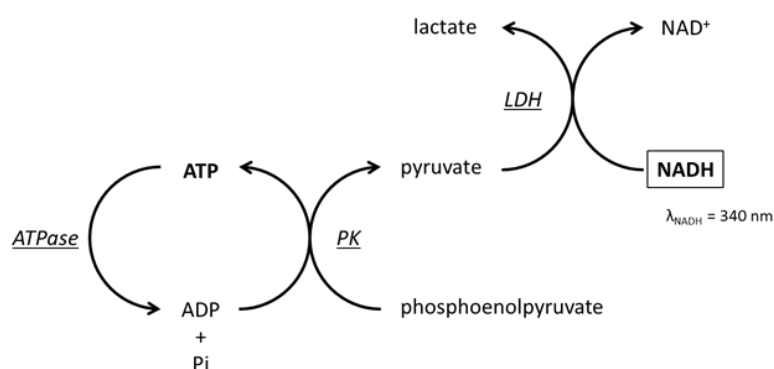


**Figure 58: Scheme of the enzyme coupled assay used to determine ATPase activity.**

*The ATPase hydrolyses the ATP. The PK uses the ADP and Phosphoenolpyruvate to regenerate ATP and produce pyruvate. The LDH uses the pyruvate and NADH to produce lactate and NAD<sup>+</sup>. The decrease of NADH is followed by the decrease of absorbance at 340 nm. PK: pyruvate kinase; LDH: lactate dehydrogenase.*

The reaction was done in a spectrophotometer cuvette at 30°C in 2 mL of SSR buffer supplemented with 0.04 mg/mL of pyruvate kinase, 0.1 mg/mL lactate dehydrogenase, 1 mM DTT, 0.2 mg/ml DDM, 1 mM phosphoenolpyruvate, 1 mM NaN<sub>3</sub> and about 2  $\mu$ g/mL of the purified complex PcATP2/PcCdc50.1. Then, 1 mM of MgATP was added and then we did the baseline on the spectrophotometer. The measure started when 250  $\mu$ M of NADH was added in the cuvette. Different lipids mixed with DDM (0.5 to 1 mg/mL) were added along the reaction as 0.1 mg/mL DOPC, 0.2 mg/mL POPS, 0.1 mg/mL POPE, 0.2 mg/mL POPC, 0.03 mg/mL PIP<sub>2</sub> and 0.03 mg/mL PI4P. 120  $\mu$ g final of

trypsin was also added and if desired AP5-A, an inhibitor of adenylate kinase, was also added at 1.1  $\mu\text{M}$  concentration. The reaction was stopped by addition of 1 mM  $\text{BeF}_3^-$  (1mM  $\text{BeCl}_2$  + 20 mM KF).

## 2. Phosphorylation assay

100  $\mu\text{L}$  of the purified PcATP2/PcCdc50.1 complex (about 2  $\mu\text{g}$  of proteins) was mixed with 2  $\mu\text{g}$  of pyruvate kinase (“loading control”). The samples were incubated on ice before the phosphorylation in the absence or presence of inhibitors as  $\text{BeF}_3^-$  (50 $\mu\text{M}$   $\text{BeCl}_2$ /1mM KF) or the compounds from the Malaria box, MMV007224 and MMV665852 (Spangenberg et al. 2013). Then, [ $\gamma$ - $^{32}\text{P}$ ] ATP was added to a final concentration of 2  $\mu\text{M}$  corresponding to 0.5 mCi/ $\mu\text{mol}$  and incubated for 2 min on ice. The reaction was stopped after the addition of an equal volume of 1 M TCA and 5 mM  $\text{H}_3\text{PO}_4$ , and left on ice for 45 min to allow the precipitation of the proteins. The samples were centrifuged at 14000  $\times g$  during 25 min at 4°C. Each pellet was washed with 100  $\mu\text{L}$  of 0.5 M TCA and 5 mM  $\text{H}_3\text{PO}_4$  followed by centrifugation at 14000  $\times g$  during 25 min at 4°C. The supernatant was removed and the pellet was centrifuged one more time at 14000  $\times g$  during 5 min at 4°C to remove the residual TCA. Then, the samples were re-suspended in 30  $\mu\text{l}$  of 1xU sarkadi loading buffer (see) and 20  $\mu\text{l}$  were loaded on 7% SDS\_PAGE sarkadi gels. The electrophoresis was run at constant intensity of 12.5 mA per gel at 4°C during 3-4 h. After the electrophoresis, the gel was stained with Coomassie blue and dried overnight. The next day the gel was placed in contact with a Phosphor screen (GE healthcare) and phosphorylated proteins were detected 72 h later with a Typhoon PhosphorImager (GE healthcare).

## V-2-6 Fluorescence Microscopy of *S. cerevisiae* cells expressing PcATP2-GFP and Cdc50.1-GFP

A small-scale culture of *S. cerevisiae* expressing PcATP2 alone or co-expressed with PcCdc50.1 was done as described in section Protein expression in *S. cerevisiae*. 1 mL of the culture was centrifuged for 5 min at 2000  $\times g$  and then washed two times with 1 mL of PBS pH 7.4. The cells were re-suspended in 1 mL of PBS pH 7.4 and 2  $\mu\text{L}$  of the cell suspension was deposited on a agarose pad made with 1% (w/v) agarose in milliQ water (see fig 59). The pictures were taken in the Light Microscopy Facility of ImaGif (I2BC) using a Leica confocal microscope SP8 controlled by the LAS-X software.

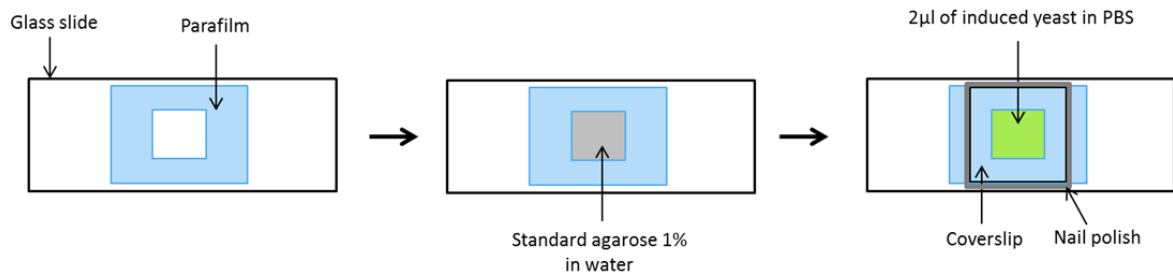


**Figure 59: Scheme of the assembly of the slide containing *S. cerevisiae* cells for confocal microscopy analysis.**

*A square is cut in a piece of parafilm and this piece is put on a glass slide. The parafilm will serve as frame to cast the agarose pad made with 1% agarose melted in milliQ water. The 2  $\mu$ l of induced *S. cerevisiae* cells are deposited on the top of the pad. Then a coverslip is placed on the top of the pad and sealed with nail polish.*

## VI. Bibliography

---

- Abdullah, Saleh, and Kaliyaperumal Karunamoorthi. 2016. "Malaria and Blood Transfusion: Major Issues of Blood Safety in Malaria-Endemic Countries and Strategies for Mitigating the Risk of Plasmodium Parasites." *Parasitology Research* 115 (1): 35–47. <https://doi.org/10.1007/s00436-015-4808-1>.
- Achan, Jane, Ambrose O Talisuna, Annette Erhart, Adoke Yeka, James K Tibenderana, Frederick N Baliraine, Philip J Rosenthal, and Umberto D'Alessandro. 2011. "Quinine, an Old Anti-Malarial Drug in a Modern World: Role in the Treatment of Malaria." *Malaria Journal* 10 (May): 144. <https://doi.org/10.1186/1475-2875-10-144>.
- Aebi, Markus. 2013. "N-Linked Protein Glycosylation in the ER." *Biochimica et Biophysica Acta - Molecular Cell Research*. <https://doi.org/10.1016/j.bbamcr.2013.04.001>.
- Amino, Rogerio, Sabine Thiberge, Béatrice Martin, Susanna Celli, Spencer Shorte, Friedrich Frischknecht, and Robert Ménard. 2006. "Quantitative Imaging of Plasmodium Transmission from Mosquito to Mammal." *Nature Medicine* 12 (2): 220–24. <https://doi.org/10.1038/nm1350>.
- Amoah, Linda E., Jacqueline K. Lekostaj, and Paul D. Roepe. 2007. "Heterologous Expression and ATPase Activity of Mutant versus Wild Type PfMDR1 Protein." *Biochemistry*. <https://doi.org/10.1021/bi7002026>.
- Angov, Evelina. 2011. "Codon Usage: Nature's Roadmap to Expression and Folding of Proteins." *Biotechnology Journal* 6 (6): 650–59. <https://doi.org/10.1002/biot.201000332>.
- Antony, Hiasindh Ashmi, and Subhash Chandra Parija. 2016. "Antimalarial Drug Resistance: An Overview." *Tropical Parasitology* 6 (1): 30–41. <https://doi.org/10.4103/2229-5070.175081>.
- Arnou, Bertrand, Cédric Montigny, Jens Preben Morth, Poul Nissen, Christine Jaxel,



- Jesper V Møller, and Marc le Maire. 2011. "The Plasmodium Falciparum Ca(2+)-ATPase PfATP6: Insensitive to Artemisinin, but a Potential Drug Target." *Biochemical Society Transactions* 39 (3): 823–31. <https://doi.org/10.1042/BST0390823>.
- Arrow, Kenneth J, Claire Panosian, and Hellen Gelband. 2004. *Saving Lives, Buying Time: Economics of Malaria Drugs in an Age of Resistance*. Institute of Medicine (US) Committee on the Economics of Antimalarial Drugs. [https://doi.org/ISBN-10: 0-309-09218-3](https://doi.org/ISBN-10:0-309-09218-3).
- Ashley, Elizabeth A, Aung Pyae Phyo, and Charles J Woodrow. 2018. "Malaria." *Lancet (London, England)* 391 (10130): 1608–21. [https://doi.org/10.1016/S0140-6736\(18\)30324-6](https://doi.org/10.1016/S0140-6736(18)30324-6).
- Autino, Beatrice, Alice Noris, Rosario Russo, and Francesco Castelli. 2012. "Epidemiology of Malaria in Endemic Areas." *Mediterranean Journal of Hematology and Infectious Diseases* 4 (1): e2012060. <https://doi.org/10.4084/MJHID.2012.060>.
- Azouaoui, Hassina, Cédric Montigny, Miriam Rose Ash, Frank Fijalkowski, Aurore Jacquot, Christina Grønberg, Rosa L. López-Marqués, et al. 2014. "A High-Yield Co-Expression System for the Purification of an Intact Drs2p-Cdc50p Lipid Flippase Complex, Critically Dependent on and Stabilized by Phosphatidylinositol-4-Phosphate." *PLoS ONE*. <https://doi.org/10.1371/journal.pone.0112176>.
- Azouaoui, Hassina, Cédric Montigny, Thibaud Dieudonné, Philippe Champeil, Aurore Jacquot, José Luis Vázquez-Ibar, Pierre Le Maréchal, et al. 2017. "High Phosphatidylinositol 4-Phosphate (PI4P)-Dependent ATPase Activity for the Drs2p-Cdc50p Flippase after Removal of Its N- and C-Terminal Extensions." *Journal of Biological Chemistry*. <https://doi.org/10.1074/jbc.M116.751487>.
- Azouaoui, Hassina, Cédric Montigny, Aurore Jacquot, Raphaëlle Barry, Philippe Champeil, and Guillaume Lenoir. 2016. "Coordinated Overexpression in Yeast of a P4-ATPase and Its Associated Cdc50 Subunit: The Case of the Drs2p/Cdc50p Lipid Flippase Complex." *Methods in Molecular Biology (Clifton, N.J.)* 1377: 37–55. [https://doi.org/10.1007/978-1-4939-3179-8\\_6](https://doi.org/10.1007/978-1-4939-3179-8_6).
- Baldrige, Ryan D, and Todd R Graham. 2013. "Two-Gate Mechanism for Phospholipid

- Selection and Transport by Type IV P-Type ATPases." *Proceedings of the National Academy of Sciences of the United States of America* 110 (5): E358-67.  
<https://doi.org/10.1073/pnas.1216948110>.
- Bannister, L.H, J.M Hopkins, R.E Fowler, S Krishna, and G.H Mitchell. 2000. "A Brief Illustrated Guide to the Ultrastructure of Plasmodium Falciparum Asexual Blood Stages." *Parasitology Today* 16 (10): 427-33. [https://doi.org/10.1016/S0169-4758\(00\)01755-5](https://doi.org/10.1016/S0169-4758(00)01755-5).
- Barbot, Thomas, Cédric Montigny, Paulette Decottignies, Marc Maire, Christine Jaxel, Nadège Jamin, and Veronica Beswick. 2016. *Regulation of Ca<sup>2+</sup>-ATPases, V-ATPases and F-ATPases*. <https://doi.org/10.1007/978-3-319-24780-9>.
- Baro, Nicholas K., Chaya Pooput, and Paul D. Roepe. 2011. "Analysis of Chloroquine Resistance Transporter (CRT) Isoforms and Orthologues in *S. Cerevisiae* Yeast." *Biochemistry*. <https://doi.org/10.1021/bi200922g>.
- Bartoloni, Alessandro, and Lorenzo Zammarchi. 2012. "Clinical Aspects of Uncomplicated and Severe Malaria." *Mediterranean Journal of Hematology and Infectious Diseases* 4 (1): e2012026. <https://doi.org/10.4084/MJHID.2012.026>.
- Baum, Jake, Tim-Wolf Gilberger, Freddy Frischknecht, and Markus Meissner. 2008. "Host-Cell Invasion by Malaria Parasites: Insights from Plasmodium and Toxoplasma." *Trends in Parasitology* 24 (12): 557-63.  
<https://doi.org/10.1016/j.pt.2008.08.006>.
- Birkholtz, Lyn-Marie, Gregory Blatch, Theresa L Coetzer, Heinrich C Hoppe, Esmaré Human, Elizabeth J Morris, Zoleka Ngcete, et al. 2008. "Heterologous Expression of Plasmodial Proteins for Structural Studies and Functional Annotation." *Malaria Journal*. <https://doi.org/10.1186/1475-2875-7-197>.
- Bleve, Gianluca, Gian Pietro Di Sansebastiano, and Francesco Grieco. 2011. "Over-Expression of Functional *Saccharomyces Cerevisiae* GUP1, Induces Proliferation of Intracellular Membranes Containing ER and Golgi Resident Proteins." *Biochimica et Biophysica Acta (BBA) - Biomembranes* 1808 (3): 733-44.  
<https://doi.org/10.1016/J.BBAMEM.2010.12.005>.

- Bornert, Olivier, Fatima Alkhalifioui, Christel Logez, and Renaud Wagner. 2012. "Overexpression of Membrane Proteins Using *Pichia Pastoris*." *Current Protocols in Protein Science*. <https://doi.org/10.1002/0471140864.ps2902s67>.
- Bushell, Ellen, Ana Rita Gomes, Theo Sanderson, Burcu Anar, Gareth Girling, Colin Herd, Tom Metcalf, et al. 2017. "Functional Profiling of a Plasmodium Genome Reveals an Abundance of Essential Genes." *Cell* 170 (2): 260–272.e8. <https://doi.org/10.1016/j.cell.2017.06.030>.
- Cardi, Delphine, Alexandre Pozza, Bertrand Arnou, Estelle Marchal, Johannes D. Clausen, Jens Peter Andersen, Sanjeev Krishna, Jesper V. Møller, Marc Le Maire, and Christine Jaxel. 2010. "Purified E255L Mutant SERCA1a and Purified PfATP6 Are Sensitive to SERCA-Type Inhibitors but Insensitive to Artemisinins." *Journal of Biological Chemistry*. <https://doi.org/10.1074/jbc.M109.090340>.
- Carter, Nicola S, Choukri Ben Mamoun, Wei Liu, Edilene O Silva, Scott M Landfear, Daniel E Goldberg, and Buddy Ullman. 2000. "Isolation and Functional Characterization of the PfNT1 Nucleoside Transporter Gene from Plasmodium Falciparum\* Downloaded From." *THE JOURNAL OF BIOLOGICAL CHEMISTRY*. Vol. 275. <http://www.jbc.org/>.
- Champeil, Philippe, Stéphane Orłowski, Simon Babin, Sten Lund, Marc le Maire, Jesper Møller, Guillaume Lenoir, and Cédric Montigny. 2016. "A Robust Method to Screen Detergents for Membrane Protein Stabilization, Revisited." *Analytical Biochemistry* 511 (October): 31–35. <https://doi.org/10.1016/j.ab.2016.07.017>.
- Chen, Chih Ying, Michael F. Ingram, Peter H. Rosal, and Todd R. Graham. 1999. "Role for Drs2p, a P-Type ATPase and Potential Aminophospholipid Translocase, in Yeast Late Golgi Function." *The Journal of Cell Biology* 147 (6): 1223–36. <https://doi.org/10.1083/JCB.147.6.1223>.
- Chen, Sophie, Jiyi Wang, Baby-Periyannayagi Muthusamy, Ke Liu, Sara Zare, Raymond J Andersen, and Todd R Graham. 2006. "Roles for the Drs2p-Cdc50p Complex in Protein Transport and Phosphatidylserine Asymmetry of the Yeast Plasma Membrane." *Traffic* 7 (11): 1503–17. <https://doi.org/10.1111/j.1600-0854.2006.00485.x>.

- Cheruiyot, Jelagat, Luicer A. Ingasia, Angela A. Omondi, Dennis W. Juma, Benjamin H. Opot, Joseph M. Ndegwa, Joan Mativo, et al. 2014. "Polymorphisms in Pf *Mdr1* , Pf *Crt* , and Pf *Nhe1* Genes Are Associated with Reduced *In Vitro* Activities of Quinine in Plasmodium Falciparum Isolates from Western Kenya." *Antimicrobial Agents and Chemotherapy* 58 (7): 3737–43. <https://doi.org/10.1128/AAC.02472-14>.
- Coelho, Camila Henriques, Justin Yai Alamou Doritchamou, Irfan Zaidi, and Patrick E. Duffy. 2017. "Advances in Malaria Vaccine Development: Report from the 2017 Malaria Vaccine Symposium." In *Npj Vaccines*. <https://doi.org/10.1038/s41541-017-0035-3>.
- Coleman, J. A., A. L. Vestergaard, R. S. Molday, B. Vilsen, and J. Peter Andersen. 2012. "Critical Role of a Transmembrane Lysine in Aminophospholipid Transport by Mammalian Photoreceptor P4-ATPase ATP8A2." *Proceedings of the National Academy of Sciences* 109 (5): 1449–54. <https://doi.org/10.1073/pnas.1108862109>.
- Coleman, Jonathan A, and Robert S Molday. 2011. "Critical Role of the  $\beta$ -Subunit CDC50A in the Stable Expression, Assembly, Subcellular Localization, and Lipid Transport Activity of the P4-ATPase ATP8A2." *Journal of Biological Chemistry* 286 (19): 17205–16. <https://doi.org/10.1074/jbc.M111.229419>.
- Counihan, Natalie A., Ming Kalanon, Ross L. Coppel, and Tania F. de Koning-Ward. 2013. "Plasmodium Rhoptry Proteins: Why Order Is Important." *Trends in Parasitology* 29 (5): 228–36. <https://doi.org/10.1016/j.pt.2013.03.003>.
- Cova, Marta, João A Rodrigues, Terry K Smith, and Luis Izquierdo. 2015. "Sugar Activation and Glycosylation in Plasmodium." *Malaria Journal*. <https://doi.org/10.1186/s12936-015-0949-z>.
- Cowell, Annie N., Eva S. Istvan, Amanda K. Lukens, Maria G. Gomez-Lorenzo, Manu Vanaerschot, Tomoyo Sakata-Kato, Erika L. Flannery, et al. 2018. "Mapping the Malaria Parasite Druggable Genome by Using *In Vitro* Evolution and Chemogenomics." *Science*. <https://doi.org/10.1126/science.aan4472>.
- Cowman, Alan F., Drew Berry, and Jake Baum. 2012. "The Cellular and Molecular Basis for Malaria Parasite Invasion of the Human Red Blood Cell." *Journal of Cell Biology*. <https://doi.org/10.1083/jcb.201206112>.

- Cowman, Alan F., Julie Healer, Danushka Marapana, and Kevin Marsh. 2016. "Malaria: Biology and Disease." *Cell*. <https://doi.org/10.1016/j.cell.2016.07.055>.
- Cox, Francis Eg. 2010. "History of the Discovery of the Malaria Parasites and Their Vectors." *Parasites & Vectors* 3 (1): 5. <https://doi.org/10.1186/1756-3305-3-5>.
- Cregg, James. 1993. "The Pichia System." *Keck Graduate Institute, Claremont, Calif*, 1–8.
- Cronan, John E. 2005. "THE JOURNAL OF BIOLOGICAL CHEMISTRY Biotination of Proteins in Viuo." Vol. 265. <http://www.jbc.org/>.
- Cui, Liwang, and Xin-zhuan Su. 2009. "Discovery, Mechanisms of Action and Combination Therapy of Artemisinin." *Expert Review of Anti-Infective Therapy* 7 (8): 999–1013. <https://doi.org/10.1586/eri.09.68>.
- David-Bosne, Stéphanie, Michael Voldsgaard Clausen, Hanne Poulsen, Jesper Vuust Møller, Poul Nissen, and Marc Le Maire. 2016. "Erratum: Reappraising the Effects of Artemisinin on the ATPase Activity of PfATP6 and SERCA1a E255L Expressed in *Xenopus Laevis* Oocytes (Nature Structural and Molecular Biology (2016) 23 (1-2))." *Nature Structural and Molecular Biology*. <https://doi.org/10.1038/nsmb0416-358a>.
- David-Bosne, Stéphanie, Isabelle Florent, Anne-Marie Lund- Winther, John B. Hansen, Morten Buch-Pedersen, Paul Machillot, Marc le Maire, and Christine Jaxel. 2013. "Antimalarial Screening via Large-Scale Purification of *Plasmodium Falciparum* Ca<sup>2+</sup>-ATPase 6 and *in Vitro* Studies." *FEBS Journal* 280 (21): 5419–29. <https://doi.org/10.1111/febs.12244>.
- Douglas, Alexander D., G. Christian Baldeviano, Carmen M. Lucas, Luis A. Lugo-Roman, Cécile Crosnier, S. Josefin Bartholdson, Ababacar Diouf, et al. 2015. "A PfrH5-Based Vaccine Is Efficacious against Heterologous Strain Blood-Stage Plasmodium Falciparum Infection in Aotus Monkeys." *Cell Host & Microbe* 17 (1): 130–39. <https://doi.org/10.1016/J.CHOM.2014.11.017>.
- Drew, David, Simon Newstead, Yo Sonoda, Hyun Kim, Gunnar von Heijne, and So Iwata. 2008. "GFP-Based Optimization Scheme for the Overexpression and Purification of Eukaryotic Membrane Proteins in *Saccharomyces Cerevisiae*." *Nature Protocols*.

- <https://doi.org/10.1038/nprot.2008.44>.
- Duraisingh, Manoj T, and Alan F Cowman. 2005. "Contribution of the Pfmdr1 Gene to Antimalarial Drug-Resistance." *Acta Tropica* 94 (3 SPEC. ISS.): 181–90. <https://doi.org/10.1016/j.actatropica.2005.04.008>.
- Eastman, Richard T, and David A Fidock. 2009. "Artemisinin-Based Combination Therapies: A Vital Tool in Efforts to Eliminate Malaria." *Nature Reviews Microbiology* 7 (12): 864–74. <https://doi.org/10.1038/nrmicro2239>.
- Eckstein-Ludwig, U, R J Webb, I D A Van Goethem, J M East, A G Lee, M Kimura, P M O'neill, P G Bray, S A Ward, and & S Krishna. 2003. *Artemisinins Target the SERCA of Plasmodium Falciparum*. [www.nature.com/nature](http://www.nature.com/nature).
- Ekberg, Kira, Michael G Palmgren, Bjarke Veierskov, and Morten J Buch-Pedersen. 2010. "A Novel Mechanism of P-Type ATPase Autoinhibition Involving Both Termini of the Protein." *Journal of Biological Chemistry* 285 (10): 7344–50. <https://doi.org/10.1074/jbc.M109.096123>.
- Ellgaard, Lars, and Ari Helenius. 2003. "Quality Control in the Endoplasmic Reticulum." *Nature Reviews Molecular Cell Biology* 4 (3): 181–91. <https://doi.org/10.1038/nrm1052>.
- Errasti-murugarren, Ekaitz, Arturo Rodríguez-banqueri, and José Luis Vázquez-ibar. 2017. "Heterologous Gene Expression in E.Coli" 1586: 181–95. <https://doi.org/10.1007/978-1-4939-6887-9>.
- Fidock, David A., Philip J. Rosenthal, Simon L. Croft, Reto Brun, and Solomon Nwaka. 2004. "Antimalarial Drug Discovery: Efficacy Models for Compound Screening." *Nature Reviews Drug Discovery*. <https://doi.org/10.1038/nrd1416>.
- Filigheddu, Nicoletta, Viola F Gnocchi, Marco Coscia, Miriam Cappelli, Paolo E Porporato, and Riccardo Tauli. 2007. "Ghrelin and Des-Acyl Ghrelin Promote Differentiation and Fusion of C2C12 Skeletal Muscle Cells." *Molecular Biology of the Cell* 18 (December): 986–94. <https://doi.org/10.1091/mbc.E06>.
- Flannery, Erika L., Arnab K. Chatterjee, and Elizabeth A. Winzeler. 2013. "Antimalarial Drug Discovery — Approaches and Progress towards New Medicines." *Nature*

- Reviews Microbiology* 11 (12): 849–62. <https://doi.org/10.1038/nrmicro3138>.
- Frame, I J, Emilio F Merino, Vern L Schramm, María B Cassera, and Myles H Akabas. 2012. “Malaria Parasite Type 4 Equilibrative Nucleoside Transporters (ENT4) Are Purine Transporters with Distinct Substrate Specificity.” *The Biochemical Journal* 446 (2): 179–90. <https://doi.org/10.1042/BJ20112220>.
- Fried, Michal, and Patrick E. Duffy. 2015. “Designing a VAR2CSA-Based Vaccine to Prevent Placental Malaria.” *Vaccine* 33 (52): 7483–88. <https://doi.org/10.1016/j.vaccine.2015.10.011>.
- Furuta, Nobumichi, Konomi Fujimura-Kamada, Koji Saito, Takaharu Yamamoto, and Kazuma Tanaka. 2007. “Endocytic Recycling in Yeast Is Regulated by Putative Phospholipid Translocases and the Ypt31p/32p-Rcy1p Pathway.” *Molecular Biology of the Cell* 18 (1): 295–312. <https://doi.org/10.1091/mbc.e06-05-0461>.
- Gantzel, Rasmus H., Louise S. Mogensen, Stine A. Mikkelsen, Bente Vilsen, Robert S. Molday, Anna L. Vestergaard, and Jens P. Andersen. 2017. “Disease Mutations Reveal Residues Critical to the Interaction of P4-ATPases with Lipid Substrates.” *Scientific Reports*. <https://doi.org/10.1038/s41598-017-10741-z>.
- García-Sánchez, Sebastián, María P. Sánchez-Cañete, Francisco Gamarro, and Santiago Castanys. 2014. “Functional Role of Evolutionarily Highly Conserved Residues, N-Glycosylation Level and Domains of the Leishmania Miltefosine Transporter-Cdc50 Subunit.” *Biochemical Journal* 459 (1): 83–94. <https://doi.org/10.1042/BJ20131318>.
- Gardner, Malcolm J., Neil Hall, Eula Fung, Owen White, Matthew Berriman, Richard W. Hyman, Jane M. Carlton, et al. 2002. “Genome Sequence of the Human Malaria Parasite Plasmodium Falciparum.” *Nature*. <https://doi.org/10.1038/nature01097>.
- Geering, Käthi. 2001. “The Functional Role of  $\beta$  Subunits in Oligomeric P-Type ATPases.” *Journal of Bioenergetics and Biomembranes*. Vol. 33. <https://link.springer.com/content/pdf/10.1023%2FA%3A1010623724749.pdf>.
- Geering, Käthi, Pascal Béguin, Haim Garty, Steven Karlsh, Maria Füzesi, Jean-Daniel Horisberger, and Gilles Crambert. 2003. “FXD Proteins: New Tissue- and Isoform-

- Specific Regulators of Na,K-ATPase." *Annals of the New York Academy of Sciences* 986 (April): 388–94. <http://www.ncbi.nlm.nih.gov/pubmed/12763855>.
- Giacomini, Kathleen M, Shiew-Mei Huang, Donald J Tweedie, Leslie Z Benet, Kim L R Brouwer, Xiaoyan Chu, Amber Dahlin, et al. 2010. "Membrane Transporters in Drug Development." *Nature Reviews. Drug Discovery* 9 (3): 215–36. <https://doi.org/10.1038/nrd3028>.
- Gosling, Roly, and Lorenz von Seidlein. 2016. "The Future of the RTS,S/AS01 Malaria Vaccine: An Alternative Development Plan." *PLoS Medicine*. <https://doi.org/10.1371/journal.pmed.1001994>.
- Graber, Joel H., Charles R. Cantor, Scott C. Mohr, and Temple F. Smith. 1999. "Genomic Detection of New Yeast Pre-mRNA 3'-End-Processing Signals." *Nucleic Acids Research* 27 (3): 888–94. <https://doi.org/10.1093/nar/27.3.888>.
- Greenwood, Brian. 2017. "Progress with the PfSPZ Vaccine for Malaria." *The Lancet. Infectious Diseases* 17 (5): 463–64. [https://doi.org/10.1016/S1473-3099\(17\)30105-6](https://doi.org/10.1016/S1473-3099(17)30105-6).
- Guarente, L, R R Yocum, and P Gifford. 1982. "A GAL10-CYC1 Hybrid Yeast Promoter Identifies the GAL4 Regulatory Region as an Upstream Site." *Proceedings of the National Academy of Sciences of the United States of America* 79 (23): 7410–14. <http://www.ncbi.nlm.nih.gov/pubmed/6760197>.
- Guttery, David S., Jon K. Pittman, Karine Frénil, Benoit Poulin, Leon R. McFarlane, Ksenija Slavic, Sally P. Wheatley, et al. 2013. "The Plasmodium Berghei Ca<sup>2+</sup>/H<sup>+</sup> Exchanger, PbCAX, Is Essential for Tolerance to Environmental Ca<sup>2+</sup> during Sexual Development." Edited by Maria M. Mota. *PLoS Pathogens* 9 (2): e1003191. <https://doi.org/10.1371/journal.ppat.1003191>.
- Habeck, Michael, Einat Kapri-Pardes, Michal Sharon, Steven J. D. Karlish, and H Ronald Kaback. 2017. "Specific Phospholipid Binding to Na,K-ATPase at Two Distinct Sites." *Proceedings of the National Academy of Sciences*. <https://doi.org/10.1073/pnas.1620799114>.
- Hansen, Martin, Jü Rgen, F J Kun, Joachim E Schultz, and Eric Beitz. 2001. "A Single, Bi-



- Functional Aquaglyceroporin in Blood-Stage Plasmodium Falciparum Malaria Parasites\*." <https://doi.org/10.1074/jbc.M110683200>.
- Harding, Clare R, and Markus Meissner. 2014. "The Inner Membrane Complex through Development of Toxoplasma Gondii and Plasmodium." *Cellular Microbiology* 16 (5): 632–41. <https://doi.org/10.1111/cmi.12285>.
- Hedfalk, Kristina, Nina Pettersson, Fredrik O " Berg, Stefan Hohmann, Euan Gordon, Fredrik Öberg, Stefan Hohmann, and Euan Gordon. 2008. "Production, Characterization and Crystallization of the Plasmodium Falciparum Aquaporin." *Protein Expression and Purification*. <https://doi.org/10.1016/j.pep.2008.01.004>.
- Heussler, Volker, Tobias Spielmann, Friedrich Frischknecht, and Tim Gilberger. 2016. "Plasmodium." In *Molecular Parasitology: Protozoan Parasites and Their Molecules*, 241–84. Vienna: Springer Vienna. [https://doi.org/10.1007/978-3-7091-1416-2\\_9](https://doi.org/10.1007/978-3-7091-1416-2_9).
- Ho, Chi-Min, Josh R Beck, Mason Lai, Yanxiang Cui, Daniel E Goldberg, Pascal F Egea, and Z. Hong Zhou. 2018. "Malaria Parasite Translocon Structure and Mechanism of Effector Export." *Nature*. <https://doi.org/10.1038/s41586-018-0469-4>.
- Holm-Bertelsen, Julia, Sinja Bock, Folknand Helmstetter, and Eric Beitz. 2016. "High-Level Cell-Free Production of the Malarial Lactate Transporter PfFNT as a Basis for Crystallization Trials and Directional Transport Studies." *Protein Expression and Purification* 126: 109–14. <https://doi.org/10.1016/j.pep.2016.06.008>.
- Huang, Wei, Guojian Liao, Gregory M. Baker, Yina Wang, Richard Lau, Padmaja Paderu, David S. Perlin, and Chaoyang Xue. 2016. "Lipid Flippase Subunit Cdc50 Mediates Drug Resistance and Virulence in Cryptococcus Neoformans." *MBio*. <https://doi.org/10.1128/mBio.00478-16>.
- Idro, Richard, Neil E Jenkins, and Charles RJC Newton. 2005. "Pathogenesis, Clinical Features, and Neurological Outcome of Cerebral Malaria." *The Lancet Neurology* 4 (12): 827–40. [https://doi.org/10.1016/S1474-4422\(05\)70247-7](https://doi.org/10.1016/S1474-4422(05)70247-7).
- Inoue, H, H Nojima, and H Okayama. 1990. "High Efficiency Transformation of Escherichia Coli with Plasmids." *Gene* 96 (1): 23–28. <http://www.ncbi.nlm.nih.gov/pubmed/2265755>.

- Jacquot, Aurore, Cédric Montigny, Hanka Hennrich, Raphaëlle Barry, Marc Le Maire, Christine Jaxel, Joost Holthuis, Philippe Champeil, and Guillaume Lenoir. 2012. "Phosphatidylserine Stimulation of Drs2p·Cdc50p Lipid Translocase Dephosphorylation Is Controlled by Phosphatidylinositol-4-Phosphate." *Journal of Biological Chemistry*. <https://doi.org/10.1074/jbc.M111.313916>.
- Jidenko, Marie, Guillaume Lenoir, José M. Fuentes, Marc le Maire, and Christine Jaxel. 2006. "Expression in Yeast and Purification of a Membrane Protein, SERCA1a, Using a Biotinylated Acceptor Domain." *Protein Expression and Purification*. <https://doi.org/10.1016/j.pep.2006.03.001>.
- Juge, Narinobu, Sawako Moriyama, Takaaki Miyaji, Mamiyo Kawakami, Haruka Iwai, Tomoya Fukui, Nathan Nelson, Hiroshi Omote, and Yoshinori Moriyama. 2015. "Plasmodium Falciparum Chloroquine Resistance Transporter Is a H<sup>+</sup>-Coupled Polyspecific Nutrient and Drug Exporter." *Proceedings of the National Academy of Sciences of the United States of America* 112 (11): 3356–61. <https://doi.org/10.1073/pnas.1417102112>.
- Kato, Utako, Hironori Inadome, Masatoshi Yamamoto, Kazuo Emoto, Toshihide Kobayashi, and Masato Umeda. 2013. "Role for Phospholipid Flippase Complex of ATP8A1 and CDC50A Proteins in Cell Migration." *Journal of Biological Chemistry* 288 (7): 4922–34. <https://doi.org/10.1074/jbc.M112.402701>.
- Kawate, Toshimitsu, and Eric Gouaux. 2006. "Fluorescence-Detection Size-Exclusion Chromatography for Precrystallization Screening of Integral Membrane Proteins." *Structure (London, England : 1993)* 14 (4): 673–81. <https://doi.org/10.1016/j.str.2006.01.013>.
- Kenthirapalan, Sanketha, Andrew P. Waters, Kai Matuschewski, and Taco W.A. Kooij. 2016. "Functional Profiles of Orphan Membrane Transporters in the Life Cycle of the Malaria Parasite." *Nature Communications*. <https://doi.org/10.1038/ncomms10519>.
- Kirk, K, R E Martin, S Bröer, S M Howitt, and K J Saliba. 2005. "Plasmodium Permeomics: Membrane Transport Proteins in the Malaria Parasite." *Current Topics in Microbiology and Immunology* 295 (January): 325–56.

- <http://www.ncbi.nlm.nih.gov/pubmed/16265897>.
- Kirk, Kiaran. 2004. "Channels and Transporters as Drug Targets in the Plasmodium-Infected Erythrocyte." *Acta Tropica*.  
<https://doi.org/10.1016/j.actatropica.2003.10.002>.
- Kirk Kiaran. 2015. "Ion Regulation in the Malaria Parasite." *Annual Review of Microbiology* 69 (1): 341–59. <https://doi.org/10.1146/annurev-micro-091014-104506>.
- Kirk, Kiaran, and Adele M Lehane. 2014. "Membrane Transport in the Malaria Parasite and Its Host Erythrocyte." *The Biochemical Journal* 457 (1): 1–18.  
<https://doi.org/10.1042/BJ20131007>.
- Klomp, Leo W. J., Julie C. Vargas, Saskia W. C. van Mil, Ludmila Pawlikowska, Sandra S. Strautnieks, Michiel J. T. van Eijk, Jenneke A. Juijn, et al. 2004. "Characterization of Mutations in *ATP8B1* Associated with Hereditary Cholestasis." *Hepatology* 40 (1): 27–38. <https://doi.org/10.1002/hep.20285>.
- Koning-Ward, Tania F De, Paul R Gilson, Justin A Boddey, Melanie Rug, Brian J Smith, Anthony T Papenfuss, Paul R Sanders, et al. 2009. "A Novel Protein Export Machine in Malaria Parasites HHS Public Access." *Nature* 459 (7249): 945–49.  
<https://doi.org/10.1038/nature08104>.
- Krishna, Sanjeev, Gill M. Cowan, Kathryn J. Robson, and John C. Meade. 1994. "Plasmodium Falciparum: Further Characterization of Putative Cation ATPases." *Experimental Parasitology*. <https://doi.org/10.1006/expr.1994.1011>.
- Kubala, Marta H., Oleksiy Kovtun, Kirill Alexandrov, and Brett M. Collins. 2010. "Structural and Thermodynamic Analysis of the GFP:GFP-Nanobody Complex." *Protein Science* 19 (12): 2389–2401. <https://doi.org/10.1002/pro.519>.
- Kühlbrandt, Werner. 2004. "Biology, Structure and Mechanism of P-Type ATPases." *Nature Reviews Molecular Cell Biology*. <https://doi.org/10.1038/nrm1354>.
- Lee, M R. 2002. "HISTORY PLANTS AGAINST MALARIA PART 1: CINCHONA OR THE PERUVIAN BARK." *J R Coll Physicians Edinb*. Vol. 32.  
[https://www.rcpe.ac.uk/sites/default/files/paper\\_7.pdf](https://www.rcpe.ac.uk/sites/default/files/paper_7.pdf).

- Lenoir, Guillaume, Thibaud Dieudonné, Anaïs Lamy, Maylis Lejeune, José Luis Vazquez-Ibar, and Cédric Montigny. 2018. "Screening of Detergents for Stabilization of Functional Membrane Proteins." *Current Protocols in Protein Science* 93: 1–27. <https://doi.org/10.1002/cpps.59>.
- Lenoir, Guillaume, Thierry Menguy, Fabienne Corre, Cédric Montigny, Per A. Pedersen, Denyse Thinès, Marc le Maire, and Pierre Falson. 2002. "Overproduction in Yeast and Rapid and Efficient Purification of the Rabbit SERCA1a Ca<sup>2+</sup>-ATPase." *Biochimica et Biophysica Acta - Biomembranes* 1560 (1–2): 67–83. [https://doi.org/10.1016/S0005-2736\(01\)00458-8](https://doi.org/10.1016/S0005-2736(01)00458-8).
- Lim, Liting, Marc Linka, Kylie A. Mullin, A. P M Weber, and Geoffrey I. McFadden. 2010. "The Carbon and Energy Sources of the Non-Photosynthetic Plastid in the Malaria Parasite." *FEBS Letters* 584 (3): 549–54. <https://doi.org/10.1016/j.febslet.2009.11.097>.
- López-Marqués, Rosa L., Joost C.M. Holthuis, and Thomas G. Pomorski. 2011. "Pumping Lipids with P4-ATPases." *Biological Chemistry*. <https://doi.org/10.1515/BC.2011.015>.
- Lopez-Marques, Rosa L., Lisa Theorin, Michael G. Palmgren, and Thomas Günther Pomorski. 2014. "P4-ATPases: Lipid Flippases in Cell Membranes." *Pflugers Archiv European Journal of Physiology*. <https://doi.org/10.1007/s00424-013-1363-4>.
- López-Marqués, Rosa L, Lisbeth R Poulsen, Susanne Hanisch, Katharina Meffert, Morten J Buch-Pedersen, Mia K Jakobsen, Thomas Günther Pomorski, and Michael G Palmgren. 2010. "Intracellular Targeting Signals and Lipid Specificity Determinants of the ALA/ALIS P4-ATPase Complex Reside in the Catalytic ALA Alpha-Subunit." *Molecular Biology of the Cell* 21 (5): 791–801. <https://doi.org/10.1091/mbc.e09-08-0656>.
- Lyons, Joseph A., Azadeh Shahsavari, Peter Aasted Paulsen, Bjørn Panyella Pedersen, and Poul Nissen. 2016. *Expression Strategies for Structural Studies of Eukaryotic Membrane Proteins. Current Opinion in Structural Biology*. Vol. 38. <https://doi.org/10.1016/j.sbi.2016.06.011>.
- "M15-A Laboratory Diagnosis of Blood-Borne Parasitic Diseases; Approved Guideline."

2000. [www.clsi.org](http://www.clsi.org).

Machault, Vanessa, Cécile Vignolles, François Borchi, Penelope Vounatsou, Frédéric Pages, Sébastien Briolant, Jean Pierre Lacaux, and Christophe Rogier. 2011. "The Use of Remotely Sensed Environmental Data in the Study of Malaria." *Geospatial Health* 5 (2): 151–68. <https://doi.org/10.4081/gh.2011.167>.

MacLennan, David H, Michio Asahi, and A Russell Tupling. 2003. "The Regulation of SERCA-Type Pumps by Phospholamban and Sarcolipin." *Annals of the New York Academy of Sciences* 986 (April): 472–80. <http://www.ncbi.nlm.nih.gov/pubmed/12763867>.

Maier, Alexander G, Brian M Cooke, Alan F Cowman, and Leann Tilley. 2009. "Malaria Parasite Proteins That Remodel the Host Erythrocyte." *Nature Reviews Microbiology* 7 (5): 341–54. <https://doi.org/10.1038/nrmicro2110>.

Maire, Marc Le, Philippe Champeil, and Jesper V. Møller. 2000. "Interaction of Membrane Proteins and Lipids with Solubilizing Detergents." *Biochimica et Biophysica Acta - Biomembranes* 1508 (1–2): 86–111. [https://doi.org/10.1016/S0304-4157\(00\)00010-1](https://doi.org/10.1016/S0304-4157(00)00010-1).

Marchand, Alexandre, Anne-Marie Lund Winther, Peter Joakim Holm, Claus Olesen, Cedric Montigny, Bertrand Arnou, Philippe Champeil, et al. 2008. "Crystal Structure of D351A and P312A Mutant Forms of the Mammalian Sarcoplasmic Reticulum Ca(2+) -ATPase Reveals Key Events in Phosphorylation and Ca(2+) Release." *The Journal of Biological Chemistry* 283 (21): 14867–82. <https://doi.org/10.1074/jbc.M710165200>.

Marchetti, Rosa V, Adele M Lehane, Sarah H Shafik, Markus Winterberg, Rowena E Martin, and Kiaran Kirk. 2015. "ARTICLE A Lactate and Formate Transporter in the Intraerythrocytic Malaria Parasite, Plasmodium Falciparum." *Nature Communications*. <https://doi.org/10.1038/ncomms7721>.

Mark, Vincent A. van der, Ronald P.J. Oude Elferink, and Coen C. Paulusma. 2013. "P4 ATPases: Flippases in Health and Disease." *International Journal of Molecular Sciences*. <https://doi.org/10.3390/ijms14047897>.

- Martin, Rowena E, Hagai Ginsburg, and Kiaran Kirk. 2009. "Membrane Transport Proteins of the Malaria Parasite." *Molecular Microbiology*.  
<https://doi.org/10.1111/j.1365-2958.2009.06863.x>.
- Martin, Rowena E, Roselani I Henry, Janice L Abbey, John D Clements, and Kiaran Kirk. 2005. "Open Access The 'permeome' of the Malaria Parasite: An Overview of the Membrane Transport Proteins of Plasmodium Falciparum."  
<http://genomebiology.com/2005/6/3/R26>.
- Martin, Rowena E, Rosa V Marchetti, Anna I Cowan, Susan M Howitt, Stefan Bröer, and Kiaran Kirk. 2009. "Chloroquine Transport via the Malaria Parasite's Chloroquine Resistance Transporter." *Science* 325 (5948): 1680–82.  
<https://doi.org/10.1126/science.1175667>.
- Mathison, Blaine A, and Bobbi S Pritt. 2017. "Update on Malaria Diagnostics and Test Utilization." *Journal of Clinical Microbiology* 55 (7): 2009–17.  
<https://doi.org/10.1128/JCM.02562-16>.
- Mbengue, Alassane, Souvik Bhattacharjee, Trupti Pandharkar, Haining Liu, Guillermina Estiu, Robert V. Stahelin, Shahir S. Rizk, et al. 2015. "A Molecular Mechanism of Artemisinin Resistance in Plasmodium Falciparum Malaria." *Nature* 520 (7549): 683–87. <https://doi.org/10.1038/nature14412>.
- Mcfadden, Geoffrey I., Ross F. Waller, Michael E. Reith, and Naomi Lang-Unnasch. 1997. "Plastids in Apicomplexan Parasites." In , 261–87. Springer, Vienna.  
[https://doi.org/10.1007/978-3-7091-6542-3\\_14](https://doi.org/10.1007/978-3-7091-6542-3_14).
- Meshnick, Steven R. 2002. "Artemisinin: Mechanisms of Action, Resistance and Toxicity." In *International Journal for Parasitology*. [https://doi.org/10.1016/S0020-7519\(02\)00194-7](https://doi.org/10.1016/S0020-7519(02)00194-7).
- Møller, Jesper V, Claus Olesen, Anne-Marie L Winther, and Poul Nissen. 2010. "The Sarcoplasmic Ca<sup>2+</sup>-ATPase: Design of a Perfect Chemo-Osmotic Pump." *Quarterly Reviews of Biophysics* 43 (4): 501–66.  
<https://doi.org/10.1017/S003358351000017X>.
- Montigny, Cédric, Hassina Azouaoui, Aurore Jacquot, Marc le Maire, Christine Jaxel,

- Philippe Champeil, and Guillaume Lenoir. 2014. "Overexpression of Membrane Proteins in *Saccharomyces Cerevisiae* for Structural and Functional Studies: A Focus on the Rabbit Ca<sup>2+</sup>-ATPase Serca1a and on the Yeast Lipid 'Flippase' Complex Drs2p/Cdc50p." In *Membrane Proteins Production for Structural Analysis*, 133–71. New York, NY: Springer New York. [https://doi.org/10.1007/978-1-4939-0662-8\\_6](https://doi.org/10.1007/978-1-4939-0662-8_6).
- Montigny, Cédric, Paulette Decottignies, Pierre Le Maréchal, Pierre Capy, Maike Bublitz, Claus Olesen, Jesper Vuust Møller, Poul Nissen, and Marc le Maire. 2014. "S-Palmitoylation and S-Oleoylation of Rabbit and Pig Sarcolipin \*." <https://doi.org/10.1074/jbc.M114.590307>.
- Montigny, Cédric, Joseph Lyons, Philippe Champeil, Poul Nissen, and Guillaume Lenoir. 2016. "On the Molecular Mechanism of Flippase- and Scramblase-Mediated Phospholipid Transport." *Biochimica et Biophysica Acta - Molecular and Cell Biology of Lipids* 1861 (8): 767–83. <https://doi.org/10.1016/j.bbalip.2015.12.020>.
- Moody, Anthony. 2002. "Rapid Diagnostic Tests for Malaria Parasites." *Clinical Microbiology Reviews* 15 (1): 66–78. <https://doi.org/10.1128/CMR.15.1.66-78.2002>.
- Mordmüller, Benjamin, Güzin Surat, Heimo Lagler, Sumana Chakravarty, Andrew S. Ishizuka, Albert Lalremruata, Markus Gmeiner, et al. 2017. "Sterile Protection against Human Malaria by Chemoattenuated PfSPZ Vaccine." *Nature*. <https://doi.org/10.1038/nature21060>.
- Natarajan, Paramasivam, Ke Liu, Dustin V. Patil, Vicki A. Sciorra, Catherine L. Jackson, and Todd R. Graham. 2009. "Regulation of a Golgi Flippase by Phosphoinositides and an ArfGEF." *Nature Cell Biology* 11 (12): 1421–26. <https://doi.org/10.1038/ncb1989>.
- O'Malley, Michelle A., Tzvetana Lazarova, Zachary T. Britton, and Anne S. Robinson. 2007. "High-Level Expression in *Saccharomyces Cerevisiae* Enables Isolation and Spectroscopic Characterization of Functional Human Adenosine A2a Receptor." *Journal of Structural Biology*. <https://doi.org/10.1016/j.jsb.2007.05.001>.
- Olesen, Claus, Martin Picard, Anne-Marie Lund Winther, Claus Gyruup, J. Preben Morth,

- Claus Oxvig, Jesper Vuust Møller, and Poul Nissen. 2007. "The Structural Basis of Calcium Transport by the Calcium Pump." *Nature* 450 (7172): 1036–42. <https://doi.org/10.1038/nature06418>.
- Ouji, Manel, Jean-Michel Augereau, Lucie Paloque, and Françoise Benoit-Vical. 2018. "Plasmodium Falciparum Resistance to Artemisinin-Based Combination Therapies: A Sword of Damocles in the Path toward Malaria Elimination." *Parasite* 25: 24. <https://doi.org/10.1051/parasite/2018021>.
- Palmgren, Michael G., and Poul Nissen. 2011. "P-Type ATPases." *Annual Review of Biophysics*. <https://doi.org/10.1146/annurev.biophys.093008.131331>.
- Parker, M D, R J Hyde, S Y Yao, L McRobert, C E Cass, J D Young, G A McConkey, and S A Baldwin. 2000. "Identification of a Nucleoside/Nucleobase Transporter from Plasmodium Falciparum, a Novel Target for Anti-Malarial Chemotherapy." *The Biochemical Journal* 349 (Pt 1): 67–75. <https://doi.org/10.1042/BJ3490067>.
- Pasini, Erica M., Joanna A. Braks, Jannik Fonager, Onny Klop, Elena Aime, Roberta Spaccapelo, Thomas D. Otto, et al. 2013. "Proteomic and Genetic Analyses Demonstrate That *Plasmodium Berghei* Blood Stages Export a Large and Diverse Repertoire of Proteins." *Molecular & Cellular Proteomics*. <https://doi.org/10.1074/mcp.M112.021238>.
- Penny, Jeffrey I, Simone T Hall, Charles J Woodrow, Gill M Cowan, Annette M Gero, and Sanjeev Krishna. 1998. "Expression of Substrate-Specific Transporters Encoded by Plasmodium Falciparum in Xenopus Lae6is Oocytes." *Molecular and Biochemical Parasitology*. Vol. 93. [https://ac.els-cdn.com/S0166685198000243/1-s2.0-S0166685198000243-main.pdf?\\_tid=7400233d-f4a5-485a-bba1-6420d3b1887d&acdnat=1537798521\\_47b9fffc037c4b318377f659e6f38571](https://ac.els-cdn.com/S0166685198000243/1-s2.0-S0166685198000243-main.pdf?_tid=7400233d-f4a5-485a-bba1-6420d3b1887d&acdnat=1537798521_47b9fffc037c4b318377f659e6f38571).
- Perandrés-López, Rubén, María P. Sánchez-Cañete, Francisco Gamarro, and Santiago Castanys. 2018. "Functional Role of Highly Conserved Residues of the N-Terminal Tail and First Transmembrane Segment of a P4-ATPase." *Biochemical Journal* 475 (5): 887–99. <https://doi.org/http://dx.doi.org/10.1042/BCJ20170749>.
- Pérez-Victoria, F. Javier, Francisco Gamarro, Marc Ouellette, and Santiago Castanys. 2003. "Functional Cloning of the Miltefosine Transporter: A Novel p-Type



- Phospholipid Translocase from *Leishmania* Involved in Drug Resistance." *Journal of Biological Chemistry*. <https://doi.org/10.1074/jbc.M308352200>.
- Petersen, Ines, Richard Eastman, and Michael Lanzer. 2011. "Drug-Resistant Malaria: Molecular Mechanisms and Implications for Public Health." *FEBS Letters* 585 (11): 1551–62. <https://doi.org/10.1016/j.febslet.2011.04.042>.
- Poespoprodjo, Jeanne R., Afdal Hasanuddin, Wendelina Fobia, Paulus Sugiarto, Enny Kenangalem, Daniel A. Lampah, Emiliana Tjitra, Ric N. Price, and Nicholas M. Anstey. 2010. "Case Report: Severe Congenital Malaria Acquired in Utero." *American Journal of Tropical Medicine and Hygiene*. <https://doi.org/10.4269/ajtmh.2010.09-0744>.
- Poulsen, L. R., R. L. Lopez-Marques, S. C. McDowell, J. Okkeri, D. Licht, A. Schulz, T. Pomorski, J. F. Harper, and M. G. Palmgren. 2008. "The Arabidopsis P4-ATPase ALA3 Localizes to the Golgi and Requires a  $\gamma$ -Subunit to Function in Lipid Translocation and Secretory Vesicle Formation." *THE PLANT CELL ONLINE*. <https://doi.org/10.1105/tpc.107.054767>.
- Poulsen, Lisbeth R., Rosa L. López-Marqués, Pai R. Pedas, Stephen C. McDowell, Elizabeth Brown, Reinhard Kunze, Jeffrey F. Harper, Thomas G. Pomorski, and Michael Palmgren. 2015. "A Phospholipid Uptake System in the Model Plant Arabidopsis Thaliana." *Nature Communications*. <https://doi.org/10.1038/ncomms8649>.
- Privé, Gilbert G. 2007. "Detergents for the Stabilization and Crystallization of Membrane Proteins." *Methods* 41 (4): 388–97. <https://doi.org/10.1016/j.ymeth.2007.01.007>.
- Puts, Cathelene F., and Joost C M Holthuis. 2009. "Mechanism and Significance of P4 ATPase-Catalyzed Lipid Transport: Lessons from a Na<sup>+</sup>/K<sup>+</sup>-Pump." *Biochimica et Biophysica Acta - Molecular and Cell Biology of Lipids*. <https://doi.org/10.1016/j.bbalip.2009.02.005>.
- Puts, Cathelene F., Radhakrishnan Panatala, Hanka Hennrich, Alina Tsareva, Patrick Williamson, and Joost C.M. Holthuis. 2012. "Mapping Functional Interactions in a Heterodimeric Phospholipid Pump." *Journal of Biological Chemistry* 287 (36): 30529–40. <https://doi.org/10.1074/jbc.M112.371088>.
- Rask-Andersen, Mathias, Markus Sällman Almén, and Helgi B Schiöth. 2011. "Trends in

- the Exploitation of Novel Drug Targets." *Nature Reviews. Drug Discovery* 10 (8): 579–90. <https://doi.org/10.1038/nrd3478>.
- Richter, Joachim, Gabriele Franken, Heinz Mehlhorn, Alfons Labisch, and Dieter Häussinger. 2010. "What Is the Evidence for the Existence of Plasmodium Ovale Hypnozoites?" *Parasitology Research*. <https://doi.org/10.1007/s00436-010-2071-z>.
- Rodríguez-Banqueri, Arturo, Ekaitz Errasti-Murugarren, Paola Bartoccioni, Lukasz Kowalczyk, Alex Perálvarez-Marín, Manuel Palacín, and José Luis Vázquez-Ibar. 2016. "Stabilization of a Prokaryotic LAT Transporter by Random Mutagenesis." *The Journal of General Physiology* 147 (4): 353–68. <https://doi.org/10.1085/jgp.201511510>.
- Roland, Bartholomew P, Tomoki Naito, Jordan T Best, Cayetana Arnaiz-Yépez, Hiroyuki Takatsu, Roger J Yu, Hye-Won Shin, and Todd R. Graham. 2018. "Identification and Characterization of Yeast and Human Glycosphingolipid Flippases." *BioRxiv*, July, 373712. <https://doi.org/10.1101/373712>.
- Rosenthal, Philip J. 2005. "Proteases and Hemoglobin Degradation." In *Molecular Approaches to Malaria*, 311–26. American Society of Microbiology. <https://doi.org/10.1128/9781555817558.ch16>.
- Rosling, James E. O., Melanie C. Ridgway, Robert L. Summers, Kiaran Kirk, and Adele M. Lehane. 2018. "Biochemical Characterization and Chemical Inhibition of PfATP4-Associated Na<sup>+</sup>-ATPase Activity in *Plasmodium Falciparum* Membranes." *Journal of Biological Chemistry* 293 (34): 13327–37. <https://doi.org/10.1074/jbc.RA118.003640>.
- Rothbauer, Ulrich, Kourosh Zolghadr, Serge Muyldermans, Aloys Schepers, M. Cristina Cardoso, and Heinrich Leonhardt. 2008. "A Versatile Nanotrap for Biochemical and Functional Studies with Fluorescent Fusion Proteins. Supplemental Data Experimental Procedures." *Molecular & Cellular Proteomics : MCP* 7 (2): 282–89. <https://doi.org/10.1074/mcp.M700342-MCP200>.
- Rotmann, Alexander, Cecilia Sanchez, Armand Guiguemde, Petra Rohrbach, Anurag Dave, Naziha Bakouh, Gabrielle Planelles, and Michael Lanzer. 2010. "PfCHA Is a Mitochondrial Divalent Cation/H<sup>+</sup> Antiporter in *Plasmodium Falciparum*."

*Molecular Microbiology* 76 (6): 1591–1606. <https://doi.org/10.1111/j.1365-2958.2010.07187.x>.

Rottmann, Matthias, Case McNamara, Bryan K.S. Yeung, Marcus C.S. Lee, Bin Zou, Bruce Russell, Patrick Seitz, et al. 2010. “Spiroindolones, a Potent Compound Class for the Treatment of Malaria.” *Science*. <https://doi.org/10.1126/science.1193225>.

Routledge, Sarah J., Lina Mikaliunaite, Anjana Patel, Michelle Clare, Stephanie P. Cartwright, Zharain Bawa, Martin D.B. B Wilks, et al. 2016. *The Synthesis of Recombinant Membrane Proteins in Yeast for Structural Studies. Methods*. Vol. 95. <https://doi.org/10.1016/j.ymeth.2015.09.027>.

Saito, K. 2004. “Cdc50p, a Protein Required for Polarized Growth, Associates with the Drs2p P-Type ATPase Implicated in Phospholipid Translocation in *Saccharomyces Cerevisiae*.” *Molecular Biology of the Cell*. <https://doi.org/10.1091/mbc.E03-11-0829>.

Saito, Koji. 2004. “Cdc50p, a Protein Required for Polarized Growth, Associates with the Drs2p P-Type ATPase Implicated in Phospholipid Translocation in *Saccharomyces Cerevisiae*.” *Molecular Biology of the Cell* 15 (7): 3418–32. <https://doi.org/10.1091/mbc.E03-11-0829>.

Saito, Koji, Konomi Fujimura-Kamada, Hisatoshi Hanamatsu, Utako Kato, Masato Umeda, Keith G. Kozminski, and Kazuma Tanaka. 2007. “Transbilayer Phospholipid Flipping Regulates Cdc42p Signaling during Polarized Cell Growth via Rga GTPase-Activating Proteins.” *Developmental Cell* 13 (5): 743–51. <https://doi.org/10.1016/j.devcel.2007.09.014>.

Salcedo-Sora, J Enrique, Edwin Ochong, Susan Beveridge, David Johnson, Alexis Nzila, Giancarlo A Biagini, Paul A Stocks, et al. 2011. “The Molecular Basis of Folate Salvage in *Plasmodium Falciparum* CHARACTERIZATION OF TWO FOLATE TRANSPORTERS \* □ S.” <https://doi.org/10.1074/jbc.M111.286054>.

Salcedo-Sora, J Enrique, Steve A Ward, and Giancarlo A Biagini. 2012. “A Yeast Expression System for Functional and Pharmacological Studies of the Malaria Parasite Ca<sup>2+</sup> /H<sup>+</sup> Antiporter.” <http://www.malariajournal.com/content/11/1/254>.

- Saliba, Kevin J., Rowena E. Martin, Angelika Bröer, Roselani I. Henry, C. Siobhan McCarthy, Megan J. Downie, Richard J. W. Allen, et al. 2006. "Sodium-Dependent Uptake of Inorganic Phosphate by the Intracellular Malaria Parasite." *Nature*, September. <https://doi.org/10.1038/nature05149>.
- Sanchez, Cecilia P., Alexander Rotmann, Wilfred D. Stein, and Michael Lanzer. 2008. "Polymorphisms within PfMDR1 Alter the Substrate Specificity for Anti-Malarial Drugs in *Plasmodium Falciparum*." *Molecular Microbiology*, September. <https://doi.org/10.1111/j.1365-2958.2008.06413.x>.
- Sarkadi, B, Agnes Enyedi, J T Penniston, A K Verma, L Dux, E Molnár, and G Gfirdos. 1988. "Characterization of Membrane Calcium Pumps by Simultaneous Immunoblotting and <sup>32</sup>p Radiography."
- Schlitzer, Martin. 2007. "Malaria Chemotherapeutics Part I: History of Antimalarial Drug Development, Currently Used Therapeutics, and Drugs in Clinical Development." *ChemMedChem* 2 (7): 944–86. <https://doi.org/10.1002/cmdc.200600240>.
- Sehgal, Pankaj, Claus Olesen, and Jesper V. Møller. 2016. "ATPase Activity Measurements by an Enzyme-Coupled Spectrophotometric Assay." In , 105–9. Humana Press, New York, NY. [https://doi.org/10.1007/978-1-4939-3179-8\\_11](https://doi.org/10.1007/978-1-4939-3179-8_11).
- Sherman, Irwin W. 2005. "The Life of Plasmodium: An Overview." In *Molecular Approaches to Malaria*, 3–11. American Society of Microbiology. <https://doi.org/10.1128/9781555817558.ch1>.
- Shor, Erika, Yina Wang, David S Perlin, and Chaoyang Xue. 2016. "Cryptococcus Flips Its Lid-Membrane Phospholipid Asymmetry Modulates Antifungal Drug Resistance and Virulence." *OPEN ACCESS / Www.Microbialcell.Com 358 Microbial Cell* 3 (8). [www.microbialcell.com](http://www.microbialcell.com).
- Sidhu, Amar Bir Singh, Dominik Verdier-Pinard, and David A Fidock. 2002. "Chloroquine Resistance in Plasmodium Falciparum Malaria Parasites Conferred by Pfcrt Mutations." *Science (New York, N.Y.)* 298 (5591): 210–13. <https://doi.org/10.1126/science.1074045>.
- Sinden, R E, A Talman, S R Marques, M N Wass, and M. J.E. Sternberg. 2010. "The

- Flagellum in Malarial Parasites." *Current Opinion in Microbiology*.  
<https://doi.org/10.1016/j.mib.2010.05.016>.
- Slater, Andrew F G. 1993. "CHLOROQUINE: MECHANISM OF DRUG ACTION AND RESISTANCE IN PLASMODIUM FALCIPARUM." *Pharmac. Ther* 57: 203–35.
- Sonoda, Yo, Alex Cameron, Simon Newstead, Hiroshi Omote, Yoshinori Moriyama, Michihiro Kasahara, So Iwata, and David Drew. 2010. "Tricks of the Trade Used to Accelerate High-Resolution Structure Determination of Membrane Proteins." <https://doi.org/10.1016/j.febslet.2010.04.015>.
- Soulié, Stéphanie, Jesper Vuust Møller, Pierre Falson, and Marc le Maire. 1992. "Urea Reduces the Aggregation of Membrane Proteins on Sodium Dodecyl Sulfate-Polyacrylamide Gel Electrophoresis." *Tetrahedron Lett.* Vol. 285. [https://ac.els-cdn.com/S0003269796901839/1-s2.0-S0003269796901839-main.pdf?\\_tid=db758c44-14a0-471c-b150-7f0ed3a72b30&acdnat=1537464014\\_9339df5a1b566e2f485b81f8e2d639e4](https://ac.els-cdn.com/S0003269796901839/1-s2.0-S0003269796901839-main.pdf?_tid=db758c44-14a0-471c-b150-7f0ed3a72b30&acdnat=1537464014_9339df5a1b566e2f485b81f8e2d639e4).
- Spangenberg, T, J N Burrows, P Kowalczyk, S McDonald, and Tnc N C Wells. 2013. "The Open Access Malaria Box: A Drug Discovery Catalyst for Neglected Diseases." *PLoS ONE* 8 (6): 62906. <https://doi.org/10.1371/journal.pone.0062906>.
- Spielmann, Tobias, Georgina N Montagna, Leonie Hecht, and Kai Matuschewski. 2012. "Molecular Make-up of the Plasmodium Parasitophorous Vacuolar Membrane." *International Journal of Medical Microbiology* 302: 179–86.  
<https://doi.org/10.1016/j.ijmm.2012.07.011>.
- Spillman, Natalie J., Richard J W Allen, Case W. McNamara, Bryan K S Yeung, Elizabeth A. Winzeler, Thierry T. Diagana, and Kiaran Kirk. 2013. "Na<sup>+</sup> regulation in the Malaria Parasite Plasmodium Falciparum Involves the Cation ATPase PfATP4 and Is a Target of the Spiroindolone Antimalarials." *Cell Host and Microbe* 13 (2): 227–37.  
<https://doi.org/10.1016/j.chom.2012.12.006>.
- Spillman, Natalie Jane, and Kiaran Kirk. 2015. "The Malaria Parasite Cation ATPase PfATP4 and Its Role in the Mechanism of Action of a New Arsenal of Antimalarial Drugs." *International Journal for Parasitology: Drugs and Drug Resistance*.  
<https://doi.org/10.1016/j.ijpddr.2015.07.001>.

- Strugatsky, David, Kay-Eberhard Gottschalk, Rivka Goldshleger, Eitan Bibi, and Steven J D Karlish. 2003. "Expression of Na<sup>+</sup>,K<sup>+</sup>-ATPase in *Pichia Pastoris*: Analysis of Wild Type and D369N Mutant Proteins by Fe<sup>2+</sup>-Catalyzed Oxidative Cleavage and Molecular Modeling." *The Journal of Biological Chemistry* 278 (46): 46064–73. <https://doi.org/10.1074/jbc.M308303200>.
- Tan, W., D. M. Gou, E. Tai, Y. Z. Zhao, and L. M.C. C Chow. 2006a. "Functional Reconstitution of Purified Chloroquine Resistance Membrane Transporter Expressed in Yeast." *Archives of Biochemistry and Biophysics* 452: 119–28. <https://doi.org/10.1016/j.abb.2006.06.017>.
- Tan, W, D M Gou, E Tai, Y Z Zhao, and L M C Chow. 2006b. "Functional Reconstitution of PuriWed Chloroquine Resistance Membrane Transporter Expressed in Yeast." *Archives of Biochemistry and Biophysics* 452: 119–28. <https://doi.org/10.1016/j.abb.2006.06.017>.
- Thomas, Jennifer A, and Christopher G Tate. 2014. "Quality Control in Eukaryotic Membrane Protein Overproduction." <https://doi.org/10.1016/j.jmb.2014.10.012>.
- Thompson, J D, D G Higgins, and T J Gibson. 1994. "CLUSTAL W: Improving the Sensitivity of Progressive Multiple Sequence Alignment through Sequence Weighting, Position-Specific Gap Penalties and Weight Matrix Choice." *Nucleic Acids Research* 22 (22): 4673–80. <http://www.ncbi.nlm.nih.gov/pubmed/7984417>.
- Tilley, Leann, Geoff McFadden, Alan Cowman, and Nectarios Klonis. 2007. "Illuminating Plasmodium Falciparum-Infected Red Blood Cells." *Trends in Parasitology*. <https://doi.org/10.1016/j.pt.2007.04.001>.
- Tindall, Sarah M., Cindy Vallières, Dev H. Lakhani, Farida Islahudin, Kang-Nee Nee Ting, and Simon V. Avery. 2018. "Heterologous Expression of a Novel Drug Transporter from the Malaria Parasite Alters Resistance to Quinoline Antimalarials." *Scientific Reports* 8 (1): 2464. <https://doi.org/10.1038/s41598-018-20816-0>.
- Tokumasu, F., G. Crivat, H. Ackerman, J. Hwang, and T. E. Wellems. 2014. "Inward Cholesterol Gradient of the Membrane System in *P. Falciparum*-Infected Erythrocytes Involves a Dilution Effect from Parasite-Produced Lipids." *Biology Open* 3 (6): 529–41. <https://doi.org/10.1242/bio.20147732>.

- Toyoshima, Chikashi, and Hiromi Nomura. 2002. "Structural Changes in the Calcium Pump Accompanying the Dissociation of Calcium." *Nature* 418 (6898): 605–11. <https://doi.org/10.1038/nature00944>.
- Traenkle, Bjoern, Philipp D. Kaiser, Ulrich Rothbauer, Bjoern Traenkle, Philipp D. Kaiser, and Ulrich Rothbauer. 2016. "Nanobody Platform for Determination of Protein Structure, Application Of." *Encyclopedia of Analytical Chemistry*, 1–14. <https://doi.org/10.1002/9780470027318.a9548>.
- Trampuz, Andrej, Matjaz Jereb, Igor Muzlovic, and Rajesh M Prabhu. 2003. "Clinical Review: Severe Malaria." *Critical Care (London, England)* 7 (4): 315–23. <https://doi.org/10.1186/cc2183>.
- Tran, Phuong N., Simon H. J. Brown, Melanie Rug, Melanie C. Ridgway, Todd W. Mitchell, and Alexander G. Maier. 2016. "Changes in Lipid Composition during Sexual Development of the Malaria Parasite Plasmodium Falciparum." *Malaria Journal* 15 (1): 73. <https://doi.org/10.1186/s12936-016-1130-z>.
- Trape, J F. 2001. "The Public Health Impact of Chloroquine Resistance in Africa." *The American Journal of Tropical Medicine and Hygiene* 64 (1–2 Suppl): 12–17. <http://www.ncbi.nlm.nih.gov/pubmed/11425173>.
- Trottein, Franfois, and A F Cowman. 1995. "Molecular Cloning and Sequence of Two Novel P-Type Adenosinetriphosphatases from Plasmodium Falciparum." *European Journal of Biochemistry / FEBS* 227 (1–2): 214–25. <http://www.ncbi.nlm.nih.gov/pubmed/7851389>.
- Tsirigos, Konstantinos D, Christoph Peters, Nanjiang Shu, Lukas Käll, and Arne Elofsson. 2015. "The TOPCONS Web Server for Consensus Prediction of Membrane Protein Topology and Signal Peptides." *Nucleic Acids Research* 43 (W1): W401–7. <https://doi.org/10.1093/nar/gkv485>.
- Vasoo, Shawn, and Bobbi S. Pritt. 2013. "Molecular Diagnostics and Parasitic Disease." *Clinics in Laboratory Medicine* 33 (3): 461–503. <https://doi.org/10.1016/j.cll.2013.03.008>.
- Velden, Lieke M. van der, Catharina G. K. Wichers, Adriana E. D. van Breevoort, Jonathan

- A. Coleman, Robert S. Molday, Ruud Berger, Leo W. J. Klomp, and Stan F. J. van de Graaf. 2010. "Heteromeric Interactions Required for Abundance and Subcellular Localization of Human CDC50 Proteins and Class 1 P<sub>4</sub>-ATPases." *Journal of Biological Chemistry* 285 (51): 40088–96.  
<https://doi.org/10.1074/jbc.M110.139006>.
- Velden, Lieke M Van Der, Catharina G K Wichers, Adriana E D Van Breevoort, Jonathan A Coleman, Robert S Molday, Ruud Berger, Leo W J Klomp, and Stan F J Van De Graaf. 2010. "Heteromeric Interactions Required for Abundance and Subcellular Localization of Human CDC50 Proteins and Class 1 P<sub>4</sub>-ATPases \* □ S." <https://doi.org/10.1074/jbc.M110.139006>.
- Vestergaard, Anna L, Jonathan A Coleman, Thomas Lemmin, Stine A Mikkelsen, L. L. Molday, Bente Vilsen, Robert S Molday, Matteo Dal Peraro, and Jens Peter Andersen. 2014. "Critical Roles of Isoleucine-364 and Adjacent Residues in a Hydrophobic Gate Control of Phospholipid Transport by the Mammalian P<sub>4</sub>-ATPase ATP8A2." *Proceedings of the National Academy of Sciences* 111 (14): E1334–43.  
<https://doi.org/10.1073/pnas.1321165111>.
- Weber, J L. 1987. "Analysis of Sequences from the Extremely A + T-Rich Genome of Plasmodium Falciparum." *Gene* 52 (1): 103–9.  
<http://www.ncbi.nlm.nih.gov/pubmed/3297924>.
- Weiner, January, and Taco Kooij. 2016. "Phylogenetic Profiles of All Membrane Transport Proteins of the Malaria Parasite Highlight New Drug Targets." *Microbial Cell*. <https://doi.org/10.15698/mic2016.10.534>.
- Wilson, Michael L. 2012. "Malaria Rapid Diagnostic Tests." *Clinical Infectious Diseases* 54 (11): 1637–41. <https://doi.org/10.1093/cid/cis228>.
- Wittekindt, Nicola E, Friedrich E Wurgler, and Christian Sengstag. 1995. "Targeting of Heterologous Membrane Proteins into Proliferated Internal Membranes in Saccharomyces Cerevisiae." Vol. 11.  
<https://onlinelibrary.wiley.com/doi/pdf/10.1002/yea.320111003>.
- Wongsrichanalai, Chansuda, Mazie J Barcus, Sinuon Muth, Awalludin Sutamihardja, and Walther H Wernsdorfer. 2007. "A Review of Malaria Diagnostic Tools: Microscopy



- and Rapid Diagnostic Test (RDT).” [www.malaria.mr4.org](http://www.malaria.mr4.org).
- Woodrow, Charles J, Richard J Burchmore, and Sanjeev Krishna. 2000. “Hexose Permeation Pathways in Plasmodium Falciparum-Infected Erythrocytes.” *Proceedings of the National Academy of Sciences of the United States of America* 97 (18): 9931–36. <https://doi.org/10.1073/pnas.170153097>.
- Woodrow, Charles J, Jeffrey I Penny, and Sanjeev Krishna. 1999. “Intraerythrocytic Plasmodium Falciparum Expresses a High Affinity Facilitative Hexose Transporter.” *Journal of Biological Chemistry* 274 (11): 7272–77. <https://doi.org/10.1074/jbc.274.11.7272>.
- World Health Organization. 2016. “WORLD MALARIA REPORT 2016 ISBN 978 92 4 151171 1.” [www.who.int/malaria](http://www.who.int/malaria).
- World Health Organization. 2017a. “World Malaria Report 2016 – English Summary.” <http://apps.who.int/bookorders>.
- World Health Organization. 2017b. *World Malaria Report 2017*. <https://doi.org/10.1071/EC12504>.
- World Health Organisation. 2018. “WHO | High-Risk Groups.” World Health Organization. [http://www.who.int/malaria/areas/high\\_risk\\_groups/en/](http://www.who.int/malaria/areas/high_risk_groups/en/).
- Wright, R, M Basson, L D’Ari, and J Rine. 1988. “Increased Amounts of HMG-CoA Reductase Induce “Karmellae”: A Proliferation of Stacked Membrane Pairs Surrounding the Yeast Nucleus.” *The Journal of Cell Biology* 107 (1): 101–14. <https://doi.org/10.1083/JCB.107.1.101>.
- Wu, Binghua, Janis Rambow, Sinja Bock, Julia Holm-Bertelsen, Marie Wiechert, Alexandra Blancke Soares, Tobias Spielmann, and Eric Beitz. 2015. “Identity of a Plasmodium Lactate/H<sup>+</sup> Symporter Structurally Unrelated to Human Transporters.” *Nature Communications* 6 (1): 6284. <https://doi.org/10.1038/ncomms7284>.
- Wunderlich, Frank, Stefan Fiebig, Henri Vial, and Hans Kleinig. 1991. “Distinct Lipid Compositions of Parasite and Host Cell Plasma Membranes from Plasmodium Chabaudi-Infected Erythrocytes.” *Molecular and Biochemical Parasitology* 44 (2):

271–77. [https://doi.org/10.1016/0166-6851\(91\)90013-V](https://doi.org/10.1016/0166-6851(91)90013-V).

Yatime, Laure, Morten J. Buch-Pedersen, Maria Musgaard, J. Preben Morth, Anne Marie Lund Winther, Bjørn P. Pedersen, Claus Olesen, et al. 2009. “P-Type ATPases as Drug Targets: Tools for Medicine and Science.” *Biochimica et Biophysica Acta - Bioenergetics*. <https://doi.org/10.1016/j.bbabi.2008.12.019>.

Youyou, Tu. 2015. “Youyou Tu - Nobel Lecture: Artemisinin - A Gift from Traditional Chinese Medicine to the World.” [https://assets.nobelprize.org/uploads/2018/06/tu-lecture.pdf?\\_ga=2.238022594.390225717.1536130040-1869620999.1536130040](https://assets.nobelprize.org/uploads/2018/06/tu-lecture.pdf?_ga=2.238022594.390225717.1536130040-1869620999.1536130040).

Zhang, Hanbang, Ellen M. Howard, and Paul D. Roepe. 2002. “Analysis of the Antimalarial Drug Resistance Protein PfCRT Expressed in Yeast.” *Journal of Biological Chemistry*. <https://doi.org/10.1074/jbc.M204005200>.

Zhang, Min, Chengqi Wang, Thomas D. Otto, Jenna Oberstaller, Xiangyun Liao, Swamy R. Adapa, Kenneth Udenze, et al. 2018. “Uncovering the Essential Genes of the Human Malaria Parasite *Plasmodium Falciparum* by Saturation Mutagenesis.” *Science* 360 (6388). <https://doi.org/10.1126/science.aap7847>.

Zhang, Xi, and Keith W. Miller. 2015. “Dodecyl Maltopyranoside Enabled Purification of Active Human GABA Type A Receptors for Deep and Direct Proteomic Sequencing.” *Molecular & Cellular Proteomics* 14 (3): 724–38. <https://doi.org/10.1074/mcp.M114.042556>.

Zhou, Xiaoming, Tessa T. Sebastian, and Todd R. Graham. 2013a. “Auto-Inhibition of Drs2p, a Yeast Phospholipid Flippase, by Its Carboxyl-Terminal Tail.” *Journal of Biological Chemistry*. <https://doi.org/10.1074/jbc.M113.481986>.

Zhou, Xiaoming, Tessa T. Sebastian, and Todd R. Graham. 2013b. “Auto-Inhibition of Drs2p, a Yeast Phospholipid Flippase, by Its Carboxyl-Terminal Tail.” *The Journal of Biological Chemistry* 288 (44): 31807–15. <https://doi.org/10.1074/jbc.M113.481986>.

# Article

---



# Screening of Detergents for Stabilization of Functional Membrane Proteins

Guillaume Lenoir,<sup>1</sup> Thibaud Dieudonné,<sup>1</sup> Anais Lamy,<sup>1</sup> Maylis Lejeune,<sup>1</sup> José-Luis Vazquez-Ibar,<sup>1</sup> and Cédric Montigny<sup>1,2</sup>

<sup>1</sup>Institute for Integrative Biology of the Cell (I<sup>2</sup>BC), CEA, CNRS, Université Paris-Sud, Université Paris-Saclay, Gif-sur-Yvette CEDEX, France

<sup>2</sup>Corresponding author: [Cedric.MONTIGNY@i2bc.paris-saclay.fr](mailto:Cedric.MONTIGNY@i2bc.paris-saclay.fr)

Membrane protein studies usually require use of detergents to extract and isolate proteins from membranes and manipulate them in a soluble context for their functional or structural characterization. However, solubilization with detergent may interfere with MP stability and may directly affect MP function or structure. Moreover, detergent properties can be affected such as critical micellar concentration (CMC) can be affected by the experimental conditions. Consequently, the experimenter must pay attention to both the protein and the behavior of the detergent. This article provides a convenient protocol for estimating the CMC of detergents in given experimental conditions. Then, it presents two protocols aimed at monitoring the function of a membrane protein in the presence of detergent. Such experiments may help to test various detergents for their inactivating or stabilizing effects on long incubation times, ranging from few hours to some days. © 2018 by John Wiley & Sons, Inc.

Keywords: detergents • Drs2p/Cdc50p • lipids • LMNG • membrane protein • stabilization • SERCA1a

## How to cite this article:

Lenoir, G., Dieudonné, T., Lamy, A., Lejeune, M., Vazquez-Ibar, J.-L., & Montigny, C. (2018). Screening of detergents for stabilization of functional membrane proteins. *Current Protocols in Protein Science*, 93, e59. doi: 10.1002/cpps.59

## INTRODUCTION

Membrane proteins (MPs) are usually solubilized in detergent for purification and downstream studies. Several detergents or polymers can be used for this purpose, and their presence is mandatory for extraction of proteins from native membranes, their purification, their functional studies and occasionally their crystallization. In the latter case, long-term MP stability is essential to perform accurate functional studies and crystallogenesis (Frauenfeld et al., 2016; le Maire, Champeil, & Moller, 2000; Popot et al., 2011; Privé, 2007). Stability of an MP can be assessed easily, for instance by ligand binding or monodispersity (Borths, Poolman, Hvorup, Locher, & Rees, 2005; see Commentary for alternate approaches).

Orwick-Rydmark, Arnold, & Linke (2016) presents an extensive review of detergent diversity and focuses on their uses for MP solubilization. Additionally, Saif Hasan et al., (2013) presents a case study that discusses specific strategies for selecting a detergent for purification and crystallization of two different integral MP complexes. Briefly, detergents are amphipathic molecules. Their chemical structures are composed primarily of phospholipids or biliary salts. Some detergents are in fact derived from lipids (e.g., lysolipids or some biliary salts). A subclass of detergent is commonly named aliphatic

detergents, as they are directly inspired from the structure of phospholipids: they have a hydrophilic headgroup attached to an aliphatic chain. The nature of the headgroup can vary greatly, e.g., sugars, hydrophilic polymers, or amino acids. Depending on the nature of this headgroup, detergents are generally categorized as non-polar, anionic, cationic, or zwitterionic, depending on their global charge at neutral pH (note that most protein purifications are done at pH ranging from 6.5 to 8.5). The length of the aliphatic chain may also vary, although detergents commonly used in MP stabilization and solubilization usually have aliphatic chains of 6 to 12 carbons (le Maire et al., 2000). Note that nonionic detergents with mid-length hydrocarbon chains (10 to 14 carbons) have proven efficient for MP stabilization in most cases. For instance, n-dodecyl- $\beta$ -D-maltopyranoside (DDM) displays a maltose headgroup attached to a 12-carbon aliphatic chain and is often used in preliminary screens as it is usually a good detergent for MP stabilization. New detergents and polymers are regularly synthesized to improve long-term stabilization of MPs (Hardy, Bill, Jawhari, & Rothnie, 2016).

Unfortunately, many MPs may become irreversibly inactive after solubilization by detergent (Columbus, 2015; le Maire et al., 2000; Privé, 2007). The presence of various osmolytes (e.g., sugars, amino acids, glycerol, betaine) in the incubation medium can slow down such irreversible inactivation. For example, sarco-endoplasmic reticulum  $\text{Ca}^{2+}$ -ATPase (SERCA1a) is stabilized by addition of glycerol or glycyl-betaine (Montigny, Arnou, Marchal, & Champeil, 2008, 2010, and references therein). Glycyl-betaine also protects the photosystem II complex from dissociation (Murata, Mohanty, Hayashi, & Papageorgiou, 1992) and the erythrocyte plasma membrane calcium pump from urea-induced denaturation (Coelho-Sampaio, Ferreira, Castro Júnior, & Vieyra, 1994). The presence of a ligand can also be critical for stabilization. For instance, addition of calcium to detergent-solubilized SERCA1a increased its long-term stability from a few hours to several days (Montigny, Arnou, & Champeil, 2010). The two bound calcium ions make several interactions with transmembrane helices and limit the movement of the transmembrane helices, consequently also limiting the insertion of detergent between the helices. Detergent properties can also be influenced by temperature (see Basic Protocol 1). While most biochemists may consider incubation at 4°C to be the most appropriate condition for storing a protein for a long time, one should consider that detergent-solubilized proteins are sometimes more stable at 20°C. For example, time-dependent irreversible inactivation of SERCA1a solubilized with either  $\text{C}_{12}\text{E}_8$  or DDM is slower at 20°C than at 6°C, regardless of the presence of calcium (Champeil, Menguy, Tribet, Popot, & le Maire, 2000; Montigny et al., 2010). Another possibility to improve the stability of an MP involves generating thermostable mutants (Magnani et al., 2016; Rodríguez-Banqueri et al., 2016; Vaidehi, Grisshammer, & Tate, 2016). However, none of these tips can fully prevent detergent-induced irreversible inactivation. Furthermore, it is essential to develop convenient protocols for screening detergents for their ability to solubilize and stabilize an MP, preferably before advancing to the purification process. Indeed, a detergent that efficiently solubilizes an MP might not necessarily be the best choice for its long-term stabilization or for downstream functional and structural characterization. The present article aims to help the experimenter by setting up protocols to screen detergents for their ability to stabilize a particular MP in its active form. Basic Protocol 1 will help the experimenter verify that detergent behavior is not perturbed excessively during the purification and functional characterization of a particular MP. Basic Protocol 2 and the Alternate Protocol take advantage of particular features of P-type ATPases, a large family of MP transporters, to assess the effect of several detergents on the long-term stabilization of the SERCA1a (Basic Protocol 2) and a yeast *trans*-Golgi flippase complex (Drs2p/Cdc50p, Alternate Protocol). Basic Protocol 2 is more appropriate for purified samples, whereas the Alternate Protocol is suitable for crude membranes analysis.

## DETERMINATION OF THE CRITICAL MIXED MICELLAR CONCENTRATION OF A DETERGENT

As is true of other amphipathic molecules, detergents are soluble in aqueous solution and can also insert into hydrophobic phases, including membranes. The critical micellar concentration (CMC) reflects the solubility of the individual detergent monomer in pure water. Above the CMC, the concentration of monomers is constant and detergent molecules in excess start to spontaneously form aggregates to prevent the exposure of their hydrophobic tails toward the aqueous phase. Such aggregates are called micelles and their size depends particularly on the chemical nature of the detergent (Helenius & Simons, 1975; Tanford & Reynolds, 1976). The number of aggregation ( $N_A$ ) corresponds to the average number of monomers found in a micelle. The concentration of detergent to be used for MP solubilization and stabilization directly depends on the CMC (see Commentary). Nevertheless, the CMC can be greatly influenced by the physical and chemical parameters of the environment such as temperature or ionic strength (Walter, Kuehl, Barnes, & VanderWaerd, 2000; also see Orwick-Rydmark et al., 2016, and references therein). In this respect, protein purification processes may sometimes require temperature variations from 4°C to 20°C, high salt concentrations (e.g., ion-exchange chromatography), and sometimes addition of stabilizing additives like glycerol, sucrose, or betaine as mentioned in the Introduction. Moreover, functional characterization usually requires long incubation of the sample to estimate activity or ligand binding ability.

The critical mixed micellar concentration (CMMC) reflects the solubility of the detergent monomer in a complex aqueous phase such as the buffer used in a particular experiment. The CMMC is usually close to, but always slightly lower than, the CMC in water. It is mandatory to check that the CMMC of a detergent does not vary significantly during the different steps of the purification, functional characterization, and possibly crystallization setup. An increase of the CMMC could result in aggregation of the MP, as the total detergent concentration becomes too low to keep the MP in a soluble state. Conversely, a decrease of the CMMC can trigger denaturation, as the amount of available detergent for interaction with the MP may increase and eventually result in destabilization of membrane bundles, dissociation of MP complexes, or removal of essential lipids for stabilization.

Several techniques have been developed for CMC and CMMC determination. Some techniques are based on measurement of surface tension or refractive index. These methods have the advantage of allowing estimation of the CMC (not only the CMMC) in pure water, i.e., in absence of any probe (see below). The oldest method, but still useful, was proposed by du Noüy (du Noüy, 1919). The force required to raise a platinum ring from the surface of a liquid depends on the surface tension. When the surface tension diminishes, the force required also decreases. The surface tension decreases when the concentration of detergent monomers increases. The CMC is reached when the force becomes constant (Benzonana, 1969). Similarly, it has been observed that the refractive index of a detergent solution changes when the CMC is reached. However, this method is more appropriate to detergents with CMCs in the millimolar range, as refractive index change becomes significant only when the total concentration of detergent is high (Tan, Huang, & Huang, 2010). Other methods involve the use of chemical probes whose absorption or fluorescence spectra changes when the probe moves from the aqueous environment to the hydrophobic core of micelles (Slavík, 1982; Jumpertz et al., 2011). Orwick-Rydmark et al. (2016) describes a protocol using pyrene fluorescence properties in hydrophobic phases (see Commentary). As most biochemistry labs possess a spectrophotometer, this protocol describes a simple method exploiting a colorimetric probe sensitive to micelle formation.

Methyl orange is generally used as pH indicator, as its color changes from red to yellow at pH 3-4 (Benzonana, 1969). However, it also changes color after incorporation into hydrophobic phases such as micelles. G. Benzonana took advantage of this property to estimate the CMC of deoxycholate, a biliary salt-derived detergent (Benzonana, 1969). Methyl orange has also proven useful for the determination of the CMC of aliphatic detergents. Figure 1 presents the use of methyl orange to estimate the effect of glycerol on the CMMC of DDM. First, glycerol itself has an effect on the absorption spectrum of methyl orange even in the absence of detergent (Fig. 1A). This may reflect a change in the polarity of the medium upon adding glycerol, as the medium becomes less polar when the concentration of glycerol increases. For this reason, the wavelength chosen to follow methyl orange spectral changes was different in the three conditions investigated (see procedure below and Ohnishi, 1978). Figure 1B depicts an example of difference spectra recorded after several additions of DDM in a buffer without glycerol. Changes in absorbance were extracted from these difference spectra (see procedure below) to obtain the values represented on Figure 1C, which show that the presence of glycerol alters the CMMC of DDM. The  $CMMC_{DDM}$  is  $\sim 80$   $\mu\text{g/ml}$  in the absence of glycerol and increases to  $\sim 90$  and  $\sim 120$   $\mu\text{g/ml}$  in the presence of 20% and 40% glycerol, respectively. Additionally, the slopes of the line segments used for CMMC estimation decrease when the amount of glycerol increases (Fig. 1C), revealing a change in the partition coefficient of methyl orange between the aqueous phase and the micelles. Similar results were obtained with  $C_{12}E_8$ , another aliphatic detergent (Aramaki, Olsson, Yamaguchi, & Kunieda, 1999). The methyl orange method is robust and suitable for estimating CMMC changes in varying chemical and physical conditions, for instance in the presence of a particular compound in the medium (e.g., glycerol; Fig. 1), in the presence of different salts concentrations, or even when the temperature varies. As an example, a few CMMC values of different detergents in various solvents determined with the methyl orange method are given in Table 1. It illustrates the effect of such parameters on CMMC, especially for detergents with high CMC values, such as n-octyl- $\beta$ -D-glucopyranoside (OG).

### Materials

Buffer A with 0%, 20%, or 40% (v/v) glycerol (see recipe)  
2 mM methyl orange (see recipe)  
20 mg/ml DDM (see recipe for detergent stock solutions)

Agilent 8453 diode array spectrophotometer with thermostatic cell holder  
(connected to a circulating water bath to ensure constant temperature and  
continuous stirring of the sample; see Troubleshooting)  
2-ml plastic or glass cuvette

1. Switch on the spectrophotometer  $\sim 15$  min before starting experiments to allow the lamps to warm up. Switch on the water bath to set up the temperature of the cell holder. Warm buffers to the desired temperature.

*The spectrophotometer will be used in a record spectra mode.*

2. Add 2 ml of the first buffer to be tested (in this example, buffer A without glycerol) to a 2-ml cuvette. Record blank from 440 to 640 nm.
3. Add 40  $\mu\text{l}$  of 2 mM methyl orange (final 40  $\mu\text{M}$ ) and record spectrum again from 440 to 640 nm (Fig. 1A, continuous line).
4. Record blank again but now in the presence of methyl orange.
5. To generate difference spectra (Fig. 1B), perform serial additions of 40  $\mu\text{g}$  DDM (2  $\mu\text{l}$  of 20 mg/ml stock) until the final concentration is  $\sim 220$   $\mu\text{g/ml}$ . After each addition,



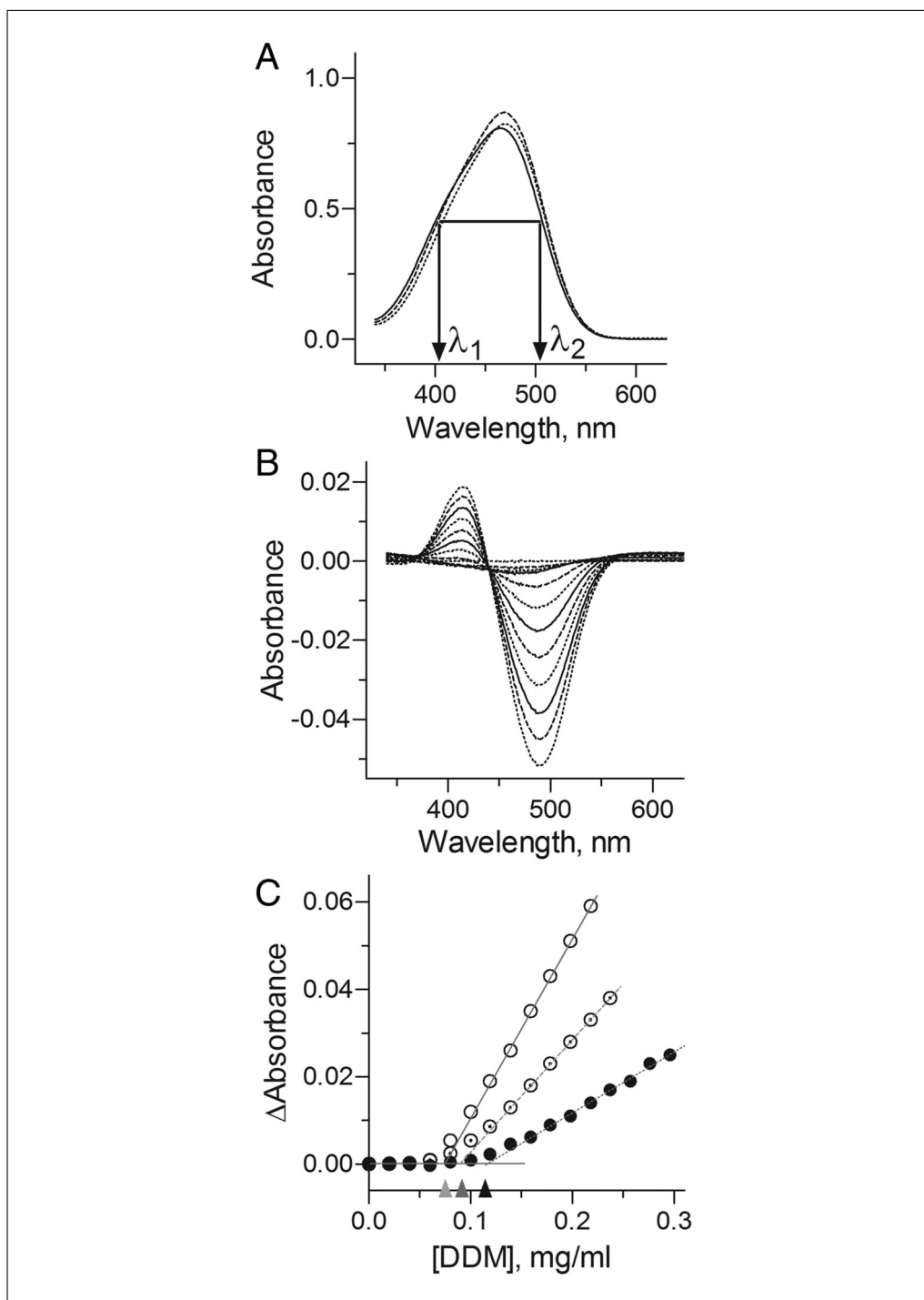


**Figure 1** Use of methyl orange for CMMC determination. The effect of glycerol on the CMMC of n-dodecyl- $\beta$ -D-maltopyranoside (DDM) is shown as an example. **(A)** Spectra of methyl orange ( $40 \mu\text{M}$ ) in buffer A alone (continuous line) or supplemented with 20% (v/v; dashed line) or 40% (dotted line) glycerol.  $\lambda_1$  and  $\lambda_2$  are two wavelengths used to follow color changes upon addition of DDM to the cuvette. They are chosen to give equal absorbance in the absence of detergent to minimize the effect of dilution upon addition of detergent (Ohnishi, 1978). **(B)** Difference spectra of methyl orange ( $40 \mu\text{M}$ ) in buffer A without glycerol upon addition of increasing concentrations of DDM (0 to  $220 \mu\text{g/ml}$ ). **(C)** Differences in absorbance measured at 0% (open symbols), 20% (dotted symbols), and 40% (closed symbols) glycerol.  $\lambda_1$  and  $\lambda_2$  were 401 and 506 nm, 410 and 507 nm, and 410 and 509 nm, respectively. The CMMC corresponds to the point where the differences in absorbance increase sharply:  $\sim 80 \mu\text{g/ml}$  in the absence of glycerol (light gray triangle),  $\sim 90 \mu\text{g/ml}$  in 20% glycerol (dark gray triangle), and  $\sim 120 \mu\text{g/ml}$  in 40% glycerol (dark gray triangle).

**Table 1** Examples of CMMC Values in Different Experimental Conditions Determined by the Methyl Orange Method<sup>a</sup>

	C <sub>12</sub> E <sub>8</sub>	DDM	OG
CMC (H <sub>2</sub> O) <sup>b</sup>	0.045	0.085	5.9
Buffer A	0.046	0.080	6.5
+20% glycerol (v/v)	0.050	0.090	7.4
+40% glycerol (v/v)	0.075	0.120	7.9
0.1 M NaCl <sup>c</sup>	n.d.	0.081	7.6
0.2 M NaCl <sup>c</sup>	n.d.	0.079	7.3
0.5 M NaCl <sup>c</sup>	n.d.	0.076	6.1
10°C	n.d.	0.097	8.7
17°C	n.d.	0.087	8.2
23°C	n.d.	0.077	7.6

<sup>a</sup>CMMC values determined in buffer A at 20°C. Concentrations are in mg/ml. CMC values measured in pure water are given for comparison (Anatrace website and references therein). C<sub>12</sub>E<sub>8</sub>, octaethylene glycol monododecyl ether; DDM, n-dodecyl-β-D-maltopyranoside; OG, n-octyl-β-D-glucopyranoside; n.d., not determined. For a more complete list of detergents and data on their properties, see Orwick-Rydmark et al. (2016) and le Maire et al. (2000).

<sup>b</sup>Values from Anatrace (see Internet Resources).

<sup>c</sup>KCl in buffer A was replaced with NaCl.

wait for a few seconds before recording the difference spectrum, as equilibrium between detergent monomers and micelles may take some time (see Troubleshooting).

6. Select two wavelengths with equal absorbance of methyl orange.

*Three characteristic wavelengths are observed on difference spectra (Fig. 1B) upon detergent additions: an increase of absorption at  $\lambda_{max} = 414$  nm, a decrease of absorption at  $\lambda_{min} = 490$  nm, and an isosbestic point at  $\lambda = 441$  nm, a wavelength where no change occurs (see Troubleshooting). Although maximum sensitivity can be achieved by using a  $\lambda_{max} - \lambda_{min}$  difference, a slight dilution effect may be observed and may perturb CMMC determination. This dilution effect can be avoided by selecting two wavelengths where the absorbance of methyl orange is the same (Fig. 1A,  $\lambda_1$  and  $\lambda_2$ ; Ohnishi, 1978).*

7. Estimate the difference in absorbance at these wavelengths ( $A_{\lambda_1} - A_{\lambda_2}$ ) on each difference spectrum (Fig. 1B) and plot them as a function of total DDM concentration in the cuvette (Fig. 1C).

*Note that the total concentration in DDM in the cuvette must be calculated for each recorded spectrum as the total volume of the cuvette increases after each addition of detergent.*

8. Determine the CMMC as the point where the difference in absorbance increases sharply.

- a. Draw a straight line segment along the points corresponding to the concentration of DDM where no significant absorption changes occur (horizontal gray line in Fig. 1C).

*This can be done manually for a quick estimate or by fitting the selected points to a linear function.*

- b. Draw another straight line segment along the points exhibiting a proportional increase in absorption as a function of detergent concentration (continuous gray line in the absence of glycerol).
- c. Determine the CMMC as the intercept of these two lines (light gray triangle on  $x$  axis in the absence of glycerol).

- Repeat steps 2 to 8 for each buffer or condition to be tested (in this example, buffer A with 20% and 40% glycerol).

## USE OF ATPASE ACTIVITY MEASUREMENTS TO SCREEN DETERGENTS FOR LONG-TERM STABILIZATION OF SERCA1a

BASIC  
PROTOCOL 2

It is not straightforward to predict the appropriate detergent to solubilize and stabilize a particular MP. In most cases, the primary goal is to achieve functional and/or structural characterization of the MP in a native-like state and under well-defined conditions. As a large panel of detergents is available for the study of MPs, simple and quick procedures that allow the screening of a large number of detergents are required. ATPase activity can be used to screen the potential stabilization effect of several detergents on MPs in the presence of remaining native lipids.

Several protocols have been developed to determine ATPase activity. Some colorimetric methods estimate the amount of inorganic phosphate ( $P_i$ ) arising from hydrolysis of ATP (Sehgal, Olesen, & Møller, 2016, and references therein). These methods are very convenient for detecting and assessing very low activity, as inorganic phosphate can be accumulated for a long period. They are also convenient for treating several samples simultaneously, e.g., screening multiple conditions by conducting the test in 96-well microplates. Unfortunately, these colorimetric methods also have several major disadvantages. First, they do not reflect fluctuations in the ATP hydrolysis rate that may occur during the incubation period, e.g., if irreversible inactivation progressively happens during turnover. Second, the accumulation of ADP during the incubation period can inhibit ATP hydrolysis, even though an ATP regenerating system can be added to the reaction medium (see below). Moreover, colorimetric assays require the use of a standard series to estimate the  $P_i$  concentration. Finally, a possible nonspecific ATP hydrolysis background may be revealed by using, for example, a control sample that has been inactivated beforehand.

The method presented here allows continuous monitoring of enzyme turnover using a spectrophotometer. ATPase activity is determined according to a method developed by Pullman and colleagues (Pullman, Penefsky, Datta, & Racker, 1960). Figure 2 presents a scheme of the principle of the method; a complete description of the procedure is found in Sehgal et al. (2016) and references therein. Briefly, ATPase hydrolyzes ATP into ADP and  $P_i$ . The ATP is regenerated by pyruvate kinase from ADP and phosphoenolpyruvate. Pyruvate kinase and phosphoenolpyruvate constitute the regenerating system. The resulting pyruvate is converted to lactate by lactate dehydrogenase with concomitant oxidation of  $NADH, H^+$  to  $NAD^+$ . As  $NADH, H^+$ , and not  $NAD^+$ , absorbs at 340 nm, the negative slope of the recorded kinetic trace will correspond to the rate of ATP hydrolysis during the experiment. Lactate dehydrogenase and  $NADH, H^+$  constitute the reporting system. Finally,

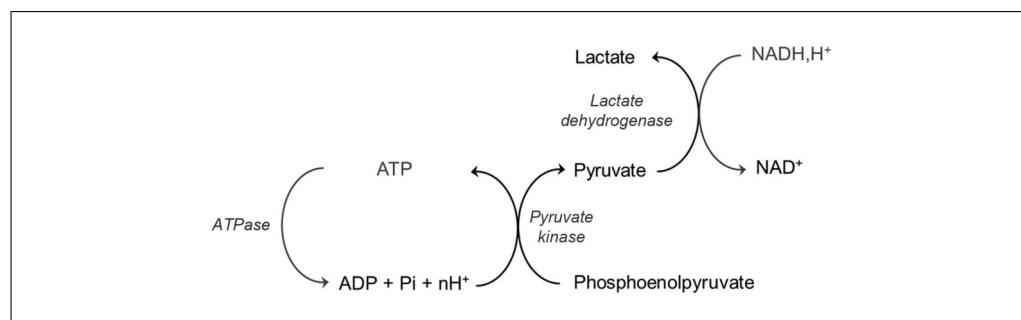


**Figure 2** Principle of the enzyme-coupled assay. Two forms of the nicotinamide adenine dinucleotide exist: an oxidized ( $NAD^+$ ) and reduced form ( $NADH, H^+$ ).  $NADH, H^+$ , not  $NAD^+$ , absorbs at 340 nm.

Lenoir et al.

7 of 27

for every mole of ATP hydrolyzed by ATPase, 1 mole of NADH,H<sup>+</sup> is consumed by the regenerating and reporting systems. The ATPase activity (in  $\mu\text{mol}$  ATP hydrolyzed/mg protein/min) can be easily calculated from the molar extinction coefficient of NADH,H<sup>+</sup> and its rate of oxidation (slope corresponding to a decrease of absorbance per second).

This method is suitable for assessing activity of various ATPases. It can be also applied to a large number of samples, although this requires an appropriate microplate reader to record numerous kinetic traces simultaneously (Zhou & Bowie, 2000). The main advantage of the method is that it allows a direct observation of possible changes in the ATP hydrolysis rate during the experiment: a stable protein with a constant ATPase activity results in a straight decrease, while curvature of the trace may reflect inactivation of the enzyme or possible interaction with cofactors (Montigny et al., 2008, 2010, 2017). Furthermore, addition of an inhibitor directly in the cuvette (here, EGTA to chelate calcium) allows simultaneous measurement of possible nonspecific ATPase activity that has to be subtracted from the rate of hydrolysis measured in the absence of inhibitor. The presence of a regenerating system maintains the concentration of ADP at a very low level and the concentration of ATP close to its maximum, ensuring constant experimental conditions. As a general comment, ATPase activity measurements are more appropriate for purified proteins, as crude extracted membranes may contain a large variety of ATPases. Use of specific inhibitors of endogenous ATPases could help improve the signal-to-noise ratio (Centeno et al., 1994).

Sarco-endoplasmic reticulum Ca<sup>2+</sup>-ATPase (SERCA1a) is a 994–amino acid integral MP. A large cytosolic domain, responsible for hydrolysis of ATP, is connected to a transmembrane domain made of ten  $\alpha$ -helices. This bundle of helices contains the calcium-binding sites (Møller, Olesen, Winther, & Nissen, 2010). SERCA1a hydrolyses ATP to drive the transport of calcium from the cytosol to the lumen of the endoplasmic reticulum against a steep concentration gradient. The ATP hydrolysis is calcium-dependent. This membrane transporter belongs to the P-type ATPase family, a large family of membrane transporters mainly involved in the transport of cations or lipids across membranes (Palmgren & Nissen, 2011). During the catalytic cycle, these enzymes are autophosphorylated from ATP, forming a phosphorylated intermediate dubbed “EP”. This autophosphorylation is a key event in the transport mechanism and a hallmark of this family of transporters (Møller et al., 2010; see Alternate Protocol dedicated to P-type ATPases). This autophosphorylation occurs on a conserved aspartate residue in the cytosolic domain of the protein and it results in the formation of an acylphosphate bond that is highly stable at acidic pH (Hokin, Sastry, Galsworthy, & Yoda, 1965). It has been demonstrated for several members of this family of transporters that dephosphorylation is the rate-limiting step of the catalytic cycle, so the phosphorylated intermediate accumulates at steady-state.

SERCA1a-enriched membranes are commonly prepared from rabbit fast-twitch skeletal muscle (as this procedure is specific for SERCA1a, it is not described here; for a detailed protocol see Møller & Olesen, 2016). These membranes contain  $\sim 0.5$  g of lipid per gram of protein and are mostly enriched in SERCA1a (Roux & Champeil, 1984). The procedure described here consists of solubilizing SERCA1a-containing membranes with a large amount of the detergent to be tested (see below for methods to predict the required amount of detergent to obtain a fully solubilized sample). Solubilization can be testified by the clear-cut drop in absorbance (turbidity of the membrane suspension in the absence or presence of detergent) observed at all wavelengths after adding the detergent. Of note, partial or total delipidation may occur at a high detergent/lipid ratio (Lund et al., 1989; Montigny et al., 2017). An aliquot of the solubilized sample is taken after different periods of incubation and this aliquot is diluted into the ATPase assay medium, which already contains C<sub>12</sub>E<sub>8</sub> at 2 mg/ml. C<sub>12</sub>E<sub>8</sub> is a nonionic detergent appropriate for preparing active and stable solubilized SERCA1a as demonstrated previously (Champeil et al.,

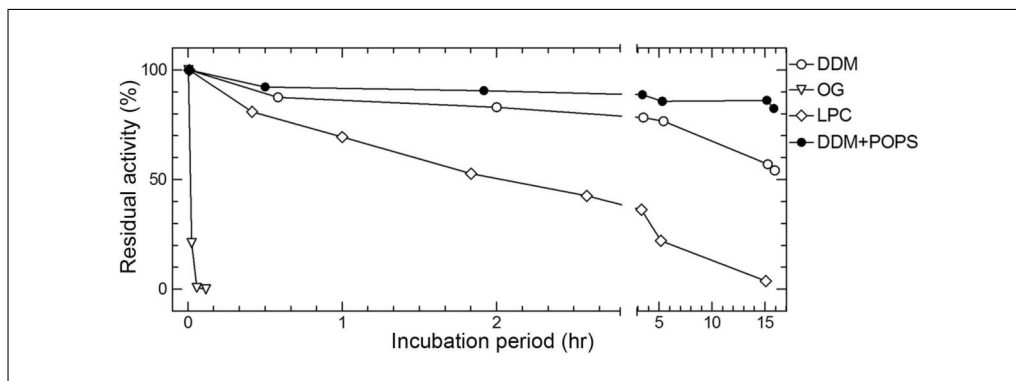


**Figure 3** Stability of SERCA1a upon long-term incubation in the presence of several detergents or detergent/lipid mixtures. SERCA1a-containing membranes were solubilized at a detergent/endogenous lipid ratio of 100:1 (w/w) and incubated for various periods in the presence of the indicated detergents with or without lipid. Residual activity was measured in the presence of 2 mg/ml  $C_{12}E_8$  and 0.02 mg/ml of the detergent tested for stabilization, resulting from a 50-fold dilution of the preincubated sample. Residual activity was 6.2, 4.4, 6.3, and 6.4  $\mu\text{mol ATP hydrolyzed/mg protein/min}$  for DDM, OG, LPC, and DDM/POPS, respectively. Relative residual activity was graphed with residual activity at time 0 set at 100%. The CMC of the detergent tested was estimated in the preincubation medium according to the methyl orange method (see Basic Protocol 1). The experiment shown here is representative of several other experiments giving similar results.

2016; Møller, Lind, & Andersen, 1980). Depending on the protein, another detergent could be used in the assay medium (for discussion, see Commentary). Consequently, the detergent tested during the preincubation period is highly diluted in  $C_{12}E_8$  micelles, and therefore barely interferes with the ATPase activity measurement, allowing assessment of the residual ATPase activity.

Figure 3 illustrates a typical experiment showing the effect of different types of detergents on the stabilization of SERCA1a. The experiment included two chemically pure non-polar detergents (DDM and OG, with 12-carbon chains and 8-carbon aliphatic chains, respectively), as well as a natural extract of 1- $\alpha$ -lysophosphatidylcholine (LPC) from soybean. In addition, the experiment illustrates the effect of additional lipid on the stabilization of SERCA1a. As previously documented (Lund et al., 1989), DDM-solubilized SERCA1a is stable for hours, as the residual ATPase activity after 3 hr of incubation at 20°C is ~80% of the initial activity. Inversely, the activity of OG-solubilized SERCA1a decreases dramatically within a few minutes of preincubation, indicating that irreversible inactivation of SERCA1a occurs quickly in the presence of OG. This test can be also used for detergent mixtures as depicted by the results obtained with LPC. The CMC of this detergent determined by the methyl orange method is about 2  $\mu\text{g/ml}$ . This low value may reflect the presence of a diversity of aliphatic chains (fatty acid distribution is available at <https://avantilipids.com/product/840072/>). SERCA1a solubilized in LPC is fairly stable, but less so than in DDM. Furthermore, lipids can be essential for MP stabilization and activity (Drachmann et al., 2014; Hunte & Richers, 2008; Picas et al., 2010; also see Commentary for procedures that allow complete delipidation of MPs). In some cases, use of detergent/lipid mixtures may help the stabilization of an MP (Azouaoui et al., 2014; Cardi et al., 2010). Incubation of the DDM-solubilized SERCA1a in the additional presence of phosphatidylserine (1-palmitoyl-2-oleoyl-sn-glycero-3-phospho-l-serine, POPS) has a higher long-term stabilizing effect than DDM alone.

The following protocol describes the procedure for measuring the residual ATPase activity of SERCA1a. It may be readily transposed to any other membrane-embedded ATPase or to transmembrane receptors, as the binding affinity for different ligands can be used as readout as well.

## Materials

40 mg protein/ml SERCA1a-containing sarco-endoplasmic reticulum membranes from rabbit muscle (for complete detailed procedure, see Møller & Olesen, 2016)

Buffer B (see recipe)

Detergents to be tested:

200 mg/ml detergent stock solutions (see recipe) of DDM, OG, and LPC

100:5 (w/w) DDM/POPS stock mixture (see recipe for detergent/lipid stock mixtures)

ATPase assay medium (see recipe)

15 mM NADH (see recipe)

0.5 M EGTA (see recipe)

Agilent 8453 diode array spectrophotometer with thermostatic cell holder (connected to a circulating water bath for constant temperature and continuous stirring of the sample)

2-ml quartz cuvette

## Prepare for assay

1. Switch on the spectrophotometer ~15 min before starting experiments to allow the lamps to warm up. Switch on the water bath to set up the temperature of the cell holder. Warm buffers to the desired temperature.

*The spectrophotometer will be used in a kinetics record mode at 340 nm.*

## Pre-incubate samples

2. Suspend SERCA1a-containing membranes in buffer B at 0.21 mg protein/ml. Adjust the protein concentration as needed to be able to detect activity (see comments about the limit of detection of the method at the end of the protocol). To avoid pipetting errors, prepare only one master suspension to cover all the needs of the experiment.

*As an example, to obtain the results presented in Figure 3, prepare 2.1 ml suspension by adding 11  $\mu$ l of 40 mg/ml membranes to 2.09 ml buffer B.*

3. Divide the suspension into five aliquots of 380  $\mu$ l (for the five detergents to be tested). Store samples on ice.
4. At time 0, add detergents at a final concentration of 10 mg/ml (e.g., 20  $\mu$ l of 200 mg/ml DDM stock solution). Homogenize the suspension using a vortex.

*When several conditions are tested in parallel, start incubations at different times (by staggering the addition of detergent) so there is enough time to measure the residual ATPase activity.*

*The SERCA1a-containing suspension is now at 0.2 mg protein/ml and should be transparent if solubilization has occurred.*

5. Incubate samples at the chosen temperature (here, 20°C). After different periods of incubation, withdraw 40  $\mu$ l (8  $\mu$ g protein) for immediate ATPase activity measurements.

## Measure residual ATPase activity

6. Add 2 ml ATPase assay medium without NADH to the cuvette and record blank.
7. Add freshly prepared NADH to a final concentration of 0.3 mM (40  $\mu$ l at 15 mM) and wait for the absorbance to stabilize.

With a freshly prepared NADH solution, starting absorbance may be close to 1.86. As the stock solution becomes older, the starting absorbance decreases. Moreover, depending on the intensity of the lamp, special attention should be paid to the linear absorbance zone. The starting absorbance must be in this linear zone.

Fresh NADH solution will be yellowish. NADH is light sensitive and is spontaneously oxidized to  $\text{NAD}^+$  if exposed to light. It should be protected from light by covering tubes with aluminum foil or using a suitable smoked-glass bottle. The molar extinction coefficient of NADH at 340 nm is 6200 M/cm. Consequently, a drop of 0.062 in absorbance at 340 nm corresponds to the oxidation of 10  $\mu\text{M}$  NADH. Photobleaching of NADH can be reduced by inserting an MTO J310A filter between the light source of the spectrophotometer and the sample to eliminate the short-wavelength UV-exciting light of the spectrophotometer lamp, as excitation of the 260 nm absorption band of NADH is much more deleterious for light stability of NADH than excitation of its 340 nm band. This setup reduces the spontaneous rate of NADH absorption changes down to  $\sim 0.00001$  mAU/sec, and therefore make it possible to detect very low activities (Azouaoui et al., 2017).

8. Add the 40- $\mu\text{l}$  sample (step 5) and wait for 1 to 3 min.

*For low activities, longer waiting times give more precise measurements.*

9. Add 1 mM EGTA (4  $\mu\text{l}$  at 0.5 M) to chelate calcium and stop hydrolysis of ATP. Wait another 1 to 3 min.
10. Stop recording.
11. Measure the slope before EGTA addition to give total activity,  $a_{\text{tot}}$ , expressed as a decay of absorbance per second.
12. Measure the slope after EGTA addition to give the calcium-independent activity,  $a_0$ , also expressed as decay of absorbance per second.
13. Calculate the calcium-dependent activity, which corresponds to the residual ATPase activity of detergent-solubilized SERCA1a, as  $a_{\text{tot}} - a_0$ .
14. Convert activity to  $\mu\text{mol}$  ATP hydrolyzed/mg protein/min according to the Beer-Lambert law:

$$A \sim 4838 \times a$$

where  $a$  is activity measured and 4838 is a factor that takes into account the NADH molar extinction coefficient at 340 nm ( $\epsilon_{\text{NADH at 340 nm}} = 6200$  liters/mol/cm), the volume of the cuvette, the concentration of protein, the conversion from seconds to minutes, the conversion from  $\mu\text{g}$  protein to mg, and the conversion from moles NADH to  $\mu\text{moles}$ .

*In Figure 3, the final ATPase concentration in the cuvette was 4  $\mu\text{g/ml}$  (see step 5). In these conditions, calcium-independent decay measured after EGTA addition was  $\sim 0.00001$ . This decay is mainly attributed to spontaneous oxidation of NADH and can be assumed as the background of the method. Additionally, the decay of absorbance measured at time 0 was about 0.0025 for each condition tested and was  $\sim 0.0001$  after a 15-hr incubation in the presence of LPC, one of the lowest activities measured in that experiment, but still about ten times higher than the background.*

*Specific activity may be slightly different at time 0 for each condition, as it may depend on the presence of the detergent tested during incubation or on the accuracy of pipetting. To make the results fully comparable, residual specific activity ( $\text{RSA}_n$ , where  $n$  is the incubation time), initially expressed in  $\mu\text{mol}$  ATP hydrolyzed/mg protein/min, can be converted as a percentage of the specific activity measured at time 0 ( $\text{RSA}_0$ ) for each condition:  $\% \text{RSA}_n = (\text{RSA}_n \times 100) / \text{RSA}_0$ .*

**USE OF A PHOSPHORYLATION ASSAY TO SCREEN DETERGENTS FOR LONG-TERM STABILIZATION OF A FLIPPASE COMPLEX IN THE PRESENCE OF LIPIDS**

As mentioned above, determination of the residual ATPase activity after incubation of SERCA1a in the presence of several detergents is a general procedure that should be readily adaptable to other membrane ATPases. In the specific case of P-type ATPases, other functional assays are available to probe the stability of an MP. A general approach in the MP field is to exploit a particular feature of the protein to develop a procedure enabling screening of several conditions for their effect on stabilization (e.g., ligand-binding assay on G protein-coupled receptors; see Magnani et al., 2016).

At acidic pH, the phosphorylated intermediate formed by P-type ATPases during turnover (dubbed EP) can be trapped and the amount of phosphorylatable proteins in a sample can be quantified (Azouaoui et al., 2016; Hatori et al., 2008). The main advantage of this technique is that it is possible to quantify the amount of phosphorylatable enzyme even in the presence of other ATPases: crude membranes may contain various ATPases, but only P-type ATPases will form a stable phosphorylated species. Furthermore, the affinity of P-type ATPases for ATP is high compared to that of other membrane-embedded ATPases (submicromolar for the former versus high micromolar or even millimolar for the others). Consequently, a low amount of radiolabeled ATP is required for the assay. Therefore, this method is highly sensitive and selective and the background is usually very low, allowing detection of a very small amount of protein.

The protocol described here shows how this particular feature of P-type ATPases, i.e., autophosphorylation, can be used to investigate the stabilizing effect of several detergent/lipid mixtures on the Drs2p/Cdc50p flippase complex. Flippases are P-type ATPases involved in active transbilayer lipid transport (Montigny, Lyons, Champeil, Nissen, & Lenoir, 2016). Drs2p, in association with its subunit Cdc50p, is a yeast flippase localized in the *trans*-Golgi network. It has been demonstrated that Drs2p is involved in phosphatidylserine (PS) transport (Natarajan, Wang, Hua, & Graham, 2004; Zhou & Graham, 2009). Its ATPase activity depends on the presence of the transported species, PS, and a physiological regulatory lipid, phosphatidylinositol-4-phosphate (PI4P; Azouaoui et al., 2014; Jacquot et al., 2012; Zhou, Sebastian, & Graham, 2013). The goal here was to test the effect of lauryl maltose neopentyl glycol (LMNG) on Drs2p/Cdc50p structural and functional integrity. LMNG is a peculiar nonpolar detergent with two 12-carbon acyl chains and a large headgroup composed of two maltose units. LMNG was described for its favorable behavior with respect to MP stabilization (Chae et al., 2010; <https://www.anatrace.com/Products/Detergents/NG-CLASS/NG310>). For instance, it was recently used for crystallization of a bacterial lipid-linked oligosaccharide transporter (Perez et al., 2015).

Drs2p and Cdc50p are co-overexpressed in *Saccharomyces cerevisiae* (Jacquot et al., 2012). Drs2p/Cdc50p-enriched membrane fractions are prepared and a complex of both proteins is purified by affinity chromatography. DDM proved to be a very good detergent for solubilization and stabilization of the Drs2p/Cdc50p complex during purification (Azouaoui et al., 2014). A procedure was previously described to measure autophosphorylation in crude yeast membranes, i.e., in the presence of endogenous lipids (Azouaoui et al., 2016). This protocol is for investigating the stability of the solubilized and purified complex in the presence of various detergent/lipid mixtures. Briefly, the purified sample in the presence of detergent or detergent/lipid mixtures is supplemented with [ $\gamma$ - $^{32}$ P]ATP. Transient phosphorylation occurs within tenths of a second. The reaction is subsequently stopped by acid quenching to precipitate and stabilize the acylphosphate intermediate EP. The sample is then filtered and the radioactivity trapped in the filter is counted by scintillation.



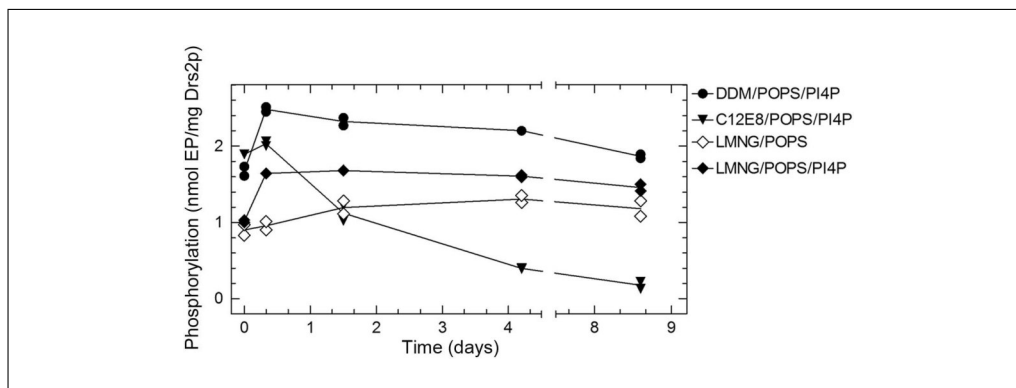


**Figure 4** Stability of the Drs2p/Cdc50p flippase complex upon long-term incubation in the presence of several detergent/lipid mixtures. Purified Drs2p/Cdc50p was incubated in the presence of the indicated mixtures. Aliquots were withdrawn after various incubation periods and submitted to phosphorylation assays. This experiment is representative of several similar independent experiments.

Figure 4 shows a typical experiment where the purified Drs2p/Cdc50p complex was incubated in the presence of different detergent/lipid mixtures for various time periods before phosphorylation was triggered by addition of  $[\gamma\text{-}^{32}\text{P}]\text{ATP}$ . In the mixtures tested here, inactivation rates are very slow, probably due to the presence of lipids. The  $t_{1/2}$  for phosphoenzyme loss is  $\sim 2$  days in  $\text{C}_{12}\text{E}_8/\text{PS}/\text{PI4P}$  at  $4^\circ\text{C}$  and increases to 8 days when  $\text{C}_{12}\text{E}_8$  is replaced by DDM or LMNG. It has been demonstrated that the rate of phosphorylation and dephosphorylation of P-type ATPases may be influenced by the presence of detergent (de Foresta, Henao, & Champeil, 1992). Therefore, variations of EP levels observed at time 0 probably reflect the fact that the maximum achievable EP level is not the same in different detergent/lipid mixtures. Additionally, the EP level increases during the first 8 hr of incubation. As the rate of detergent-to-lipid exchange (and vice versa) may be very slow at  $4^\circ\text{C}$ , this increase in the EP level during the first 8 hr of incubation may simply reflect the time necessary for this protein/detergent/lipid system to reach equilibrium (Montigny et al., 2017). Consequently, as the EP level is greatly dependent on the nature of the detergent, one should consider the variations of the EP level for estimating the stability of the Drs2p/Cdc50p complex, once the maximum has been reached. As seen in Figure 4, it appears that at  $4^\circ\text{C}$ , irrespective of the presence of PI4P, LMNG supplemented with PS confers the highest stability to the Drs2p/Cdc50p complex.

**CAUTION:** When working with radioactivity, take appropriate precautions to avoid contamination of the experimenter and the surroundings. Carry out the experiment and dispose of wastes in appropriately designated areas, following guidelines provided by your local radiation safety officer.

### Materials

Buffer C (see recipe)

0.2-0.3 mg/ml purified Drs2p/Cdc50p obtained as in Azouaoui et al. (2014) and stored in buffer C supplemented with 0.5 mg/ml DDM and 0.025 mg/ml POPS

Detergent stock solutions and detergent/lipid stock mixtures (see recipes):

50 mg/ml DDM or  $\text{C}_{12}\text{E}_8$

25 mg/ml LMNG

DDM/POPS or  $\text{C}_{12}\text{E}_8/\text{POPS}$  at 50 and 10 mg/ml, respectively

LMNG/POPS at 25 and 10 mg/ml, respectively

DDM/PI4P or  $\text{C}_{12}\text{E}_8/\text{PI4P}$  at 50 and 5 mg/ml, respectively

LMNG/PI4P at 25 and 5 mg/ml, respectively

20  $\mu\text{M}$   $[\gamma\text{-}^{32}\text{P}]\text{ATP}$  (0.25-1 mCi/ $\mu\text{mol}$  ATP)

Quenching solution (see recipe)  
Rinsing solution: 0.1 × quenching solution

4-ml polycarbonate test tubes  
Cellulose GS filters (0.22- $\mu\text{m}$  porosity, Millipore), presoaked in quenching solution  
Scintillation vials (Perkin Elmer)  
Filter-count scintillation solution (Packard Biosciences, 6013149)  
Liquid scintillation counter (Beckman Coulter LS-5801)

1. Dilute purified Drs2p/Cdc50p complex to 11  $\mu\text{g}/\text{ml}$  in buffer C supplemented with 1 mg/ml detergent, POPS at 50  $\mu\text{g}/\text{ml}$ , and if necessary PI4P at 25  $\mu\text{g}/\text{ml}$  by combining the different detergents or detergent/lipid mixtures available. Adjust the sample volume to the number of measurements to be made and the amount of protein required for each measurement.

*Typically, the experiment presented in Figure 4 requires 30  $\mu\text{l}$  of 11  $\mu\text{g}/\text{ml}$  Drs2p/Cdc50p complex per measurement and five measurements are made for each series over nine days (i.e., 150  $\mu\text{l}$  enzyme for each series). For long-term incubation at 4°C, samples are stored in the refrigerator.*

2. As soon as the protein sample is diluted into the detergent/lipid-containing buffer, withdraw 27  $\mu\text{l}$  for measurement at  $t_0$  and store on ice.
3. Initiate phosphorylation by adding 3  $\mu\text{l}$  of 20  $\mu\text{M}$  [ $\gamma$ - $^{32}\text{P}$ ]ATP (final 2  $\mu\text{M}$ ). Mix thoroughly and immediately transfer to 30°C.
4. Incubate 1.5 min, then immediately withdraw 10  $\mu\text{l}$  and transfer it to a 4-ml test tube containing 1 ml quenching solution, on ice, to stop the phosphorylation reaction ( $t_0$ , sample 1, tube 1).
5. Withdraw another 10  $\mu\text{L}$  from the same sample (~15-30 sec after the previous aliquot) and place it in a second 4-ml test tube containing 1 ml quenching solution on ice ( $t_0$ , sample 1, tube 2). Once samples have been acid quenched, keep them on ice for at least 30 min (a period sufficient for aggregation of the precipitated protein and therefore retention by the filter).

*This second point may correspond to a duplicate. It aims at verifying that the maximum EP level was already reached after the first 1.5 min of phosphorylation. The EP level may be the same for tubes 1 and 2, resulting in the obtaining of a duplicate.*

6. Filter the precipitated samples on GS filters that have been pre-soaked in quenching solution for several minutes.
7. Carefully rinse the tubes with 4 ml rinsing buffer and apply it to the same filters. Repeat for a total of three rinses.
8. Place each filter in a scintillation vial and add 4 ml Filter-count solution. Shake vials until the filter is completely dissolved.
9. Measure radioactivity by scintillation counting.
10. Repeat steps 4-9 at the appropriate times to complete the time course (e.g., Fig. 4).
11. Convert counts per min (cpm) to moles of phosphoenzyme (EP) formed. For conversion, measure the radioactivity of several dilutions of 20  $\mu\text{M}$  [ $\gamma$ - $^{32}\text{P}$ ]ATP stock solution to make a standard curve.

## REAGENTS AND SOLUTIONS

All reagents and chemicals should be of analytical grade. Milli-Q water or other ultrapure type I water should be used to prepare buffers and solutions.

For convenience, some of buffer components can be prepared as concentrated stock solutions (e.g., 500 mM MOPS-Tris, pH 7; 500 mM TES-Tris, pH 7.5; 3 M KCl; 2 M MgCl<sub>2</sub>; 1 M CaCl<sub>2</sub>). Solutions should be filtered through a 0.22- $\mu$ m porosity filter and stored up to several months at 4°C.

### **[ $\gamma$ -<sup>32</sup>P]ATP, 20 $\mu$ M**

Mix radiolabeled [ $\gamma$ -<sup>32</sup>P]ATP (250  $\mu$ Ci, 10 mCi/ml, 3000 Ci/mmol; Perkin Elmer, cat. no. BLU002A) with nonradioactive ATP to reach a specific radioactivity of 0.25–1 mCi/ $\mu$ mol. Typically, 1 ml of 20  $\mu$ M nonradioactive Mg-ATP solution (20 nmol Mg-ATP) is supplemented with 2  $\mu$ l freshly synthesized [ $\gamma$ -<sup>32</sup>P]ATP (20  $\mu$ Ci) to obtain a radioactive Mg- $[\gamma$ -<sup>32</sup>P]ATP working solution at 20  $\mu$ M with a specific activity of 1 mCi/ $\mu$ mol.

The half-life of <sup>32</sup>P is 14.3 days. Thus, [ $\gamma$ -<sup>32</sup>P]ATP should be used ideally within ~4 weeks (about two periods) following shipment from the supplier. Otherwise, the volume of the supplier's solution should be adjusted to achieve the required final specific radioactivity of 0.25–1 mCi/ $\mu$ mol.

**CAUTION:** High-energy  $\beta$  emissions from <sup>32</sup>P can present a substantial skin and eye dose hazard. Always use appropriate self-protection equipment (gloves, glasses, lab coat). Stock solutions received from the provider must be manipulated under a chemical hood to avoid inhalation. Use a 1-cm thickness Plexiglas screen for proper protect from irradiation. Diluted solutions prepared from the provider's stock solution can be manipulated out from the hood but they should be transported in a 1-cm thickness Plexiglas chamber or pot. Manipulate in a restricted and clearly identified area behind a Plexiglas screen. Use a dedicated and clearly identified bin for waste. As regulation may change from one country to the other, contact the laboratory or institutional Health and Safety Manager for local rules on the use of radiolabeled molecules before planning experiments. For a Safe Handling Guide, please refer also to [https://www.perkinelmer.com/lab-solutions/resources/docs/TCH\\_Phosphorus32.pdf](https://www.perkinelmer.com/lab-solutions/resources/docs/TCH_Phosphorus32.pdf).

### **ATPase assay medium**

Buffer B (see recipe) supplemented with:

5 mM Mg-ATP (from 200 mM stock; see recipe)

40  $\mu$ g/ml pyruvate kinase (buffered aqueous glycerol solution from rabbit muscle, ~3.8 mg/ml; Sigma, cat. no. P7768)

100  $\mu$ g/ml lactate dehydrogenase (buffered aqueous glycerol solution from bovine heart, ~9.4 mg/ml; Sigma, L1006)

1 mM phosphoenolpyruvate (from 50 mM phospho(enol)pyruvic acid cyclohexylammonium salt; Sigma, cat. no. P3637)

2 mg/ml C<sub>12</sub>E<sub>8</sub> (from 200 mg/ml stock; see recipe for detergent stock solutions)

Prepare fresh (store up to 1 day at room temperature)

Mg-ATP, phosphoenolpyruvate, and C<sub>12</sub>E<sub>8</sub> stock solutions prepared from powders can be stored up to several years at –20°C. Pyruvate kinase and lactate dehydrogenase stock solutions can also be stored up to several years at –20°C as indicated by the provider.

### **Buffer A**

50 mM MOPS (3-(*N*-morpholino)propanesulfonic acid; Sigma, cat. no. M1254)

50 mM KCl (Sigma, cat. no. P9541)

5 mM MgCl<sub>2</sub> (hexahydrate; Merck, 118A568633)

Adjust to pH 7 at 20°C with saturated Tris (Trizma base; Sigma, cat. no. T1503)

Store up to several months at 4°C

### **Buffer B**

50 mM TES (2-[(2-hydroxy-1,1-bis(hydroxymethyl)ethyl)amino]ethanesulfonic acid; Sigma, cat. no. T1375)  
100 mM KCl (Sigma, P9541)  
1 mM MgCl<sub>2</sub> (hexahydrate; Merck, 118A568633)  
50 μM CaCl<sub>2</sub> (Carl Roth, CN93.1)  
Adjust to pH 7.5 at 20°C with saturated Tris (Trizma base; Sigma, T1503)  
Store up to several months at 4°C

### **Buffer C**

Buffer A (see recipe) with 20% (v/v) glycerol (Merck, cat. no. 1.04092.1000)  
Store up to several months at 4°C

### **Detergent stock solutions**

n-Dodecyl-β-D-maltopyranoside (DDM; Anatrace, cat. no. D310)  
Octa(ethylene glycol) dodecyl monoether (C<sub>12</sub>E<sub>8</sub>; Nikkol, BL-8SY)  
n-Octyl-β-D-glucoside (OG; Anatrace, O311)  
Soy lysophosphatidylcholine (LPC; Avanti Polar Lipids, 840072)  
Lauryl maltose neopentyl glycol (LMNG; Anatrace, NG310)

*Preparation of detergent stock solutions:* Dissolve detergent powder at the desired concentration in Milli-Q water or other ultrapure type I water. Store up to several days at 4°C or up to several years at –20°C. Add detergent to buffers immediately before use.

*Storage and handling of detergent powders:* Store up to several years at –20°C under an argon or nitrogen atmosphere. To avoid condensation, remove the flacon from the freezer and warm at room temperature for ~10 min before opening. After taking the required amount of powder, fill the flacon with dry nitrogen or argon before closing and returning to the freezer.

*Condensation may cause oxidation or partial hydrolysis of detergent. A desiccator can be used, if available.*

**CAUTION:** *Detergent powders may be dangerous when inhaled and may be harmful upon contact with skin or eyes. Wear appropriate personal protective equipment and clothing, including lab coat, safety glasses, gloves, and mask when manipulating powders. Collect residual powders in a manner that does not create dust, and place in a suitable waste container. Use adequate ventilation or work under a chemical fume hood.*

### **Detergent/lipid stock mixtures**

POPS (1-palmitoyl-2-oleoyl-sn-glycero-3-phospho-l-serine; Avanti Polar Lipids, cat. no. 840034P)  
PI4P (1-α-phosphatidylinositol-4-phosphate extract from porcine brain; Avanti Polar Lipids, 840045P)

*Preparation of detergent/lipid mixtures:* Dissolve 20 mg POPS in 4 ml of 100 mg/ml detergent stock solution (see recipe) to achieve a final detergent/POPS mixture at 100 and 5 mg/ml, respectively. Mix vigorously. Store up to several days at 4°C or several years at –20°C. Pay attention to thawing when removing a stock solution from the freezer, as phase transition can occur with temperature changes. Mix vigorously after reaching room temperature to obtain a clear solution.

*The final solution should be visually clear at 20°C. Note that the detergent/lipid ratio in the final mixture may depend on the solubilities of the detergent and lipid. If the final mixture is not limpid, the detergent/lipid ratio must be increased until complete clarification.*

For DDM/POPS, a 5:1 (w/w) ratio is a maximum. However, it is obviously possible to prepare stock solutions with a lower detergent/lipid ratio, depending on the need of the experiment.

Lipids should be added to buffers just before use.

**Storage and handling of lipid powders:** Store up to several years at  $-20^{\circ}\text{C}$  under an argon or nitrogen atmosphere. To avoid condensation, remove the flacon from the freezer and warm at room temperature for  $\sim 10$  min before opening. After taking the required amount of powder, fill the flacon with dry nitrogen or argon before closing and returning to the freezer.

Condensation may cause oxidation or partial hydrolysis of detergent. A desiccator can be used, if available.

### **EGTA, 0.5 M**

Dissolve 1.9 g ethylene glycol-bis(2-aminoethylether)-*N,N,N',N'*-tetraacetic acid (EGTA, Sigma, cat. no. E0396) in Milli-Q water and adjust pH to 7 with NaOH. Adjust volume to 10 ml. Store up to several years at  $4^{\circ}\text{C}$ .

### **Methyl orange, 2 mM**

Dissolve 13 mg methyl orange (Carl Roth, cat. no. T118.1) in 20 ml Milli-Q water or other ultrapure type I water. Store up to several years at  $4^{\circ}\text{C}$ .

### **Mg-ATP stock solution, 200 mM**

Prepare a 220 mM solution of  $\text{Na}_2\text{-ATP}$  (Sigma, cat. no. A2383) in Milli-Q water or other ultrapure type I water. Adjust to pH 7.5 with NaOH. Mix 9 volumes with 1 volume of 2 M  $\text{MgCl}_2$  hexahydrate (Merck, cat. no. 118A568633). Store up to several years at  $-20^{\circ}\text{C}$ .

The molar extinction coefficient of Mg-ATP at 260 nm is 15.4 mM/cm.

### **NADH, 15 mM**

Dissolve NADH powder ( $\beta$ -nicotinamide adenine dinucleotide, reduced disodium salt hydrate; Roche Diagnostic, cat. no. 621676) in Milli-Q water or other ultrapure type I water. Prepare fresh.

### **Quenching solution**

500 mM trichloroacetic acid (Sigma, cat. no. T6399)  
30 mM  $\text{H}_3\text{PO}_4$  (phosphoric acid solution at  $\sim 8.7$  M; Sigma, W290017)  
Store in a dry place at  $4^{\circ}\text{C}$  (stable for weeks)

TCA crystals are highly hygroscopic and should be stored in a closed container, if possible, in a dry place to limit absorption of water.

CAUTION: TCA powders and highly concentrated stock solutions are corrosive. Use appropriate equipment (nitrile gloves, glasses, lab coat) when handling. Dissolving TCA powder is an exothermic reaction. Use an appropriate container to prepare it.

## **COMMENTARY**

### **Background Information**

Integral MPs are by nature embedded in cell membranes, but most of the functional or structural approaches require isolating the MP from its native environment. Although detergents are essential tools for biochemists to isolate and study MPs, extracting MPs from their surrounding lipids, which usually stabilize the hydrophobic core of these proteins, re-

mains a difficult task. Exposure of hydrophobic regions to aqueous solvent and/or removal of essential lipids may indeed lead to irreversible inactivation or aggregation of the protein (Hunte & Richers, 2008). Thus, while the ultimate goal probably consists in understanding the mechanism of the protein of interest, acquiring knowledge about the behavior of the protein in detergent and developing tools to

study protein-detergent interactions is another key aspect of MP biochemistry.

#### ***Use of other probes for CMC determination***

As mentioned above, detergent behavior in aqueous solvent, in absence of lipids or proteins, can be summed up to two main features: the CMC and the aggregation number,  $N_A$ . As mentioned in Basic Protocol 1, these two features are generally influenced by the physical and chemical parameters of the solvent. Consequently, methods have been developed to check the possible effect of experimental conditions on detergents to anticipate their behavior during isolation and purification of MPs. Some of these methods are briefly discussed in the Basic Protocol 1 introduction. In Orwick-Rydmark et al. (2016), a method to determine detergent CMMC using pyrene fluorescence is described. Pyrene fluorescence is highly sensitive to the environment, especially when it partitions in hydrophobic phases, and has been widely used to study micellar systems (Kalyanasundaram & Thomas, 1977). The main advantage of this technique is its high sensitivity, as the quantum yield of pyrene is very high in the presence of hydrophobic phases. Nonetheless, pyrene needs to be used with caution. First, pyrene belongs to the polycyclic aromatic hydrocarbon family, so it is potentially toxic. It requires the use of appropriate protective equipment to avoid inhalation and contact with skin or eyes, and also the use of a suitable waste container. Second, its solubility in aqueous buffer is very low and it may form aggregates known as excimers when used in buffers suitable for biochemical studies. Excimers have particular fluorescence properties (Mataga, Okada, & Yamamoto, 1967) and their presence may mask micelle formation and consequently result in mis-estimation of the CMMC. Depending on the nature of the detergent, pyrene may also interact with detergent monomers before micelle formation, also contributing to mis-estimation of the CMMC (Mukerjee & Mysels, 1955). The use of pyrene at very low concentration (1-3  $\mu\text{M}$ ) together with repeating CMMC determination at different probe concentrations may help prevent these problems (Kalyanasundaram & Thomas, 1977). Note that several other fluorescent probes have been used to study hydrophobic environments and micelle formation. 1-Anilino-8-naphthalene (ANS) is one of those common probes and has the advantage of being markedly less toxic than pyrene (Slavík, 1982). However, ANS is a charged molecule, so its use is limited to nonionic detergents.

The present article presents a procedure using the properties of methyl orange (see Basic Protocol 1). The advantages of methyl orange are that it is non-toxic and its measurement requires only a spectrophotometer, as interaction with micelles leads to spectral changes in the visible wavelength range. Nevertheless, methyl orange also has some drawbacks. It is sensitive to pH changes, and consequently should be used in a buffered medium. Furthermore, fluorescent probes are generally more sensitive than methyl orange and consequently more appropriate for detergents with very low CMC.

In summary, the most reasonable way to determine CMMC of a detergent is probably to measure it using two or three different methods to avoid bias due to the probe. Additionally, one should be aware that neither the CMMC nor the CMC are exact values. Depending on the method used for their estimation, micelles can be detected at a very early stage in their formation, i.e., when just a few detergent monomers start to interact with each other. Therefore, the values determined by these methods provide ranges rather than exact values. One solution to overcome this issue could be to continuously inject the detergent in the medium used for measurement instead of adding a fixed amount of detergent as shown in Figure 1. If the method is highly sensitive, it may be possible to reveal the formation of the earliest aggregates. However, in the particular context of purification and stabilization of membrane proteins, one is not interested in exact CMMC values, but rather a verification that no sudden and substantial changes in CMMC will occur during the study of the protein (Table 1), as such changes are likely to lead to irreversible inactivation of the protein.

#### ***Interaction of detergents with membrane proteins during extraction and purification***

The nature of the detergent is critical for MP stability. However, its concentration is also critical, as a large excess may trigger removal of essential lipids or cofactors and, in some cases, induce membrane complex dissociation or denaturation (Hunte & Richers, 2008; le Maire et al., 2000; Lee, 2011). Methods described as Basic Protocol 2 and the Alternate Protocol may help to determine the nature of the best detergent to be used for long-term stabilization. Afterwards, the next experiment may consist of testing several concentrations of the selected detergent to determine the best conditions for stabilization. The

detergent/protein ratio and detergent/lipid ratio are critical. During the solubilization step that precedes purification of a membrane protein, it may be important to optimize these ratios. As colloidal systems, membranes in solution produce light scattering. This light scattering is observable on a simple spectrophotometer. The sample may become transparent following detergent addition. One useful technique is to monitor light scattering during continuous addition of detergent into the sample-containing cuvette to obtain solubilization curves. The obtained curves may reveal at least two important pieces of information: the saturation point and the solubilization point (Lichtenberg, Ahyayauch, Alonso, & Goñi, 2013; Paternostre, Roux, & Rigaud, 1988). The saturation point corresponds to the maximum amount of detergent that can be incorporated in the membrane before solubilization. The solubilization point corresponds to the minimum amount of detergent necessary to complete clarification of the sample. Parallel aliquots can be taken to detect the protein of interest (for instance, by western blotting) to define the minimum amount of detergent necessary to extract the protein from the membrane (i.e., after ultracentrifugation, the solubilized protein should be recovered in the supernatant). Interestingly, it is sometimes not necessary to attain complete solubilization of the membrane to release the protein of interest into the solubilized phase. As native membranes are heterogeneous media (e.g., nature of the lipids, micro-domains) and MPs behave differently in the presence of different detergents, some MPs can be extracted at a detergent concentration in the range of the concentrations necessary to attain saturation and solubilization of the membrane, i.e., before reaching complete clarification of the sample (Kragh-Hansen, le Maire, & Møller, 1998; Lichtenberg et al., 2013). As lipids can be essential for MP stabilization and activity (Hunte & Richers, 2008), complete solubilization of the membrane is not necessarily desirable, as it can be important to avoid removal of critical lipids from the protein. The total detergent concentration in the sample  $[\text{det}]_{\text{total}}$  (in moles) can be defined as followed:

$$[\text{det}]_{\text{total}} = [\text{det}]_{\text{free}} + [\text{det}]_{\text{bound}}$$

where  $[\text{det}]_{\text{bound}}$  corresponds to the detergent present in the membrane phase and  $[\text{det}]_{\text{free}}$  corresponds to the detergent that remains in the aqueous phase.  $[\text{det}]_{\text{free}}$  is a constant, as it corresponds to the monomeric detergent. In fact, as soon as micelles form, lipids will

partition into these micelles to form detergent-lipid mixed micelles. The amount of micelle is negligible until saturation of the membrane, as a detergent “prefers” to partition into the lipid phase instead of interacting with itself, i.e., the hydrophobic environment is more favorable than the aqueous phase. Consequently,  $[\text{det}]_{\text{free}}$  is approximately equal to the CMMC and  $[\text{det}]_{\text{total}}$  can be expressed as:

$$[\text{det}]_{\text{total}} = \text{CMMC} + ([\text{det}]_{\text{bound}}/[\text{lip}]_{\text{total}}) \times [\text{lip}]_{\text{total}}$$

where  $[\text{lip}]_{\text{total}}$  corresponds to the total amount of lipid in the sample. Consequently, this equation now corresponds to a linear dependence of  $[\text{det}]_{\text{total}}$  on  $[\text{lip}]_{\text{total}}$ , where the CMMC corresponds to the intercept at  $[\text{lip}] = 0$  and the ratio  $R = [\text{det}]_{\text{bound}}/[\text{lip}]_{\text{total}}$  corresponds to the slope. Interestingly, saturation and solubilization points may be generally anticipated. Empirically, and primarily for aliphatic detergents, the value of  $R$  at saturation ( $R_{\text{sat}}$ ) is close to 1 mole of detergent per mole of lipids, and the value at solubilization ( $R_{\text{sol}}$ ) is close to 3 moles of detergent per mole of lipids (Kragh-Hansen et al., 1998). Note that a rough estimate of the concentration of detergent to use for an initial solubilization trial can be obtained by considering the detergent/protein mass ratio instead of detergent/lipid molar ratio. As lipids and detergents have molecular weights in the same order of magnitude, and considering that the lipid/protein ratio in biological membranes is generally in the range of 0.5 to 2 (g/g), a starting attempt at a 3:1 detergent/protein weight ratio (g/g) corresponds to about a 3:1 to 10:1 detergent/lipid molar ratio, i.e., a ratio close or even above the empirical value of 3 for  $R_{\text{sol}}$ . This rough estimate is certainly useful for low-CMMC detergents, i.e., when the CMMC is negligible in comparison to the total amount of detergent used. For high-CMMC detergents, i.e., detergents for which the CMMC is not negligible in comparison to the total amount of detergent used, biochemists have to consider the second equation above. From this equation, the CMMC of a detergent can be determined by repeating the experiment with different concentrations of membranes (for a detailed procedure and more theoretical concept, see le Maire et al., 2000; Lichtenberg et al., 2013).

In these equations, it should be kept in mind that the concentration of proteins and detergents can vary greatly during purification

processes. Stabilization of an MP requires maintaining a sufficient amount of detergent around its hydrophobic core to prevent aggregation. When the MP is purified through a column, the  $[\text{det}]_{\text{total}}$  should remain constant, especially during the washing and elution steps. Accidental dilution of the detergent below its CMMC often results in aggregation of the MP, as it is no longer solubilized. Similarly, concentration of purified proteins by ultrafiltration can be fraught with potential problems for solubilized MPs. First, filter units must be carefully rinsed with a detergent-containing buffer before use in order to limit nonspecific binding of the detergent (and especially of the protein) to the filter. The choice of the molecular weight cut-off should take into account the size of the detergent/protein complex and the size of the detergent micelles. As the detergent/protein complex is concentrated on the top of the filter unit, detergent micelles have to pass through the filter pore to limit the concentration of the detergent and to prevent exposure of the MP to high detergent concentrations that may eventually induce inactivation, dissociation, or denaturation of the protein. Additionally, inactivation of MPs by detergents can result from loss of essential partners such as cofactors, lipids, or proteins that may be dispersed in the micellar phase. Working as close as possible to the CMMC of the detergent can limit this effect.

It should also be stressed that an appropriate detergent for solubilization is not necessarily the best detergent for long-term stabilization. Some detergents can be incompatible with some functional assays or with some structural biology approaches. Crystallography of an MP may occur in the presence of a given detergent but not in the presence of another with similar properties. For instance, recombinant SERCA1a was crystallized in the presence of  $\text{C}_{12}\text{E}_8$ , but initial solubilization and purification from yeast membranes were performed in the presence of DDM, because poor solubilization was observed with  $\text{C}_{12}\text{E}_8$  (Clausen et al., 2013; Jidenko et al., 2005; Lenoir et al., 2002; Marchand et al., 2008). In this case, the DDM-to- $\text{C}_{12}\text{E}_8$  exchange was done by size-exclusion chromatography (for SEC analysis of MPs, see Korepanova & Matayoshi, 2012; le Maire et al., 2008) and was mandatory to obtain crystals (Sørensen, Olesen, Jensen, Møller, & Nissen, 2006). Moreover, detergent-to-detergent (or lipid-to-detergent) exchange is not an instantaneous phenomenon. Equilibrium between monomers and micelles requires

a few seconds to be achieved when adding detergent from a concentrated stock solution to the cuvette, and the lipid-to-detergent exchange around a protein may be very slow depending on the nature of the molecules and the parameters of the experiment (e.g., temperature, viscosity, relative affinity of the protein for the molecule of concern; see Carney et al., 2006, and Montigny et al., 2017, for methods to follow detergent/protein or lipid/protein interactions). For instance, a lipid-to-detergent exchange that occurs within a minute at  $30^\circ\text{C}$  could need  $>10$  min at  $4^\circ\text{C}$ , the latter being a temperature usually used in purification procedures. Consequently, addition of detergent or detergent/lipid mixtures to investigate their potential stabilizing effect on an MP must be monitored at various incubation time points, with the aim of reaching an equilibrium state between protein, detergent, and lipids. Additionally, it has been demonstrated that the rate of addition of a detergent to the membranes can have an impact on the rate of solubilization; addition that is too rapid may lead to an overestimation of  $R_{\text{sat}}$  and  $R_{\text{sol}}$  (Paternostre et al., 1988) and consequently an overestimation of the amount of detergent necessary to extract a particular protein from its membrane.

#### ***Methods for assessing the effect of detergent on the overall structure of membrane proteins***

The present article focuses on functional assays to assess the stability of an MP in the presence of detergents. However, several protocols are also available to easily and quickly detect the deleterious effect of detergent on the overall structure of an MP. Interestingly, some MPs have associated chromophores whose absorption spectra depend on their environment, thereby reflecting overall protein structure (e.g., bacteriorhodopsin, rhodopsin, or light-harvesting complexes). Detergent destabilization of such MPs leads to significant changes in their absorption spectra in the UV/visible range. Therefore, the stability of such proteins can be easily monitored by spectrophotometry (Arluison, Seguin, & Robert, 2002; Breyton, Chabaud, Chaudier, Pucci, & Popot, 2004; Meyer, Ollivon, & Paternostre, 1992). However, a few MPs have chromophores. Alternatively, SEC is a powerful technique to study the structural integrity or possible aggregation of a solubilized MP (le Maire et al., 2000; see also Korepanova & Matayoshi, 2012). This allows monitoring of monodispersity (i.e., the homogeneity of the protein)



and also subunit association in the case of MP complexes, as subunit interactions can be perturbed or abolished by detergents (Boulter & Wang, 2001). Moreover, if an expressed MP is fused to a GFP or another analog fluorescent protein, Fluorescence-SEC (F-SEC) can allow a quick upstream analysis of unpurified proteins and may give information about the behavior of the GFP-fused MP in crude solubilized membranes, i.e., before any purification (Kawate & Gouaux, 2006). Along those lines, F-SEC can be used to monitor a protein after each step of a purification procedure (Drew et al., 2008; Ellinger, Kluth, Stindt, Smits, & Schmitt, 2013). It should be kept in mind, however, that monodispersity of a protein in the presence of detergent is sometimes not an indicator of proper function. For instance, detergents may compete for inter- or intramolecular interactions with partners or within the protein, respectively (Cross, Sharma, Yi, & Zhou, 2011). The detergent may sometimes stabilize misfolded conformations that are not functional as shown for the NMR structure of the uncoupling protein (UCP2) in dodecylphosphocholine (DPC; Berardi, Shih, Harrison, & Chou, 2011). By combining biochemistry and molecular dynamics, it was demonstrated that DPC severely alters the structure as well as the function of UCP2, even though a high-resolution structure was obtained (Zoonens et al., 2013). DPC probably induced misfolding of UCP2 by intercalating between the transmembrane helices. This last point highlights the importance of the choice of a proper detergent for MP handling. To limit this mechanism of inactivation and improve the stability of MPs, new detergents derived from DDM and including a more rigid hydrophobic tails have been developed (Chae et al., 2010; Hong et al., 2010; Hovers et al., 2011).

### Critical Parameters

The availability of an MP is often the main limiting parameter for its functional and/or structural characterization. Membrane proteins are usually expressed at low levels in the cell. Even though heterologous expression can be used to increase the yield of expression, obtaining pure, active, and stable MPs still remains a major bottleneck for biochemists (Andréll & Tate, 2013; Montigny et al., 2014). Experiments presented here can be carried out with small amounts of protein. The ATPase assays can be miniaturized by adapting the enzyme-coupled assay to 96-well microplates (Zhou & Bowie, 2000). Moreover,

as detergents could trigger MP aggregation, a simple ultracentrifugation after a period of incubation in the presence of the detergent, followed by western blotting of the supernatant, will also yield information on the stability of the protein, even though it does not provide information regarding its function (Ellinger et al., 2013).

A word should also be said about the detergent used in the assay medium. In the present protocol, C<sub>12</sub>E<sub>8</sub> is appropriate to maintain long-term activity of SERCA1a (Lund et al., 1989). However, when working with a new MP sample, without any idea of the ability of a given detergent to stabilize the protein, C<sub>12</sub>E<sub>8</sub> could be replaced by the detergent used during the pre-incubation period. However, it is essential to verify that this detergent does not interfere with the enzyme-coupled assay. As mentioned above, 1 mole of NADH is converted to NAD<sup>+</sup> when 1 mole of ATP is regenerated. Consequently, addition of ADP should result in a decrease of absorbance corresponding to the amount of ATP synthesized from the ADP. Additionally, if signals are integrated on a second timescale, the kinetics of ATP regeneration (NADH consumption) should also be controlled. In normal conditions, addition of 10 μM ADP should result in a drop in absorbance of 0.062 in about 6 to 10 sec at 20°C.

### Troubleshooting

Basic Protocol 1 describes approaches to correct the dilution effect that may be observed during CMC determination using methyl orange or any other colorimetric assay (Fig. 1A; Ohnishi, 1978). The isobestic point is an indication that the probe is only interacting with one component: the detergent, in the present case. If ternary complexes form with another compound present in the medium, this isobestic point will no longer exist. For example, as glycerol affects the absorption spectra of methyl orange (Fig. 1A), other compounds in the assay medium may obviously also affect it. Ionic strength also affects methyl orange spectra, but does not interfere with the CMMC estimate. The presence of other hydrophobic macromolecules in the medium could obviously interfere with the assay. Methyl orange may partition in hydrophobic phases like lipid phases. It may also interact with hydrophobic patches on proteins or other macromolecules containing such patches. For example, interactions with human serum albumin have been reported (Ito & Yamamoto, 2015). To our knowledge, methyl orange alone does not interact with DNA; however, when used in

combination with other dyes like crystal violet or indole blue, the resulting complexes are able to interact with DNA (Hwang, Jin, Yoo, & Choi, 2006; Yang, Jung, Bai, Yoo, & Choi, 2001). In such delicate conditions, another method for CMC determination should be considered.

The methyl orange method can be used for a wide range of CMCs. When a detergent has a high CMC, the volume of detergent added starts to be pretty high compared to the volume of the cuvette. In that case, the dilution of methyl orange with each detergent addition, before micelle formation, is not negligible and the experimenter should take into account the dilution factor even when using the Ohnishi method. For a low-CMC detergent, the limit depends particularly on the spectrophotometer. Some diode array spectrophotometers allow accurate measurement of absorbance changes in the  $10^{-3}$  range, making it possible to determine CMMCs of detergents close to 0.08-0.09 mM (e.g., for  $C_{12}E_8$ ). For detergents with lower CMC (e.g., LMNG, CMC < 0.01 mM), this method is not sensitive enough.

Achieving equilibrium between monomers and micelles requires a few seconds. Consequently, it is critical to wait for a few seconds after adding detergent to the cuvette. Continuous stirring and temperature regulation of the medium using a temperature-controlled cell holder is mandatory.

Basic Protocol 2 allows one to follow the ATPase activity of solubilized membrane ATPases. It should be kept in mind that protein aggregation may occur because the detergent is present at a fairly high concentration in the cuvette. Protein aggregates generate light scattering. Thus, it is important to follow simultaneously the absorbance at 340 nm (to observe NADH consumption) and the absorbance at 500-600 nm (to look at possible variations in light scattering). NADH does not absorb at such wavelengths.

The Alternate Protocol takes advantage of a specific feature of P-type ATPases, namely formation of a stable phosphoenzyme (EP). In the present experiment, the signal-to-noise ratio is good, with raw data gathered from 60 to 1400 cpm for samples and 20 to 25 cpm for background. If the background is high, check that the filters were rinsed properly. If available, a specific inhibitor of the protein can be used to evaluate the background.

Although the present experiment used GS nitrocellulose filters, other filters are avail-

able and may be compared for their tendency to nonspecifically bind compounds in the medium that could increase background. For instance, glass fiber filters (type A/E, porosity 1  $\mu$ m) represent an alternative to GS filters. For phosphorylation measurements, the question arises as to whether the acid-denatured detergent-solubilized Drs2p would be retained efficiently by the filters, in view of the presence of detergents. In this respect, incubation of the acid-quenched proteins on ice for a period sufficient for aggregation is a critical step, as efficient and reproducible aggregation is a prerequisite for further retention by filters. In our case, samples had to be incubated on ice for at least half an hour for aggregation and therefore retention by filters. Additionally, for several detergents, when two filters were used on top of each other, the bottom filter contained about 10-20% of the total radioactivity, with the main part being recovered on the top filter. Therefore, it may be necessary in some cases to use two filters for maximal recovery of precipitated proteins.

### Anticipated Results

The experiments described in this article will help the experimenter to identify an appropriate detergent for long-term stabilization of a particular integral membrane protein. From Basic Protocol 1, the experimenter will obtain the CMMC of a detergent in specific experimental conditions. High variation in the value of the CMMC will suggest that the detergent concentration needs to be adapted during the different steps of the experiment in order to maintain the protein in an appropriate environment. Typically, the experimenter must take into account the CMMC values to define the protocol for detergent screening. The screening methods described in Basic Protocol 2 and the Alternate Protocol should result in the selection of the best detergent to ensure long-term stability of an active and functional membrane protein. The experimental conditions arising from this screen hopefully will be important for subsequent purification, functional characterization, and crystallogenesis. The latter usually requires a careful estimation and adjustment of the amount of detergent around the protein to favor crystal contact (Dahout-Gonzalez, Brandolin, & Pebay-Peyroula, 2003; Parker & Newstead, 2016; Sørensen et al., 2006).

### Time Considerations

Preparing detergent solutions and detergent/lipid mixtures can take a few hours. The

determination of the CMMC for one detergent by the methyl orange method takes about 1 hr to be performed twice. From the moment the solutions are prepared, measuring an ATPase activity takes about 5 to 15 min depending on the activity (for low activity, it will be necessary to wait longer in order to distinguish the activity of the protein of interest from that of the background). For instance, the experiment shown in Figure 3 takes 1.5 days. Similarly, the time required for phosphorylation assays depends on the number of samples. For the experiment shown in Figure 4, each series of samples (8 tubes per series) takes about 2 hr from phosphorylation to first counting results.

### Acknowledgments

This work was supported by the Centre National de la Recherche Scientifique (CNRS), by ANR grant ANR-14-CE09-0022 to GL (AsymLip), and by the French Infrastructure for Integrated Structural Biology (FRISBI; ANR-10-INSB-05). We are grateful to Marc le Maire for critical reading of this manuscript and pertinent suggestions. CM would like to address his heartfelt thanks to Philippe Champeil for his teachings and for all the insightful discussions of the past sixteen years.

### Conflicts of Interest

The authors declare that they have no conflicts of interest with the contents of this article.

### Literature Cited

- Andréll, J., & Tate, C. G. (2013). Overexpression of membrane proteins in mammalian cells for structural studies. *Molecular Membrane Biology*, *30*, 52–63. doi: 10.1099/09687688.2012.703703.
- Aramaki, K., Olsson, U., Yamaguchi, Y., & Kunieda, H. (1999). Effect of water-soluble alcohols on surfactant aggregation in the C12CO8 system. *Langmuir*, *15*, 6226–6232. doi: 10.1021/la9900573.
- Arluison, V., Seguin, J., & Robert, B. (2002). The reaction order of the dissociation reaction of the B820 subunit of *Rhodospirillum rubrum* light-harvesting I complex. *FEBS Letters*, *516*, 40–42. doi: 10.1016/S0014-5793(02)02469-9.
- Azouaoui, H., Montigny, C., Ash, M.-R., Fijalkowski, F., Jacquot, A., Grönberg, C., ... Lenoir, G. (2014). A high-yield co-expression system for the purification of an intact Drs2p-Cdc50p lipid flippase complex, critically dependent on and stabilized by phosphatidylinositol-4-phosphate. *PLoS One*, *9*, e112176. doi: 10.1371/journal.pone.0112176.
- Azouaoui, H., Montigny, C., Dieudonné, T., Champeil, P., Jacquot, A., Vázquez-Ibar, J. L., ... Lenoir, G. (2017). A high and phosphatidylinositol-4-phosphate (PI4P)-dependent ATPase activity for the Drs2p/Cdc50p flippase after removal of its N- and C-terminal extensions. *Journal of Biological Chemistry*, *292*, 7954–7970. doi: 10.1074/jbc.M116.751487.
- Azouaoui, H., Montigny, C., Jacquot, A., Barry, R., Champeil, P., & Lenoir, G. (2016). Coordinated overexpression in yeast of a P4-ATPase and its associated Cdc50 subunit: The case of the Drs2p/Cdc50p lipid flippase complex. *Methods in Molecular Biology*, *1377*, 37–55. doi: 10.1007/978-1-4939-3179-8\_6.
- Benzonana, G. (1969). Study of bile salts micelles: Properties of mixed oleate-deoxycholate solutions at pH 9.0. *Biochimica et Biophysica Acta*, *176*, 836–848.
- Berardi, M. J., Shih, W. M., Harrison, S. C., & Chou, J. J. (2011). Mitochondrial uncoupling protein 2 structure determined by NMR molecular fragment searching. *Nature*, *476*, 109–113. doi: 10.1038/nature10257.
- Borths, E. L., Poolman, B., Hvorup, R. N., Locher, K. P., & Rees, D. C. (2005). In vitro functional characterization of BtuCD-F, the *Escherichia coli* ABC transporter for vitamin B12 uptake. *Biochemistry*, *44*, 16301–16309. doi: 10.1021/bi0513103.
- Boulter, J. M., & Wang, D. N. (2001). Purification and characterization of human erythrocyte glucose transporter in decylmaltoside detergent solution. *Protein Expression and Purification*, *22*, 337–348. doi: 10.1006/prep.2001.1440.
- Breyton, C., Chabaud, E., Chaudier, Y., Pucci, B., & Popot, J.-L. (2004). Hemifluorinated surfactants: A non-dissociating environment for handling membrane proteins in aqueous solutions? *FEBS Letters*, *564*, 312–318. doi: 10.1016/S0014-5793(04)00227-3.
- Cardi, D., Pozza, A., Arnou, B., Marchal, E., Clausen, J. D., Andersen, J. P., ... Jaxel, C. (2010). Purified E255L mutant SERCA1a and purified PfATP6 are sensitive to SERCA-type inhibitors but insensitive to artemisinins. *Journal of Biological Chemistry*, *285*, 26406–26416. doi: 10.1074/jbc.M109.090340.
- Carney, J., East, J. M., Mall, S., Marius, P., Powl, A. M., Wright, J. N., & Lee, A. G. (2006). Fluorescence quenching methods to study lipid-protein interactions. *Current Protocols in Protein Science*, *45*, 19.12.1–19.12.17. doi: 10.1002/0471142301.ps1912s45.
- Centeno, F., Deschamps, S., Lompré, A. M., Anger, M., Moutin, M. J., Dupont, Y., ... Falson, P. (1994). Expression of the sarcoplasmic reticulum Ca<sup>2+</sup>-ATPase in yeast. *FEBS Letters*, *354*, 117–122. doi: 10.1016/0014-5793(94)01104-4.
- Chae, P. S., Rasmussen, S. G. F., Rana, R. R., Gotfryd, K., Chandra, R., Goren, M. A., ... Gellman, S. H. (2010). Maltose-neopentyl glycol (MNG) amphiphiles for solubilization, stabilization and crystallization of membrane proteins. *Nature Methods*, *7*, 1003–1008. doi: 10.1038/nmeth.1526.
- Champeil, P., Menguy, T., Tribet, C., Popot, J. L., & le Maire, M. (2000). Interaction of amphipols with sarcoplasmic reticulum Ca<sup>2+</sup>-

- ATPase. *Journal of Biological Chemistry*, 275, 18623–18637. doi: 10.1074/jbc.M000470200.
- Champeil, P., Orłowski, S., Babin, S., Lund, S., le Maire, M., Møller, J., ... Montigny, C. (2016). A robust method to screen detergents for membrane protein stabilization, revisited. *Analytical Biochemistry*, 511, 31–35. doi: 10.1016/j.ab.2016.07.017.
- Clausen, J. D., Bublitz, M., Arnou, B., Montigny, C., Jaxel, C., Møller, J. V., ... le Maire, M. (2013). SERCA mutant E309Q binds two Ca<sup>2+</sup> ions but adopts a catalytically incompetent conformation. *The EMBO Journal*, 32, 3231–3243. doi: 10.1038/emboj.2013.250.
- Coelho-Sampaio, T., Ferreira, S. T., Castro Júnior, E. J., & Vieyra, A. (1994). Betaine counteracts urea-induced conformational changes and uncoupling of the human erythrocyte Ca<sup>2+</sup> pump. *European Journal of Biochemistry*, 221, 1103–1110. doi: 10.1111/j.1432-1033.1994.tb18830.x.
- Columbus, L. (2015). Post-expression strategies for structural investigations of membrane proteins. *Current Opinion in Structural Biology*, 32, 131–138. doi: 10.1016/j.sbi.2015.04.005.
- Cross, T. A., Sharma, M., Yi, M., & Zhou, H.-X. (2011). Influence of solubilizing environments on membrane protein structures. *Trends in Biochemical Sciences*, 36, 117–125. doi: 10.1016/j.tibs.2010.07.005.
- Dahout-Gonzalez, C., Brandolin, G., & Pebay-Peyroula, E. (2003). Crystallization of the bovine ADP/ATP carrier is critically dependent upon the detergent-to-protein ratio. *Acta Crystallographica. Section D, Biological Crystallography*, 59, 2353–2355. doi: 10.1107/S0907444903020699.
- Drachmann, N. D., Olesen, C., Møller, J. V., Guo, Z., Nissen, P., & Bublitz, M. (2014). Comparing crystal structures of Ca<sup>2+</sup>-ATPase in the presence of different lipids. *The FEBS Journal*, 281, 4249–4262. doi: 10.1111/febs.12957.
- Drew, D., Newstead, S., Sonoda, Y., Kim, H., von Heijne, G., & Iwata, S. (2008). GFP-based optimization scheme for the overexpression and purification of eukaryotic membrane proteins in *Saccharomyces cerevisiae*. *Nature Protocols*, 3, 784–798. doi: 10.1038/nprot.2008.44.
- du Noüy, P. L. (1919). A new apparatus for measuring surface tension. *Journal of General Physiology*, 1, 521–524. doi: 10.1085/jgp.1.5.521.
- Ellinger, P., Kluth, M., Stindt, J., Smits, S. H. J., & Schmitt, L. (2013). Detergent screening and purification of the human liver ABC transporters BSEP (ABCB11) and MDR3 (ABCB4) expressed in the yeast *Pichia pastoris*. *PLoS One*, 8, e60620. doi: 10.1371/journal.pone.0060620.
- de Foresta, B., Henao, F., & Champeil, P. (1992). Kinetic characterization of the perturbation by dodecylmaltoside of sarcoplasmic reticulum Ca<sup>2+</sup>-ATPase. *European Journal of Biochemistry*, 209, 1023–1034. doi: 10.1111/j.1432-1033.1992.tb17378.x.
- Frauenfeld, J., Löving, R., Armache, J.-P., Sonnen, A. F.-P., Guettou, F., Moberg, P., ... Nordlund, P. (2016). A saposin-lipoprotein nanoparticle system for membrane proteins. *Nature Methods*, 13, 345–351. doi: 10.1038/nmeth.3801.
- Hardy, D., Bill, R. M., Jawhari, A., & Rothnie, A. J. (2016). Overcoming bottlenecks in the membrane protein structural biology pipeline. *Biochemical Society Transactions*, 44, 838–844. doi: 10.1042/BST20160049.
- Hatori, Y., Hirata, A., Toyoshima, C., Lewis, D., Pilankatta, R., & Inesi, G. (2008). Intermediate phosphorylation reactions in the mechanism of ATP utilization by the copper ATPase (CopA) of *Thermotoga maritima*. *Journal of Biological Chemistry*, 283, 22541–22549. doi: 10.1074/jbc.M802735200.
- Helenius, A., & Simons, K. (1975). Solubilization of membranes by detergents. *Biochimica et Biophysica Acta*, 415, 29–79. doi: 10.1016/0304-4157(75)90016-7.
- Hokin, L. E., Sastry, P. S., Galsworthy, P. R., & Yoda, A. (1965). Evidence that a phosphorylated intermediate in a brain transport adenosine triphosphatase is an acyl phosphate. *Proceedings of the National Academy of Sciences of the United States of America*, 54, 177–184. doi: 10.1073/pnas.54.1.177.
- Hong, W.-X., Baker, K. A., Ma, X., Stevens, R. C., Yeager, M., & Zhang, Q. (2010). Design, synthesis, and properties of branch-chained maltoside detergents for stabilization and crystallization of integral membrane proteins: Human connexin 26. *Langmuir*, 26, 8690–8696. doi: 10.1021/la904893d.
- Hovers, J., Potschies, M., Polidori, A., Pucci, B., Raynal, S., Bonneté, F., ... Welte, W. (2011). A class of mild surfactants that keep integral membrane proteins water-soluble for functional studies and crystallization. *Molecular Membrane Biology*, 28, 171–181. doi: 10.3109/09687688.2011.552440.
- Hunte, C., & Richers, S. (2008). Lipids and membrane protein structures. *Current Opinion in Structural Biology*, 18, 406–411. doi: 10.1016/j.sbi.2008.03.008.
- Hwang, S.-Y., Jin, L.-T., Yoo, G.-S., & Choi, J.-K. (2006). Counterion-dye staining for DNA in electrophoresed gels using indoine blue and methyl orange. *Electrophoresis*, 27, 1739–1743. doi: 10.1002/elps.200500640.
- Ito, S., & Yamamoto, D. (2015). Structure of the methyl orange-binding site on human serum albumin and its color-change mechanism. *Biomedical Research*, 36, 247–252. doi: 10.2220/biomedres.36.247.
- Jacquot, A., Montigny, C., Hennrich, H., Barry, R., le Maire, M., Jaxel, C., ... Lenoir, G. (2012). Phosphatidylserine stimulation of Drs2p-Cdc50p lipid translocase dephosphorylation is controlled by phosphatidylinositol-4-phosphate. *Journal of Biological Chemistry*, 287, 13249–13261. doi: 10.1074/jbc.M111.313916.

- Jidenko, M., Nielsen, R. C., Sørensen, T. L.-M., Møller, J. V., le Maire, M., Nissen, P., & Jaxel, C. (2005). Crystallization of a mammalian membrane protein overexpressed in *Saccharomyces cerevisiae*. *Proceedings of the National Academy of Sciences of the United States of America*, *102*, 11687–11691. doi: 10.1073/pnas.0503986102.
- Jumpertz, T., Tschapek, B., Infed, N., Smits, S. H. J., Ernst, R., & Schmitt, L. (2011). High-throughput evaluation of the critical micelle concentration of detergents. *Analytical Biochemistry*, *408*, 64–70. doi: 10.1016/j.ab.2010.09.011.
- Kalyanasundaram, K., & Thomas, J. (1977). Environmental effects on vibronic band intensities in pyrene monomer fluorescence and their application in studies of micellar systems. *Journal of the American Chemical Society*, *99*, 2039–2044. doi: 10.1021/ja00449a004.
- Kawate, T., & Gouaux, E. (2006). Fluorescence-detection size-exclusion chromatography for precrystallization screening of integral membrane proteins. *Structure*, *14*, 673–681. doi: 10.1016/j.str.2006.01.013.
- Korepanova, A., & Matayoshi, E. D. (2012). HPLC-SEC characterization of membrane protein-detergent complexes. *Current Protocols in Protein Science*, *68*, 29.5.1–29.5.12. doi: 10.1002/0471140864.ps2905s68.
- Kragh-Hansen, U., le Maire, M., & Møller, J. V. (1998). The mechanism of detergent solubilization of liposomes and protein-containing membranes. *Biophysical Journal*, *75*, 2932–2946. doi: 10.1016/S0006-3495(98)77735-5.
- Lee, A. G. (2011). Biological membranes: The importance of molecular detail. *Trends in Biochemical Sciences*, *36*, 493–500. doi: 10.1016/j.tibs.2011.06.007.
- Lenoir, G., Menguy, T., Corre, F., Montigny, C., Pedersen, P. A., Thinès, D., ... Falson, P. (2002). Overproduction in yeast and rapid and efficient purification of the rabbit SERCA1a Ca<sup>2+</sup>-ATPase. *Biochimica et Biophysica Acta*, *1560*, 67–83. doi: 10.1016/S0005-2736(01)00458-8.
- Lichtenberg, D., Ahyayauch, H., Alonso, A., & Goñi, F. M. (2013). Detergent solubilization of lipid bilayers: A balance of driving forces. *Trends in Biochemical Sciences*, *38*, 85–93. doi: 10.1016/j.tibs.2012.11.005.
- Lund, S., Orłowski, S., de Foresta, B., Champeil, P., le Maire, M., & Møller, J. V. (1989). Detergent structure and associated lipid as determinants in the stabilization of solubilized Ca<sup>2+</sup>-ATPase from sarcoplasmic reticulum. *Journal of Biological Chemistry*, *264*, 4907–4915.
- Magnani, F., Serrano-Vega, M. J., Shibata, Y., Abdul-Hussein, S., Lebon, G., Miller-Gallacher, J., ... Tate, C. G. (2016). A mutagenesis and screening strategy to generate optimally thermostabilized membrane proteins for structural studies. *Nature Protocols*, *11*, 1554–1571. doi: 10.1038/nprot.2016.088.
- le Maire, M., Arnou, B., Olesen, C., Georgin, D., Ebel, C., & Møller, J. V. (2008). Gel chromatography and analytical ultracentrifugation to determine the extent of detergent binding and aggregation, and Stokes radius of membrane proteins using sarcoplasmic reticulum Ca<sup>2+</sup>-ATPase as an example. *Nature Protocols*, *3*, 1782–1795. doi: 10.1038/nprot.2008.177.
- le Maire, M., Champeil, P., & Møller, J. V. (2000). Interaction of membrane proteins and lipids with solubilizing detergents. *Biochimica et Biophysica Acta*, *1508*, 86–111. doi: 10.1016/S0304-4157(00)00010-1.
- Marchand, A., Winther, A.-M. L., Holm, P. J., Olesen, C., Montigny, C., Arnou, B., ... Maire, M. (2008). Crystal structure of D351A and P312A mutant forms of the mammalian sarcoplasmic reticulum Ca<sup>2+</sup>-ATPase reveals key events in phosphorylation and Ca<sup>2+</sup> release. *Journal of Biological Chemistry*, *283*, 14867–14882. doi: 10.1074/jbc.M710165200.
- Mataga, N., Okada, T., & Yamamoto, N. (1967). Electronic processes in hetero-excimer and the mechanism of fluorescence quenching. *Chemical Physics Letters*, *1*, 119–121. doi: 10.1016/0009-2614(67)85003-6.
- Meyer, O., Ollivon, M., & Paternostre, M. T. (1992). Solubilization steps of dark-adapted purple membrane by Triton X-100. A spectroscopic study. *FEBS Letters*, *305*, 249–253. doi: 10.1016/0014-5793(92)80679-B.
- Møller, J. V., Lind, K. E., & Andersen, J. P. (1980). Enzyme kinetics and substrate stabilization of detergent-solubilized and membraneous (Ca<sup>2+</sup> + Mg<sup>2+</sup>)-activated ATPase from sarcoplasmic reticulum. Effect of protein-protein interactions. *Journal of Biological Chemistry*, *255*, 1912–1920.
- Møller, J. V., & Olesen, C. (2016). Preparation of Ca<sup>2+</sup>-ATPase1a enzyme from rabbit sarcoplasmic reticulum. In M. Bublitz (Ed.), *P-type ATPases* (pp. 11–17). New York, NY: Springer.
- Møller, J. V., Olesen, C., Winther, A.-M. L., & Nissen, P. (2010). The sarcoplasmic Ca<sup>2+</sup>-ATPase: Design of a perfect chemi-osmotic pump. *Quarterly Reviews of Biophysics*, *43*, 501–566. doi: 10.1017/S003358351000017X.
- Montigny, C., Arnou, B., & Champeil, P. (2010). Glycyl betaine is effective in slowing down the irreversible denaturation of a detergent-solubilized membrane protein, sarcoplasmic reticulum Ca<sup>2+</sup>-ATPase (SERCA1a). *Biochemical and Biophysical Research Communications*, *391*, 1067–1069. doi: 10.1016/j.bbrc.2009.12.021.
- Montigny, C., Arnou, B., Marchal, E., & Champeil, P. (2008). Use of glycerol-containing media to study the intrinsic fluorescence properties of detergent-solubilized native or expressed SERCA1a. *Biochemistry*, *47*, 12159–12174. doi: 10.1021/bi8006498.
- Montigny, C., Azouaoui, H., Jacquot, A., le Maire, M., Jaxel, C., Champeil, P., & Lenoir, G. (2014). Overexpression of membrane proteins in *Saccharomyces cerevisiae* for structural

- and functional studies: A focus on the rabbit  $\text{Ca}^{2+}$ -ATPase Serca1a and on the yeast lipid “flippase” complex Drs2p/Cdc50p. In I. Mus-Veteau (Ed.), *Membrane proteins production for structural analysis* (pp. 133–171). New York, NY: Springer.
- Montigny, C., Dieudonné, T., Orłowski, S., Vázquez-Ibar, J. L., Gauron, C., Georgin, D., ... Lenoir, G. (2017). Slow phospholipid exchange between a detergent-solubilized membrane protein and lipid-detergent mixed micelles: Brominated phospholipids as tools to follow its kinetics. *PLoS One*, *12*, e0170481. doi: 10.1371/journal.pone.0170481.
- Montigny, C., Lyons, J., Champeil, P., Nissen, P., & Lenoir, G. (2016). On the molecular mechanism of flippase- and scramblase-mediated phospholipid transport. *Biochimica et Biophysica Acta*, *1861*, 767–783. doi: 10.1016/j.bbalmem.2015.12.020.
- Mukerjee, P., & Mysels, K. (1955). A re-evaluation of the spectral change method of determining critical micelle concentration. *Journal of the American Chemical Society*, *77*, 2937–2943. doi: 10.1021/ja01616a003.
- Murata, N., Mohanty, P. S., Hayashi, H., & Papageorgiou, G. C. (1992). Glycinebetaine stabilizes the association of extrinsic proteins with the photosynthetic oxygen-evolving complex. *FEBS Letters*, *296*, 187–189. doi: 10.1016/0014-5793(92)80376-R.
- Natarajan, P., Wang, J., Hua, Z., & Graham, T. R. (2004). Drs2p-coupled aminophospholipid translocase activity in yeast Golgi membranes and relationship to in vivo function. *Proceedings of the National Academy of Sciences of the United States of America*, *101*, 10614–10619. doi: 10.1073/pnas.0404146101.
- Ohnishi, S. T. (1978). Characterization of the murexide method: Dual-wavelength spectrophotometry of cations under physiological conditions. *Analytical Biochemistry*, *85*, 165–179. doi: 10.1016/0003-2697(78)90287-7.
- Orwick-Rydmark, M., Arnold, T., & Linke, D. (2016). The use of detergents to purify membrane proteins. *Current Protocols in Protein Science*, *84*, 4.8.1–4.8.35. doi: 10.1002/0471140864.ps0408s84.
- Palmgren, M. G., & Nissen, P. (2011). P-type ATPases. *Annual Review of Biophysics*, *40*, 243–266. doi: 10.1146/annurev.biophys.093008.131331.
- Parker, J. L., & Newstead, S. (2016). Membrane protein crystallisation: Current trends and future perspectives. *Advances in Experimental Medicine and Biology*, *922*, 61–72. doi: 10.1007/978-3-319-35072-1\_5.
- Paternostre, M. T., Roux, M., & Rigaud, J. L. (1988). Mechanisms of membrane protein insertion into liposomes during reconstitution procedures involving the use of detergents. 1. Solubilization of large unilamellar liposomes (prepared by reverse-phase evaporation) by Triton X-100, octyl glucoside, and sodium cholate. *Biochemistry*, *27*, 2668–2677. doi: 10.1021/bi00408a006.
- Perez, C., Gerber, S., Boilevin, J., Bucher, M., Darbre, T., Aebi, M., ... Locher, K. P. (2015). Structure and mechanism of an active lipid-linked oligosaccharide flippase. *Nature*, *524*, 433–438. doi: 10.1038/nature14953.
- Picas, L., Suárez-Germà, C., Montero, M. T., Vázquez-Ibar, J. L., Hernández-Borrell, J., Prieto, M., & Loura, L. M. S. (2010). Lactose permease lipid selectivity using Förster resonance energy transfer. *Biochimica et Biophysica Acta*, *1798*, 1707–1713. doi: 10.1016/j.bbamem.2010.
- Popot, J.-L., Althoff, T., Bagnard, D., Banères, J.-L., Bazzacco, P., Billon-Denis, E., ... Zoonens, M. (2011). Amphipols from A to Z. *Annual Review of Biophysics*, *40*, 379–408. doi: 10.1146/annurev-biophys-042910-155219.
- Privé, G. G. (2007). Detergents for the stabilization and crystallization of membrane proteins. *Methods*, *41*, 388–397. doi: 10.1016/j.ymeth.2007.01.007.
- Pullman, M. E., Penefsky, H. S., Datta, A., and Racker, E. (1960). Partial resolution of the enzymes catalyzing oxidative phosphorylation: I. Purification and properties of soluble, dinitrophenol-stimulated adenosine triphosphatase. *Journal of Biological Chemistry*, *235*, 3322–3329.
- Rodríguez-Banqueri, A., Errasti-Murugarren, E., Bartoccioni, P., Kowalczyk, L., Perálvarez-Marín, A., Palacín, M., & Vázquez-Ibar, J. L. (2016). Stabilization of a prokaryotic LAT transporter by random mutagenesis. *Journal of General Physiology*, *147*, 353–368. doi: 10.1085/jgp.201511510.
- Roux, M., & Champeil, P. (1984).  $^{31}\text{P}$  NMR as a tool for monitoring detergent solubilization of sarcoplasmic reticulum membranes. *FEBS Letters*, *171*, 169–172. doi: 10.1016/0014-5793(84)80481-0.
- Saif Hasan, S., Baniulis, D., Yamashita, E., Zhalnina, M. V., Zakharov, S. D., Stoffeth, J. T., & Cramer, W. A. (2013). Methods for studying interactions of detergents and lipids with  $\alpha$ -helical and  $\beta$ -barrel integral membrane proteins: Interactions of detergents and lipids with membrane proteins. *Current Protocols in Protein Science*, *74*, 29.7.1–29.7.30. doi: 10.1002/0471140864.ps2907s74.
- Sehgal, P., Olesen, C., & Møller, J. V. (2016). ATPase activity measurements by an enzyme-coupled spectrophotometric assay. In M. Bublitz (Ed.), *P-type ATPases* (pp. 105–109). New York, NY: Springer.
- Slavík, J. (1982). Anilidonaphthalene sulfonate as a probe of membrane composition and function. *Biochimica et Biophysica Acta*, *694*, 1–25. doi: 10.1016/0304-4157(82)90012-0.
- Sørensen, T. L.-M., Olesen, C., Jensen, A.-M. L., Møller, J. V., & Nissen, P. (2006). Crystals of sarcoplasmic reticulum  $\text{Ca}^{2+}$ -ATPase. *Journal of Biotechnology*, *124*, 704–716. doi: 10.1016/j.jbiotec.2006.02.004.
- Tan, C. H., Huang, Z. J., & Huang, X. G. (2010). Rapid determination of surfactant crit-

- ical micelle concentration in aqueous solutions using fiber-optic refractive index sensing. *Analytical Biochemistry*, 401, 144–147. doi: 10.1016/j.ab.2010.02.021.
- Tanford, C., & Reynolds, J. A. (1976). Characterization of membrane proteins in detergent solutions. *Biochimica et Biophysica Acta*, 457, 133–170. doi: 10.1016/0304-4157(76)90009-5.
- Vaidehi, N., Grisshammer, R., & Tate, C. G. (2016). How can mutations thermostabilize G-protein-coupled receptors? *Trends in Pharmacological Sciences*, 37, 37–46. doi: 10.1016/j.tips.2015.09.005.
- Walter, A., Kuehl, G., Barnes, K., & VanderWaerd, G. (2000). The vesicle-to-micelle transition of phosphatidylcholine vesicles induced by nonionic detergents: Effects of sodium chloride, sucrose and urea. *Biochimica et Biophysica Acta*, 1508, 20–33. doi: 10.1016/S0304-4157(00)00005-8.
- Yang, Y., Jung, D. W., Bai, D. G., Yoo, G. S., & Choi, J. K. (2001). Counterion-dye staining method for DNA in agarose gels using crystal violet and methyl orange. *Electrophoresis*, 22, 855–859. doi: 10.1002/1522-2683(200105)22:5<855::AID-ELPS855>3.0.CO;2-Y.
- Zhou, X., & Graham, T. R. (2009). Reconstitution of phospholipid translocase activity with purified Drs2p, a type-IV P-type ATPase from budding yeast. *Proceedings of the National Academy of Sciences of the United States of America*, 106, 16586–16591. doi: 10.1073/pnas.0904293106.
- Zhou, X., Sebastian, T. T., & Graham, T. R. (2013). Auto-inhibition of Drs2p, a yeast phospholipid flippase, by its carboxyl-terminal tail. *Journal of Biological Chemistry*, 288, 31807–31815. doi: 10.1074/jbc.M113.481986.
- Zhou, Y., & Bowie, J. U. (2000). Building a thermostable membrane protein. *Journal of Biological Chemistry*, 275, 6975–6979. doi: 10.1074/jbc.275.10.6975.
- Zoonens, M., Comer, J., Masscheleyn, S., Pebay-Peyroula, E., Chipot, C., Miroux, B., & Dehez, F. (2013). Dangerous liaisons between detergents and membrane proteins. The case of mitochondrial uncoupling protein 2. *Journal of the American Chemical Society*, 135, 15174–15182. doi: 10.1021/ja407424v.

### Internet Resources

<https://www.anatrace.com>

Anatrace website for references and physical and chemical parameters of detergents. Brochures are sometimes downloadable. Frequently asked questions sections usually contain good advice on the use of detergents.

<https://avantilipids.com>

Avanti Polar lipids website for references and resources. Chemical formulas of lipids are available.

[https://www.perkinelmer.com/lab-solutions/resources/docs/TCH\\_Phosphorus32.pdf](https://www.perkinelmer.com/lab-solutions/resources/docs/TCH_Phosphorus32.pdf)

Safe handling guide is available on Perkin Elmer website.





## Résumé en français

---

Le paludisme est une maladie causée par une infection par un parasite du genre *Plasmodium*. Elle touche 91 pays dans le monde et, en 2016, a causé la mort de 450 000 personnes. Cinq espèces sont responsables de la maladie chez l'Homme, *P. falciparum*, *P. vivax*, *P. ovale*, *P. malariae* and *P. knowlesi*. Le cycle de vie du parasite est complexe, une partie se déroulant chez l'insecte vecteur, le moustique femelle du genre *Anopheles*, et une partie chez l'hôte. Chez ce dernier, le stade intra-érythrocytaire est responsable des différents symptômes observés. Malgré les différents traitements et contrôles mis en place, la lutte contre le paludisme reste difficile du fait de l'apparition de souches résistantes aux traitements et à leur rapide propagation. C'est pour cela qu'il est nécessaire de trouver de nouvelles molécules, mais aussi de nouvelles cibles thérapeutiques contre le parasite. Il est donc important de comprendre la biologie du parasite. Au stade érythrocytaire, le parasite intracellulaire a besoin de la présence de transporteurs membranaires afin d'acquérir des nutriments, évacuer ses métabolites et conserver l'homéostasie ionique. A ce jour, très peu de transporteurs membranaires ont été caractérisés chez *Plasmodium*. De récentes études ont montré que ATP2, un transporteur putatif de la famille des ATPases de type P4, ou flippases, est essentiel à la survie du parasite. Les ATPases de type P4 permettent le maintien de l'asymétrie en lipide dans les membranes biologiques en transportant les lipides du feuillet externe vers le feuillet interne de la membrane, et elles sont impliquées dans différents processus biologiques comme la formation de vésicules, l'apoptose ou la signalisation cellulaire par exemple. Ces transporteurs sont associés à une sous-unité de la famille des CDC50 et trois sous-unités putatives sont trouvées dans le génome de *P. falciparum*.

La thèse a pour but d'initier la caractérisation biochimique d'ATP2 pour lequel aucune étude fonctionnelle n'a été réalisée à ce jour. Les questions que nous pouvons nous poser sont : est-ce que ATP2 est bien une flippase ? Peut-elle s'associer à une ou différentes sous-unités Cdc50 ? Quels sont les lipides transportés par ATP2 ? Pour essayer de répondre à ces questions, nous avons entrepris de cloner et d'exprimer chez la levure *Saccharomyces cerevisiae* ATP2 avec les différentes sous-unités Cdc50 putatives afin de caractériser l'association entre les deux protéines et, par la suite, débiter la caractérisation fonctionnelle d'ATP2.

Nous avons décidé de ne pas seulement travailler sur les séquences d'ATP2 et des trois sous-unités Cdc50 correspondantes de *P. falciparum* mais aussi sur celles de deux autres espèces infectant les rongeurs, *Plasmodium berghei* et *Plasmodium chabaudi*. L'identité de séquence est de 50 à 60% entre les séquences homologues d'ATP2 chez ces différentes espèces de *Plasmodium*. Afin de pouvoir exprimer les gènes de *Plasmodium* dans la levure, nous avons utilisé des séquences optimisées pour l'expression chez *S. cerevisiae*, pour diminuer le taux élevé en AT dans le génome de *P. falciparum*. La stratégie de clonage, mise en place au laboratoire pour d'autres ATPases de type P4, est de construire un vecteur de co-expression. Les séquences de la flippase et de la sous unité sont clonées dans le même vecteur, chaque séquence sous le contrôle de son propre promoteur. La séquence de la flippase est clonée avec un domaine accepteur de biotine positionné en N- ou C- terminal de la protéine et une étiquette 10 histidines est clonée en C-terminal des différentes sous unités Cdc50. Les différents vecteurs de co-expression n'ont pu être obtenus pour l'espèce *P. berghei*. Les tests d'expression ont donc été faits avec les espèces *P. falciparum* et *P. chabaudi*. Seules les constructions pour *P. chabaudi* ont montré une co-expression de PcATP2 et des sous unités correspondantes. Les co-expressions PcATP2/PcCdc50.1 et PcATP2/PcCdc50.3 ont donné les résultats les plus encourageants pour la suite. Un fractionnement membranaire a été réalisé pour chaque construction et celui-ci nous a montré que la distribution d'ATP2 dans les différentes fractions membranaires n'était pas la même selon la sous-unité co-exprimée. Nous avons également démontré que la sous-unité PcCdc50.3 possède un site de glycosylation et est glycosylée chez la levure mais sans pouvoir conclure quant à son rôle dans notre système d'expression. Nous avons réussi à solubiliser une faible fraction d'ATP2 et les PcCdc50 à l'aide d'un détergent dit doux et un dérivé du cholestérol, le cholesteryl hemisuccinate, mais suffisamment pour continuer nos analyses. Nous avons ensuite inséré la Green Fluorescent Protein (GFP) afin d'utiliser des techniques plus sensibles pour détecter notre flippase. Grâce à la GFP, nous avons pu étudier la localisation d'ATP2 et PcCdc50.1 dans la levure par microscopie confocale. Nous avons également démontré par co-immunoprécipitation à l'aide de nanobodies ciblant la GFP, qu'ATP2 était capable de s'associer à PcCdc50.1 et à PcCdc50.3. Nous avons étudié la stabilité d'ATP2 et PcCdc50 en détergent en utilisant la chromatographie d'exclusion stérique couplée à la détection par fluorescence. Cette étude nous a permis de voir que la présence d'ATP2 permettait à PcCdc50.1 d'être plus

stable. Du fait des résultats obtenus pour l'association entre ATP2 et PcCdc50.1, nous avons entrepris la purification du complexe. En parallèle, nous avons obtenu les mutants non-fonctionnels d'ATP2, E235Q et D596N, respectivement mutés dans le domaine de déphosphorylation et dans le domaine contenant l'aspartate phosphorylé durant le cycle catalytique, nous permettant ainsi d'avoir des contrôles négatifs. Les premiers tests fonctionnels de phosphorylation, en utilisant de l'ATP radioactif, et les tests d'activité ATPasique n'ont, à ce jour, pas donné de résultats concluants. Cependant, d'autres possibilités peuvent être encore testées comme l'utilisation d'autres substrats phospholipidiques ou un autre détergent pour la stabilité et la fonction du complexe.

Pour résumer, nous avons réussi à produire une flippase putative, ATP2, de *P. chabaudi* en complexe avec sa sous-unité Cdc50 associée. Nos études ont également démontré que les deux sous-unités PcCdc50.1 et PcCdc50.3 étaient capables de s'associer à PcATP2. Nous avons pu voir que la sous-unité PcCdc50.3 était glycosylée dans la levure. Malgré le faible niveau d'expression et le faible taux de solubilisation, nous avons pu purifier le complexe PcATP2/PcCdc50.1 à l'aide de nanobodies ciblant l'étiquette GFP.

Afin d'obtenir plus de matériel pour les futurs tests fonctionnels, il est nécessaire d'optimiser les différentes étapes de production et de purification de notre complexe. Dans un premier temps, pour tenter d'exprimer plus de protéines, nous avons entrepris le clonage des séquences d'ATP2 et des sous-unités Cdc50 pour l'expression chez la levure *Pichia pastoris* également largement utilisée pour la production de protéines membranaires. Une autre technique que nous avons testée est l'harmonisation de codons, c'est-à-dire l'incorporation de codons peu utilisés par les ribosomes afin de permettre de ralentir la traduction et permettre un meilleur repliement de la protéine.



### Flippases de parasites du genre *Plasmodium* : de la production hétérologue vers la caractérisation fonctionnelle

Mots clés : ATPase de type P4; sous unités Cdc50; protéines membranaires; expression hétérologue; purification; paludisme

Le paludisme est une maladie dévastatrice causée par un parasite du genre *Plasmodium*. Du fait de la propagation de souches résistantes aux actuels antipaludéens, il est nécessaire de comprendre la biologie du parasite afin de trouver de nouvelles cibles thérapeutiques. Les transporteurs membranaires sont une classe importante de cibles du fait de leur rôle physiologique essentiel pour la cellule. Cependant, seulement quelques transporteurs ont été biochimiquement caractérisés chez les parasites du genre *Plasmodium*. Des études récentes de délétion de gènes dans un modèle murin ont montré qu'une ATPase de type P4 de *Plasmodium*, ou flippase, est essentielle à la survie du parasite. Chez les Eucaryotes, l'activité de translocation des lipides des ATPases de type P4 est nécessaire pour maintenir l'asymétrie des membranes, un élément clé dans de nombreux processus essentiels comme la formation de vésicules ou l'apoptose. Les flippases forment des complexes hétéromériques avec les protéines de la famille Cdc50 qui sont également trouvées dans le génome de *Plasmodium*. Pour comprendre le rôle fonctionnel de ces transporteurs putatifs durant l'infection par le parasite, nous avons besoin d'étudier leur mécanisme de transport et d'identifier leur (s) substrat (s). Nous avons entrepris l'expression hétérologue chez *Saccharomyces cerevisiae* d'ATP2, une ATPase de type P4, et des sous unités Cdc50 de trois espèces différentes de *Plasmodium*. Nous avons réussi à co-exprimer PcATP2 de *P. chabaudi* et les sous unités correspondantes. Par co-immuno précipitation et une chromatographie d'exclusion stérique détectée par fluorescence, nous sommes parvenus à identifier quelle sous unité peut être associée à PcATP2. Nous avons ensuite purifié le complexe PcATP2/PcCdc50.1 en utilisant des nanobodies reconnaissant la GFP fusionnée à l'extrémité C-terminale de PcATP2 et nous avons initié la caractérisation fonctionnelle avec des tests d'activité ATPasique

### Lipid flippases of *Plasmodium* parasites: from heterologous production towards functional characterization

Keywords : P4-ATPases; Cdc50 subunits; membrane proteins; heterologous expression; purification; malaria

Malaria is a devastating disease caused by a parasite of the genus *Plasmodium*. Due to the spread of resistant strains to current antimalarial drug, it is necessary to understand the biology of the parasite in order to find new drug targets. The membrane transporters are an important class of drug targets as they have an essential role in the physiology of the cell. However, from *Plasmodium* parasites, just a few membrane transporters have been biochemically described. Recent gene-deletion studies in malaria mouse models have shown that one *Plasmodium* P4-ATPase, or lipid flippase, is essential for the parasite survival. In eukaryotes, the phospholipid translocation activity of P4-ATPases is needed to maintain the asymmetric distribution of membranes, a key element in many essential processes like vesicle budding or apoptosis. Lipid flippases form heteromeric complexes with members of the Cdc50 protein family, also found in the genomes of *Plasmodium* parasites. To understand the functional role of these still putative transporters during malaria infection we need to study their transport mechanism and identify their substrate(s). We have conducted the heterologous expression in *Saccharomyces cerevisiae* of ATP2, a P4-ATPase, and Cdc50 subunits from three different *Plasmodium* species. We succeeded to co-express PcATP2 from *P. chabaudi* and the related putative PcCdc50 proteins. By co-immunoprecipitation and Fluorescence-detection Size Exclusion Chromatography, we have managed to identify which  $\beta$ -subunit can be associated to PcATP2. We then purified the complex PcATP2/PcCdc50.1 using immobilized nanobodies that recognize the GFP fused at the C-terminal end of PcATP2 and we initiated the functional characterization using ATPase activity assays

